Mathematical Modelling of Drying Food Products: Application to Tropical Fruits

Nor Azni Shahari, MSc

Thesis submitted to the University of Nottingham
for the degree of Doctor of Philosophy

February, 2012

Abstract

Drying is an old traditional method of removing liquid from inside material, such as wood, food, paper, ceramics, building materials, textiles, granular products, pharmaceutical and electronic devices. The kinetics of this liquid removal depends on the material properties of the solid phase as well as on cellular structure.

The aim of this project is to understand the effect of complex interaction of heat, moisture and shrinkage to create a detailed mathematical modelling to quantify the drying of a food product and tropical fruits in particular, which typically have high water content. To this purpose, in first part of the thesis, an initial simple coupled diffusion model with Fickian moisture transfer and Fourier heat transfer by Wang and Brenann [122] has been extended. A one-dimensional model is applied with the effect of shrinkage for a prediction of moisture and temperature distribution during drying. Constant physical and thermal properties are used relevant to tropical fruits. A numerical solution technique, based on the method of lines, is used with local finite difference methods approximation to the drying. The results match well with published food drying simulation studies and the anticipated final state of shrinkage in particular.

To obtain a detailed understanding of simultaneous heat and liquid transfer during drying of fruits, the internal structure has to be modelled. In fruit tissue, intercellular space existing within a highly complicated network of gaseous channels can be considered as a porous medium. Guided by this, an extended model of drying, incorporating the heterogeneous properties of the tissues and their cellular structure, is recognized and simplified to represent the physical model. In this model, a distinction is made between the different classes of water present in the material (free water, bound water and water vapour) and the conversion between them. Evaluation is applied to the range of one-dimensional structures of increasing complexity: the first is an isothermal model without consideration of heat effects; the remaining have heat effects but differ in the correlated spatial arrangement of micro and macro pores. All results are given as drying curves and phase distributions during drying.

Acknowledgements

I would like to thank my principal supervisor, Associated Professor Dr Stephen Hibberd, for his expert guidance, invaluable advice, supervision and patient encouragement throughout this research which has enabled me to complete this thesis successfully. He has never been lacking in kindness and support.

Moreover, I appreciate the excellent support, helpful comments, guidance and advice given by my co-supervisor, Professor Dr Sandra Hill. I am also grateful for the advise of Dr Pragnesh Gajjar and Dr Norma Alias. I would also like to thank Dr Greg Tucker for the advice about food structure properties.

I gratefully acknowledge that this research is jointly funded by Universiti Teknologi MARA, Malaysia and the Ministry of Higher Education, Government of Malaysia. Thanks go to them for giving me the opportunity to help them to achieve their vision and mission whilst giving me the chance to realise my dream.

I cannot express how much I would like to say thank you to my husband, Khairulanwar, who has supported me from day one and my children Khairi, Aidah, Laila, Imran and Hafizul. They have always been there for me, no matter what the situation, and I am forever in their debt.

Contents

List of Tables

List of Figures

Chapter 1

Introduction to the Modelling of Drying Fruits

1.1 Introduction and Motivation

Drying is described as the reduction of product moisture to the required dryness values as a definite process [18]. Solid drying is of interest in different fields, such as food processing, building materials (such as brick [138, 6] and wood [116, 110]), pharmaceutical products, paper and ceramic etc. This thesis centres on the drying of food products, especially the drying of tropical fruits, which is characterized by a cellular internal structure and high levels of initial moisture. Over the years, research on drying common fruits has been extensively carried out, for example, apples, grapes, berries, bananas, pears, potatoes etc. However, reports on other fruits especially tropical fruits are rather scarce [45].

Fresh fruit waste and the increasing demand for dry fruits have given a new initiative for food manufactures to produce dried fruit products [36]. Furthermore, an estimated 30%-40% damage and wastage of seasonal fruits in many countries is attributed to a lack of proper processing [65]. The drying applied to fruits serves a number of aims, the most important of which is the reduction of moisture content to a required level to prevent growth of mould and microbes, allowing safe storage and preventing microbial development or other harmful reactions. In the food industry, drying of food is an important aspect of the production of various types of food.

This process can be very challenging: using a mathematical model, a new dryer can be developed, the appearance of the product can be enhanced, the original flavour encapsulated and nutritional value maintained [22].

Currently, most dehydrated fruits are produced by the technique of hot air drying, which is the simplest and most economical of the various methods [45]. Several other drying techniques have been proposed, such as a combination of osmotic dehydration with hot air drying or a combination of freeze drying followed by air drying, superheated steam etc. However, for modelling purposes, in this study, conventional hot air drying is assumed to be applied to the surface. The main feature of such a system is its ability to predict moisture and temperature inside the product, which is a very important way of providing structural knowledge of the quality of the new product.

A mathematical modelling approach is suggested as an approach that is complementary to existing laboratory experiments. To reflect the diversity of the applications and to maximize the potential use of a drying model, several important aspects are considered in its development, such as the simplification of problem formulation applicability to various food processes and the inclusion of dominant internal process in a mathematical representation [34]. The goal is to keep as many details of the process as possible, without creating unnecessary computational complexity or time commitment [34]. Comprehensiveness also has long been an issue in developing drying models in food. However, many modelling approaches that claim to be comprehensive are limited in practical applications due to models that contain large numbers of parameters. These not only make the models less interpretable but also make the numerical process slower. One of the common solutions to the above issue is to build either observation based models, which are able to induce more comprehensive models, or so-called empirical models, which are capable of producing high performance for limited data sets.

In this thesis, we aim to increase the understanding of the movement of water and heat during the drying of tropical fruits. In this chapter we give a brief overview of drying method applicable to drying tropical fruits and identify the underlying physical processes. This chapter is organized as follows: section 1.2 discusses the major approach to quantifying drying process in fruits in order to give some basis to this project. Section 1.3 discusses the development of some mathematical drying

models for food; their applications and restrictions are reviewed with examples of some of the models presented. Finally, methods and results of some research groups involved in the drying of food by various methods will be described.

1.2 Major approaches to quantifying the drying process in foods

Modelling of the drying processes can be formally characterized by two different approaches: physical based modelling and empirical modelling. Physical based modelling is mathematically formulated from the basic physical principles of the drying process. However, evaluation of some of the detailed physical properties and complex processes are very difficult to quantify and the relevance of these models is typically limited by the approximation made. According to Datta [34], in a comprehensive review of food science and food safety, observation based models provide a starting point but they are primarily empirical in nature. In contrast, a physical based model should describe the presumed physical phenomena, even in the absence of experimental data [34]. Early physical based diffusion modelling in drying, together with an analytical solution, is associated with the work of Crank [27].

The existing models of thermal processes in food can be broadly divided into four groups. The first group consists of totally lumped models for heat and mass transport that do not include any important physics. Such models are based entirely on empirical data, are suited for a specified product and processing conditions, and, therefore, cannot be applied to a general class of food processes or even a slightly different situation (for example [118, 68, 122]). The development of empirical models includes lumped parameter models, generally predicting only average moisture content as a function of drying time.

The second group consists of slightly improved models that assume conductive heat transfer for energy and diffusive transport for moisture, solving a transient diffusion equation using experimentally determined effective diffusivity. Evaporation was included using a surface boundary condition in the heat equation. Evaporation inside the food domain is ignored, even though the temperature inside the food

reaches 80^{o}C. Lumping together all modes of water transport within the product as diffusion cannot be justified in all situations, especially when other phenomena, such as pressure-driven flow due to intensive heating or transport due to physicochemical changes in the porous medium, become important [51]. Also, the use of effective diffusivity does not yield insights into the prevalent transport mechanisms. These models might provide good matches with trial experimental results, but they cannot be generalized to other conditions. These types of models typically predict moisture content that varies with time and space and describe the physical transport of moisture within the material, giving results of more fundamental value than purely empirical models. However, for practical purposes, empirical models are simpler to develop than the diffusion models and, because of this they are comprehensively applied to the study of food drying [7].

Diffusion of liquid may not be the only mechanism responsible for moisture migration inside the food. It is evident that, during drying, significant water evaporation takes place inside the material as well as on the external surface of food [111, 125, 23]. The comparisons between the experiment and predicted water content show that, in some instances, an evaporation front in the drying model is valid to describe the diffusion mechanism, such as in bread [111] and bananas [125]. This third group of models, with a significantly improved formulation, compared with those of simple diffusion models, assumes a sharp moving boundary separating the dry and wet regions (e.g., deep-fat frying models [43]). This assumption is analogous to that made in freezing and thawing models of a pure material, where a sharp front separates the frozen and unfrozen regions. Such models have separated regions, such as core and crust with a moving boundary.

In contrast to sharp boundary models, distributed evaporation models assume that evaporation occurs over a zone rather than at an interface (for example see [84, 131, 135]). In a given situation, it is possible that the real evaporation zone is very narrow, closer to the sharp interface, and that a distributed evaporation formulation will in fact predict such a narrow evaporation zone. At a high rate of internal evaporation, significant pressure driven flow can be present for all phases and throughout the material. In this group, evaporation of water is considered as an intensive heating food process, such as deep-fat frying and drying, and has usually been modelled using an

equilibrium formulation, wherein liquid water present in the food is always assumed to be in equilibrium with water vapour present in the pore space ([84, 131, 135]). This is may not always be true, since water vapour is not always in equilibrium with liquid water. To overcome this problem, (for example [88, 53, 51]) an approach has recently been developed that uses an explicit formulation of the evaporation rate, known as a 'non-equilibrium' approach to frying and baking, based on the expression developed by Fang and Ward [42]. A non-equilibrium formulation that can also be used to enforce equilibrium constitutes a more general approach and appears to be the obvious alternative.

This study includes the development of a coupled transport mathematical model that is relevant to tropical fruits, in which all the parameters are based on existing data within the open literature. As with other research, the development of a comprehensive governing equation for drying has been hindered by the lack of accurate data for thermal and transport properties such as permeability, effective moisture diffusivity, bound water diffusivity and thermal conductivity. In this study, consideration is more restricted to that of tropical fruits and the available data. A direct comparison of predicted values with dedicated experiments is not possible at this time; the process of validation is based on literature data.

Close similarities between drying fruits and porous media has led us to a multidisciplinary cooperation in order to describe a physically based model of transport phenomena. Such a model takes into account the basic transport phenomena on the pore scale, where Darcy's Law for liquid transport is introduced alongside Fick's Law of moisture diffusion. Most fruit cells are dominated by a vacuole containing large amounts of dissolved sugars and organic acids, in addition to smaller amounts of other constituents, such as phenolic [86]. In plant tissue there is an extracellular space of gas canals for the transport of respiratory gases. Factors such as cell size and shape, the vacuolar composition, the size and shape of the extracellular gas space, as well as the properties of the cell wall and the cell membranes, probably have a bearing on the drying behavior. This is not reflected in the existing mathematical models of fruit drying, which are mainly based on a physical approach. However, an exception is an attempt to model the drying behavior of plant tissue considering four different compartments: vacuole, cytoplasm, cell wall, and extracellular space (Crapiste et al.

[28]). The latter authors developed a model in which the material is treated as cellular, incorporating knowledge of tissue structure. The model, which is based on a physical and chemical approach, is restricted to isothermal drying under conditions where cellular structure prevails. Several studies (e.g. [57, 114, 92]) represent the structure of fruit tissue using ellipse tessellation in developing a model to represent the liquid transport mechanism.

Previous studies using modelling approach of a food product provide a basic approach for this research. The model of Wang and Brenann [124] will be used initially in the model developed for heat and mass transfer that includes the shrinkage effect of liquid removal. This insight into the heat and mass transfer principle can then be used to develop more detailed models. The model was further developed by using Crapiste *et al.* [28] approach. The principle of transport of liquid water divides into two paths: through the cell or through the pores, where the food is now treated as porous media. In the cellular region, the assumption is made that separate consideration is needed for bound and free water. This distinction is clearly demonstrated in other material such as brick and wood [138, 6, 116, 110]. For this section of the study we restrict our model to non-shrinkage foods.

1.3 Drying models

In this section we identify different mathematical modelling techniques for the drying of food and we assess their merit. Initially we look at the movement of water. In many drying cases, heat also has a major effect in the movement of water and this is considered in details in later chapters.

Representative mathematical models of drying are identified, such as experiment based models (Empirical drying rate models)(e.g. [7, 106, 19, 120, 2]), models based on heat and mass transfer ([123, 8, 68, 59, 60, 141, 49, 65, 119, 61]), models based on porous media theory with an equilibrium approach ([28, 35, 131, 85, 23, 44, 39]) or a model based on a non-equilibrium approach ([53, 51, 88]. We will discuss different types of this mathematical modelling.

1.3.1 Experimental based modelling (Empirical model)

Generally, the development of experiment based models is mathematically and computationally easier. Simple empirical process modelling involves the varying of specific input setup parameters, such as temperature, relative humidity and air velocity provided to the experiment apparatus, and the measuring of output quantities by a data logging system (see illustration Figure 1.1). Correlations are derived to provide predictive capabilities; such an approach, however, makes this model system specific ([77, 106]). Appropriate statistically designed experiments offer a valid basis for developing an empirical model which can be used to derive correlations to approximate unknown functions from numerical data. Thus, the empirical models only consider average conditions of moisture content and temperature, which restricts their use for general predictions.

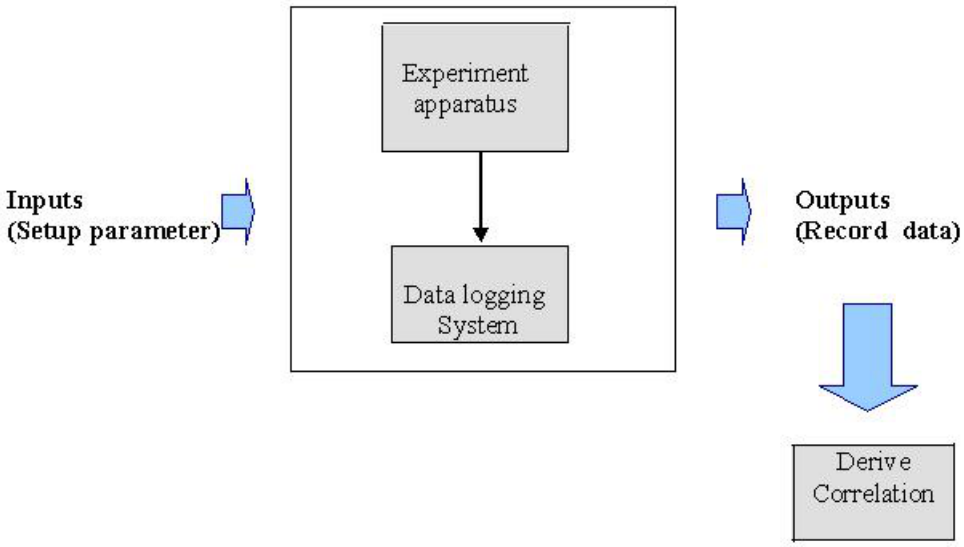

Figure 1.1: Empirical process modelling.

Experiment observations have become important for drying models in the food science literature. In this type of approach, an experiment is done in the laboratory to find a mathematical function to represent the data observed, based on different temperature and air velocity conditions. The limitations of this approach are as fol-

lows: the process of obtaining data from experiment is time consuming, it is difficult to obtain accurate measurements, different experiments may derive different equations, which makes the system too specific and only average moisture content can be measured using the experiment data [7, 106].

Numerous experimental studies have been carried out on the determination of drying kinetics for various food products [19, 120, 2, 118, 106]. In these cases, a set of measured experimental values are used directly to infer drying behaviour under specific conditions. Experimental studies relevant to the drying of fruits have been conducted on various food products such as avocado and banana [19], red chilli peppers, lemon grass and leech lemon leaves [120], potato slices [2], apple [118] and kiwi [106]. A large number of empirical and semi-empirical models have been introduced for specific foods such as Page, Newton (exponential) and Lewis model. Other models include Wang and Singh, Logarithmic, parabolic model as well as Henderson and Pabis, two-term exponential and modified Page. Details of these are provided by [2].

On measuring the drying moisture content $M(t)$ with time t, the drying curve of each experiment is obtained by plotting the decay of dimensionless moisture in the sample with the drying time, where M_0 is the initial moisture content and k is drying rate constant. The basic decay equation that is normally used is an assumed exponential model for the moisture ratio,

$$MR = \frac{M - M_e}{M_0 - M_e} = \exp(-kt). \tag{1.1}$$

The basic exponential model (equation (1.1)) is commonly based on the assumption of Fickian moisture migration, negligible shrinkage, constant diffusion coefficients and isothermal conditions.

Drying kinetic models have gained wide acceptance in the design of a new or simulate of an existing system and in describing the drying behavior of food materials [19, 2, 62]. However, these models although useful for individual practical proposes, fail to identify the general complexity of the drying processes. A more robust mathematical model for drying kinetics is normally based on physical mechanisms such as the effect of air temperature, air humidity and air velocity and characteristics of sample size (i.e multi-dimensional parameter space). For example, the empirical model found by Ceylan *et al.* [19], showed that the empirical drying model can give

good agreement of drying kinetics with different ranges of application, depending on the model selected. However, the drying kinetics discussed only take the average moisture content as a function of drying time. During the drying process, gradients of moisture content and temperature arise inside the material. Correspondingly, variations in moisture content as a function of both time and space exist within the drying material, but this is not included in empirical models, which may limit their application to drying. Furthermore, not only the average temperature and moisture content, but their distributions of temperature and moisture characterize the quality indicator during drying. For instance, in the case of food preservation, the growth of micro-organisms that can give rise to food poisoning needs to be prevented. This can only be achieved by studying safe moisture content on every location in the material and by using a mathematical modelling that involves simultaneous moisture and heat transfer under transient conditions, with variations in moisture content for both time and space. In the next section, we discuss and review some of single phase mathematical models that have been used in drying.

1.3.2 Single phase model of heat and mass transfer

Single phase heat and mass models have been widely used to describe the movement of water and heat during drying. The food is often modelled as a homogeneous medium. Lewis and Sherwood are known as pioneers in the development of mathematical drying models by the application of the Fourier equation of heat conduction to the drying of solids, using Fick's Law. Moisture transport involves two dependent processes: the evaporation of moisture at the solid surface that needs heat from the air and the internal diffusion of liquid to the surface.

The governing physical equations for simultaneous transfer of moisture $M(t)$ and temperature $T(t)$ in an isotropic food with no internal sources of moisture are given by the coupled pdes,

$$\frac{\partial M}{\partial t} = \nabla.(D\nabla M), \tag{1.2}$$

$$\rho c_p \frac{\partial T}{\partial t} = \nabla.(k\nabla T). \tag{1.3}$$

where D is diffusion coefficient, ρ is density, c_p is specific heat capacity and k is thermal conductivity. In the above, temperature is given from a standard heat conduction

formulation (see Carslaw and Jaeger [17]), where the conductive temperature flux $\mathbf{q} = -k\nabla T$. Equation (1.2) represents the moisture movement in the interior of the product during drying and equation (1.3) represents the temperature evolution in the interior of the product. In general, equations (1.2) and (1.3) may be limited by drying conditions at the surface of the food or internally: $D = D(M, T)$ and $k = k(M)$, such food proceeds through a glass transition phase. Glass transition temperature (T_g), can be defined as the temperature at which an amorphous system changes from a glassy to a rubbery state. At the beginning of drying, T_g is high because moisture content is high. During hot drying, moisture content decreases, leading to an increased in glass transition temperature. This phenomenon could be considered as directly related to the drying temperature during the process and particulary affected the diffusion coefficient of the food.

For a one-dimensional geometry with constant diffusivities D_{eff} and constant thermal diffusivity α, the simultaneous heat and moisture transfer problem with effective diffusion D_{eff} and conductivity k simplify to become

$$\frac{\partial M}{\partial t} = D_{eff}\frac{\partial^2 M}{\partial x^2}, \tag{1.4}$$

$$\frac{\partial T}{\partial t} = \alpha\frac{\partial^2 T}{\partial x^2}. \tag{1.5}$$

where $\alpha = k/\rho c_p$. A one-dimensional slab is defined by taking a region $-L(t) < x < L(t)$. Initial constant conditions are given by

$$M = M_0 \quad \text{and} \quad T = T_0 \quad \text{at} \quad t = 0. \tag{1.6}$$

A symmetry boundary condition is applied at the centre for equal drying from both slab surfaces:

$$\frac{\partial M}{\partial x} = 0 \quad \text{and} \quad \frac{\partial T}{\partial x} = 0 \quad \text{at} \quad x = 0. \tag{1.7}$$

Dependent on the drying conditions applied to the surface, two types of boundary conditions are typically used: equilibrium boundary conditions or flux boundary conditions. Equilibrium boundary conditions are given by

$$M = M_e \quad \text{and} \quad T = T_e \quad \text{at} \quad x = L(t). \tag{1.8}$$

with M_e and T_e are equilibrium moisture and temperature respectively. This is equivalent to the specific moisture and temperature applied at the surface.

Table 1.1: Average Moisture Diffusivity at 60^oC of fruits reported by different authors. Source Pavon *et al.*[90]

Product	Moisture Diffusivity (m^2/s)	References
Carrot	7.517×10^{-10}	Mulet [80]
Potato	2.553×10^{-10}	Mulet [80]
Grape	2.22×10^{-10}	Simal *et al.* [107]
Mango	8.56×10^{-10}	Hernandez *et al.* [56]
Cassava	4.93×10^{-10}	Hernandez *et al.* [56]
Apple	8.121×10^{-9}	Zogzas and Maroulis [142]

Flux boundary conditions are relevant in the absence of any moisture or temperature surface layer and correspond to transfer of external air flow, given by

$$D_{eff}\frac{\partial M}{\partial x} = -h_m(C_{sur} - C_{air}) \quad \text{at} \quad x = L(t), \tag{1.9}$$

$$\text{and} \qquad k\frac{\partial T}{\partial x} - \lambda D_{eff}\frac{\partial M}{\partial x} = -h(T_{sur} - T_{air}) \quad \text{at} \quad x = L(t). \tag{1.10}$$

In the above, h_m is moisture transfer coefficient, h a temperature transfer coefficient, C_{sur} is concentration of water at the surface, C_{air} is air concentration and λ latent heat of evaporation. All of these conditions are based on a bulk transfer model between the values at the surface of the food and external conditions. The external moisture and temperature are taken as M and T.

The effective diffusion coefficient D_{eff} is normally determined experimentally by the 'method of slope' approach that is widely used to estimate the effective diffusion coefficient. For example, this method was used by [106, 62, 70, 15, 82, 119, 61]. Experimental data of the effective diffusion coefficient (moisture diffusivity) of selected fruit are collated in Table 1.1 for later modelling purposes. The magnitude of the moisture diffusivity of food material is considerable and ranges from 10^{-13} to 10^{-7} m^2/s.

Experimental data of the average thermal conductivity (k) and specific heat (C_p) of selected fruits are collated in Table 1.2 below for later modelling purposes. It is assumed that the diffusivity is constant over the whole drying period. However,

Table 1.2: Average conductivity (k) and specific heat (C_p) and thermal conductivity α for foodstuffs reported by different authors.

Product	k (W/m K)	C_p(KJ/kg K)	$\alpha(m^2/s)$	References
Carrot	0.530	3.81-3.935		Singh [108]
Potato	0.554	3.517	1.70×10^{-5}	Singh [108]
Banana	0.475		1.18×10^{-5}	Singh [108]
Mango pulp	0.562	3.621	1.49×10^{-4}	Bon, *et al.* [13]
Apple	0.567	1.926-3.683		Feng *et al.*[44]

experimental studies also suggest that the physical processes are sometimes nonlinear and the transport properties inside the food are dependent on moisture content and temperature. Based on collected experiment data, it is suggested that the effective diffusion coefficient D_{eff} should be taken as varying with moisture, $D_{eff} = D(M)$, varying with temperature $D_{eff} = D(T)$ or varying with temperature and moisture $D_{eff} = D(T, M)$ during drying and leading to a more general model (see Crank [26]).

Moisture diffusivity is widely considered as a function of temperature, usually of an Arrehenius type dependence, which is reasonable on account of the increase in the molecular kinetic energy when temperature rises. Typically, the effective diffusivity, in this sense, is given by

$$\overline{D}(T) = D_0 \exp(\frac{-E_T}{RT}). \tag{1.11}$$

In the above, D_0=Arrhenius factor (m^2s^{-1}), E_T=Activation energy ($kJmol^{-1}$), T=Temperature (in Kelvin) and R=Gas constant ($kJmol^{-1}$). Values D_0 and E_T are usually estimated from experiment data (see for example [105, 70, 119, 61]). Example value of E_T is 39.4 $kJmol^{-1}$ for potato, 23.6 kJmol¹ for kiwi [105]. An example of this function was given by Simal *et al.* [106] as

$$\overline{D}(T) = 1.476 \times 10^{-5} \exp(\frac{-26950}{RT}), \tag{1.12}$$

with activation energy 26.950 KJ/mol.

A more extensive dependence on diffusivity is required to produce effects, such as glass transition, where diffusivity changes with local values of moisture and tempera-

ture. More generally, the effective diffusion coefficient may be taken as a function of process and involves a dependence on both material temperature and moisture content [55, 71, 20, 49]. The effective moisture diffusivity will be treated as a function of material moisture content and temperature, as suggested by Kiranoudis [71] and given by the following expression

$$\widetilde{D}(T, M) = K \exp(\frac{-E_T}{RT}) \exp(\frac{-E_M}{M}), \tag{1.13}$$

with E_M is parameter of the Arrhenius-type equation for moisture diffusivity expressing material moisture content dependence.

For example, based on the formula given by equation (1.13), Kiranoudis [71] developed a model for diffusivity ($D = \widetilde{D}(T, M)$) using optimal Bayesian estimation for potato given by

$$\widetilde{D}(T, M) = 1.29 \times 10^{-6} \exp(\frac{-2044}{T}) \exp(\frac{-0.0725}{M}). \tag{1.14}$$

The most common single phase modelling in foods involves one-dimensional heat and moisture transfer, equation (1.4) and (1.5) with empirical values of effective diffusivity such as that given by equation (1.11) or (1.13).

This method has been used by Hussain and Dincer [59], Kaya *et al.* [68], Zhou *et al.* [141], Wang and Brenann [123], Balaban and Pigott [8], Villa-Corrales *et al.* [119], Janjai *et al.*[61]. The use of finite-difference approach [59, 60, 68, 119] or finite element approach [141, 61] to compute the behaviour of the distribution of heat and mass transfer is widely adopted to solve the resulting equations. Difference between models depends mainly upon the assumptions about the surface, such as the use of equilibrium boundary conditions at the surface [106, 74, 94] or convective boundary conditions [59, 68].

Hussain and Dincer [59, 60] analyse two-dimensional heat and moisture transfer with convective boundary conditions at the surface. In this model, latent heat is not considered and gives an uncoupled model at the surface for isothermal conditions. The temperature increases rapidly compared to the change in moisture, which is not always the case: in the experiment findings by Pavon *et al.* [90] the surface food temperature of mango and cassava did not reach the air temperature instantaneously.

An additional result obtained by Kaya *et al.* [68], suggests the use of a variable convective heat (h) and mass transfer coefficient (h_m) during the drying period. Their

results show that the temperature gradient along the surface of the product is non-uniform because the heat transfer coefficient along the surface is non-uniform. They also found that moisture and temperature distribution inside the object are non-symmetrical compared to those observed for the constant convective heat and mass transfer coefficient. An interesting contribution of this paper is the local distribution of the convective mass transfer coefficient through the analogy between the thermal and concentration boundary layer numerically predicted using Fluent CFD package. However, the applicability of this model is restricted to that model and use of variable convective heat and mass transfer coefficients makes the model significantly more complex.

A more intensive and complex model is presented by Curcio *et al.* [31] and Curcio and Aversa [30], who analyse the simultaneous heat and mass transfer in both air and food for single food particles and one-dimensional, hot dry air flow. They state that the heat and mass transfer rate depends not only on temperature and concentration difference but also on the air velocity field, which strongly influences the transfer rate at the food-air interface. This gives the coupled boundary condition at the surface between the temperature and air velocity as well as concentration with air velocity. The model for food is the same as that used by Hussain and Dincer [59, 60] and includes latent heat effects at the surface; the model for overlying air has been modelled by the well-known $k - \varepsilon$ model. The model is solved by finite element method using COMSOL Multiphysics. It is observed that the air characteristics such as relative humidity and inlet velocity, influence drying performance. However, this model is very computationally intensive and some of the parameters involved need semi empirical transport equations, such as $k-\varepsilon$ turbulent kinetic energy and energy dissipation rate.

Overall, there are many advantages to using a single phase mass and heat model to capture the behaviour of heat and mass during drying for use in the development of enhanced food processing. Firstly, they are generally fairly simple and contain few parameters. It is also relatively straightforward to include changes in shape and size as a result of water removal and internal collapse during the drying process. In light of these benefits, we employ a mass and heat model assuming diffusion and conduction of moisture and temperature during drying in chapter 2 and extend the

model to include the effect of shrinkage in chapter 3. However, there are several disadvantages to this approach. Foods are not treated as distinct entities; foods with porous internal structure and those from more solid structures can differ. This causes difficulties when one attempts to incorporate sub-cellular features, such as the different pathways for the transport of water during drying: cell to cell and cell to intercellular space (void). Furthermore, single phase liquid diffusion may not be the only relevant mechanism inside the food during drying so, in the next section we look at other relevant mechanisms of transport used in drying.

1.3.3 Multiphase model using a porous media approach

In modelling the coupled heat and moisture transfer, internal water evaporation during drying may be significant and therefore simultaneous heat, water and vapour diffusion should be considered when simulating the drying processes [111]. Comparisons between experiment and predicted water content in the drying model in foods such as bread [111] and bananas [125] show the formation of an evaporation front. Other mechanisms for the transport of water during drying, such as pressure driven flow and capillary flow, link to the mechanism of drying with a porous media approach. The transport mechanisms of drying of porous media have been investigated by many research groups using experiments or simulations in a wide variety of physical applications.

The development of a mathematical model capable of predicting transport through porous media structure dates to 1856, when Darcy proposed a direct relationship between flow rate and applied pressure difference as

$$\boldsymbol{u}_i = -\frac{k}{\mu}\nabla P. \tag{1.15}$$

with k is permeability of the medium, μ is viscocity of the medium and ∇P pressure gradient vector. This has been widely adapted, together with modifications e.g. for unsteady flow in porous food (see Datta [34]). Fick's law of diffusion is used, along with Darcy's law, in the description of moisture movement in drying. Darcy's law, in its simplest form, expresses the proportionality between the average velocity of fluid flow and flow potential, comprising the pressure gradient through porous media [67].

In recent years, more comprehensive theories have been developed to describe the simultaneous heat and mass transfer processes on a microscopic scale, on the basis of diffusion theory, capillary flow theory, and evaporation condensation theory. In particular, increasing attention on heat and mass transfer in porous media has resulted in many experimental and theoretical investigations for different applications. Examples include approaches developed by Luikov [75] and Whittaker [126]. Luikov used thermodynamic theory of irreversible processes to describe the temperature, moisture, and pressure distribution within porous media during drying in a phenomenological manner. These studies have typically used mass and energy conservation equations with phenomenological relationships to describe water and vapour mass fluxes and heat flux within porous media. Whitaker introduced a volume averaging technique to formulate fluid flow and heat transfer in porous media as a continuum. Whittaker [126] presented a set of equations to describe the simultaneous heat, mass and momentum transfer of porous media. Based on traditional conservation laws, an important milestone in the development of drying theory, they incorporated all mechanisms for heat and mass transfer. The mechanisms were as follows: liquid flow due to capillary forces, vapour and gas flow due to convection and diffusion, internal evaporation of moisture and heat transfer by convection, diffusion and conduction. By using a formal volume averaging method, the microscopic differential equations were defined in terms of average field quantities. The rigorous study of the transition from an individual phase at the microscopic level to representative average volume at the macroscopic level provides a fundamental and convincing basis [32]. The advantage of Whitaker's model is that it offers a clear representation of the physical phenomena occurring in porous media during drying. However the problem encountered with the use of Whitaker's model is difficulty in determining parameters within a transport equation, such as effective diffusivity and permeability, which depend strongly on the material properties and structure. The volume averaging method has become a popular approach for theoretically modelling the drying of porous media, for example, Plumb [91], Colomba [37], Constant *et al.* [25], Nasrallah and Perre, [81], Quintard and Whitaker [93].

Luikov's equation and Whitaker's approach are usually used for non-hydroscopic material, such as sand, polymer particles and ceramics where the transport of material

does not cause additional complications and the phases are clearly separated. For food material, which is hydroscopic porous media, an equivalent porosity and equivalent water saturation have been introduced by researchers such as Yamsaengsung and Moreira [131], for frying of potato chips, Feng *et al.* [44] for drying of apple, Ni *et al.* [85], Datta and Ni [35] for microwave drying, Ousegui *et al.* [88], Zhang and Datta [134], Zhang *et al.* [135] and Dincov *et al.* [39] for bread baking.

The formulation of equations for hygroscopic porous media analogous to those equations well-established for non-hygroscopic porous media was developed in terms of drying of food using either Luikov or Whitaker's approach. Analogous to Whitaker's approach, the mass conservation equations for water vapour, liquid water, air and energy relevant to the drying of food based of porous media are presented in general terms of the mass conservation of three phases- vapour, water and air - as

$$\frac{\partial c_v}{\partial t} + \nabla.(\mathbf{n}_v) = \dot{I}, \tag{1.16}$$

$$\frac{\partial c_w}{\partial t} + \nabla.(\mathbf{n}_w) = -\dot{I}, \tag{1.17}$$

$$\frac{\partial c_a}{\partial t} + \nabla.(\mathbf{n}_a) = 0, \tag{1.18}$$

and overall conservation of energy as

$$\frac{\partial}{\partial t}(c_v h_v + c_w h_w c_s h_s) + \nabla.(\mathbf{n}_v h_v + \mathbf{n}_w h_w + \mathbf{n}_a h_a) = \nabla.(k_{eff}\nabla T) - \lambda\dot{I} + \boldsymbol{q}. \tag{1.19}$$

$\mathbf{n}_v$, $\mathbf{n}_w$, $\mathbf{n}_a$ represent the vapour, liquid water and air flux based on assumptions made by the researcher, c_v, c_w, c_a are concentrations of each phase that are transformed in terms of porosity and saturation, $\dot{I}$ is the rate of evaporation which represents the mass of liquid water that becomes vapour per unit volume, λ is latent heat and $\boldsymbol{q}$ is heat source. Fluid velocities in a multiphase porous medium are given by a generalized Darcy's law as

$$\mathbf{u}_w = -\frac{k_w}{\mu_w}\nabla(P - p_c), \tag{1.20}$$

$$\mathbf{u}_g = -\frac{k_g}{\mu_g}\nabla P, \tag{1.21}$$

k_w and k_g is permeability of the liquid phase and gas phase respectively, μ_w and μ_g is the viscosity of the liquid phase and gas phase respectively, $P - p_c$ is the difference between gas pressure and capillary pressure. Diffusive flux of vapour and air is

governed by Fick's Law as

$$\mathbf{j}_v = \rho_g D_v \nabla c_v = \mathbf{j}_a. \tag{1.22}$$

Total liquid water flux results from convective flow, due to the gradient in total gas pressure, and capillary flow, due to the gradient of capillary force, such as

$$\mathbf{n}_w = -\rho_w \mathbf{u}_w = -\rho_w \frac{k_w}{\mu_w} \nabla P - \rho_w \frac{k_w}{\mu_w} \nabla p_c. \tag{1.23}$$

Total flux of vapour $\mathbf{n}_v$ and air $\mathbf{n}_a$ are composed of convective flow and diffusion flux, such as

$$\mathbf{n}_v = \rho_v \mathbf{u}_v + \mathbf{j}_v = -\rho_v \frac{k_g}{\mu_g} \nabla P - \rho_v D_v \nabla c_v, \tag{1.24}$$

$$\mathbf{n}_a = \rho_a \mathbf{u}_a + \mathbf{j}_a = -\rho_a \frac{k_g}{\mu_g} \nabla P - \rho_a D_a \nabla c_a. \tag{1.25}$$

The formulation above covers the vast majority of food processing situations when interest is focussed on transport within the food tissues or the structure of food material. These formulations are generally quite similar to each other such as used by Yamsaengsung and Moreira [131], Ni *et al.* [85], Datta and Ni [35] for drying and frying. Nevertheless most of the drying models that describe the drying of foodstuffs are constructed on the basics of theories commonly used with conventional porous materials and without acknowledging the features that makes this particular problem unusual [28]. An assumption made of most multiphase porous media, between all of the phases at any location, concerns thermal equilibrium, with only one temperature for any given location. Furthermore, transport mechanisms such as the effect of temperature on the diffusion coefficient, are generally considered small, and seldom used and shrinkage is generally ignored.

Perhaps the earliest model in food that utilized Darcy's flow was that of Farkas *et al.* [43], which included pressure driven flow. A two region detailed model was developed - core and crust - providing different sets of equations for these two regions, separated by a moving boundary and showing differences in temperature between them. The physical assumption was made that water flow took place within the core region and that water vapor movement was pressure-driven only in the crust region. Diffusion flow in the crust region and pressure driven flow in the core region were ignored, which is a limitation of the model. Halder *et al.* [52], reviewing the hypothesis of this model, stated that, by neglecting the vapor flux in the core and

the liquid flux in the crust, mathematical complications were reduced but important physics sacrificed. A limitation of the sharp boundary model is that it ignores the presence of air/pores inside the food domain. As we can see from food structure, the cell is surrounded by intercellular space (air). It is assumed that vapour pressure drives the flow of vapour towards the surface so that the crust region develops and the moving boundary separates these two regions. But, as evaporation takes place, the vapour was produced then expels the air and occupies its space. Although Farkas' model was able to include the structure of the food, it failed to model or capture the interaction between the two-phase regions, only the moving boundary that separated the two-regions.

Ni and Datta [84] extend the model by Farkas by adding the oil phase conservation equation, with the introduction of equivalent porosity and equivalent water saturation. They added capillary flow in liquid water transport and diffusive flow in vapour transport, which are not considered in Farkas' model. They considered only one region with three-phases in continuum: the liquid phase combination of equation of vapour and water in term of one equation of the liquid phase, the air phase and the oil phase. The conservation equations for vapour, liquid water, air and energy are written as above (equation (1.16) - (1.19)), and the conservation equation is transformed into variable saturation S_w, temperature T and pressure P as in the Luikov approach. Because the evaporation rate is unknown, equations (1.16) and (1.17) are combined to form a total moisture equation. Subsequently, this model was used by Ni *et al.* [85] for intensive microwave heating, using a one region model with two phase in continuum: a liquid phase (water and vapour) and an air phase. Others who followed the same approach but made different assumptions include Yamsaengsung and Moreira [131] who included shrinkage, Feng *et al.* [44] who introduced the migration of bound water, Chua *et al.* [23], Zhang and Datta [134], Zhang *et al.*[135] and Dincov *et al.* [39].

The main advantage of the model discussed above is that, compared to the empirical and single phase models, they can include precise modelling of the different phases. However, further investigation using the initial form of the model report serious numerical difficulties, such as converging to the solution. According to experiments by Halder *et al.* [50], using porosimetry and bioimpedance analyses of potato

tissue, most water is not in the pores but in the cell, so the use of equivalent water saturation analogous to porous media is not appropriate.

Furthermore, they assumed that liquid water and water vapour is in equilibrium. This is because the evaporation rate is unknown; Measurement of the evaporation rate is difficult and the parameters are not available from experiment. The assumption that the evaporation rate is unknown leads to $\dot{I}$ being eliminated in the governing equation, based on a combination of liquid water and water vapour equations, to form one liquid phase equation. The evaporation rate in the energy equation used the equilibrium formulation of evaporation common in the literature $p_v = p_{equi}$, where vapour is always in equilibrium with water. The use of evaporation rate $\dot{I}$ maybe inappropriate, as this term is eliminated in the governing equation of liquid phase. It is more relevant to divide the region into the liquid phase (containing free water and bound water) and the air phase (containing water vapour and air) and then to derive an equation similar to the evaporation rate relevant to the experiment findings (e.g. see [57, 50]), involving cell to cell transport because of pressure difference ([86]), and cell to pore transport.

Thus, an improved model was suggested that would replace the instantaneous phase change of liquid to vapour by introducing an evaporation rate term equation and using non-equilibrium approach derive from an expression by Fang and Ward [42]. Since water vapour is not always in equilibrium with liquid water, Ousegui *et al.* [88] and Halder *et al.* [53, 54, 51], developed a multiphase model using a non-equilibrium formulation for evaporation, which is the latest mathematical modelling for drying and frying. The non-equilibrium approach leads to an explicit formulation of $\dot{I}$, such as [53],

$$\dot{I} = K.(\rho_{v,equi} - \rho_v), \tag{1.26}$$

K is a parameter signifying the constant rate of evaporation, ρ_v is a vapour density at the location and $\rho_{v,equi}$ is the equilibrium vapour pressure of pure water. In recent years, Ousegui *et al.* [88] have simulated the baking process of bread using this formulation and Halder *et al.* [51] have applied this model to the drying of more general of hydroscopic food material.

All the models discussed above developed a formulation analogous to those equations well-established for non-hygroscopic porous media but do not reflect the com-

plexity of cellular structure in their modelling. Structure heterogeneity of biological material, such as fruit, brings additional complexity to the water migration in a porous solid system. The cellular fruit tissues are multiphase systems and water can migrate out of the cell in three possible ways: transmembrane transport, symplastic transport and apoplastic transport.

Wood *et al.* [127] identify a multiscale model to include mass transfer in cellular systems by a complex multiphase process involving diffusion within the cell and diffusion across cell wall/ cell membranes. In a series of publications, Wood and Whittaker [128], study cellular scale structure equations describing transport and phase concentration in an extracellular phase and intercellular phase, including enzyme mediated intercellular reaction.

An interesting study regarding cellular material is made by Crapiste *et al.* [28]. In this work, the author applied Whitaker's model to investigate the drying of cellular materials for isothermal drying with the influence of shrinkage. They recognize the complex cellular structure and consider four phases: vacuole, cytoplasm, cell wall and intercellular space and develop a model of multiphase systems that considers the different mechanisms of water transport. It was shown that the water transport during drying occurs by the contribution of three main fluxes: diffusive water vapour flow through the intercellular air space (intercellular space), capillary flux of water through cell walls (wall to wall), and flux of liquid water through the vacuoles, the cytoplasm and the cell membranes (cell to cell). It was shown that water transport during drying occurs by the contribution of these three fluxes, and an equation for the fluxes was developed. The initial 'conceptual' model lead to a volume average equation comprising coupled diffusion and reaction equation containing effective parameters quantifying the sub-cellular geometries, kinematic reaction parameters and diffusivity. This will be more relevant than the development of a formulation analogous to those equations well-established for non-hygroscopic porous media such as discussed in Whitaker's approach. However, taking a microscale continuum equation to the macroscale is a formidable task. The approach taken to date proposes a macroscale continuum approach.

As discussed above, for accurate prediction of temperature and moisture content in cellular tissue during drying, it is important to understand the various pathways

along which water can move during drying, which are characterized by the structure of cellular tissue. Halder *et al.* [50], in a recent experimental study, investigated the water transport of cellular tissue and stated that the pathways for water transport during drying are extracellular pathways (pores) and intercellular pathways (cell). When drying at lower temperatures, the pathways of moisture transport are through intracellular cells but if drying at higher temperature, pathways of water are through intercellular pores. This study concluded that the different pathways for the transport of water during drying exist.

An understanding of cell structure to describe material behaviour helps to understand the physics for the purpose of modelling. The relationship between macroscopic representative properties and microscopic features is important for the development of the representative continuum model approach. The structure of many hydroscopic materials, such as food products, is basically an array of cells (Chen and Pei [21]). It is recognized that, although the cell structure maybe very similar in nature, the composite tissue may differ widely in porosity. The intercellular space, like void space in a porous material, is interconnected and filled with air and free water; the cells themselves also contain bound water. Xiong *et al.* [129] define bound water as water molecules that are strongly connected to the material molecules and free water as loosely connected to the material molecules. The conversion between these two forms of water molecule, modelled as a reversible reaction may be an important part of modelling, particularly within the later stage of drying.

The multiphase approach offers an advantage over the traditional single phase approach when a number of different interacting fluid phases are present. A multiphase formulation naturally lends itself to modelling of the drying process and has been used by many authors. The approach detailed in this section will be developed for a drying model and presented in Chapter 4.

1.4 Thesis Objectives

The objectives of this research are

(1) To investigate transport phenomena during the thermal processing of slab fruit products, considering fruit to be a homogenous mixture. The effect of thickness

change is also investigated. This objective will be accomplished by developing a one-dimensional mathematical model and associated numerical scheme. The computer simulation will be based on a process model that takes into account the food values relevant to tropical fruits. Comparison will be made with existing macro-scale models and available experimental studies.

(2) Based on a process model, to develop an enhanced model between the macrostructure of porous material and microscopic drying behaviour by using the cell level structure of fruits. The transport phenomena will be developed that are based on the heterogenous properties of tropical fruits for both isothermal and non-isothermal conditions. Numerical solutions and cases will be considered using COMSOL.

(3) To investigation the influence of material properties, such as permeability and diffusivity on the drying process on a macroscopic scale by varying their values numerically.

(4) Comparing the drying simulation with data reported from the literature.

1.5 Thesis outline

This chapter explains the reason for conducting this research, the main characteristics of the drying model and gives examples of the major approaches to drying. It also describes several important aspects in the development of the drying model and states the aim of this research, which is to developed a new approach. It concludes with a brief description of the thesis results and their significance.

This thesis has four main parts: an introduction to modelling food drying of fruits and a literature review about drying; the development of a homogeneous model on a process level, using heat and mass transfer; the development of a more physical based model, using a porous media approach and the presentation and discussion of the results, including validation of the model. Figure 1.2 shows a schematic overview of the thesis.

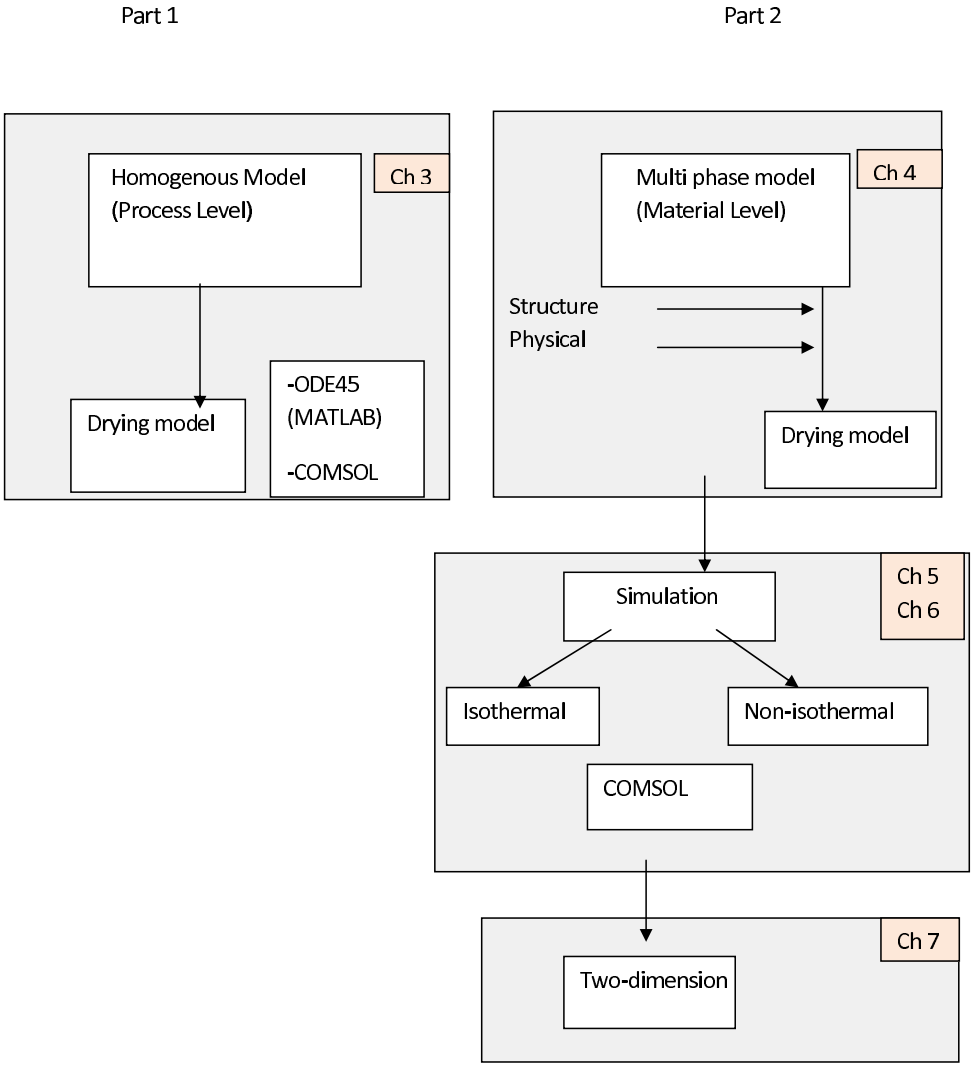

Figure 1.2: A schematic overview of the thesis.

- Chapter one explains the current approach to developing a drying model in which more attention is given to fruit drying. It begins with a description of the general approach used in designing a drying model and is followed by a discussion of the physical process employed in designing the drying model. The important part of this chapter is a review of the historical development of drying models and their application. Examples of several drying models for

approximate distribution of moisture and temperature are also presented. The discussion of the results on drying from past research groups is reviewed.

- The homogenous model in this project is based on the work of Wang and Brenann [122], as discussed in chapters two and three. A heat and mass transfer model, including the effect of shrinkage for homogenous food, is derived. The shrinkage effect is derived and solved numerically by transforming the governing equation of heat and mass transfer to a changing coordinate system. Outcomes of this model include analysis and comparison with existing data.

- The development of a multiphase model is discussed in chapter four. This chapter consists of two sections. The first part of this chapter briefly reviews the properties of food structure. In the second part, the mathematical formulation of the drying processes of fruit incorporates the heterogeneous properties of tissues and complex cellular structure is recognized and simplified to a representative physical model. Based on these basic concepts of cellular structure, a representative macrostructure model for the multiphase transport of water relevant to tropical fruits is developed. This model takes into account diffusion through cellular membranes and diffusion and convection through intercellular spaces, based on the microstructural properties of the fruit tissue.

- The results of the numerical simulation for multiphase drying are presented in chapters five and chapter six. The results are divided into a corresponding isothermal model and non-isothermal model. For each model, the influence of bound water is evaluated in order to establish its influence on drying behaviour. Comparison is made between these two models. A parametric study is conducted to verify the models' properties, using data from the open literature.

- In chapter seven, the two-dimensional multiphase model for drying under non-isothermal conditions is presented, corresponding to the model developed in chapter four.

- In chapter eight, the final conclusions and recommendations for further research are presented.

Chapter 2

Single phase moisture and heat model of drying food

2.1 Overview

We formulate and analyse a mathematical model applicable to tropical fruits and the system introduced in section §1.3.2. As a first approximation, we employ a simple one-dimensional and two-dimensional model of heat and mass transfer that assumes fruits as a homogenous structure, as discussed by Wang and Brenann [123], Balaban and Pigoet [8]. In this model, we do not consider changes in dimension, such as changes of thickness, length and width.

The model combines the principle of mass balance with heat balance for movement of moisture and heat. We use this model to study two different situations. In the first model, we consider an isothermal condition with negligible latent heat, which gives uncoupled boundary condition to the governing equation at the surface. In this situation, the temperature of fruit increases rapidly compared to the change in moisture, so the equation for moisture was solved without the heat equation. In the second model, we considered the effect of latent heat term $\overline{\lambda}$ which is especially important at the fruit-air interface, where evaporation occurs. Numerical solutions are presented corresponding to one-dimensional and two-dimensional fruit tissues with constant diffusivity and diffusivity dependent on temperature and moisture.

2.2 Mathematical formulation of one-dimensional moisture and heat models

In this section we formulate the general heat and mass transfer formulation to develop a simple model of distribution of moisture and heat during the drying of fruits. The physical problem involves a single slice of food of thickness $2L$, initially at a uniform temperature T_0 and a uniform moisture content M_0. Drying is taken as effective only at the surfaces $x = \pm L$. The surface of the drying body is in contact with drying air, providing a convective boundary condition for moisture content M, and constant air temperature T_{air}. The problem considered is symmetric relative to the midplane of the food slice, as shown in Figure 2.1.

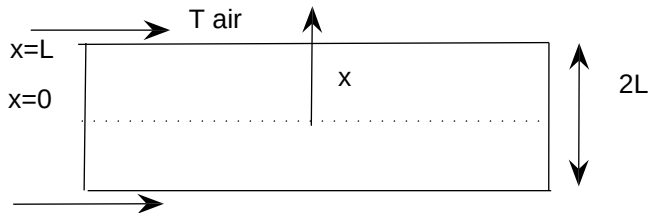

Figure 2.1: Schematic of one-dimensional model of food drying process

During drying, heat is transferred mainly by convection from air to the product surface and by conduction from the surface towards the product centre. Meanwhile, moisture diffuses outwards towards the surface and is vaporized into the air. Such a coupled mechanism provides the basis for a simultaneous heat and moisture transfer model. In the case of a slab of infinite length, the moisture content $M(x,t)$ across the slab and unsteady temperature $T(x,t)$ are expressed by the well known system of partial differential equations (PDEs) for moisture and energy transport [124],

$$\rho_s \frac{\partial M}{\partial t} = \frac{\partial}{\partial x}(D\rho_s \frac{\partial M}{\partial x}) \; ; \quad 0 < x < L(t), \tag{2.1}$$

$$\rho_s C_p \frac{\partial T}{\partial t} = \frac{\partial}{\partial x}(k\frac{\partial T}{\partial x}) \quad ; \quad 0 < x < L(t). \tag{2.2}$$

with D is diffusion coefficient, ρ_s is solid density, c_p is specific heat capacity and k is thermal conductivity. Due to symmetry, the solution is sought from the centre line at $x = 0$ to the surface $x = L(t)$. Taking constant thermal diffusivity $\alpha = \dfrac{k}{\rho_s C_p}$ and

constant diffusion coefficient $D = D_0$, equations (2.1) and (2.2) gives

$$\frac{\partial M}{\partial t} = D_0 \frac{\partial^2 M}{\partial x^2} \; ; \; 0 < x < L(t), \tag{2.3}$$

$$\frac{\partial T}{\partial t} = \alpha \frac{\partial^2 T}{\partial x^2} \quad ; \; 0 < x < L(t). \tag{2.4}$$

A generalization of the above general approach is to take diffusivity dependent on temperature [123, 8]. Taking diffusivity dependent on temperature $D = \overline{D}(T)$ equation (2.1) becomes

$$\frac{\partial M}{\partial t} = \overline{D} \frac{\partial^2 M}{\partial x^2} + \frac{\partial M}{\partial x} \frac{\partial T}{\partial x} \overline{D}^{'}, \tag{2.5}$$

where $\overline{D}^{'} = \dfrac{d\overline{D}}{dT}$.

Taking Diffusivity dependent on moisture and temperature $D = \widetilde{D}(T, M)$ equation (2.1) becomes

$$\frac{\partial M}{\partial t} = \widetilde{D} \frac{\partial^2 M}{\partial x^2} + \widetilde{D}^{'}_{T} \frac{\partial M}{\partial x} \frac{\partial T}{\partial x} + \widetilde{D}^{'}_{M} (\frac{\partial M}{\partial x})^2, \tag{2.6}$$

where $\widetilde{D}^{'}_{T} = \dfrac{\partial \widetilde{D}}{\partial T}$ and $\widetilde{D}^{'}_{M} = \dfrac{\partial \widetilde{D}}{\partial M}$.

The values of diffusivity $\overline{D}(T)$ and $\widetilde{D}(T, M)$ are discussed in section §1.3.2. At the onset of the drying process, the moisture content, temperature and the thickness of the product are taken as uniform; initial conditions are thus

$$M = M_0, \quad T = T_0, \quad L = L_0 \quad \text{at} \quad t = 0. \tag{2.7}$$

Imposing symmetry, there are no temperature and moisture concentration gradients at the centre of the product, and so the following conditions hold:

$$\frac{\partial M}{\partial x} = 0 \quad \text{and} \quad \frac{\partial T}{\partial x} = 0, \quad \text{at} \quad x = 0. \tag{2.8}$$

Heat transfer at the surface boundary occurs by convection to the dry overlying air, typically modelled through the use of a heat transfer coefficient h. Some heat is also absorbed by the moisture in transferring to a vapour phase, and the boundary condition at the surface is given by,

$$k \frac{\partial T}{\partial x} - \lambda D_0 \, \rho_s \frac{\partial M}{\partial x} = -h(T_{sur} - T_{air}) \quad \text{at} \quad x = L(t). \tag{2.9}$$

where λ is the heat of vaporization (latent heat).

In developing a drying boundary condition for moisture at the surface, we need to consider a driving gradient from the surface to the air that involves partial pressure and temperature at the surface. The driving force for the flux water vapour from the wetted surface to the air is the difference between the moisture content in the air, C_{air} and the water content in the form of liquid water film at the surface C_{sur} [41]. In this case, the boundary condition at the surface becomes

$$-D_0\rho_s\frac{\partial M}{\partial x} = h_m(C_{sur} - C_{air}), \quad \text{at} \quad x = L(t). \tag{2.10}$$

2.3 One-dimensional model: case study

The fruit sample is a hygroscopic porous media, yet it is assumed to be a fictitious continuum. Weak internal evaporation and transport of vapour within the dehydrated fruits towards the external food surface have not being considered. In the first instance, we consider models with no shrinkage ($x = L_0$) associated with isothermal diffusion and constant moisture diffusivity ($D = D_0$) and heat diffusivity $k = k_0$ with constant initial moisture level $M = M_0$ and $T = T_0$. In this simplest case we solve equations (2.3) and (2.4), together with boundary conditions (2.7) - (2.10). In this model the moisture is removed from the fruit when the air temperature $T_{air} > T_0$ gives a surface temperature of food T_{sur} to generate a moisture gradient from the evaporation of moisture at the external surface. Governing equations become

$$\frac{\partial M}{\partial t} = D_0\frac{\partial^2 M}{\partial x^2} \; ; \; 0 < x < L_0, \tag{2.11}$$

$$\frac{\partial T}{\partial t} = \alpha_0\frac{\partial^2 T}{\partial x^2} \quad ; \; 0 < x < L_0. \tag{2.12}$$

Boundary conditions are

$$\frac{\partial M}{\partial x} = 0 \quad \text{and} \quad \frac{\partial T}{\partial x} = 0, \quad \text{at} \quad x = 0. \tag{2.13}$$

$$\text{and} \quad -D_0\rho_s\frac{\partial M}{\partial x} = h_m(C_{sur} - C_{air}), \quad \text{at} \quad x = L_0, \tag{2.14}$$

$$k\frac{\partial T}{\partial x} - \lambda\rho_s D_0\frac{\partial M}{\partial x} = -h(T_{sur} - T_{air}), \quad \text{at} \quad x = L_0, \tag{2.15}$$

where λ is the heat of vaporization.

Taking non-dimensional variables

$$\overline{M} = \frac{M}{M_0}, \quad \overline{T} = \frac{T - T_0}{T_{air} - T_0}, \quad \tau = \frac{D_0 t}{L_0^2} \quad \text{and} \quad \xi = \frac{x}{L_0}, \tag{2.16}$$

we obtain governing diffusion and heat equations as

$$\frac{\partial \overline{M}}{\partial \tau} = \frac{\partial^2 \overline{M}}{\partial \xi^2}, \quad \text{and} \quad \frac{\partial \overline{T}}{\partial \tau} = Le \frac{\partial^2 \overline{T}}{\partial \xi^2}. \tag{2.17}$$

Initial conditions become $\overline{M} = 1$, and $\overline{T} = 0$, at $\tau = 0$ and boundary conditions

$$\xi = 0: \quad \left(\frac{\partial \overline{T}}{\partial \xi}\right) = 0, \quad \text{and} \left(\frac{\partial \overline{M}}{\partial \xi}\right) = 0, \tag{2.18}$$

and at ξ=1:

$$\frac{\partial \overline{M}}{\partial \xi} = -Sh \left(\overline{C}_{sur} - 1\right), \tag{2.19}$$

$$\frac{\partial \overline{T}}{\partial \xi} = -Nu \left(\overline{T}_{sur} - 1\right) + \overline{\lambda} \frac{1}{Le} \frac{\partial \overline{M}}{\partial \xi}. \tag{2.20}$$

Several non-dimensional groups are defined as:
$Sh = \frac{h_m L_0}{D_0 M_0} \frac{C_{air}}{\rho_s}$, $\overline{C}_{sur} = \frac{C_{sur}}{C_{air}}$, $Nu = \frac{hL_0}{k}$, $Le = \frac{\alpha}{D_0}$, and $\overline{\lambda} = \frac{\lambda}{C_p} \frac{M_0}{(T_{air} - T_0)}$.

Condition (2.19) links the surface condition directly to the surface temperature and incorporates surface water concentrations under local psychrometric conditions. In dynamic studies of water movement through porous materials, researchers customarily use the partial water vapour pressure, measured in Pascal, as a concentration. The relationship between vapour pressure and concentrations of water vapour in the air is defined in any gas as

$$C_{air} = 2.1667 \times 10^{-3} \times \frac{P_\nu(T_{air})}{T_{air} + 273.16}. \tag{2.21}$$

During drying, the temperature of drying air is typically constant and the relative humidity (RH) of drying air is fixed. Practically, the partial pressure of air is unchanged so the concentration of drying air is unchanged throughout drying. Thus the C_{air} is given by

$$C_{air} = 2.1667 \times 10^{-3} \times \frac{RH}{100} \times \frac{P_{\nu s}(T_{air})}{T_{air} + 273.16}. \tag{2.22}$$

The relation $P_{\nu s}(T_{air})$ is defined by [89] as

$$P_{\nu s}(T_{air}) = 610.78 \exp\left(\frac{17.2694 T_{air}}{T_{air} + 238.3}\right). \tag{2.23}$$

For example, water vapour concentration in air with temperature 60^{o}C and RH=20%, using the definition above, C_{air}=0.025169 kg/m^3.

Thermodynamic equilibrium relationship between water concentrations in the air and water concentrations on the external surface of food has been used to calculate C_{sur}. The relationship between water vapour pressure and concentrations of water vapour at the surface, involving the surface concentration C_{sur} and surface temperature T_{sur}(in ^{o} Kelvin) are linked (see Wang and Brenann [124]). We take

$$C_{sur} = 2.1667 \, \frac{P_\nu(T_{sur})}{T_{sur}}. \tag{2.24}$$

Partial pressure of water vapour P_ν is determined using the water activity relationship

$$a_w = \frac{P_\nu}{P_{\nu s}}. \tag{2.25}$$

A relationship between a_w and the moisture content M is given by Wang and Brenann [123] as

$$M = 0.062 \left(\frac{a_w}{1 - a_w} \right)^{0.42}. \tag{2.26}$$

This gives,

$$\frac{C_{sur}}{C_{air}} = f(M) \times \frac{P_{\nu s}(T_{sur})}{T_{sur}}, \tag{2.27}$$

with

$$f(M) = \sigma \frac{M^{2.38}}{0.062^{2.38} + M^{2.38}}, \tag{2.28}$$

with $\sigma = \dfrac{2.1667}{C_{air}}$.

Water activity is a distinctive parameter for each type of food that, as a function of its own structure, determines the strength of the bond between food and water. According to the literature, the mathematical representation of these isotherms could be considered using numerous relationships, as outlined by Mujumdar [79]. To estimate the relationship between a_w with moisture at the surface known as moisture isotherm, more equations experimentally obtained from the literature (for example [105, 8, 56]) can be used. Unfortunately, time constraints prevented us from using these other equations. Further, $P_{\nu s}$ can be expressed as a function of the surface temperature T_{sur} (in ^{o}Kelvin) [16], and used by [8, 124] and given by

$$P_{\nu s}(T_{sur}) = \exp\left(A - \frac{B}{T_{sur}} - C \, \ln T_{sur} \right). \tag{2.29}$$

Experimental results suggest typical dimensional values for $A = 53.33$, $B = 6834.27$ and $C = 5.169$ [123]. These values A, B and C are in dimensional form. In non-dimensional form

$$\overline{\beta}(\overline{T}_{sur}) = \frac{P_{\nu s}(T_{sur})}{T_{sur}} = \overline{A}\,\overline{T}_{sur}^{2} + \overline{B}\,\overline{T}_{sur} + \overline{C}, \tag{2.30}$$

with $\overline{A} = 0.0364$, $\overline{B} = 0.0108$ and $\overline{C} = 0.0119$ for initial temperature $T_0 = 25$ and air temperature $T_{air} = 60^o$C. The values of $\overline{A}$, $\overline{B}$ and $\overline{C}$ will depend on the values of the initial temperature and the air temperature.

Surface boundary condition, equation (2.19) becomes

$$\frac{\partial \overline{M}}{\partial \xi} = -Sh\,\left(\overline{\beta}(\overline{T}_{sur})\, f(\overline{M}) - 1\right), \tag{2.31}$$

$\overline{\beta}(\overline{T}_{sur})$ defined by equation (2.30) and $f(\overline{M})$ is defined by

$$f(\overline{M}) = \frac{\sigma \overline{M}^{\zeta}}{\varphi^{\zeta} + \overline{M}^{\zeta}}. \tag{2.32}$$

The value of $\sigma = \dfrac{2.1667}{C_{air}}$, $\varphi = \dfrac{0.062}{M_0}$ and $\zeta = 2.38$. The value of C_{air} will depend on the temperature of air and given by equation (2.22). For the temperature of air $T_{air} = 60^o$C and RH=20%, σ= 84.55.

2.3.1 Numerical solution

The COMSOL Multiphysics program is used to stimulate the dehydration process in the drying system, which corresponds to the numerical solution of these model equations. The above system of non linear partial differential equations, together with the described set of initial and boundary conditions, has been solved by Finite Element Method implementation by COMSOL Multiphysics 3.4. We fix the geometry of the model, fix the boundary setting, the mesh parameters and compute the final solution. The domains in the food were discretized into a total number of 320 elements. The time-dependent problem was solved by an implicit time-stepping scheme, leading to a non linear system equation for each time step. Newton's method was used to solve each non-linear system of equations, whereas a direct linear system solver (UMFPACK) was adopted to solve the resulting systems of linear equations. The relative and absolute tolerance were set to 0.001 and 0.0001, respectively. Equations

(2.17) were input into COMSOL Multiphysics (PDE) solver with the general form for moisture content and temperature. The details of the numerical procedure can be found in Appendix A.

2.3.2 Input Parameters

The input parameters used in this drying simulation is given by Table 2.1 for the generic drying conditions for tropical food.

Table 2.1: Input parameters used in the simulations of drying of tropical fruits.

Parameter and Symbol	Range of value	Units and sources
Density of water (ρ_w)	1000	kg/m^3
Density of solid (ρ_s)	1080	kg/m^3
Diffusivity (D_0)	$8.56 \times 10^{-10} - 8.121 \times 10^{-9}$	m/s [56]
Length (L_0)	$10^{-3} - 10^{-4}$	m
Mass transfer coefficient (h_m)	$8 \times 10^{-3} - 4 \times 10^{-4}$	m/s [10]
Heat transfer coefficient (h)	20-250	W/m^2 K [59]
Thermal conductivity (k)	0.475-0.567	W/m K (Table 1.2)
Thermal diffusivity (α)	1.31×10^{-7}	m^2/s [59]
Heat capacity (C_p)	1.9-3.683	kJ/kg K [44]
Latent heat evaporation (λ)	2.345×10^3	kJ/kg [33]

Based on input parameter above, the following reference non-dimension parameter was obtained, given by Table 2.2.

Table 2.2: Drying conditions and product properties used in the simulation.

Parameter	Properties
C_{air}	0.025625 kg/m^3 based on T_{air}=60^{o}C and RH=20%
M_0	0.8 kg water/kg moist sample
Sh	20
Le	5
Nu	0.3
$\overline{\lambda}$	0.5

2.3.3 Isothermal solution

Negligible latent heat ($\overline{\lambda} = 0$)

We pause to remark here that, in view of non-dimensionalisation $\tau = \dfrac{D_0 t}{L_0^2}$, the timescale of interest is the time taken for moisture to be diffused to the surface along the thickness of the fruits. The diffusion coefficient of moisture D_0 is given for the fruits around 10^{-9} m/s and for fruits with thickness of 5-10 mm (0.005-0.01 m). If the drying time to obtain equilibrium is taken as 15000-36000 seconds [40] for the drying of a mango slice is given a time scale of approximation 0.36-1.44. We also take the same timescale for temperature, but equation (2.33) shows that heat transfer by conduction is Le times the mass transfer by diffusion. From the values in Table 2.1, the the value for Le is around 10-100. This is very short compared with the timescale for moisture, which means that the air drying temperature is 10-100 times faster than the time needed to reach the equilibrium moisture.

In this section, the formulation presented in section §2.3 is simplified by assuming that temperature increases rapidly compared to the changes in moisture. For cases, in which $\overline{\lambda}$ is small, then the governing equation for temperature is uncoupled with the governing equation for moisture to give

$$\frac{\partial \overline{T}}{\partial \tau} = Le \frac{\partial^2 \overline{T}}{\partial \xi^2}, \quad 0 < \xi < 1, \tag{2.33}$$

$$\frac{\partial \overline{T}}{\partial \xi} = 0, \quad \text{at} \quad \xi = 0, \tag{2.34}$$

$$\text{and} \quad \frac{\partial \overline{T}}{\partial \xi} = Nu(\overline{T} - 1), \quad \text{at} \quad \xi = 1. \tag{2.35}$$

with initial $\overline{T} = 0$.

Solutions can be readily obtained analytically as analogous to classic diffusion with surface evaporation (see Crank page 60 [26] and Carslaw and Jaeger page 122 [17]). The solution can be written as an infinite series as

$$\overline{T} = \frac{T - T_0}{T_{air} - T_0} = 1 - \sum_{n=1}^{\infty} \frac{2\,Nu \times\ cos(\beta_n \xi) \exp(-{\beta_n}^2 \tau)}{(\beta_n^2\ +\ Nu^2\ +\ Nu)\, cos(\beta_n)}. \tag{2.36}$$

where the β_ns are the positive roots of $\beta\, tan\, \beta = Nu$ and $Nu = \dfrac{hL_0}{D_0}$ a non-dimension parameter.
The steady state temperature corresponds to $\dfrac{\partial \overline{T}}{\partial \tau} \longrightarrow 0$, giving $\dfrac{\partial \overline{T}}{\partial \tau} = 0$ and $\overline{T} \longrightarrow 1$. The total amount of heat of drying is given by

$$T_{total} = \int_0^{\tau} \frac{\partial \overline{T}}{\partial \tau}\, d\tau. \tag{2.37}$$

This is equivalent to Crank ([26] page 60 equation 4.53). The time scale for temperature changes is by $\mathrm{O}(\tau^{\frac{1}{2}})$ and hence $\tau >> 1$ then $\overline{T} \longrightarrow 1$ rapidly compared to change in moisture. In this limit, the boundary conditions for the moisture can be approximated by $\overline{\beta}(\overline{T}) = \overline{\beta}(\overline{T} = 1) = \overline{\beta}_1$ and the moisture obtained from the simple equation

$$\frac{\partial \overline{M}}{\partial \tau} = \frac{\partial^2 \overline{M}}{\partial \xi^2}, \quad 0 < \xi < 1. \tag{2.38}$$

$$\left(\frac{\partial \overline{M}}{\partial \xi}\right) = 0, \quad \text{at} \quad \xi = 0. \tag{2.39}$$

$$\frac{\partial \overline{M}}{\partial \xi} = -Sh \times C_{air} \left(\overline{\beta}_1\, f(\overline{M}) - 1\right) \quad \text{at} \quad \xi = 1. \tag{2.40}$$

Residual steady state moisture $\overline{M}_\infty$ is given by
$\overline{\beta}_1 f(\overline{M}_\infty) = 1$ i.e $\overline{M}_\infty = \left(\dfrac{\varphi^\zeta}{\sigma - 1}\right)^{\frac{1}{\zeta}}$. The value of ζ by experiment suggested by Wang *et al.* [123] is 2.38, with σ=84.55, $\varphi = \dfrac{0.062}{M_0}$ for drying of air temperature 60^{o}C and RH=20%.

Theoretical studies on drying of foodstuffs based on isothermal mass transfer, neglect the heat transfer and its effect on drying; in this case moisture transfer occurs by simple diffusion and capillary action [65]. For drying processes with small Nu

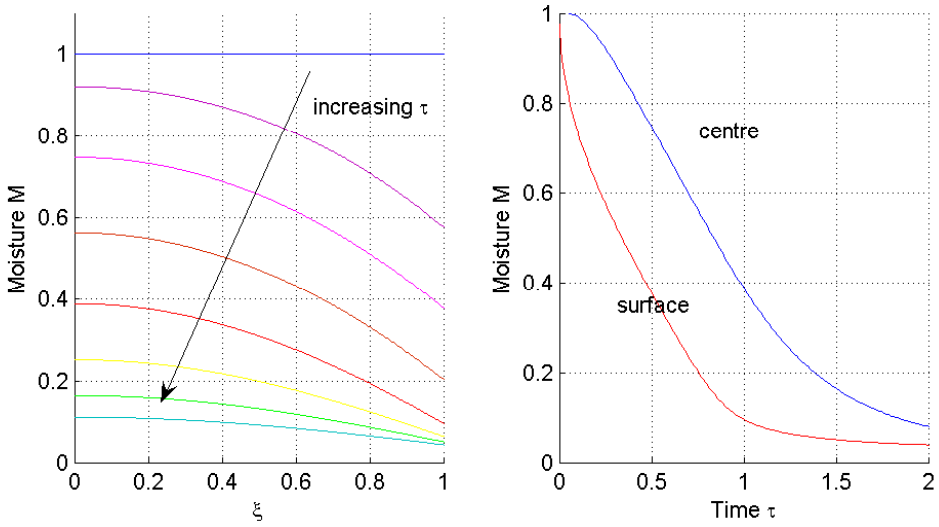

Figure 2.2: Profile of (a) moisture through the sample, with elapsed time τ=0-2 in step of 0.25 (b) Moisture profile at the surface and centre. Parameter value Sh=10.

number, a uniform temperature profile in the food can be assumed in the simulation and a single mass transfer model thus can be used to describe the drying process [125]. In this case, when temperature is uniform and increases rapidly compared to the loss of moisture, identified as an isothermal condition, the diffusion equations (equation (2.38)-(2.40)) can be solved without consideration of a heat equation and boundary condition approximated by $\overline{\beta}(\overline{T}) = \overline{\beta}(\overline{T} = 1) = \overline{\beta}_1$. Figure 2.2 shows moisture distribution as a function of time and space during drying. Each curve represents the gradient of moisture at different times. Figure 2.2 shows that, as time increases, moisture at each location decreases with time. The moisture gradient between centre and the surface decreases with drying time. Experiment findings that use drying kinetics (for example [106, 94]) show a similar profile of moisture to that in Figure 2.2(b).

The only parameter that gives effects in this case is Sh. Sh number represents the surface convection mass transfer with respect to the diffusivity of water. Figure 2.3 shows the behaviour of moisture $\overline{M}$ profile, varying the parameter Sh. From Figure 2.3, we see that Sh has a great impact. If $Sh = 1$, the results suggest that, at any time during the transient process, it is reasonable to assume a uniform moisture distribution across the food. This is not the case for drying, where the moisture

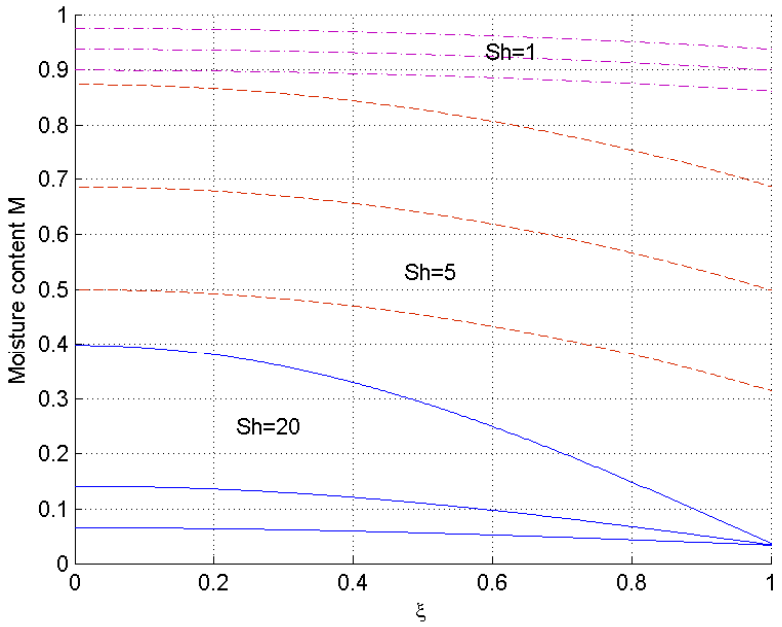

Figure 2.3: Profile of moisture at time τ=0.5,1 and 1.5 for different values of Sh and a fixed value of $\zeta = 2.38$.

gradient within the foods is significant (consistent with the experiment findings for banana [74] and mango [119]). For example, the mass transfer coefficient h_m for fruits is 10^{-3} to 10^{-6}, thickness of 0.005-0.01 m with $D_0 = 10^{-10}$(for eg. [10]), which gives the value of Sh as more then 10. This gives resistance to diffusion within the food as much more than the resistance to convection across the fluid boundary layer, where the $Sh > 1$, and therefore this phenomenon is diffusion control. For drying with diffusion control, the value of Sh is more than 20 for fruit and under these conditions, air velocity or air moisture has no effect on drying. In experiments by [90], when Sh number is bigger than 30 and change of air velocity was made, the drying curve of moisture is practically overlapped, which shows that drying is by diffusion control. In the simulation, we also observed that an increase in Sh causes a much faster decrease in moisture and the moisture gradient between the surface and centre is much bigger.

Figure 2.4 shows a plot amount of moisture loss by evaporation with different values of Sh, and consistent with the graph showing $\frac{M_t}{M_\infty}$ given by Newman (in Crank [26]) showing residual moisture left at the surface with time; the bigger the Sh number, the faster the moisture equilibrium with drying air.

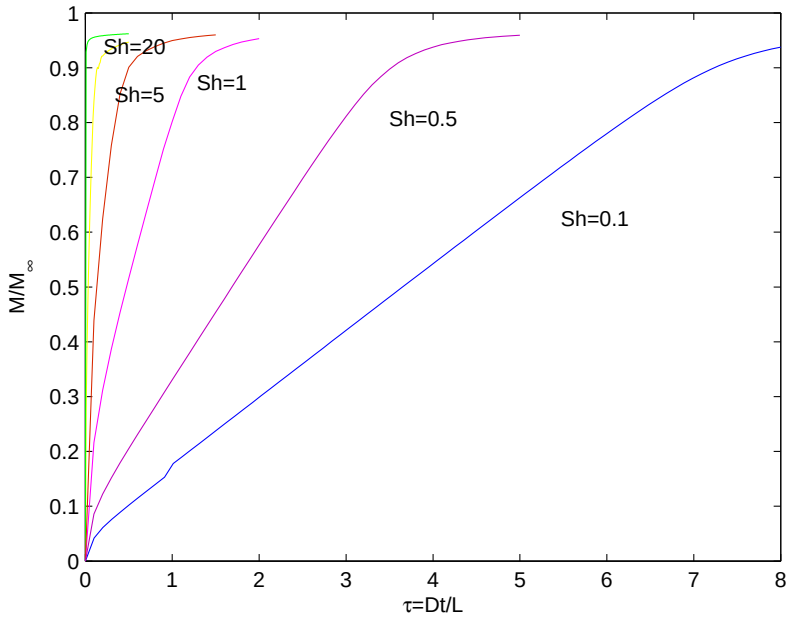

Figure 2.4: Amount of moisture loss by evaporation at the surface with different values of Sh.

To show the effect of temperature during drying, we put the boundary conditions for the moisture at the surface $\overline{\beta}(\overline{T})$, with different values of temperature $\overline{T}$, compared with $\overline{T} = 1$. Figure 2.5 gives significant difference effect in the drying rate where moisture decreases more slowly if the temperature is lower. Experimental finding by [124, 58, 56, 8, 119] show that a different drying temperature gives different drying curve. From these two phenomena, we conclude that temperature affects drying, so neglecting the heat transfer during drying is not significant.

The other parameter that may affect the transfer of moisture is the value of ζ, in equation (2.32). The value of ζ represents the relationship between the a_w with moisture at the surface. Fig 2.6 shows the behaviour of $\overline{M}$ as a function of time, varying the parameter ζ, for $Sh = 20$. We observe that an increase in ζ causes a more rapid decrease in moisture. As ζ behaves like Figure 2.6, we will set ζ=2.38. Ideally we would create or use many more equations from the literature (for example [105, 8, 56]) to estimate the relationship between a_w with moisture at the surface. Unfortunately, time constraints prevented us from using these other equations.

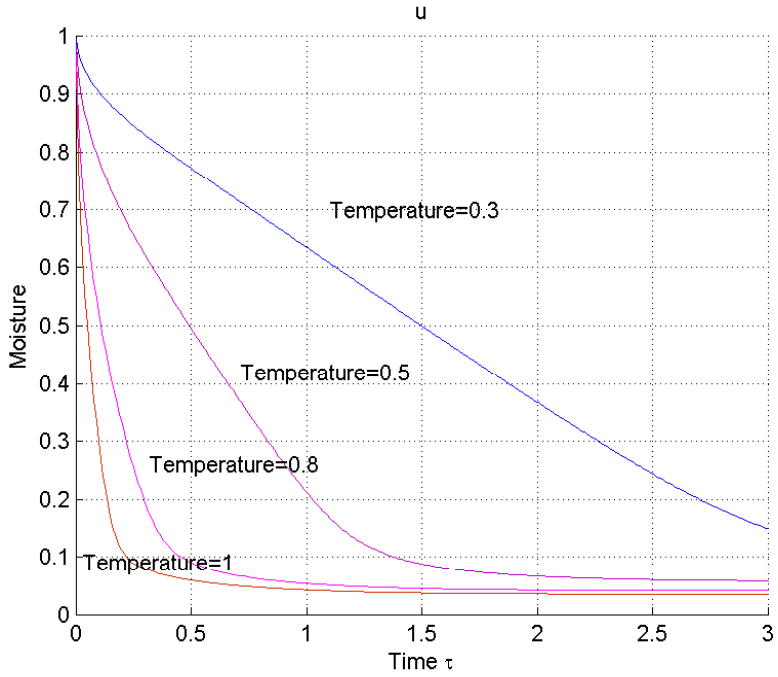

Figure 2.5: Moisture at $\xi = 1$ against time for different values of $\overline{T}$. Fixed value of $\zeta = 2.38$ and $Sh = 20$.

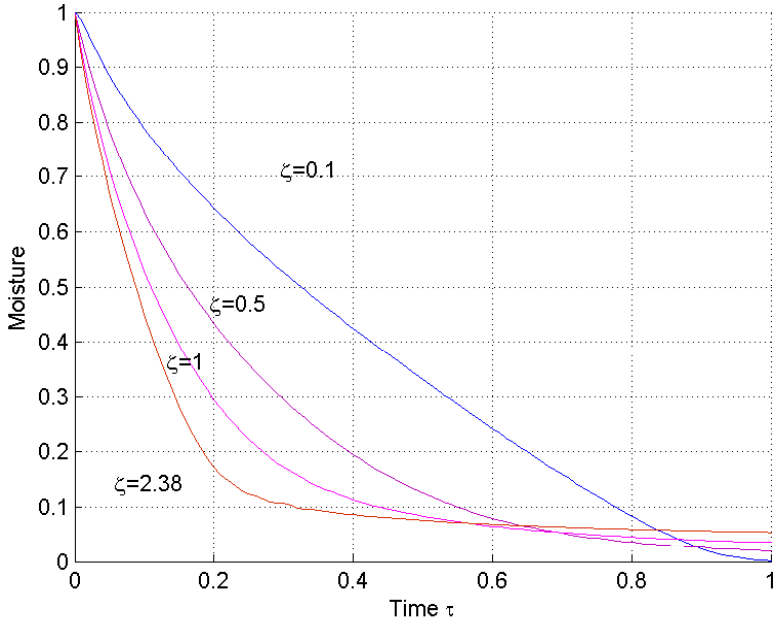

Figure 2.6: Moisture at $\xi = 1$ against time for different values of ζ and fixed value of $Sh = 20$.

From these Figures (2.3)-(2.6), we have verified numerically that in the isothermal solution case, where the increase in temperature rapidly creates flux at the surface much more quickly. This is dependent on the number of Sh. The bigger the number of Sh, the faster the drying rate and the faster the diffusion. We also conclude that temperature affect drying, so neglected the heat transfer during drying is not significant.

2.3.4 Non-isothermal solution

Drying is a fundamental problem involving simultaneous heat and mass transfer under transient conditions. Where the Nu number is large, coupled heat and mass transfer should be taken into account in the simulation. The modification of the isothermal model is to solve the heat equation together with the diffusion equation. For this non-isothermal situations, temperature profiles will develop inside the material during drying [66] and a differential energy balance is used to determine these temperature profiles.

More generally, latent heat is an important consideration, and moisture and temperature equations must be solved simultaneously. In food-air interfaces, some heat is used for water evaporation (see equation(2.20)). This gives a coupled governing equation for heat and mass transfer at the surface. From these equations, it is deduced that the heat transferred to the interior of the food, and therefore the food temperature, depends upon the relation between Nu and $\overline{\lambda}$. Non-isothermal equations for heat and mass transfer (equation (2.17)), together with the boundary condition at the surface (equations (2.20) and (2.31)), were solved together. For this simulation, we fix the temperature of air $T_{air} = 60^{o}$C.

Figure 2.7(a) shows the moisture profile through the sample of the fruit with increasing time. Moisture decreased but this was a little slower compared to isothermal case. Figure 2.7(b) shows temperature and moisture profiles at the surface. The small value of Nu number, Nu=0.3 gives a slower increase in temperature and this affects the moisture profile, which decreased more slowly than in isothermal case.

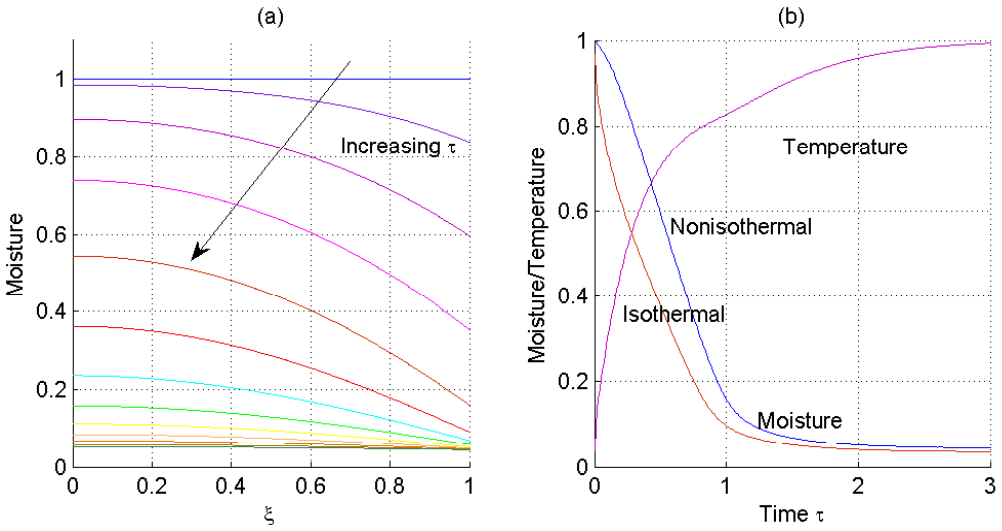

Figure 2.7: Profile of (a) moisture through the sample, with elapsed time τ=0-3 in step of 0.25 (b) Moisture and temperature profile at the surface and compared with the isothermal case. Parameter values Sh=10, Nu=0.3 and $\overline{\lambda}$=0.5.

2.3.5 Effect of diffusivity

To put the effect diffusivity into the model, equation (2.5), diffusivity dependent on temperature, and equation (2.6), diffusivity dependent on moisture and temperature, were used and applying the same non-dimensional scale variable as equation (2.16), these equations become

$$\frac{\partial \overline{M}}{\partial \tau} = \overline{\mathbf{D}}\frac{\partial^2 \overline{M}}{\partial \xi^2} + \overline{\mathbf{D}}'\frac{\partial \overline{M}}{\partial \xi}\frac{\partial \overline{T}}{\partial \xi}, \tag{2.41}$$

$$\frac{\partial \overline{M}}{\partial \tau} = \widetilde{\mathbf{D}}\frac{\partial^2 \overline{M}}{\partial \xi^2} + \frac{\partial \overline{M}}{\partial \xi}\frac{\partial \overline{T}}{\partial \xi}\widetilde{\mathbf{D}}'_{\overline{T}} + \frac{\partial \overline{M}}{\partial \xi}\frac{\partial \overline{M}}{\partial \xi}\widetilde{\mathbf{D}}'_{\overline{M}}. \tag{2.42}$$

with
$\overline{\mathbf{D}} = \dfrac{\overline{D}}{D_0}$, $\overline{\mathbf{D}}' = \dfrac{d\overline{\mathbf{D}}}{d\overline{T}}$. $\widetilde{\mathbf{D}} = \dfrac{\widetilde{D}}{D_0}$, $\widetilde{\mathbf{D}}'_{\overline{M}} = \dfrac{\partial \widetilde{\mathbf{D}}}{\partial \overline{M}}$ and $\widetilde{\mathbf{D}}'_{\overline{T}} = \dfrac{\partial \widetilde{\mathbf{D}}}{\partial \overline{T}}$.
The equation for heat that is the same as equation (2.12), is

$$\frac{\partial \overline{T}}{\partial \tau} = Le\frac{\partial^2 \overline{T}}{\partial \xi^2}. \tag{2.43}$$

Taking symmetry boundary conditions in the mid-plane of the drying slice, gives

$$\xi = 0: \quad \left(\frac{\partial \overline{T}}{\partial \xi}\right) = 0, \quad \text{and} \quad \left(\frac{\partial \overline{M}}{\partial \xi}\right) = 0. \tag{2.44}$$

At the surface, moisture and temperature boundary conditions of the drying body in contact with drying air become

$$\frac{\partial \overline{M}}{\partial \xi} = \frac{Sh}{\mathbf{D}} \left(\overline{\beta}(\overline{T}_{sur}) f(\overline{M}) - 1 \right), \tag{2.45}$$

$$\frac{\partial \overline{T}}{\partial \xi} = -Nu \left(\overline{T}_{sur} - 1 \right) + \mathbf{D} \overline{\lambda} \frac{1}{Le} \frac{\partial \overline{M}}{\partial \xi}. \tag{2.46}$$

with $\mathbf{D}=\overline{\mathbf{D}}$ for diffusivity dependent on temperature and $\mathbf{D}=\widetilde{\mathbf{D}}$ for diffusivity dependent on temperature and moisture.

Figure 2.8 shows the moisture decrease and temperature increase profile at the centre of the fruit with different values of diffusivity. It can be seen that moisture decreased more quickly for diffusivity dependent on temperature $\overline{D}(T)$ compared to D constant and $\widetilde{D}(T, M)$. This is because a temperature increase gives an increase in diffusivity during drying. When we take D as constant, the value of diffusivity remains one during drying. When we take diffusivity dependent on temperature and moisture during drying, as the temperature increases at the beginning diffusivity increases significantly but when the moisture become low, diffusivity starts to decrease until the end of drying. These two effects of temperature and moisture to diffusivity give different profiles of decreases in moisture. As a result, there are the same decreases of moisture at the beginning for $\overline{D}(T)$ and $\widetilde{D}(T, M)$, but at the end, the moisture decreases more quickly for diffusivity dependent on temperature $\overline{D}(T)$.

2.3.6 Sensitivity analysis

The development of a non-isothermal model involves a number of parameters and, for realistic models, the choice of suitable values for the parameter is very important. Detailed material properties are generally unavailable and variability in these properties can significantly affect the final result. Based on the values of thermo-physical properties reported in the literature [99], the non-dimension value was around 0.5 for $\overline{\lambda}$ and 0.2-1 for Nu. For this sensitivity study, we fixed these values as 0.5 for $\overline{\lambda}$ and 0.3 for Nu. Sensitivity analysis was carried out by varying another two parameter properties in the model, Sh and Le.

The properties used as for references correspond to case 0 in Table 2.3. The properties' values for other cases (i.e. case 1-2) were obtained by varying each parameter,

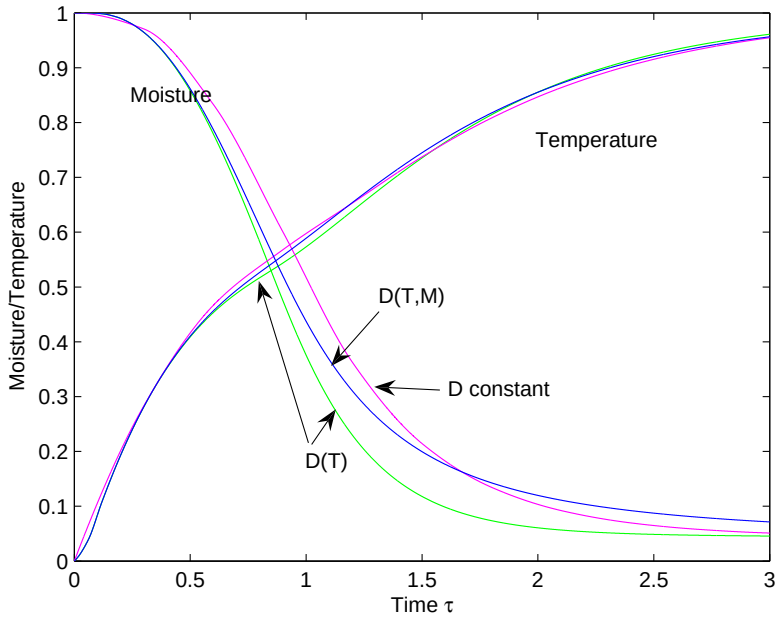

Figure 2.8: Profile of moisture and temperature at the centre for different values of diffusivity. Parameter values Sh=10, Nu=0.3 and λ=0.5.

whilst keeping the other values constant. Each parameter value was varied; the first variation denoted the lower limit while the second variation denoted the upper limit of the parameter considered. Simulations were conducted and the moisture and temperature distribution for the values of the properties corresponding to each of the cases given in Table 2.3 was predicted. Figure 2.9(a) shows the temperature evolu-

Table 2.3: Input data for parameter analysis.

Case	Sh	Le
0	20	5
1	**10-200**	5
2	20	**5-100**

tion at the surface with fixed value of Le=5 and variable values of Sh. With larger values of Sh, the temperature increased slowly while the process developed. This trend shows that the temperature would not reach the air drying temperature. This

is consistent with experimental data for mango and cassava [90]; in these experiments mango temperature did not reach the air temperature during 10 hours of drying. This phenomenon has also been observed by other researchers (Hussain and Dincer [60], Wang and Brenann [123]). Figure 2.9(b) shows moisture at the surface of a typical fruit with a fixed value of Le and variable values of Sh. It can be concluded the larger the value of Sh, the faster the drying. According to Pavon *et al.* [90], if the value of Sh is greater than 30, drying is diffusion controlled.

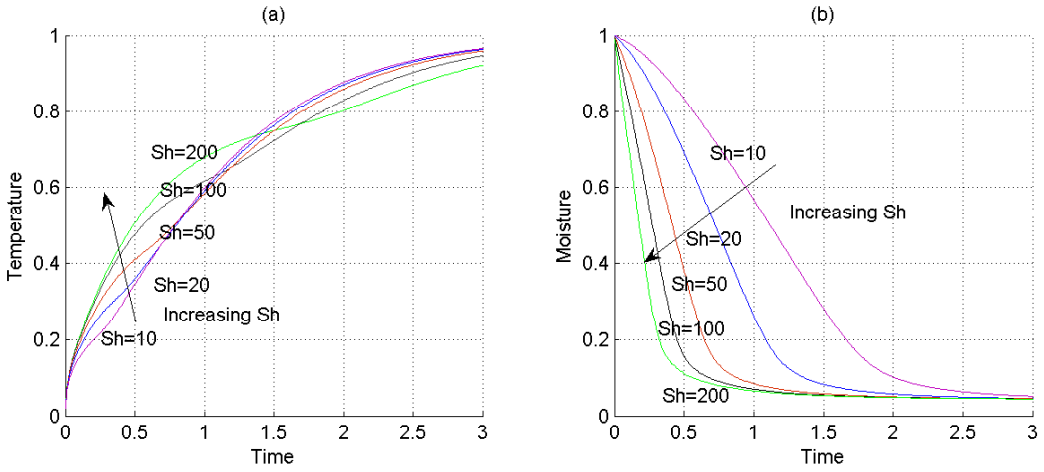

Figure 2.9: Temperature and moisture at surface $\xi = 1$ against time for different values of Sh. Parameter values $Le = 5$, Nu=0.3, $\overline{\lambda}$=0.5).

Figure 2.10(a) shows the temperature evolution. With increased value of Le, the temperature evolution increases. The larger the value of Le, the temperature increases more quickly. Based on the literature [90], the suitable value of Le is more than 100, which gives an interior temperature that is approximately equal to the surface temperature. Figure 2.10(b) shows the moisture at the surface with fixed a value of Sh and variable values of Le. An increased value of Le has the impact of moisture decrease. Moisture evolution at the surface decreased more quickly for a larger value of Le. From Figures 2.9 and 2.10, we concluded that Le and Sh has an effect on drying: the larger these values, the faster of drying.

To see the effect the value of $\overline{\lambda}$ and Nu, we fixed the value of Le=5 and $Sh = 20$ and a parametric study was conducted by varying another two parameter properties

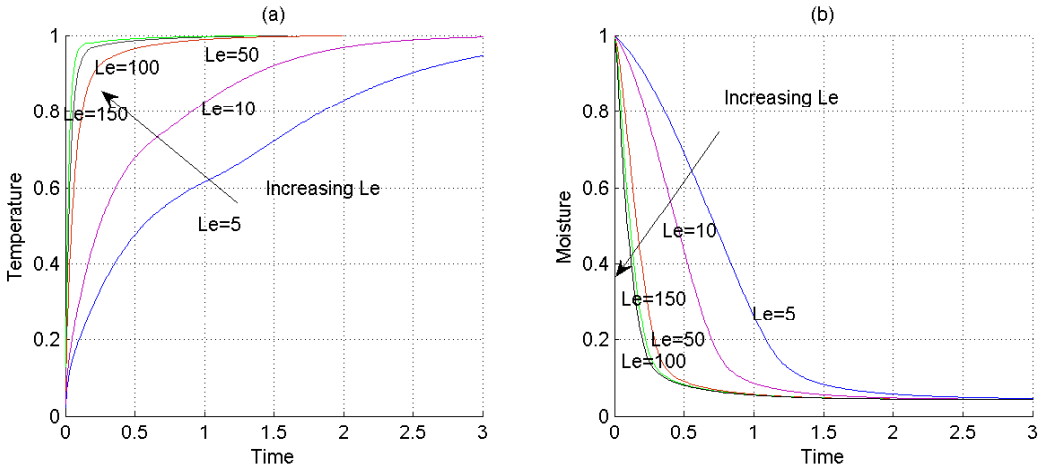

Figure 2.10: Temperature and moisture at $\xi = 1$ against time for different values of Le. Parameter values $Sh = 20$, Nu=0.3, λ=0.5).

in the model $\overline{\lambda}$ and Nu. The properties, used as references, correspond to case 0 in Table 2.4. The properties' values for the cases (i.e. case 1-2) were obtained by varying each parameter whilst keeping the other values constant. Each parameter value was varied; the first variation denoted the lower limit while the second variation denoted the upper limit of the parameter considered. Simulations were conducted and the moisture and temperature distribution for the values of the properties corresponding to each of the cases given in Table 2.4 were predicted.

Table 2.4: Input data for parameter analysis.

Case	$\overline{\lambda}$	Nu
0	0.5	0.3
1	**0-10**	0.3
2	0.5	**0.1-50**

Figure 2.11 shows the temperature evaluation at the surface with a fixed value of $Nu = 0.3$ and variable value of $\overline{\lambda}$. From the Figure, when the value of $\overline{\lambda}$ increased to 5 to 10, the temperature increased very slowly and was relatively flat at time $\tau = 0.2$ and $\tau = 0.3$. This is not the case for drying, where the temperature usually increases to nearly the same as the air temperature. Thus, from this we can conclude with

the $Nu = 0.3$, the approximation of the value of $\overline{\lambda}$ will be between $0.1 - 1$. This is consistent with finding by Pavon-Melendez [90] that the value of $\overline{\lambda}$ is around 0.5 for fruits.

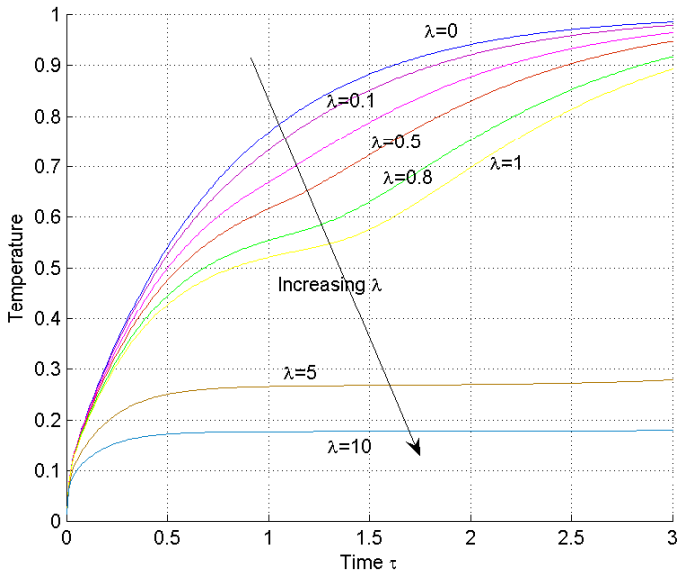

Figure 2.11: Temperature at $\xi = 1$ against time for different values of $\overline{\lambda}$ ($Nu = 0.3$).

Based on Figure 2.11, we have now fixed the value of $\overline{\lambda} = 0.5$. We change the value of Nu, based on case 2. Figure 2.12(a) and Figure 2.12(b) show the profile of temperature and moisture with different values of Nu. Increasing the value of Nu, the temperature increases rapidly and moisture decreases rapidly. When $Nu > 1$ convection heat transfer offers little resistance to heat transfer and the temperature increases rapidly, but for $Nu < 1$, the conduction heat transfer gives little resistance and leads to a slow increase in temperature.

Based on parametric study, the choice of parameters Sh, Nu, Le and λ depends on the type of fruit and the drying temperature. Different types of fruit give different values of these numbers. For example, in the study of diffusivity by Villa *et al.* [119], the heat transfer coefficient and the mass transfer coefficient of Mango Ataulfo contrasted with that of other authors, as different varieties of mango may have different physical and chemical characteristics.

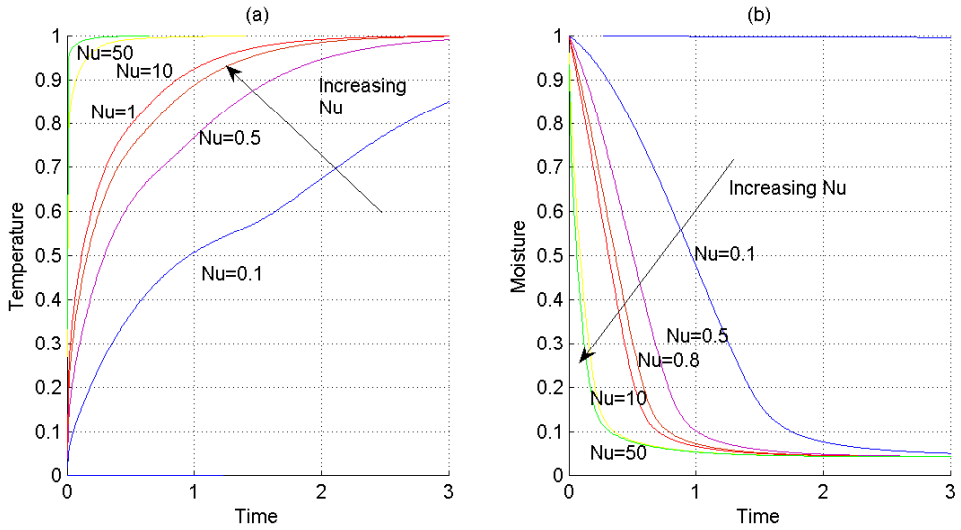

Figure 2.12: Moisture at $\xi = 1$ against time for different values of Nu (Fixed $\overline{\lambda} = 0.5$).

2.4 Two-dimensional models

In the one-dimensional model, we assume fruits of infinite length with moisture and temperature given across the thickness of the fruit. We now consider drying a slice of food with the cross-section area of a rectangle $-L_x < x < L_x$, $-L_y < y < L_y$ with surface $x = \pm L_x$, $y = \pm L_y$.

Two-dimensional isotropic foodstuff, for symmetric drying conditions as illustrated in Figure 2.13.

$$\rho_s \frac{\partial M}{\partial t} = \frac{\partial}{\partial x}(D\rho_s \frac{\partial M}{\partial x}) + \frac{\partial}{\partial y}(D\rho_s \frac{\partial M}{\partial y}), \tag{2.47}$$

$$\rho_s C_p \frac{\partial T}{\partial t} = \frac{\partial}{\partial x}(k\frac{\partial T}{\partial x}) + \frac{\partial}{\partial y}(k\frac{\partial T}{\partial y}), \quad 0 < x < L_x, \quad 0 < y < L_y. \tag{2.48}$$

Due to symmetry, the solution is sought from the centre line. Taking $\alpha = \dfrac{k}{\rho_s C_p}$ and constant diffusion coefficient $D = D_0$, equations (2.47) and (2.48) give

$$\frac{\partial M}{\partial t} = D_0 \left(\frac{\partial^2 M}{\partial x^2} + \frac{\partial^2 M}{\partial y^2} \right), \tag{2.49}$$

$$\frac{\partial T}{\partial t} = \alpha \left(\frac{\partial^2 T}{\partial x^2} + \frac{\partial^2 T}{\partial y^2} \right). \tag{2.50}$$

Initial conditions are taken as

$$M = M_0, \quad T = T_0, \quad \text{at} \quad t = 0. \tag{2.51}$$

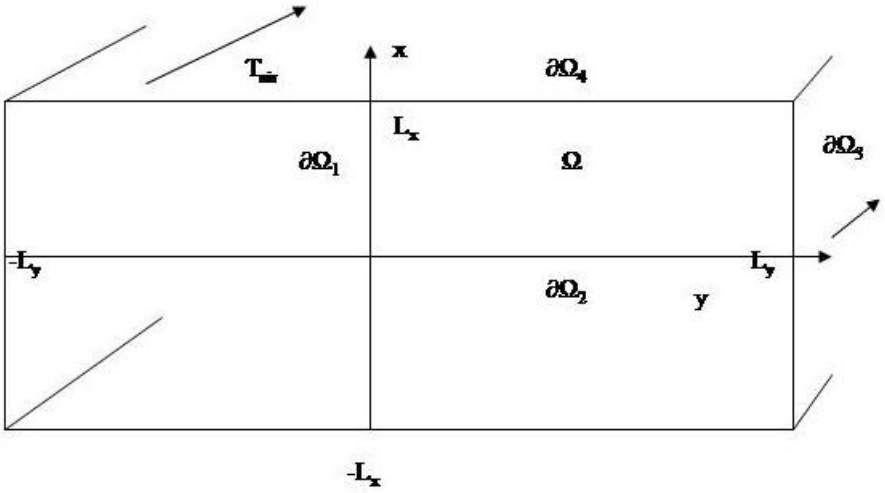

Figure 2.13: Schematic of two-dimensional model food drying process.

Imposing symmetry, there are no temperature and moisture concentration gradients at the centre of the product ($d\Omega_1$ and $d\Omega_2$), and so the following conditions hold:

$$\frac{\partial M}{\partial x} = 0 \quad \text{and} \quad \frac{\partial T}{\partial x} = 0, \quad \text{at} \quad x = 0, \tag{2.52}$$

$$\frac{\partial M}{\partial y} = 0 \quad \text{and} \quad \frac{\partial T}{\partial y} = 0, \quad \text{at} \quad y = 0. \tag{2.53}$$

At the surface, boundary conditions ($d\Omega_3$ and $d\Omega_4$) become

$$k\frac{\partial T}{\partial x} - \lambda D_0 \frac{\partial M}{\partial x} = -h(T_{sur} - T_{air}), \quad \text{and} \quad D_0 \frac{\partial M}{\partial x} = -h_m(C_{sur} - C_{air}) =, \quad \text{at} \quad x = L_x, \tag{2.54}$$

$$k\frac{\partial T}{\partial y} - \lambda D_0 \frac{\partial M}{\partial y} = -h(T_{sur} - T_{air}), \quad \text{and} \quad D_0 \frac{\partial M}{\partial y} = -h_m(C_{sur} - C_{air}), \quad \text{at} \quad y = L_y. \tag{2.55}$$

Taking $\dfrac{L_x}{L_y} = 1$, in non-dimension form equation (2.49-2.55) become

$$\frac{\partial \overline{M}}{\partial \tau} = \frac{\partial^2 \overline{M}}{\partial \xi_1^2} + \frac{\partial^2 \overline{M}}{\partial \xi_2^2} \quad \text{and} \quad \frac{\partial \overline{T}}{\partial \tau} = Le\left(\frac{\partial^2 \overline{T}}{\partial \xi_1^2} + \frac{\partial^2 \overline{T}}{\partial \xi_2^2}\right). \tag{2.56}$$

with initial conditions $\overline{M} = 1$, and $\overline{T} = 0$, at $\tau = 0$ and boundary conditions

$$\xi_1 = 0: \quad \left(\frac{\partial \overline{T}}{\partial \xi_1}\right) = 0, \quad \text{and} \left(\frac{\partial \overline{M}}{\partial \xi_1}\right) = 0, \tag{2.57}$$

$$\xi_2 = 0: \quad \left(\frac{\partial \overline{T}}{\partial \xi_2}\right) = 0, \quad \text{and} \left(\frac{\partial \overline{M}}{\partial \xi_2}\right) = 0. \tag{2.58}$$

At $\xi_1 = 1$

$$\frac{\partial \overline{M}}{\partial \xi_1} = -\overline{Sh}\,\left(\overline{\beta}(\overline{T}_{sur})\, f(\overline{M}) - 1\right), \tag{2.59}$$

$$\text{and} \quad Le\,\frac{\partial \overline{T}}{\partial \xi_1} = -Nu\,Le\,\left(\overline{T}_{sur} - 1\right) + \overline{\lambda}\,\frac{\partial \overline{M}}{\partial \xi_1}. \tag{2.60}$$

At $\xi_2 = 1$

$$\frac{\partial \overline{M}}{\partial \xi_2} = -\overline{Sh}\,\left(\overline{\beta}(\overline{T}_{sur})\, f(\overline{M}) - 1\right), \tag{2.61}$$

$$\text{and} \quad Le\,\frac{\partial \overline{T}}{\partial \xi_2} = -Nu\,Le\,\left(\overline{T}_{sur} - 1\right) + \overline{\lambda}\,\frac{\partial \overline{M}}{\partial \xi_2}, \tag{2.62}$$

with

$$\overline{\beta}(\overline{T}_{sur}) = 0.0364\,\overline{T}_{sur}^{2} + 0.0108\,\overline{T}_{sur} + 0.0119, \tag{2.63}$$

$$f(\overline{M}) = \frac{\sigma \overline{M}^{\zeta}}{\varphi^{\zeta} + \overline{M}^{\zeta}}. \tag{2.64}$$

The value of σ=84.55, $\varphi = \dfrac{0.062}{M_0}$ and $\zeta = 2.38$.

The COMSOL Multiphysics program is used to simulate the dehydration process in a drying system that corresponds to the numerical solution of these model equations as seen in the one-dimensional problem in section §2.3.1 . The above system of non linear partial differential equations, together with the described set of initial and boundary conditions, has been solved by Finite Element Method implementation by COMSOL Multiphysics 3.4. Equations (2.56) were input into COMSOL Multiphysics using a partial differential equation (PDE) solver with the general form for moisture content and temperature. Details of the numerical procedure can be found in Appendix B.

2.4.1 Isothermal solution

Simulation for isothermal conditions are carried inside the rectangular moist product, such as mango (Sh=20). For this case, the latent heat term $\overline{\lambda}$ was not considered. Because of the rapid temperature change compared to the change of moisture (without latent heat term), the equation for $\overline{\beta}(\overline{T}_{sur})$ for the moisture boundary condition at the surface will be approximate as $\overline{\beta}_1$.

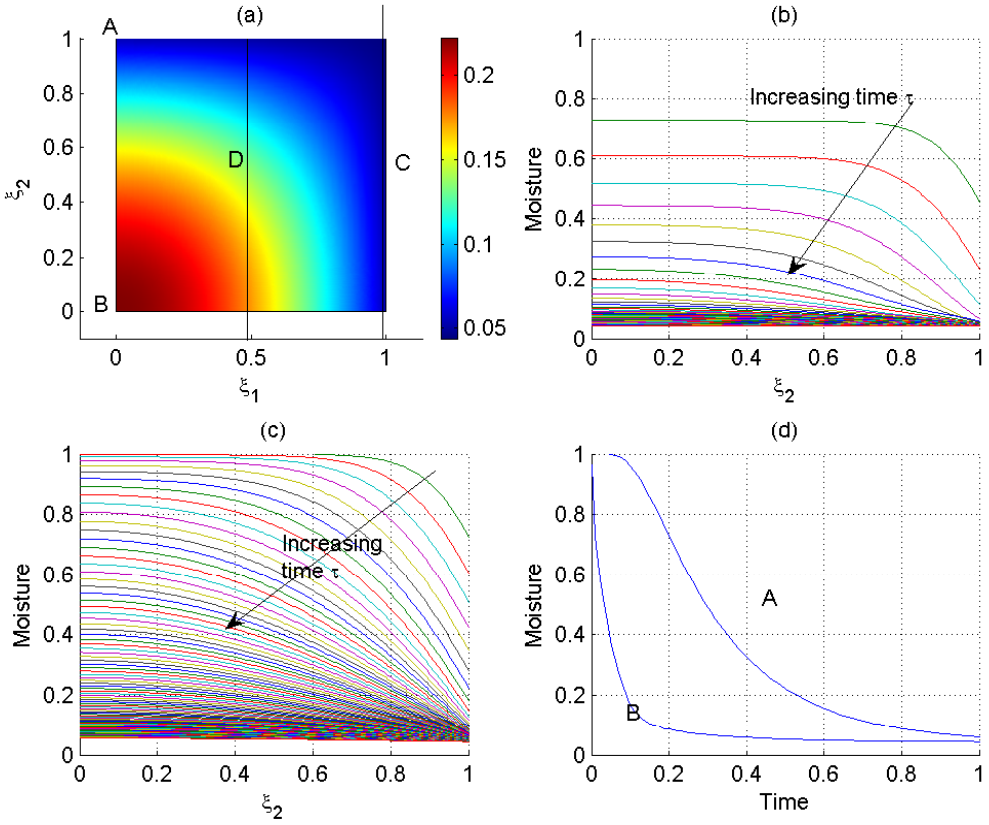

Figure 2.14: (a) Surface plot of residual free water moisture field at time τ=0.5 (b) Moisture across a line passing through the surface(line C) (c) Moisture across a line passing through the centre (line D) with increasing time τ=0-1(in step of 0.01) (d) moisture decreasing at selected points A and B.

As an example case, Figure 2.14(a) illustrates the moisture contour field inside the object at time τ=0.5. As seen from the distribution, the moisture gradient obtained at the surface ($d\Omega_3$ and $d\Omega_4$) is higher than inside the fruits ($d\Omega_1$ and $d\Omega_2$). At time=0.5, moisture at the surface is 0.06, whereas the centre moisture is still higher at 0.22. In order to have a better view of the decreasing moisture inside the object, variations of non-dimension moisture across a line passing the surface (line C) and centre (line D) are shown in Figure 2.14(b)and (c) and moisture decreases at points A and B, shown in Figure 2.14(d). It can be seen that the moisture across a line passing the surface (line C) is decreasing faster than the moisture across a line passing the centre (line D) of the product.

2.4.2 Non-isothermal solution

For non-isothermal conditions, equations (2.56)-(2.64) were solved for comparison with isothermal conditions with non-dimensional values $Sh = 20$, $Le = 5$, $Nu = 0.3$ and latent heat value $\overline{\lambda} = 0.5$.

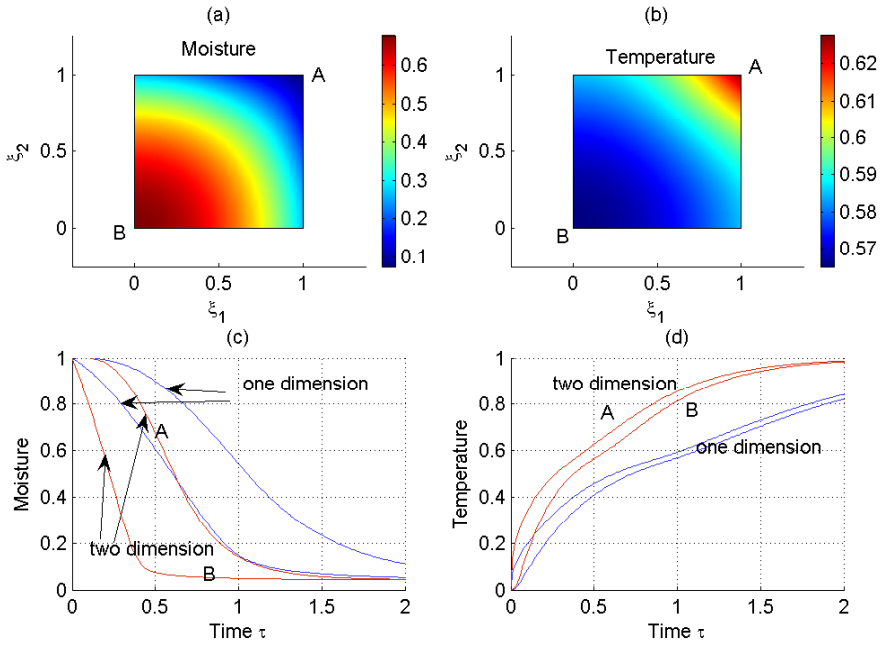

Figure 2.15: (a) Surface plot of moisture (b) temperature at time=0.5 (c) surface and centre moisture (d) surface and centre temperature for one and two-dimensions.

The temperature distribution in Figure 2.15(b), on the two exposed side boundaries ($d\Omega_3$ and $d\Omega_3$), found that the corner of the food is at much higher temperature. The temperature is found to be more 0.05 warmer on the surface leading edge (A) compared to the symmetry leading edge (B). The lowest temperature is detected at bottom edge of the (B). As we can see from Figure 2.15(a), moisture at the surface corner is 0.1 compared the bottom edge at 0.6. The moisture profiles are in agreement with drying phenomena where the moisture at the centre of the fruit is much higher at the edge, with the difference being more predominant during the initial drying. The evaporation and depletion of water is more effective at the leading edge, where the temperature is highest. Based on this two-dimensional model, we can describe temperature and spatial moisture distribution on fruit at any time. This is highly relevant from a food safety point of view, which allows detection of the regions within the food core where high values of moisture content might determine microbial spoilage. Figures 2.15(c) and (d) show the moisture and temperature profile for one-dimensional and two-dimensional models at the surface (A) and centre (B). As we can see from the profile, moisture is decreasing and temperature increasing much faster in the two-dimensional model than the one-dimensional model because of the effect of the surface area.

2.5 Discussion and conclusion

In this chapter, we have employed simple one-dimensional and two-dimensional models of heat and mass transfer that assume fruit as a homogenous structure, as discussed by Wang and Brenann [123], Balaban and Pigoet [8]. We have applied this framework to one-dimensional and two-dimensional diffusion models to represent the movement of water. Using numerical simulation, the behaviour of moisture and temperature subject to underlying air flow was calculated for constant diffusivity and diffusivity dependent on temperature and moisture content. First, we studied cases in which diffusion process occurs only as an isothermal model. An assumption that a uniform temperature profile exists inside the fruit gives the single mass transfer model which can thus be used to describe the drying process. The results reveal that, with the use of the diffusion process alone, the movement of moisture can simulate the drying

process. The results presented in this chapter provide information about moisture reduction during drying. Motivated by parameter estimation, we employed the simplifying limit of the drying process as diffusion control. Taking the Sh number as 20, we may describe the resistance to diffusion within the food as much more than the resistance to convection across the fluid boundary layer. This is consistent with experimental findings by [3] which indicate that the rate of water loss from the samples appears to be limited by the diffusion of water through the sample but not the rate of evaporation from the surface.

However, for typical drying process, it was found that temperature is an important consideration, taking into account a couple of heat and mass transfers in the simulation. This situation applies to the non-isothermal model. The numerical solution for the unsteady-state heat and mass balance equations was performed by finite element method using Comsol Multiphysic. Our analysis indicates that an increase in temperature and decrease in moisture during drying depend on the value of the parameters at the surface boundary Sh, Nu and latent heat λ. By changing these parameter values, we can control the drying process, depending on the type of food. If the mass transfer is diffusion controlled, the Sh numbers should be more than 20. If the $Nu > 1$, convection offer little resistance to heat transfer, this leads to the surface temperature instantaneously reaching air temperature. This is usually controlled by the velocity of the drying air: the higher the velocity, the bigger the Nu number. This phenomenon is represented by the boundary condition (2.20). Therefore, food temperature evolution depends upon the relationship between Nu and $\overline{\lambda}$ numbers. If Nu is similar or in the same order of magnitude as $\overline{\lambda}$, the food temperature increases slowly while the process develops. If $Nu >> \overline{\lambda}$, the surface temperature does not reach the air temperature instantaneously. Pavon-Melendez *et al.* [90] reported that the $\overline{\lambda}$ value obtained was around 0.5 for fruit when the air temperature is 60^oC. On the other hand, there is a great dispersion in the heat transfer coefficient values reported for foods, and therefore the estimation of food Nu number values are in the range 0.2-1 [90]. Therefore, in the drying of fruit, with properties similar to those mentioned by [90], the surface temperature does not instantaneously reach the air temperature .

Experiment results in [105, 122, 119] indicate that diffusivity depends on temper-

ature; changing the temperature leads to increases in diffusivity. This will affect the rate of moisture removal, due to high level of moisture at the beginning [97, 71]. Our simulation result is consistent with these findings. If the temperature is increased, the diffusivity will increase, which leads to a faster decrease in moisture during drying. The majority of models reported in the literature suggest that effective mass diffusivity increases with the material moisture content up to a certain level, which is regarded as a function of the material temperature [71]. The form of the mass diffusivity shape suggests that water molecules have to overcome a certain energy barrier as the material moisture content decreases, and, therefore, mass transfer slows in the last stages of drying [71]. Indeed, guided by our simulation, we predict slower moisture removal at the end of drying due to a low level of moisture, modelled through diffusivity that is dependent on moisture and temperature.

In a one-dimensional model, the effect of thickness is considered only in cases in which the fruit is assumed to be a thin infinite slab. To include the effect of length in the modelling, a two-dimensional model was developed. Using a numerical solution in the two-dimensional model, the behaviour of moisture and temperature predicted by the model was observed. It was observed that the temperature is higher at the surface corner of the leading edge and lower at the symmetry leading edge. The depletion of water is more effective at the higher temperature of the surface, where the surface moisture is less than that at the surface corner. The detection of this region is a very important aspect in terms of food safety.

Sensitivity analysis has been carried out for certain parameters to show their relative influence on drying. The sensitivity analysis should also guide us into selecting properties that are involved in drying. The simple heat and mass model is capable of describing the transport of both water and heat within the fruit. It is flexible and can be easily adapted to any drying conditions but it also has plenty of limitations based on the assumptions made. An additional limitation of this simple heat and mass transfer model is that, since change of volume is not considered, we are unable to model any change of shape in the system. In the chapters that follow, we develop mathematical models to account for fruit sample shrinkage during drying.

Chapter 3

Shrinkage models of drying fruit

3.1 Overview

The model presented in chapter 2 is now extended to include the effect of shrinkage in the drying model discussed in section §2.2. As a first approximation, we present a simple one-dimensional time varying model of heat and mass transfer that assumes food to have a homogenous structure. The development of this model is based on work of Wang and Brenann [124] and Balaban and Pigott [8]. A diffusion model is developed to describe the drying process, which includes a shrinkage condition and maintains a direct conservation requirement into the governing equation. Previous models, such as those presented by [124] [8], are too dependent on data from experiments with regard to the process of estimating the shrinkage effect. In this model, simultaneous moisture and heat transfer together with boundary conditions are used to estimate the heat and moisture transport rates, without resorting to any externally imposed empirical correlation. A convected coordinate system is introduced in order to fix the surface interfaces within the numerical computations. The shrinkage condition was developed on the basis of a simple mechanism of volume of evaporated water that takes place during drying. Finally, the complete model will be implemented in a computer program (MATLAB) and applied to typical tropical fruit data and comparison made with existing work.

3.2 Review of shrinkage models

In the case of food products with high moisture content, the presence of significant shrinkage during drying has been reported [107]. This may arise from a moisture gradient within the particle that induces microstructure stresses, leading to shrinkage [76]. Further, shrinkage will decrease the diffusion path of heat transfer processes and is extremely important in drying because it produces a variation in the distance required for the movement of water molecules [56]. Mayor and Sereno [76] reviewed a number of shrinkage models for food material with different geometries (cylinder, sphere, ellipsoid, slab, and cube) and different reduced dimensions (volume, radius, thickness, width, length, diameter, and surface area). Empirical models (linear and nonlinear) and fundamental models (linear, deviations of linear behavior, and explicit variation of porosity) were discussed in this review. These models usually present a good fit with experimental data, but their wider predictive use is limited because of their dependence on the drying conditions and material characteristics.

Wang and Bremann [124] have proposed a mathematical model of simultaneous moisture and heat transfer with the effect of shrinkage for the prediction of moisture and temperature distributions during drying in a slab shape solid of potato. These authors take the governing equations for heat and moisture as

$$\rho_s \frac{\partial M}{\partial t} = \frac{\partial}{\partial x}(D\rho_s \frac{\partial M}{\partial x}) \; ; \quad 0 < x < L(t),$$

$$\texttt{and} \quad \rho_s C_p \frac{\partial T}{\partial t} = \frac{\partial}{\partial x}(k \frac{\partial T}{\partial x}) \quad ; \quad 0 < x < L(t).$$

and convective surface boundary conditions to include a latent heat effect for the evaporation of moisture at the surface as

$$-D\rho_w \frac{\partial M}{\partial x} = h_m(C_{sur} - C_{air}),$$

$$\texttt{and} \quad -k \frac{\partial T}{\partial x} = h(T_{air} - T_{sur}) + \lambda D\rho_w \frac{\partial M}{\partial x}.$$

Shrinkage is one of major changes taking place during the drying process. During drying, the shape and size of the food particles are constantly changing as a result of water removal and internal collapse. These dimensional changes are variable during drying: some change is observed in dimension or shape and occasional cracking of the

product may take place. Reduction in diameter and length of dried fruits reduces the volume itself. Normally, an empirical fitting through experimental test is used to find an equation for shrinkage ([94, 123, 7, 20, 107, 74]). In order to quantify the effect of shrinkage, Wang *et al.* [123] fitted the thickness, length and width, correlated by a linear relationship with moisture as

$$L = A + B.M, \tag{3.1}$$

in which L is the thickness of the sample, A and B are taken as constants and the equation (3.1) is fitted with the experiment data. This method was also used by Quiroz *et al.* [94], who developed a shrinkage equation by fitting the mean radius r of banana and the moisture content from an initial radius r_o by a linear regression, as

$$\frac{r}{r_o} = A + B.M; \tag{3.2}$$

Subsequent computation gave $A = 0.4721$ and $B = 0.1819$.

On the other hand, Lima *et al.* [74], for the drying of banana, and Simal *et al.* [107], for the drying of kiwi, included shrinkage into the model using a correlation that relates volume and average moisture content $\overline{M}(t)$ as

$$\frac{V_t}{V_o} = \beta_1 + \beta_2 \overline{M}, \tag{3.3}$$

where β_1 and β_2 are shrinkage coefficients obtained by fitting the equation (3.3) with the experiment result. Baini and Langrish [7] included shrinkage as

$$\frac{r}{r_o} = (\frac{V}{V_o})^{1/2} = (0.6\frac{M}{M_o} + 0.4)^{1/2}. \tag{3.4}$$

Typically, empirical fitting through experiment is used to find shrinkage equations (3.2-3.4), such as those used by the authors above. Using these conditions, the thickness or radius of the sample is adjusted at each time step during the calculation of the governing equations for heat and mass. This numerical approximation is one of the limitations used; detailed experimental results on specific tropical fruits were used to find the empirical shrinkage equation before mathematical modelling is solved.

In the early stage of drying, the properties of material surface layer do not differ much from the centre [123]. As drying proceeds, the surface deforms due to viscoelastic behaviour of the solid food particles. When water is removed from the solid

material, a pressure imbalance is produced between the inner and the external pressure, generating contracting stresses that can lead to material shrinkage or collapse. The tissues in the food are unable to hold their structure when the space taken by the water is continuously removed. Shrinkage reduces the path length of the material through which diffusion occurs. This phenomenon may also reduce the surface area for heat and mass transfer, which may also affect the overall drying rate. Chemkhi *et al.* [20] developed the shrinkage phenomena due to the stress and deformation of strained solids during drying based on the viscoelastic behaviour of the material. The displacement of the solid phase (strain) during drying is a function of moisture content of the product, known as solid velocity u, represented as,

$$u = \frac{\rho_b}{1 + \beta\, M.} \tag{3.5}$$

The shrinkage coefficient (β), is known as the contraction coefficient of the material, and is found by an ideal deformation ratio $\frac{\rho_s}{\rho_{s0}}$. The corresponding stress and strain relation is developed. A model of simultaneous heat and moisture transfer of potato was coupled with a model of stress and strain and solved numerically using the finite difference method. An approach used by Hassini *et al.* [55] used strain as above but did not consider the model of stress in the coupled of heat and moisture. The simulation results produced by [20] for this model, were applied to the shrinkage of a highly deformable products such as potato, which shrinks from an initial 10 mm to a final thickness of 1.5mm after approximately three and a half hours of drying. This shrinkage value was consistent with findings by Hassini *et al.* [55] that the potato shrank by about 77% of its initial volume. The displacement of the solid needs to be found experimentally, limiting the usage of this model.

A slightly different approach is used by Hadrich and Kechaou [49], Guiné *et al.* [48] and Balaban and Pigot [8] employing density values to account for volumetric shrinkage. This is similar to the suggestion by [76] that porosity formation occurs during the drying process, which can be produced either by the inclusion of the density or through the ratio of air volume in the sample to the total volume. Guiné *et al.* [48] include the shrinkage effect by using dry solid concentration ρ_s which relates the mass of dry solid to the total volume that varies in the drying of pears. The dry solid concentration equation is a function of bulk density ρ_b and moisture content

determined by experiments as

$$\rho_s = \rho_b \left(\frac{1}{1+M}\right). \tag{3.6}$$

Hadrich and Kechaou [49] also use product density ratio $\frac{\rho_s}{\rho_b}$ as a linear function of moisture content, which varies during the drying of potato in their model as

$$\rho_s = \rho_b \left(1 + 1.4855M\right). \tag{3.7}$$

These shrinkage equations (3.6 and 3.7), were put into a governing equation of mass and heat transfer, which varies with drying. As before, the need for detailed experiment results to find an empirical equation of density ratio limits the use of the model. Furthermore, these models usually present a good fit with the experiment data, but their use is limited because of their dependence on drying conditions and material characteristics.

Karim and Hawladar [65, 64] consider that material surface shrinks at a velocity $u(x)$ toward the material sample. In that case, the shrinkage effect appears explicitly in terms of convective velocity in the heat and mass transfer equations as

$$\frac{\partial T}{\partial t} + u\frac{\partial T}{\partial x} = \alpha\frac{\partial^2 T}{\partial^2 x}, \tag{3.8}$$

$$\frac{\partial M}{\partial t} + u\frac{\partial M}{\partial x} = \alpha\frac{\partial^2 M}{\partial^2 x}. \tag{3.9}$$

To determine shrinkage velocity in order to solve governing equations, they state that shrinkage velocity cannot be predicted and experimental determination is also difficult. They make the assumption that linear shrinkage velocity can be expressed as

$$u(x) = u(L)\frac{x}{L}.$$

This is one of the limitations of this model.

The rate of water removal will also influence shrinkage. A slow drying product shrinks nearly uniformly into a solid core as the magnitude of internal stress is low. During rapid drying, the surface is much drier than the interior, resulting in better preservation of the original shape at the surface, with cracks and voids forming inside while the interior shrinks [103]. Khraisheh *et al.* [70] found that the degree of

shrinkage of potato during low temperature drying was greater than with high temperature drying, due to high internal pore development and surface case hardening at high temperature. Karathanos *et al.* [63] attributed the structured collapse to the high mobility of the matrix composed of water and soluble solids within the cell wall polymer, when the temperature was above glass transition temperature. This suggests that products, for instance with higher sugar, would exhibit a continous collapse phenomenon due to their low glass transition temperature.

Several different types of shrinkage behaviour have been identified: ideal, elastic, and viscoelastic. Mayor and Sereno [76] found that factors affecting the magnitude of shrinkage included the volume removal of water, the mobility of solid matrix, the drying rate and other processing conditions. Shrinkage has been included in studies in order to improve the physical representation of the process and also to increase confidence in the drying parameters obtained. However, in most cases, the shrinkage models used adjust the thickness of the sample at each time step through an external (often empirical) algorithm and do not include a direct conservation requirement into the governing model formulation.

3.3 Mathematical formulation of a one-dimensional shrinkage model

During drying, heat is transferred mainly by convection from air to the product surface and by conduction from the surface towards the product centre. Meanwhile, moisture diffuses outwards towards the surface and gets vaporized into the air. Such a coupled mechanism provides the basis for a simultaneous heat and moisture transfer model. In the case of an infinite slab of finite thickness $L(t)$, the moisture content $M(x,t)$ across the slab and temperature $T(x,t)$ are expressed by the well known system of partial differential equations (PDEs) for moisture and energy transport [124] (discussed in chapter 2) as,

$$\rho_s \frac{\partial M}{\partial t} = \frac{\partial}{\partial x}(D\rho_s \frac{\partial M}{\partial x}) \; ; \quad 0 < x < L(t), \tag{3.10}$$

$$\rho_s C_p \frac{\partial T}{\partial t} = \frac{\partial}{\partial x}(k \frac{\partial T}{\partial x}) \quad ; \quad 0 < x < L(t). \tag{3.11}$$

At the onset of the drying process, the moisture content, temperature and the thickness of the product are taken as uniform; initial conditions are thus

$$M = M_0, \quad T = T_0, \quad L = L_0 \quad \text{at} \quad t = 0. \tag{3.12}$$

Imposing symmetry, there are no temperature and moisture concentration gradients at the centre of the product, and so the following conditions hold:

$$\frac{\partial M}{\partial x} = 0 \quad \text{and} \quad \frac{\partial T}{\partial x} = 0, \quad \text{at} \quad x = 0. \tag{3.13}$$

Heat transfer at the surface boundary occurs by convection to the overlying air, typically modelled through the use of a heat transfer coefficient h. Some heat is also absorbed by the moisture in the transfer to a vapour phase, and the boundary condition at the surface is given by,

$$k\frac{\partial T}{\partial x} - \lambda D\rho_s \frac{\partial M}{\partial x} = -h(T_{sur} - T_{air}) \quad \text{at} \quad x = L(t), \tag{3.14}$$

where λ is the heat of vaporization. The moisture boundary condition at the surface becomes

$$D\rho_s \frac{\partial M}{\partial x} = -h_m(C_{sur} - C_{air}), \quad \text{at} \quad x = L(t). \tag{3.15}$$

3.3.1 Constant diffusivity

The one-dimensional mathematical model discussed in chapter 2 section §2.2 will be used with a shrinkage condition associated with constant diffusion D_0 and heat diffusivity k. The equations are represented by equations (3.10) and (3.11), together with boundary conditions equations (3.12) - (3.15). A complicating factor for the solution is the changing region of the sample, with interface $x = L(t)$ decreasing with drying. To track the interface position, it is convenient to fix its location within a changing coordinate grid [26]. Using the transformation $\xi = \dfrac{x}{L(t)}$, the surface interface corresponds to a fixed value ξ=1, a revised formulation for equations (3.10) and (3.11), in the form of independent state variables (ξ, t), replacing (x, t), become,

$$\frac{\partial M}{\partial t} = \frac{D_0}{L^2(t)}\frac{\partial^2 M}{\partial \xi^2} + \frac{\xi}{L(t)}\frac{dL}{dt}\frac{\partial M}{\partial \xi}, \tag{3.16}$$

$$\frac{\partial T}{\partial t} = \frac{\alpha}{L^2(t)}\frac{\partial^2 T}{\partial \xi^2} + \frac{\xi}{L(t)}\frac{dL}{dt}\frac{\partial T}{\partial \xi}. \tag{3.17}$$

Non-dimensional scaled variables are used: a representative diffusion timescale τ, interface position $s(\tau)$, scaled moisture content $\overline{M}$, and scaled temperature $\overline{T}$ are defined by

$$\tau = \frac{D_0 t}{L_0^2}, s(\tau) = \frac{L(t)}{L_0},$$
$$\overline{M} = \frac{M}{M_0}, \quad \text{and} \quad \overline{T} = \frac{T - T_0}{T_{air} - T_0}.$$

In a non-dimensional formulation, the interface $x = L(t)$ decreases with drying from $x = 1$ to an irreducible final state $x = x_f$, corresponding to the foodstuff reaching a dry state. The resulting system for the moisture and temperature is

$$\frac{\partial \overline{M}}{\partial \tau} = \frac{1}{s^2(\tau)} \frac{\partial^2 \overline{M}}{\partial \xi^2} + \xi \frac{1}{s(\tau)} \frac{ds}{d\tau} \frac{\partial \overline{M}}{\partial \xi}, \tag{3.18}$$

$$\frac{\partial \overline{T}}{\partial \tau} = Le \frac{1}{s^2(\tau)} \frac{\partial^2 \overline{T}}{\partial \xi^2} + \xi \frac{1}{s(\tau)} \frac{ds}{d\tau} \frac{\partial \overline{T}}{\partial \xi}. \tag{3.19}$$

Initial conditions associated with constant conditions are

$$\tau = 0 : \ \overline{T}(\xi, 0) = 0, \ \overline{M}(\xi, 0) = 1, \ s(0) = 1. \tag{3.20}$$

Taking symmetry boundary conditions in the mid-plane of the drying slice gives

$$\xi = 0 : \quad \left(\frac{\partial \overline{T}}{\partial \xi}\right) = 0, \quad \text{and} \ \left(\frac{\partial \overline{M}}{\partial \xi}\right) = 0. \tag{3.21}$$

At the surface, moisture and temperature boundary conditions of the drying body in contact with drying air become

$$\frac{\partial \overline{M}}{\partial \xi} = -s(\tau) \, \overline{Sh} \, \left(\overline{\beta}(\overline{T}_{sur}) f(\overline{M}) - 1\right), \tag{3.22}$$

$$\frac{\partial \overline{T}}{\partial \xi} = -s(\tau) \, Nu \left(\overline{T}_{sur} - 1\right) + \overline{\lambda} \frac{1}{Le} \frac{\partial \overline{M}}{\partial \xi}. \tag{3.23}$$

Using the relationship given by Wang and Brenann [123] which links the surface concentration C_{sur} and surface temperature T_{sur}, the non-dimensional form of equation $f(\overline{M})$ and $\overline{\beta}(\overline{T}_{sur})$ discussed in chapter 2 for air temperature $T_{air} = 60^o$C, is given by,

$$f(\overline{M}) = 84.55 \frac{\overline{M}^{2.38}}{(\frac{0.062}{M_o})^{2.38} + \overline{M}^{2.38}}, \tag{3.24}$$

$$\text{and} \quad \overline{\beta}(\overline{T}_{sur}) = 0.0364 \, \overline{T}_{sur}^2 + 0.0108 \, \overline{T}_{sur} + 0.0119, \tag{3.25}$$

In the above, several non-dimensional controlling parameters are defined by,

$$\overline{Sh} = \frac{h_m\, L_0\, C_{air}}{D_0\, M_0\, \rho_s}, \quad Nu = \frac{hL_0}{k},$$
$$Le = \frac{\alpha}{D_0} \quad \text{and} \quad \overline{\lambda} = \frac{\lambda\, M_0}{C_p\, (T_{air} - T_0)}.$$

3.3.2 Diffusivity dependent on temperature

Taking diffusivity as dependent on temperature $\overline{D}(T)$, equation (3.10) becomes

$$\begin{aligned}\frac{\partial M}{\partial t} &= \frac{\xi}{L(t)}\frac{dL(t)}{dt}\frac{\partial M}{\partial \xi} + \frac{\overline{D}}{L^2(t)}\frac{\partial^2 M}{\partial \xi^2} \\ &\quad + \frac{1}{L^2(t)}\frac{\partial M}{\partial \xi}\frac{\partial T}{\partial \xi}\overline{D}^{'}(T). \end{aligned} \tag{3.26}$$

Using the same non-dimensional scale variable as above, equation (3.26) becomes,

$$\begin{aligned}\frac{\partial \overline{M}}{\partial \tau} &= \frac{1}{s^2(\tau)}\overline{\mathbf{D}}\frac{\partial^2 \overline{M}}{\partial \xi^2} + \xi\frac{1}{s(\tau)}\frac{ds(\tau)}{d\tau}\frac{\partial \overline{M}}{\partial \xi} \\ &\quad + \frac{1}{s^2(\tau)}\overline{\mathbf{D}}^{'}\frac{\partial \overline{M}}{\partial \xi}\frac{\partial \overline{T}}{\partial \xi}, \end{aligned} \tag{3.27}$$

with $\overline{\mathbf{D}} = \dfrac{\overline{D}}{D_0}$, $\overline{\mathbf{D}}^{'} = \dfrac{d\overline{\mathbf{D}}}{d\overline{T}}$.
The equation for heat, the same as equation (3.19), is

$$\frac{\partial \overline{T}}{\partial \tau} = Le\,\frac{1}{s^2(\tau)}\,\frac{\partial^2 \overline{T}}{\partial \xi^2} + \xi\,\frac{ds}{d\tau}\,\frac{\partial \overline{T}}{\partial \xi}. \tag{3.28}$$

Initial conditions associated with constant conditions are

$$\tau = 0:\ \overline{T}(\xi, 0) = 0,\ \overline{M}(\xi, 0) = 1,\ s(0) = 1. \tag{3.29}$$

Taking symmetry boundary conditions in the mid-plane of the drying slice, gives

$$\xi = 0: \quad \left(\frac{\partial \overline{T}}{\partial \xi}\right) = 0, \quad \text{and} \ \left(\frac{\partial \overline{M}}{\partial \xi}\right) = 0. \tag{3.30}$$

At the surface, moisture and temperature boundary conditions of the drying body in contact with drying air become

$$\frac{\partial \overline{M}}{\partial \xi} = -s(\tau)\,\frac{\overline{Sh}}{\overline{\mathbf{D}}}\,\left(\overline{\beta}(\overline{T}_{sur})f(\overline{M}) - 1\right), \tag{3.31}$$

$$\frac{\partial \overline{T}}{\partial \xi} = -s(\tau)\,Nu\,\left(\overline{T}_{sur} - 1\right) + \overline{\mathbf{D}}\,\overline{\lambda}\frac{1}{Le}\,\frac{\partial \overline{M}}{\partial \xi}. \tag{3.32}$$

3.3.3 Diffusivity dependent on moisture and temperature

Taking diffusivity dependent on moisture and temperature $\widetilde{D}(T, M)$, equation (3.10) becomes

$$\begin{aligned}\frac{\partial M}{\partial t} &= \frac{\xi}{L(t)}\frac{dL(t)}{dt}\frac{\partial M}{\partial \xi} + \frac{\widetilde{D}}{L^2(t)}\frac{\partial^2 M}{\partial \xi^2} \\ &+ \frac{1}{L(t)^2}\frac{\partial M}{\partial \xi}\frac{\partial T}{\partial \xi}\widetilde{D}_T \\ &+ \frac{1}{L(t)^2}\frac{\partial M}{\partial \xi}\frac{\partial M}{\partial \xi}\widetilde{D}_M. \end{aligned} \tag{3.33}$$

Using the same non-dimensional scale variable as mentioned above, equation (3.33) gives

$$\begin{aligned}\frac{\partial \overline{M}}{\partial \tau} &= \frac{1}{s^2(\tau)}\widetilde{\mathbf{D}}\frac{\partial^2 \overline{M}}{\partial \xi^2} + \xi\frac{1}{s(\tau)}\frac{ds(\tau)}{d\tau}\frac{\partial \overline{M}}{\partial \xi} \\ &+ \frac{1}{s^2(\tau)}\frac{\partial \overline{M}}{\partial \xi}\frac{\partial \overline{T}}{\partial \xi}\widetilde{\mathbf{D}}'_{\overline{T}} \\ &+ \frac{1}{s^2(\tau)}\frac{\partial \overline{M}}{\partial \xi}\frac{\partial \overline{M}}{\partial \xi}\widetilde{\mathbf{D}}'_{\overline{M}}. \end{aligned} \tag{3.34}$$

with $\widetilde{\mathbf{D}} = \dfrac{\widetilde{D}}{D_0}$, $\widetilde{\mathbf{D}}'_{\overline{M}} = \dfrac{\partial \widetilde{\mathbf{D}}}{\partial \overline{M}}$ and $\widetilde{\mathbf{D}}'_{\overline{T}} = \dfrac{\partial \widetilde{\mathbf{D}}}{\partial \overline{T}}$.
The equation for heat, the same as equation (3.19), is

$$\frac{\partial \overline{T}}{\partial \tau} = Le\,\frac{1}{s^2(\tau)}\,\frac{\partial^2 \overline{T}}{\partial \xi^2} + \xi\,\frac{ds}{d\tau}\,\frac{\partial \overline{T}}{\partial \xi}. \tag{3.35}$$

Initial conditions associated with constant conditions are

$$\tau = 0:\ \overline{T}(\xi, 0) = 0,\ \overline{M}(\xi, 0) = 1,\ s(0) = 1. \tag{3.36}$$

Taking symmetry boundary conditions in the mid-plane of the drying slice, gives

$$\xi = 0: \quad \left(\frac{\partial \overline{T}}{\partial \xi}\right) = 0, \quad \text{and } \left(\frac{\partial \overline{M}}{\partial \xi}\right) = 0. \tag{3.37}$$

At the surface, moisture and temperature boundary conditions of the drying body in contact with drying air become

$$\frac{\partial \overline{M}}{\partial \xi} = -s(\tau)\,\frac{\overline{Sh}}{\widetilde{\mathbf{D}}}\,\left(\overline{\beta}(\overline{T}_{sur})f(\overline{M}) - 1\right), \tag{3.38}$$

$$\frac{\partial \overline{T}}{\partial \xi} = -s(\tau)\,Nu\left(\overline{T}_{sur} - 1\right) + \widetilde{\mathbf{D}}\overline{\lambda}\frac{1}{Le}\,\frac{\partial \overline{M}}{\partial \xi}. \tag{3.39}$$

3.4 Shrinkage condition

For foodstuffs with high moisture content, shrinkage is one of the major changes to take place during the drying process. This complex phenomenon reduces the thickness of the sample and so affects the transfer of heat to the medium and the transfer of moisture to the surface. In this section, a simple mechanism is developed to highlight the effect of shrinkage on drying solutions. Initially it is assumed that no gas phase (air or vapour) is present and that the material consists only of solid and liquid phases. An equation for the shrinkage is obtained from the overall mass conservation balance of liquid in the food, in the absence of any void creation.

Consider that the semi-thickness region of non-porous food is time varying with $L = L(t)$ and given by an integration of the local moisture level and the food solid density value. Taking initially a Cartesian framework with the medium of fixed unit area A and thickness $L(t)$ which comprise liquid and solid compositions, the semi-thickness is given by,

$$A \,.\, L(t) = \int_{V_m(t)} dV,$$

where $V_m(t)$ is material region of the foodstuff.
The time rate of change of the liquid property is defined by

$$\frac{dL}{dt} = \frac{1}{A}\frac{d}{dt}\int_{V_m(t)} dV. \tag{3.40}$$

From the Reynolds transport theorem(see Slattery [109] and Nhan [83]), the general quantity $\psi(x,t)$ is defined as

$$\begin{aligned} \frac{d}{dt}\int_{V_m(t)} \psi(x,t)\, dV &= \int_{V_m(t)} \frac{\partial \psi}{\partial t}\, dV \\ &+ \int_{S_m(t)} \psi\, \mathbf{v.n}\, dS, \end{aligned} \tag{3.41}$$

where $S_m(t)$ is the enclosing surface area, $\mathbf{n}$ is a unit normal to the surface and $\mathbf{v}$ is surface velocity. The first term on the right hand side of equation (3.41) is the rate of change of volume within $V_m(t)$, and the second term is the rate of liquid being transported through the surface. Within this shrinkage model, the flux of liquid that is being transported through the surface is given by

$$\mathbf{v.n} = \text{volume of flux leaving the surface/unit area,}$$

$$\mathbf{v.n} = \frac{\text{mass flux of liquid leaving the surface}}{\text{density of liquid}}.$$

Using the underlying assumption of Fick's Law, and assuming all liquid is evaporated to the air flow at the surface,

$$\mathbf{v.n} = \frac{\rho_s D \dfrac{\partial M}{\partial x}}{\rho_w}. \tag{3.42}$$

Taking (3.41), and using (3.42), and a fixed unit area $A = 1$, the mass balance of liquid in the surface is then given by,

$$\frac{dL}{dt} = \frac{d}{dt}\int_{V_m(t)} dV = \int_{S_m(t)} \frac{\rho_s}{\rho_w} D \frac{\partial M}{\partial x}\, dS. \tag{3.43}$$

For the one-dimensional case, a shrinkage condition is defined by the thickness of the slice ($0 < x < L$). In this instance, shrinkage is in the cross-sectional direction and is given by

$$\frac{dL}{dt} = \left[\frac{\rho_s}{\rho_w} D \frac{\partial M}{\partial x}\right]_{x=0}^{x=L}. \tag{3.44}$$

Noting that $\dfrac{\partial M}{\partial x} = 0$ at x=0, this gives the shrinkage condition to be applied at $x = L$ as,

$$\frac{dL}{dt} = \frac{\rho_s}{\rho_w} D \frac{\partial M}{\partial x}\Bigg)_{x=L}. \tag{3.45}$$

Thus, equation (3.45) provides a conservation requirement for the shrinkage of volume arising from a volumetric loss of moisture, and the numerical solution procedure directly involves the governing equation. This additional shrinkage condition is required to determine the position of the food interface. In transformed and non-dimensional variables the shrinkage condition (3.45),

$$\frac{ds}{d\tau} = \mathbf{D}\,\frac{\rho_s}{\rho_w}\,\frac{M_0}{s(\tau)}\,\frac{\partial \overline{M}}{\partial \xi}, \quad \text{at} \qquad \xi = 1. \tag{3.46}$$

where $\mathbf{D} = 1$ if $\mathbf{D} = D_0$ or $\mathbf{D} = \overline{\mathbf{D}}$ if $\mathbf{D} = \overline{D}(T)$ or $\mathbf{D} = \widetilde{\mathbf{D}}$ if $\mathbf{D} = \widetilde{D}(T, M)$. The speed at which the surface interface reduces is directly dependent on the initial density ratio $\dfrac{\rho_s}{\rho_w}$ and the initial moisture content M_0.

3.5 Numerical solutions

3.5.1 Computational formulation

A numerical solution, such as discussed by Crank [27] for the case of Stefan problem (in which the interface condition is associated with melting at a moving interface), was obtained using the method of lines [102, 4]. Discretizing the fixed integration region $0 \leq \xi \leq 1$ into N sub-intervals, gives a system of 2N+3 ordinary differential equations for $\overline{M}_j(\tau)$, $\overline{T}_j(\tau)$, and shrinkage $s(\tau)$. This system of equations was then solved numerically using MATLAB ODE45 solver, which is based on an order-5 Runge Kutta-Fehlberg Method (RK45).

We consider a special case of $D = D_0$, and using a spatial discretized with N grid point $\xi_j = j\Delta\xi$ with $\Delta\xi = 1/N$.

Discretising equation (3.18) with a central difference approximation becomes

$$\frac{d\overline{M}_j}{d\tau} = \frac{1}{s(\tau)^2}\frac{\overline{M}_{j-1} - 2\overline{M}_j + \overline{M}_{j+1}}{(\Delta\xi)^2} + \xi_j \frac{1}{s(\tau)}\frac{ds}{d\tau}\frac{\overline{M}_{j+1} - \overline{M}_{j-1}}{2\Delta\xi}, \tag{3.47}$$

at general index point j with $\overline{M}_j = \overline{M}(\xi_j)$ for j=1,...,N-1.

To apply the symmetry condition a fictitious grid point at ξ_{-1} is involved and equation (3.47) evaluated at ξ_0 and the value of $\overline{M}_{-1}$ eliminated using the central difference approximation of equation (3.21) as

$$\frac{\overline{M}_1 - \overline{M}_{-1}}{2\Delta\xi} = 0.$$

This gives the condition,

$$\frac{d\overline{M}_o}{d\tau} = \frac{1}{s^2(\tau)}\frac{(2\overline{M}_1 - 2\overline{M}_o)}{(\Delta\xi)^2}. \tag{3.48}$$

Applying the surface condition equation (3.22) by introducing a fictitious grid point at ξ_{N+1} gives

$$\overline{M}_{N+1} - \overline{M}_{N-1} = -2\Delta\xi \times \overline{Sh} \times s(\tau)(\overline{\beta}(\overline{T}_{sur})f(\overline{M}) - 1).$$

Applying a discretization of equation (3.18) at ξ_N and using the above to eliminate $\overline{M}_{N+1}$ in (3.22) gives

$$\begin{aligned}\frac{d\overline{M}_N}{d\tau} &= \frac{1}{s^2(\tau)}\frac{(2\overline{M}_{N-1} - 2\overline{M}_N - 2\Delta\xi\overline{Sh} \times s(\tau)(\overline{\beta}(\overline{T}_{sur})f(\overline{M}) - 1)}{\Delta\xi^2} \\ &\quad + \frac{\xi}{s(\tau)}\frac{ds}{d\tau}(\frac{3\overline{M}_N - 4\overline{M}_{N-1} + \overline{M}_{N-2}}{2\Delta\xi}).\end{aligned} \tag{3.49}$$

A higher order discretization of the gradient term at the boundary is taken inline with the recommendation for the analogous Stefan problem by Furzeland (in Crank [27]). Discretization of the shrinkage condition in equation (3.46) is given by

$$\frac{ds}{d\tau} = \frac{\rho_s}{\rho_w}\frac{1}{s(\tau)}M_o\frac{(3\overline{M}_N - 4\overline{M}_{N-1} + \overline{M}_{N-2})}{2\Delta\xi}. \tag{3.50}$$

Discretising Equation (3.19) with a central difference approximation becomes

$$\frac{d\overline{T}_j}{d\tau} = Le\frac{1}{s^2(\tau)}\frac{\overline{T}_{j-1} - 2\overline{T}_j + \overline{T}_{j+1}}{(\Delta\xi)^2} + \xi_j\frac{1}{s(\tau)}\frac{ds}{d\tau}\frac{\overline{T}_{j+1} - \overline{T}_{j-1}}{2\Delta\xi}, \tag{3.51}$$

at a general index point j with $\overline{T}_j = T(\xi_j)$for j=1,...,n-1 and $Le = \dfrac{\alpha}{D}$.
To apply the symmetry conditions, a fictitious grid point at ξ_{-1} is involved and equation (3.51) evaluated at ξ_0 and the value of $\overline{M}_{-1}$ eliminated using the central difference approximation of equation (3.21) as

$$\frac{\overline{T}_1 - \overline{T}_{-1}}{2\Delta\xi} = 0.$$

This leads to the condition,

$$\frac{d\overline{T}_o}{d\tau} = Le\frac{1}{s^2(\tau)}\frac{(2\overline{T}_1 - 2\overline{T}_o)}{(\Delta\xi)^2}. \tag{3.52}$$

Applying the surface condition equation (3.23) by introducing a fictitious grid point at ξ_{N+1} gives

$$\overline{T}_{N+1} - \overline{T}_{N-1} = -2\Delta\xi \times Nu \times s(\tau)(\overline{T}_{sur} - 1) + \overline{\lambda}\frac{1}{Le}(3\overline{M}_N - 4\overline{M}_{N-1} + \overline{M}_{N-2}).$$

Applying a discretization of equation (3.18) at ξ_N and using the above to eliminate $\overline{M}_{N+1}$ in (3.23) gives

$$\begin{aligned}\frac{d\overline{T}_N}{d\tau} &= \frac{Le}{s^2(\tau)}\Big[\frac{2\overline{T}_{N-1} - 2\overline{T}_N - 2\Delta\xi Nu \times s(\tau)(\overline{T}_{sur} - 1) + \overline{\lambda}\frac{1}{Le}(3\overline{M}_N - 4\overline{M}_{N-1} + \overline{M}_{N-2})}{\Delta\xi^2}\Big] \\ &\quad + \frac{\xi}{s(\tau)}\frac{ds}{d\tau}\Big(\frac{3\overline{T}_N - 4\overline{T}_{N-1} + \overline{T}_{N-2}}{2\Delta\xi}\Big).\end{aligned} \tag{3.53}$$

3.5.2 Input parameters

The non-dimension parameters used in the equations for the generic drying condition for tropical foods are listed in Table 3.1 and these correspond to the typical values of tropical fruits, as discussed in chapter 2 (section §2.3 for a non shrinkage model).

Table 3.1: Drying conditions and product properties used in the simulation.

Product	Properties
C_{air}	0.025625 kg/m^3 based on T=60^{o}C and RH=20%
M_0	0.8 kg water/kg moist sample
Sh number	20
Le number	5
Nu number	0.3
$\overline{\lambda}$	0.5

3.6 Results of drying of tropical fruits

The analysis of transport phenomenon presented here is based on the time evolution of variables, i.e. the non-dimension moisture content and temperature at each exposed surface. As an example, we undertake the simulation study for moisture transfer during drying of a moist slab of tropical fruits to predict the moisture profile inside the food. The simulations are divided into two parts. In the first simulation, a constant value of effective diffusivity was taken. Simulation at different values of diffusivity, $\overline{D}(T)$ and $\widetilde{D}(T, M)$ were used to show how diffusivity influences the drying process and, in particular, the drying rate.

3.6.1 Constant diffusivity $D = D_0$

In this part, simulation of a system of equations (3.18)-(3.23) and (3.46) with a value of diffusivity is taken as constant $D = D_0$. The present model was used to predict the moisture distribution inside the solid. Moisture within the food is initially scaled to unity and a final steady state close to zero is eventually reached. Figure 3.1 shows the moisture distribution as a function of both position ξ and drying time τ, during drying. The drying air temperature is used in the non-dimensional model through C_{air} as given by [47], and depends on the air temperature and partial pressure. Simulation results show the highest moisture content in the centre of the product, decreasing monotonically to the lowest level at the surface of the product. The reduction rate of

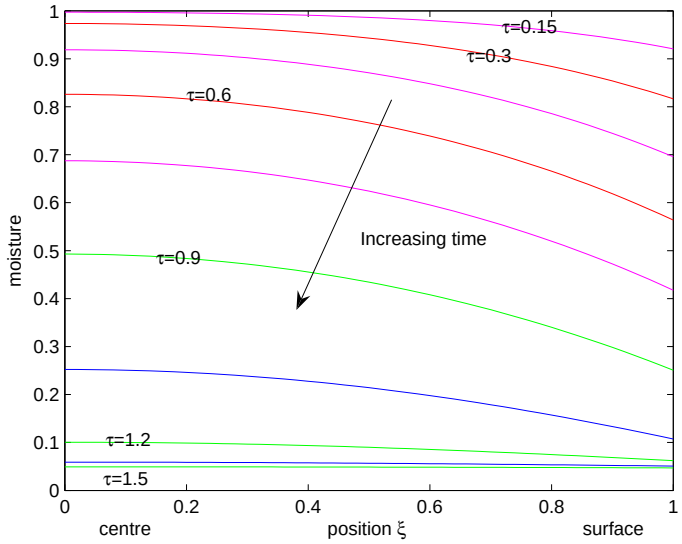

Figure 3.1: Non-dimension moisture content profile inside the food slab with increasing τ. Parameter values given by $Sh = 20$, $Le = 5$, Nu=0.3, $\overline{\lambda} = 0.5$.

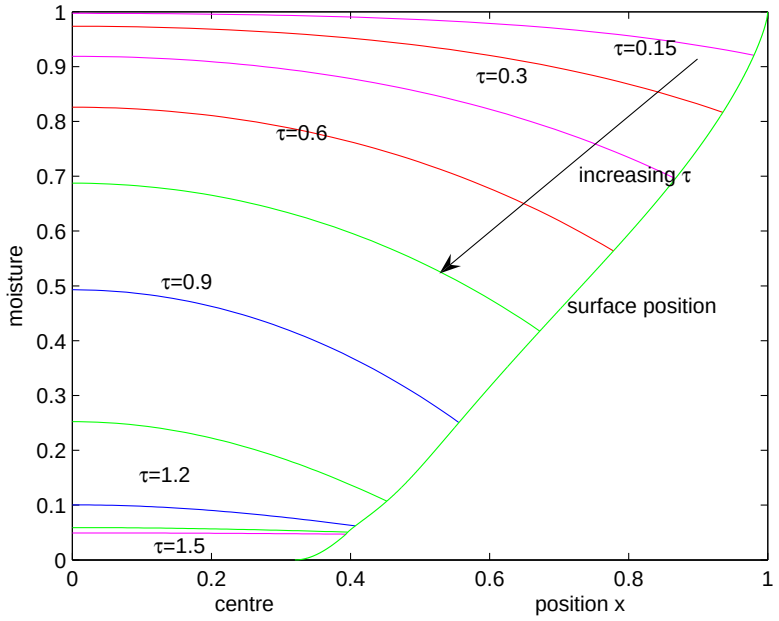

Figure 3.2: Non-dimension moisture content profile inside the food slab with increasing τ in terms of physical Cartesian distance x. Parameter values the same as Figure 3.1.

moisture in the region near the surface is higher than the interior of the object because of the high initial moisture gradient in this region, which drives diffusion from the inside to the surface. Moreover, in the early drying period ($\tau < 1.2$), the moisture content reduces rapidly. Due to the diffusion limitation of the drying process, the surface moisture content reaches the equilibrium value almost immediately and, as the drying period progresses ($1.2 < \tau < 1.5$), the rate of reduction of moisture content becomes almost steady before settling slowly to show release of residual moisture.

Figure 3.2 shows the corresponding moisture distribution prediction in terms of physical Cartesian distance x and includes the location of the free surface during shrinkage. These profiles identify that the surface quickly reaches equilibrium when a moisture gradient is developed between the surface and the rest of the sample. The shrinkage of the product is shown by the change in the thickness of the sample. In the early drying period ($\tau < 0.15$), the moisture content reduces rapidly near the surface and establishes a gradient through out the slab and shrinkage is relatively small. For the period $0.15 < \tau < 1.2$, the rate increases rapidly, moisture content reduces steadily throughout and shrinkage moves to a period of almost constant rate before finishing at the expected end position. The final value of shrinkage in this model can be determined readily as only solid mass is left at the end of drying. This situation corresponds to ideal shrinkage, where the decrease of material volume is equal to the volume of water removed. In the case of a real food system, not all liquid is removed and the calculations are terminated when an irreducible value of moisture content inside the food is reached (e.g. see [48]).

The evolution of moisture content at early times and longer times is given in Figure 3.3. At early times, the decrease in moisture is influenced by wet moisture at the surface and a small decrease in size (length) of the body. At later times, when the moisture content is very low, the decrease in moisture is influenced by drying air and a very small decrease in size can also be observed.

Simultaneously, calculation of food temperature is made within the varying food regions. Temperature is initially constant, scaled to zero and reaches a final steady value of $T = 1$. Figure 3.4 shows temperature profile in the food as function of both position and time, during drying. Temperatures at each location increase with drying time, which is due to the higher drying air temperature. The temperature

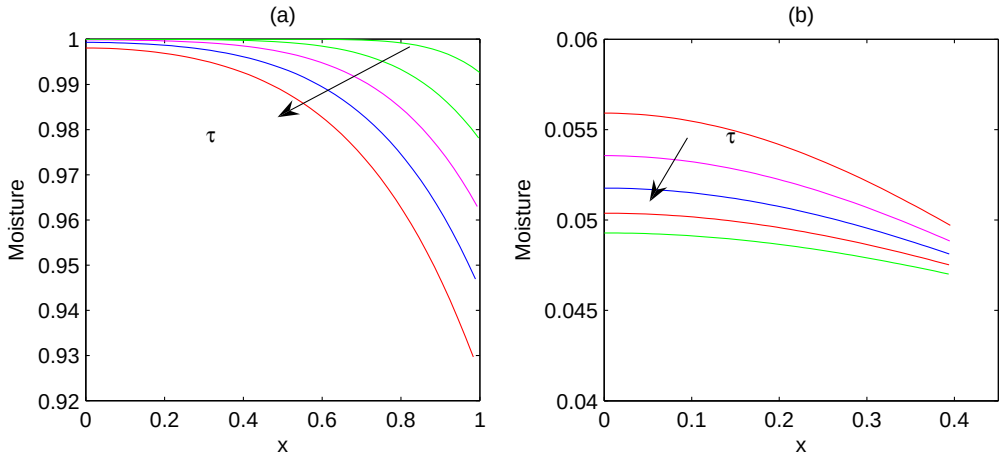

Figure 3.3: Evolution of non-dimension moisture content profile inside the food slab with increasing τ in term of physical Cartesian distance x for (a) early times:τ=0-0.135 with little shrinkage and (b) longer times: τ=1.38-1.5 (in step τ=0.03) with nearly full shrinkage. Parameter values the same as Figure 3.1.

gradient between the centre and the surface decreases with drying time. It was found that the temperature profile rises rapidly in the early period of heating ($\tau < 0.5$) due to the difference between air temperature and food temperature. As the heating period progresses $0.5 < \tau < 1$, the rise in temperature attains an almost uniform profile. This arises because the surface has high moisture and most of the heat is used for evaporation near the surface. This behaviour is controlled by the value of $\overline{\lambda}$: the bigger the value of $\overline{\lambda}$, the slower the increase in temperature. After some time ($\tau > 1.2$), when the surface moisture becomes low, the increase in temperature become faster. Subsequently, only a small quantity of heat is used for evaporation and the increase in heat flux raises the food temperature.

The temperature profiles in the sample at a Cartesian distance x including shrinkage are presented in Figure 3.5 and identify further that the temperature rises rapidly in the early period of heating ($\tau < 0.5$). As heating progresses and the shrinkage reduces the distance between the surface and the centre, the rise in temperature is relatively slow and almost uniform. At the end of drying, the temperature rises rapidly throughout the food as only small quantities of heat are needed for evaporation.

Figure 3.6 compares the position of the food surface with different initial moisture contents. The shrinkage equation (3.46) arising from volumetric loss of moisture,

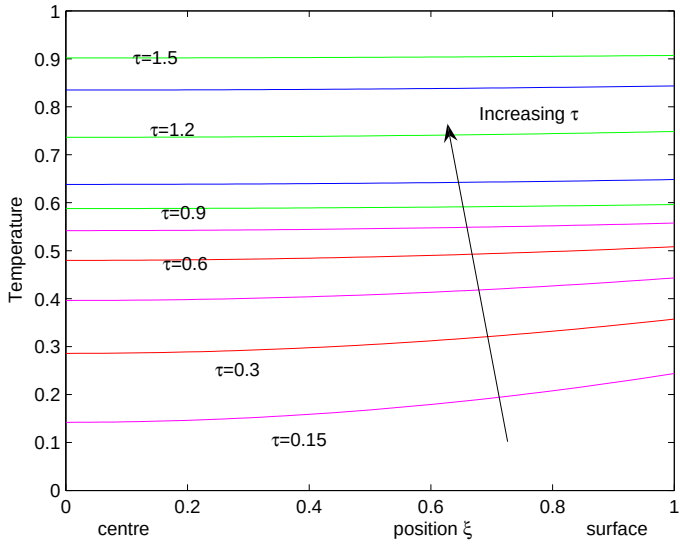

Figure 3.4: Non-dimension temperature profile inside the food slab with increasing τ. Parameter values the same as Figure 3.1.

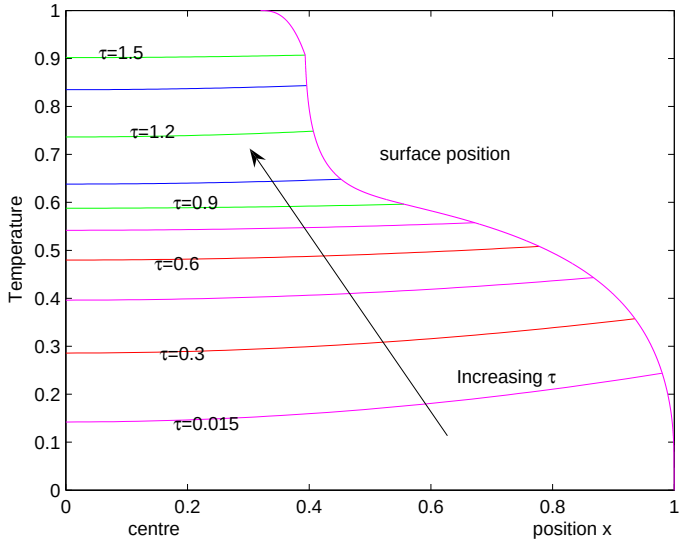

Figure 3.5: Contour profile of temperature for non-dimensional time τ and surface position x. Parameter values the same as Figure 3.1.

$\frac{\rho_s}{\rho_w}\frac{M_0}{s(\tau)}\frac{\partial \overline{M}}{\partial \xi}$ and reduced of interfaces is directly dependent on initial density ratio $\frac{\rho_s}{\rho_w}$ and initial moisture content M_0. It can be observed that the shrinkage profiles are self-similar and a constant rate of shrinkage can be observed before finishing at the expected end position.

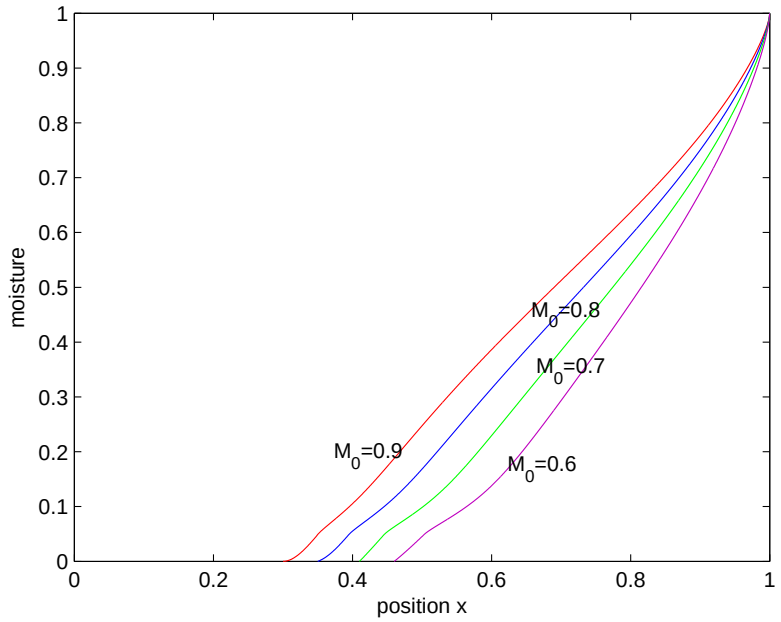

Figure 3.6: Position of food surface with different initial moisture content.

Figure 3.7 represents the comparison of moisture and temperature gradients at the centre of the fruits, with and without shrinkage effect. It can be seen that the temperature without shrinkage predicts a higher temperature at a specific time compared to that with shrinkage especially at the beginning of drying. Figure 3.7 also shows that the predicted moisture content was lower when the shrinkage effect was included in the model. Therefore, the model with shrinkage needs a shorter time for drying. Physically, the thickness of the sample decreases due to shrinkage and, correspondingly, the moisture has less distance to cover and hence reaches the surface faster, before it can diffuse to the air. This is consistent with findings reported by Wang and Brenann [124] of the shrinkage effect on drying behavior.

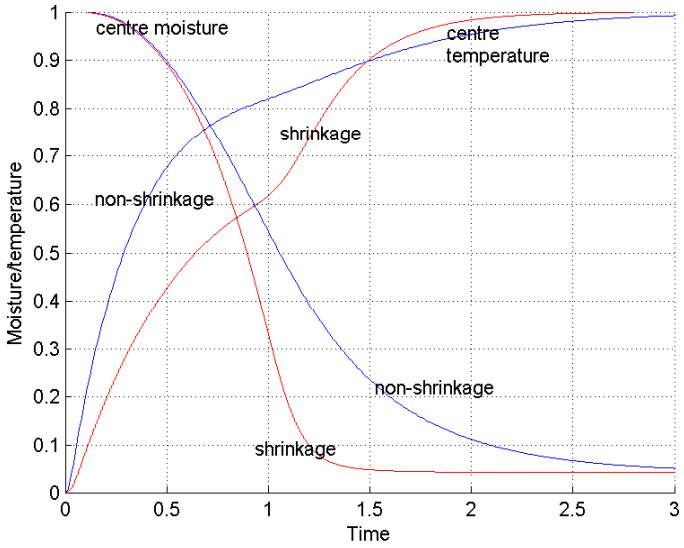

Figure 3.7: Profile of temperature and moisture at the centre of the food, with and without shrinkage effect. The non-shrinkage model refers to equations (2.17)-(2.20). Parameter values the same as Figure 3.1.

3.6.2 Diffusivity dependent on moisture and temperature $D = \overline{D}(T)$ and $D = \widetilde{D}(T, M)$

There is experimental evidence that the shrinkage extent during drying is strongly related to drying conditions [76]. These relations are expressed in the form of the glass transition temperature theory ([96, 67]). The glass transition theory is one of the concepts proposed to explain the process of shrinkage and collapse during drying. According to the concept, there is negligible collapse (of pores) in material below the glass transition temperature, and the higher the difference between the process temperature (air temperature) and the glass temperature, the higher the degree of collapse. In this way, the material may undergo transition from the glassy to the rubbery state; the lower the drying temperature, the quicker this transition occurs. As this transition restricts the volume reduction (shrinkage), lower drying temperatures lead to lower shrinkage extent values and, as a consequence, higher material porosities. This theory gives only the effect of the temperature of the material during the drying. However, as water possesses a plasticizing effect in amorphous materials, the higher moisture content may lower the glass transition temperature of the solid

[96]. Furthermore, during drying, moisture content will decrease, leading to an increased glass transition temperature [96]. This is due to the strong plasticizing effect of water; the material undergoes this transition only towards the end of drying [67]. Bodhrioua *et al.* [14] reported a glass transition temperature for dried Cavendish sp. bananas of approximately 40^oC. Thus, the samples dried above this temperature become malleable at low moisture content and undergo unrestricted shrinking. Samples dried below this temperature become rigid, as moisture content approaches to zero and, therefore, have lower volume reduction (less shrinkage) [67]. For example, at 30^oC, the material undergoes a glass transition for all the conditions and, therefore, it presents lower volume reduction(less shrinkage). At 40^oC, the transition probably occurs at a later instant, in a way that the material shrinks more before becoming glassy. At 50^oC, the material does not undergo transition and shrinks during the entire process.

This phenomenon could be considered to be directly related to the drying temperature during the process and affected, in particular by the diffusion coefficient of the food. An experimental study by Rahman *et al.* [97] stated that, in the glass transition region, an increase in effective diffusivity was detected and, in the rubbery region, diffusivity remained nearly constant. Diffusivity in the rubbery region is higher than that in the glassy region. In this section, a simulation was performed to learn more about the theory of glass transition. Different values of diffusivity were put into the model to evaluate the effect of glass transition. The variation in effective diffusivity as a function of temperature $\overline{D}(T)$, and a function of material moisture content and temperature $\widetilde{D}(T, M)$, is given in section §1.3.2, by

$$\widetilde{D}(T, M) = 1.29 \times 10^{-6} \exp(\frac{-2044}{T}) \exp(\frac{-0.0725}{M}). \tag{3.54}$$

In a non-dimension form

$$\begin{aligned} \widetilde{\mathbf{D}}(\overline{T}, \overline{M}) &= \frac{\widetilde{D}(T, M)}{\widetilde{D}(T_0, M_0)} \\ &= 934.13 \exp(\frac{-0.090625}{\overline{M}}) \exp(\frac{-2044}{30\overline{T} + 303}) \end{aligned} \tag{3.55}$$

To put only effect of temperature to diffusivity, we assume moisture treated as constant $M = M_0 = 0.8$ (initial moisture content), the diffusivity is dependent only on

the value of temperature $D = \overline{D}(T)$ given by,

$$\overline{D}(T) = 1.178 \times 10^{-6} \exp(\frac{-2044}{T}). \tag{3.56}$$

In a non-dimension form,

$$\begin{aligned} \overline{\mathbf{D}}(\overline{T}) &= \frac{\overline{D}(T)}{\overline{D}(T_0)} \\ &= \exp(\frac{202.38\overline{T}}{30\overline{T} + 303}) \end{aligned} \tag{3.57}$$

In this part, the simulation will be based on the system of equations (3.27)-(3.32) and (3.46) for diffusivity dependent on temperature and equations (3.34)-(3.39) and (3.46) for diffusivity dependent on temperature and moisture with the value of diffusivity above: (3.55) and (3.57). The overbar notation in the graph is dropped as clarity.

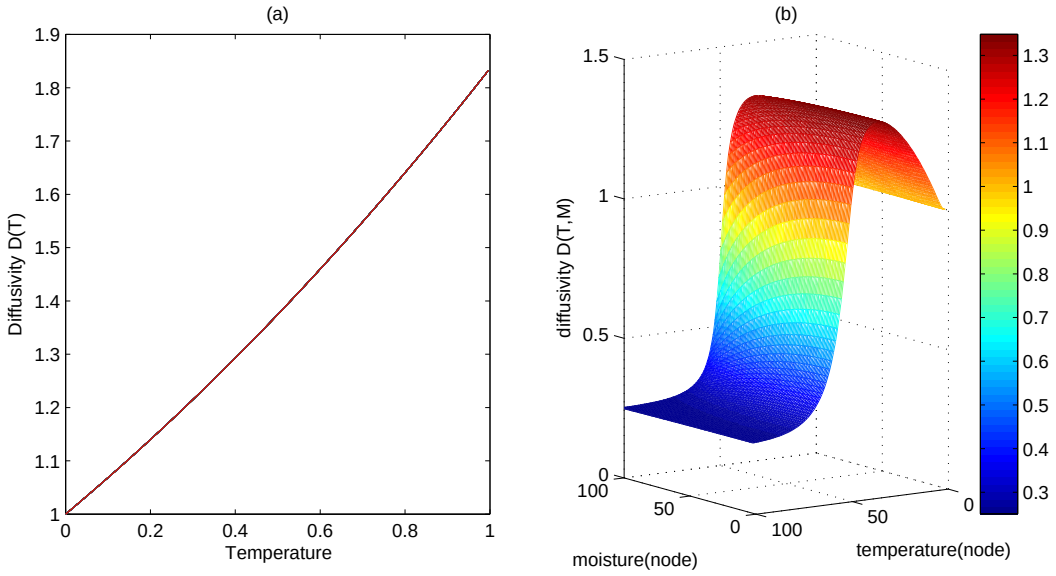

Figure 3.8: Diffusivity plot of $\overline{D}(\overline{T})$ and $\widetilde{D}(\overline{T}, \overline{M})$.

Dependency of the diffusion coefficient on local moisture content and temperature brings physical changes to the food, which arise from heating. This phenomenon could be considered as directly related to the drying temperature during the process and affects in particular the diffusion coefficient of the material. A profile of diffusivity with different local moisture and temperature is shown in Figure 3.8. Figure 3.8(a) shows that increased temperature gives increased diffusivity $\overline{\mathbf{D}}(\overline{T})$. An experimental

study also suggests that samples drying below 60^{o}C are in the glassy state and drying above 80^{o}C, in the rubbery state [3]. In the glassy sate, the diffusivity increases significantly (for example see [97, 95]) and is consistent with Figure 3.8(a).

Figure 3.8(b) shows the influence of moisture and temperature on diffusivity. At the beginning, as moisture $\overline{M} = 1$ and the temperature $\overline{T} = 0$, the diffusivity is scaled to $\widetilde{\mathbf{D}}(\overline{T}, \overline{M})$=1. As time increases, the temperature increases and moisture decreases, which leads to increases in diffusivity until a certain time. Furthermore, as the moisture continues to decrease, the diffusivity starts to decrease and is then constant at the end of drying. A present result similar to that of Rahman *et al.* [97], comes to the conclusion that diffusivity increases significantly at the beginning of drying and is constant during the end of drying.

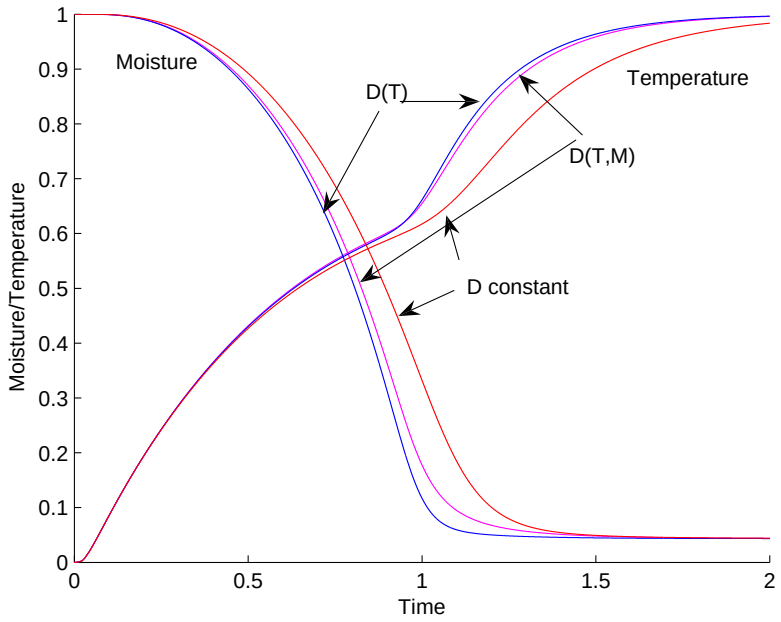

Figure 3.9: Moisture and temperature in the centre of the fruits with different diffusivity. Non-dimension parameter values given by $Sh = 20$, $Le = 5$, Nu=0.3, $\overline{\lambda} = 0.5$.

A profile of the moisture content and temperature at the centre of the fruit is presented in Figure 3.9. It can be observed that the moisture content shows a rapid decrease when diffusivity is dependent on temperature and diffusivity is dependent on moisture and temperature were taken in the model. This profile identifies that the

variation in moisture and temperature inside the product influences liquid diffusivity movement to the surface, which affects the rate of moisture diffusion in the food and is consistent with experiment findings [3]. From Figure 3.9, at the beginning of drying process ($0 < \tau < 1$), the temperature of the food increases slowly; at this time, most of the heat is used to evaporate water at the surface. About 70% of the water has evaporated. For a fruit such as mango, with high sugar, the glass transition temperature Tg is very low [9], at the beginning when the temperature is at Tg, the food is in the glassy state. At this T_g, diffusivity increases significantly (Figure 3.8). This increase allows the movement of water molecules to increase more freely, hence the moisture content reduces rapidly within this period. At the end of drying, when moisture becomes low, most of the heat is used to raise the temperature of the fruit, hence temperature rises rapidly ($1.3 < \tau < 2$). At this stage, the fruit is in the rubbery state, and molecule movement is low at this high viscosity [1]. This leads to a slow reduction in moisture at the end of drying.

In order to understand the glass transition phenomena, we used the diffusivity $\widetilde{D}(\overline{T}, \overline{M})$ in the model. We have little direct evidence of the biological mechanisms of drying behavior unless a morphological study is done. However, conclusions from the physical data can be drawn in the light of existing knowledge in biology. For example, cases based on a value of glass transition beginning at temperature 25^oC with moisture content 25% are given by [96], so we change the diffusivity $\widetilde{D}(\overline{T}, \overline{M})$ using a logistic function for a smooth approximation to a step function, with the value of K=0.5. The transition occurring at 25% moisture, gives

$$\widetilde{\mathbf{D}}(\overline{M}, \overline{T}) = D_1 + D_2 Tanh(K \times (\overline{M} - 0.25)), \tag{3.58}$$

with $D_1 = 667.067 \exp(\frac{-0.090625}{\overline{M}}) \exp(\frac{-2044}{30\overline{T} + 303})$

and $D_2 = 267.065 \exp(\frac{-0.090625}{\overline{M}}) \exp(\frac{-2044}{30\overline{T} + 303})$

Based on values of glass transition that begins at temperature 25^oC with moisture content 25% [96], the value of diffusivity against moisture and temperature is given by Figure 3.10. From the figure it can be observed that diffusivity is increased when the temperature exceeds the glass transition and continues to increase with a rise in temperature. It is noted that, at certain levels of moisture content, diffusivity starts to slow down because movement of water molecules is decreased.

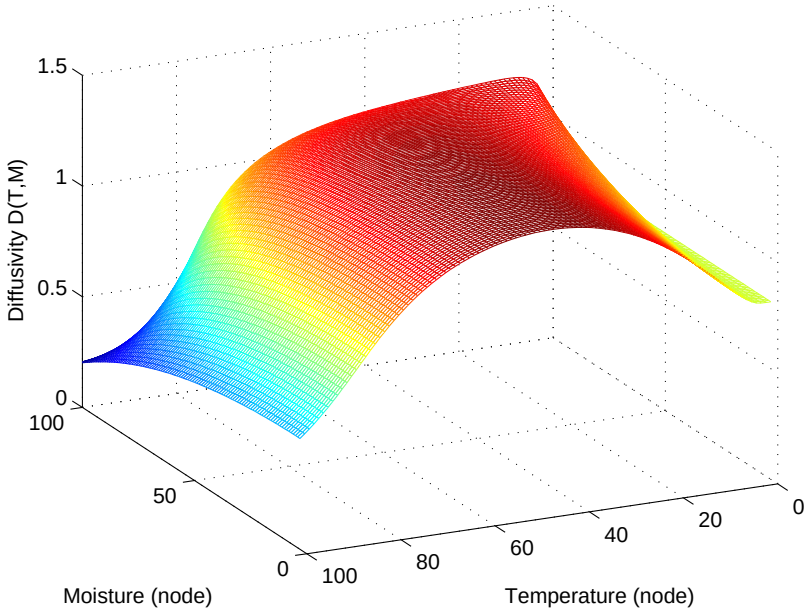

Figure 3.10: Diffusivity plot dependent on temperature and moisture using logistic function.

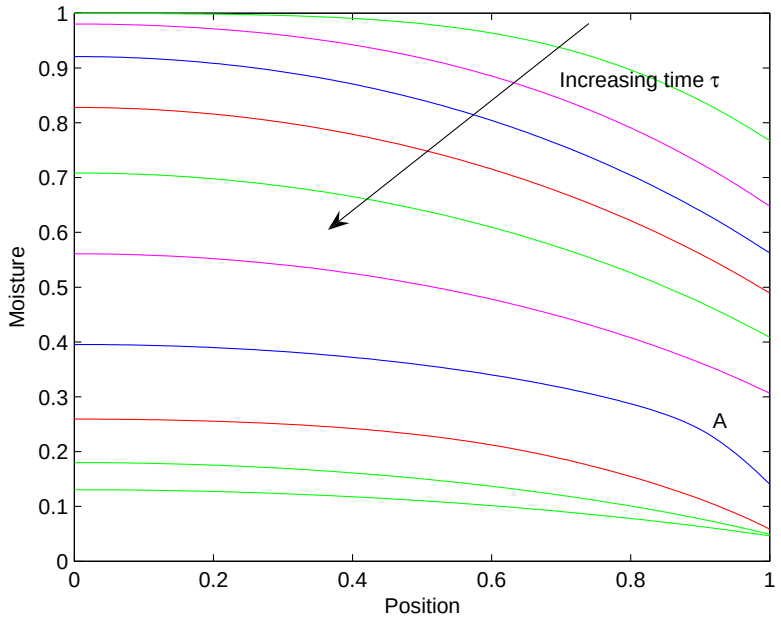

Figure 3.11: Profile of moisture inside the food slab with elapsed time τ=0-1 in step of 0.1 with effect of glass transition.

The region of moisture at around 25% where the glass transition is evident is given by Figure 3.11. From Figure 3.11, it can be observed that moisture drops rapidly (point A) near the surface when the glass transition happens at time $\tau = 0.8$. This is consistent with the experiment finding [67] that glass transition occurs at the end of drying. The contour plot of the region where the rubbery and glassy state

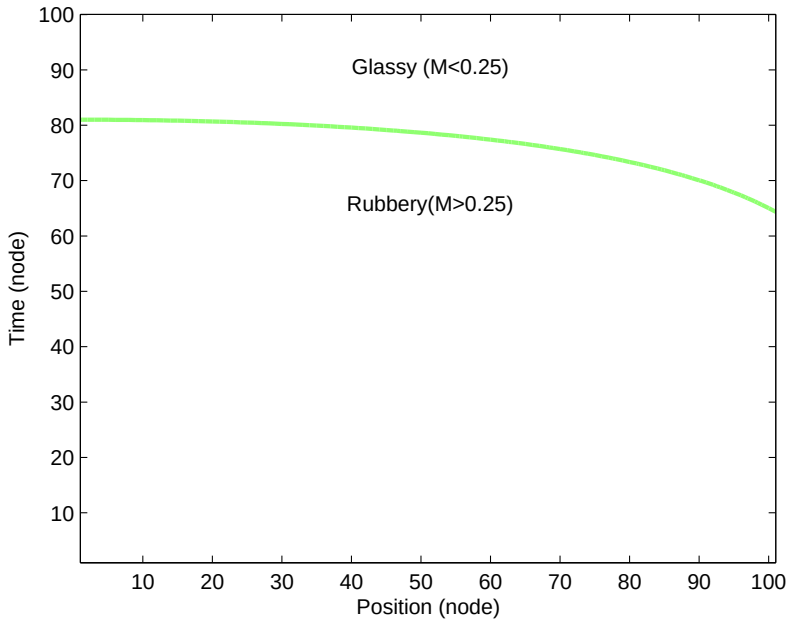

Figure 3.12: Contour plot of the region showing the rubbery and glassy states.

is given by Figure 3.12. At the centre the transition from rubbery to glassy state happen at time ($\tau = 0.81$) but at the surface this transition at time $\tau = 0.65$. From the plot it can be seen that the transition from rubbery to glassy occurs at the end of drying.

3.7 Model validation

Closely coupled with an accurate formulation of the problem is validation of the model computations. This can comprise a mesh convergence study, checking for mistakes, checking if the results can be explained using common-sense physics and comparing the results with experimental data.

3.7.1 Time step and numerical accuracy

In simulations, convergence of the numerical results was verified through mesh convergence, going up to 500 nodes in the 1 non-dimensional thickness to achieve a statistically accurate and converged solution. The input parameters used in this study are shown in Table 3.1. The number of nodes analysed include 50 and 500. The time step used in the simulation is 0.03 in terms of non-dimension time steps. Simulation of system (equations (3.18)-(3.23) and (3.46)) were used for constant diffusivity and results obtained using ODE45. Figure 3.13 illustrates the effects of changing the number of nodes on moisture and temperature distribution. The effects of changing the numbers of mesh on moisture and temperature gives an absolute error of 10^{-3}. From this plot, the results for various numbers of nodes agree well.

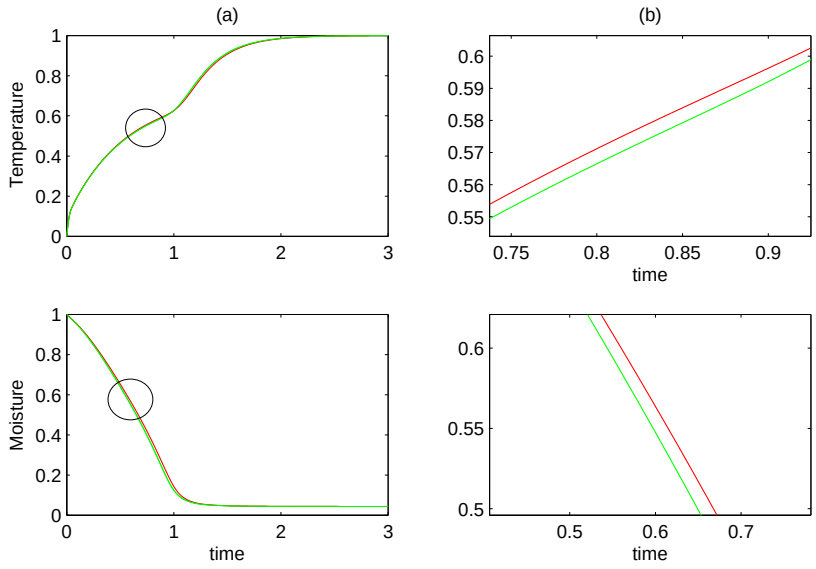

Figure 3.13: Convergence checks for different numbers of nodes and mesh refinement. (a) Evolution of moisture and temperature at the surface position (b) a magnified region to show the detail more clearly.

The numerical test was also conducted using different time steps: fixing the value of the node as 500, with time steps of change from 50 to 100. Figure 3.14 illustrates the effects of changing the number of time steps on moisture and temperature. The effects of changing the number of time steps on moisture and temperature gives an

absolute error of 10^{-6}. From this plot, the results from different numbers of time steps agree well.

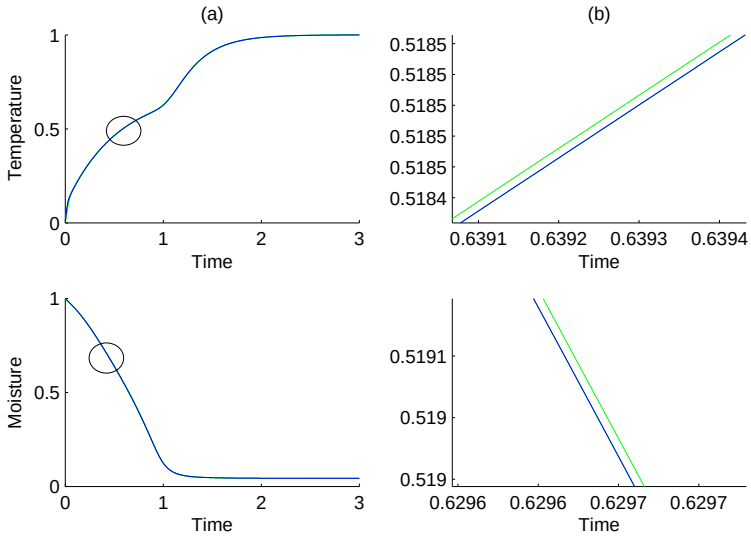

Figure 3.14: Convergence checks for different numbers of time steps. Non-dimension moisture content and temperature profile inside the food slab with increasing τ.

3.7.2 Comparison with the literature data

Many authors report results from drying experiments; these differ in terms of food types, geometrical shape and range of air temperature, air humidity and air velocity. In this section, as well as the numerical simulation carried out, a comparison is undertaken with the specific aim of verifying the model. This was attained by checking the agreement between the model's theoretical prediction and a set of experiment data found in the open literature for the drying of fruits and vegetables.

In synthesis, the non-dimension equations (3.18)-(3.23), together with equation (3.46) for constant diffusivity, represent a general description of food drying behaviour. The non-dimension numbers included in this equation Sh, Le, Nu and $\overline{\lambda}$ used in numerical solution to predict heat and mass during food drying, as given in the Table 3.1. Comparison was made with Pavón *et al.* [90], who conducted a non dimensional analysis for drying heat and mass transfer during the drying of food,

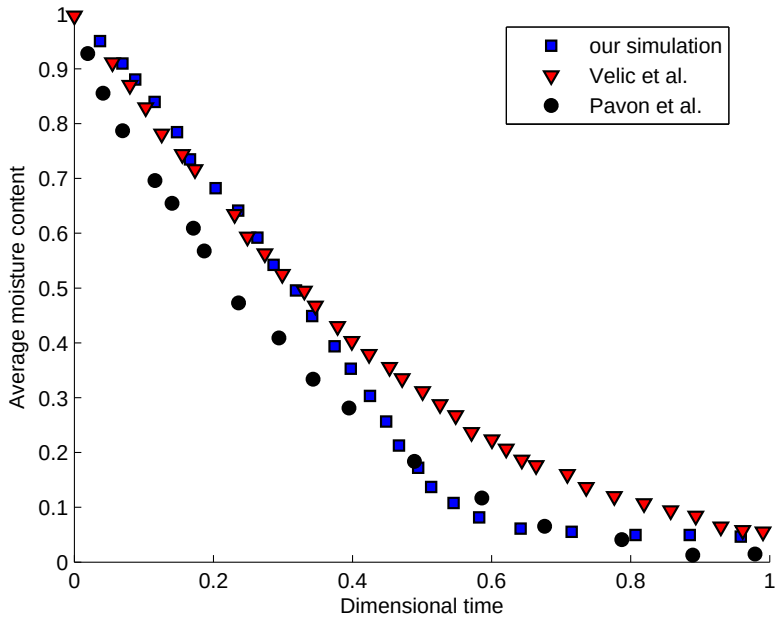

Figure 3.15: Comparison between numerical solutions for average moisture with experimental data from the literature by Pavón *et al.* [90] and Velic *et al.* [118]. Dimensional parameter values for our model given by $Sh = 20$, $Le = 5$, Nu=0.3, $\overline{\lambda} = 0.5$.

along with Velic *et al.* [118]. An experiment test was performed on mango slices to find the average moisture and temperature evolution during drying, with air temperatures 70^{o}C and 50^{o}C, slab thickness 0.75 and air velocity 1.75 m/s, and by Velic *et al.* [118] for drying apple slices with air velocity=1 m/s, temperature=60^{o}C, Relative humidity, RH=9%, length=5mm. Their results were compared with our numerical solution. Figure 3.15 shows the comparison between the experiment results of average moisture and model prediction without any parameter adjustment. There is remarkable agreement at the beginning, especially with Velic *et al.* during the first non dimensional time 0.4 when experimental data and theoretical predictions overlap. Later on, a slight deviation with Velic *et al.* can be observed but there is an overlap with Pavon *et al.*.

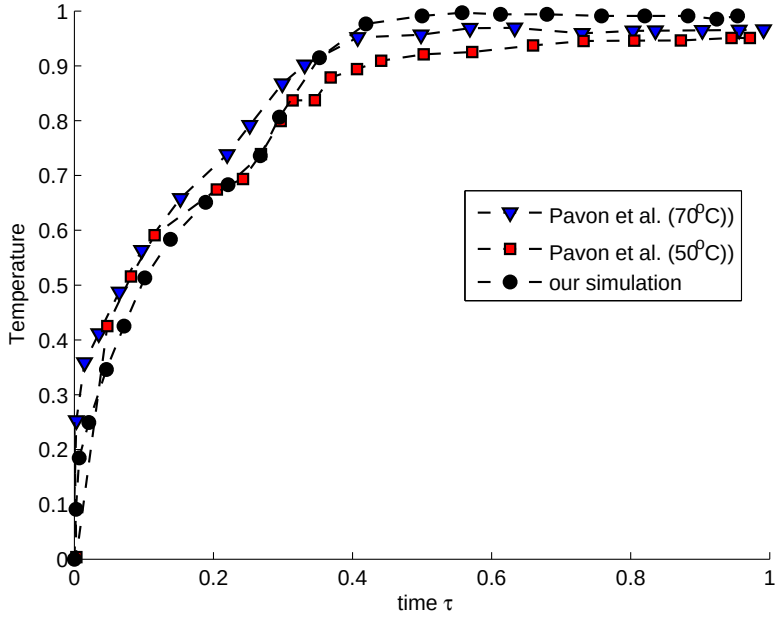

Figure 3.16: Comparison between numerical solutions for surface temperature with experimental data from the literature by Pavón-Melendez *et al.* [90]. Non-dimension parameter values for our model are given by $Sh = 20$, $Le = 5$, Nu=0.5, $\overline{\lambda} = 0.5$.

Figure 3.16 shows the comparison for surface temperature experiment data (Pavon *et al.* 70^{o}C and 50^{o}C, thickness=0.5cm air velocity=1.75m/s) with model prediction at the surface. Good agreement is observed at the beginning, but deviating for the

middle non-dimension time before the trends becoming similar at the end. From this Figure, some difference can be observed at the end of drying where our model predicts a slightly higher temperature, but the difference is in the magnitude of the experiment dispersion. A slight deviation can therefore describe the effect of shrinkage in our model at the end of drying.

In order to make more comparison with the other shrinkage model, the numerical results of predicted moisture profile during the drying of apple, based on Crapiste *et al.* [29] in terms of reduced coordinates following shrinkage, are shown in Figure 3.17(b). The moisture profiles are shown versus the non-dimension spatial coordinate $x = \frac{\xi}{L_o}$. The numerical solutions are provided by Chemkhi *et al.* [20] for the drying of potato (Figure 3.17(a)). The numerical solution of this model is shows in 3.17(c). From Figure 3.17, we can conclude that the shrinkage conditions show a similar pattern but the models differ from each other. Chemkhi *et al.* consider elastic deformation, and Crapiste *et al.* consider employing density values to account for shrinkage velocity as a function of moisture content. It is noted that Crapiste *et al.* consider an isothermal model, i.e. without the effect of temperature.

3.8 Summary and conclusions

We have developed a mathematical model describing simultaneous heat and mass transfer processes with the effect of shrinkage during the drying of food products with high moisture content. The shrinkage condition was developed on the basis of a simple mechanism of volume of evaporated water that takes place during drying. In this model, the shrinkage effects were put into models of heat and mass transfer without resorting to any externally imposed empirical correlation. A numerical solution of the model equation was produced and temperature and moisture distribution with the embedded effect of shrinkage using direct conservation were predicted.

First, we studied the case for diffusivity as constant. Using a numerical solution, the behaviour of moisture and temperature subject to shrinkage was predicted for constant diffusivity. We show that moisture content decreased more quickly than in the non shrinkage model (chapter 2), which concludes that the model with shrinkage effect needs a shorter time for drying and is consistent with experiment findings

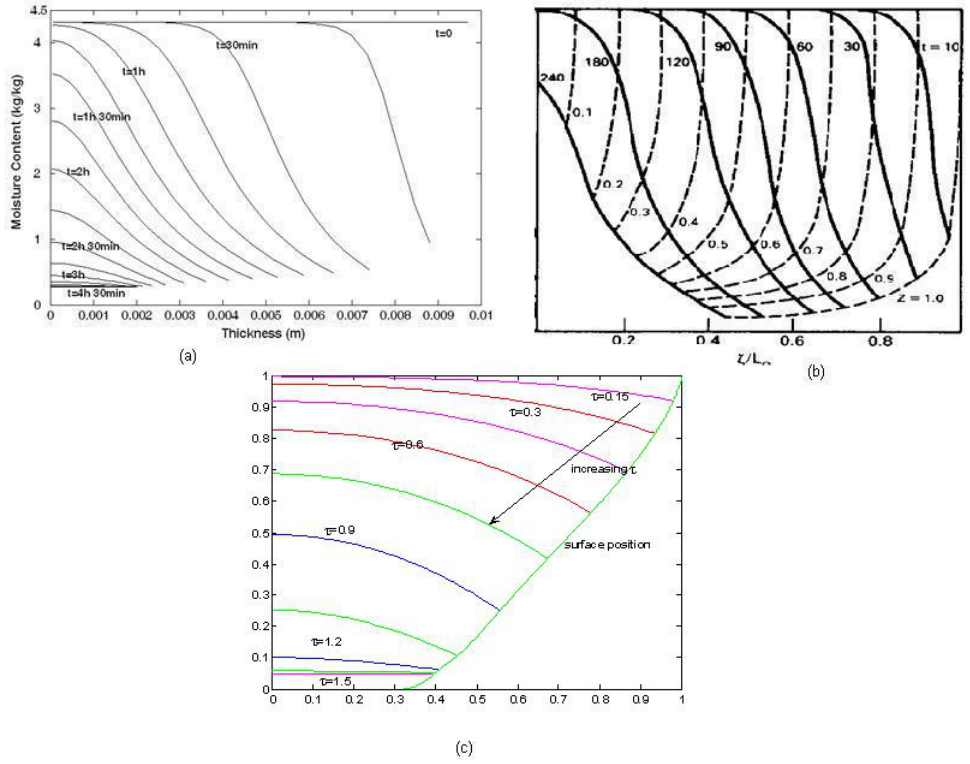

Figure 3.17: Simulated moisture content profiles versus x of the 1D moisture transport problem. (a) Chemkhi *et al.* [20], (b) Crapiste *et al.*[29], (c) this model.

[122, 107]. An example results in giving the shrinkage values from 1.0 to 0.28 for the initial moisture content $M_0 = 0.8$. In an extreme case, in which all liquid in the product is removed, shrinkage is about 72% of initial volume. Our model is consistent with the experiment findings by Yan *et al.* [132], which show that a mango slice shrank during drying to 17% wet base (83% of initial volume), and a banana [55] shrank to 77% of its initial volume. Results show that the model incorporating the effect of shrinkage is capable of describing the behaviour of moisture and temperature in the food during drying.

Experiment results from [97, 95, 71] indicate that diffusivity increases with a higher drying temperature, which speeds up the drying rate [95, 67]. Reduced moisture content will increase the glass transition temperature [97] and decrease the drying rate. Based on the experiment results, the model formulation was further extended to account for differences in diffusivity. This was achieved by replacing the constant diffusivity (D_0) with an appropriate functional form. Modification of diffusivity was put into the model and we studied cases in which diffusivity was dependent on temperature and cases in which diffusivity dependent on moisture and temperature. Simulations were presented, showing that the moisture decrease is profoundly altered by these effects, reducing much faster than constant diffusivity. This is consistent with the findings in our heat and mass transfer without shrinkage (detailed in §2.3.5), that moisture decreases much more quickly, compared to constant diffusivity. These simulations clearly demonstrate the important of considering the effect of diffusivity within drying.

The shrinkage effect was developed, on the basis of a simple mechanism of volume of evaporated water that takes place during drying and is not dependent on data from experiment. This is one of the strengths of the model and comparison with experiment findings shows a good correlation in term of moisture and temperature. A further strength of our model is that we are able to describe shrinkage phenomena with relatively few parameters. However, there are some weaknesses. Our model makes no distinction between the region inside the tissues, which is present as cellulose capsules that contain the cell wall, cell membrane and vacuole: these phenomena are combined in a single lumped parameter. It would be interesting to see, by modelling the effects separately, which of these enable the interaction between the regions to be

captured. During drying of heat and moisture sensitive products, the model has to consider external and internal limitations to mass and heat transfer on material level. This could be addressed by developing a new continuum model where each effect is modelled separately by recognising the heterogeneous properties of the tissues. This could then be compared to our continuum single phase model.

In spite of its weaknesses, the model will be improved on the basis of more sophisticated mathematical modelling to incorporate the two-phase (or porous) nature of the food-stuff with water and temperature simultaneously moving through both, solid food-stuff and void space (water vapour). Such a formulation may give insight into the limitations and applicability of homogeneous single phase models.

Chapter 4

A Multiphase Model for Drying Tropical Fruits

4.1 Introduction

In chapter 2, we describe how a homogenous model can be used to study the movement of water and temperature within a slab during drying and, in chapter 3, we include the effect of shrinkage into the model. The model is useful for describing certain aspects of the movement of water but there are several weaknesses that need to be addressed. One of the main problems with the homogenous model is that we cannot easily include detailed information relevant to the ongoing interaction between each of the phases. In the homogenous model, a single aggregate phase was considered. It is known that fruit contains water, air spaces and, under drying, the movement of water is not just in terms of the liquid phase but also in the vapour phase. Additional transfer mechanisms other than diffusion may be required to describe the movement of liquid water within general tropical fruit.

Possible modelling of these processes includes the use of a multiphase model framework. In this chapter we develop a model to investigate the mass and heat transfer phenomena during drying of fruits by developing a representative model relevant to tropical fruit based on their cellular structure. By initially investigating between individual cells, we can assign specific properties to each phase, and incorporate sub-cellular features within a multi-phase model. This allows the study of water movement

in several phases, for example, a liquid phase and a vapour phase; these will form the basis of a multiscale model of movement of water during drying. We seek a continuous representative model for drying fruit based on the transfer of water between the main constituents when viewed at the microscopic scale. The macroscopic properties of the fruit will depend on the various microscopic histological and cellular features [78]. Each material constituent is considered as a distinct phase within the multiphase material with attendant constitutive laws describing its material properties and its interaction with the neighbouring phase. Interaction between neighbouring phases, can be incorporated by introducing an appropriate source/sink term into the appropriate mass balance equations. Fruits in general have a micro-porous structure; in this chapter we adapt a porous media approach to describe the movement of water vapour within the air spaces, together with diffusion processes to describe movement in a liquid water phase.

This chapter consists of two sections. The first part of this chapter briefly reviews the properties of food structure. In the second part of this chapter, the mathematical formulation of the drying processes of fruits, incorporating the heterogeneous properties of the tissues and complex cellular structure, is recognized and simplified to a representative physical model. Based on these basic concepts of cellular structure, a representative macrostructure model for the multi-phase transport of water relevant to tropical fruits is developed. This model takes into account mass transfer through cellular membranes and diffusion through intercellular spaces, based on the microstructural properties of the fruit tissue.

4.2 Cell Level Structure of Tropical Fruits

There are two basic scale level approaches to the modelling of dehydration processes: a macroscopic approach and a microscopic approach. For a macroscopic approach we assume the product is homogenous and isotropic on the macro scale. This modelling is carried out when water diffusivity D_{eff} is taken as a single average of material property. On the other hand the microscopic approach recognizes the heterogeneous properties of the tissues and complex cellular structure, a framework that is then simplified to provide the basis of a representative model. The alternative approach is

concerned with the structure of food material at the microscopic level as deformable cellular vegetable/fruit tissue. The microscopic plant cell will be considered as a parenchymatic cell (vacuole and cytoplasm) and intercellular space (void), separated by cell membranes and cell walls.

In this section, we give a short description of this cellular system and the properties of its main components. It is important to identify the main modelling components. The tissue is viewed as a random aggregate of parenchymatic cells and intercellular spaces, with the following characteristics. A representative cell of this type is like a cellulose capsule filled with liquid. A thin cell wall composed of cellulose and other polysaccharides envelops the cell. The porosity of such cell walls is high, and correspondingly has high permeability to water, so that water retention occurs mainly by surface tension effects. Inside the cell wall and enclosing the cytoplasm there is also a semi-permeable membrane, called the plasma lemma. Within each cell, the cytoplasm contains a variety of organelles related to the metabolic activity of the cell, such as the nucleus, mitochondria and others; it is internally bounded by a membrane known as a tonoplast. Inside the tonoplast there is the vacuole, which has the highest water content of the cell phases described, reaching levels of about 98%, together with sugars, organic acids, salts and colloidal materials. The membranes are semi-permeable and with the vacuolar solution solute concentration, this results in an osmotic effect. The water chemical potential external to the vacuole generates hydrostatic pressure, which maintains the protoplast firmly pressed against the cell wall and hence keeps the tissue firm. This means that, loss of water is accompanied by a loss of internal pressure, with the tissue becoming flaccid. This pressure is known as turgor pressure and plays an important role in the rheology and texture of the tissue [87]. The shape of vegetal cells is polyhedral [73] with a variable number of faces ranging from 9 to 20 averaging 13.8, and high number of five-edged faces, as shown in Figure 4.1. In addition, there are protoplasmic connections or plasmodesmata that connect the protoplasm of joining cells.

Surrounding the cells are intercellular spaces (pores) that are randomly distributed among the cells. Their size and number depend upon the product considered; in apple tissue the pores are large and interconnected, while in potato they are tiny and isolated ([98]). Most fruits have void spaces that range between 2 to 10% but some

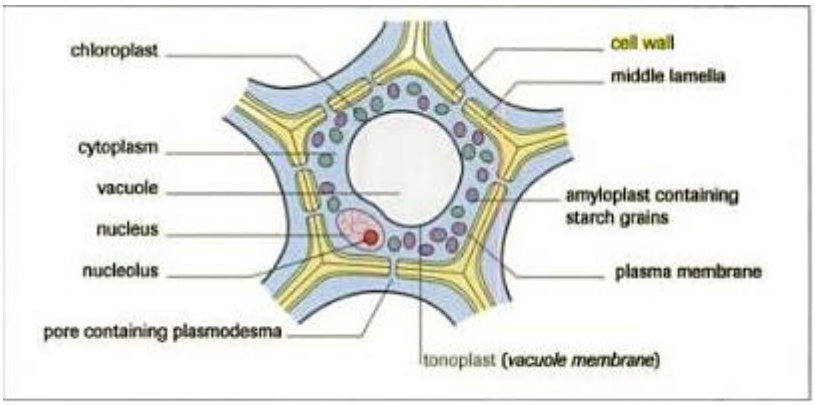

Figure 4.1: Structure of Plant Cell [114].

fruits such as apples and pears, have up to 25% void spaces [101].

A consideration of cell structure is a prerequisite to an understanding of the transport mechanism for modelling. The structure of many hydroscopic materials such as food products is basically an array of cells (Chen and Pei [21]). Although individual cells are very similar in nature, the tissues may differ widely in terms of porosity and water content. The intercellular spaces between the tissues may be interconnected and filled with air. A further model relevant for fruit is that provided by Ho *et al.* [57], who studied microscale modelling in pear tissue. This model represents the structure of fruit tissues using Ellipse tessellation before modelling the gas transport in pear tissues. Gas transport is modelled by a diffusion equation incorporating gas transport via pore, cell or cell wall processes and interior cell reaction processes. They found that filled intercellular spaces are thought to be the main pathways the gas transport (CO_2 and O_2) that plant organs need for respiration. They also found that gas is transported within the liquid phase by transfer from cell to cell. Following this mechanism, we consider the transport of water (liquid and vapour) and will examine the two different pathways: intercellular space in term of vapour transport and, from cell to cell, in terms of liquid transport.

The application of the multiphase model using porous media models of drying of food has become important. These models have been successfully been utilized in analyzing heat and mass transport problems during drying, and important findings have been obtained. Thus, to reach our goal of understanding water transport during

the drying of tropical fruits, we start to consider the tissues as a porous medium and look into how cellular structure affects such transport. Following all the studies in literature, and including cellular features, in the next section we develop a model based on this multiphase model.

4.3 Model Development

The work contained in this chapter uses models developed from a multiphase approach; each material constituent is considered as a distinct phase within the multiphase structure with constitutive laws describing the material properties and its interactions with neighboring phases. Formal averaging techniques were not used in this thesis as we formulate the process in macroscopic quantities, from the precise details at the microscopic level, based on information from previous work ([28, 43, 85, 86]). The drying process is taken as simultaneous transport of heat, momentum and mass through a two phase porous medium exposed to convective heating at its surface. A slab of tropical fruit is modelled as a matrix of cells and a void volume, formed by pores. The basic two-phase transport of water vapour, as a mixture of air and water vapour through the pores is considered as flow through a porous structure, that interacts with the cell structure.

Structural heterogeneity of fruit tissues brings additional complexity to water migration in a porous solid system. Cellular fruit tissues are taken as a combination of cell body, cell wall and membrane and intercellular space as shown in Figure 4.2 and as given by [114]. Water can migrate out of the cell in three possible ways: transmembrane transport through tonoplast and plasmalemma membrana boundaries, sympalstic transport involving transport of water from one cell directly into another by means of small channels (plasmodesmata) and apoplastic, which is defined as movement of water into the cell wall and the intercellular free space. According to Nobel [86], the symplastic flow may be generated from deeper cells towards the surface of the tissues by differences in cellular pressure. The analysis is confined to that part of the drying process in which most of the cell membranes remain intact and the structure prevails.

The motion of liquid water and water vapour through the cellular structure is

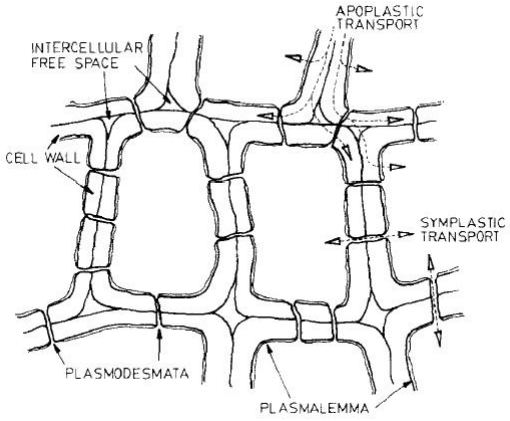

Figure 4.2: Mass transport pathways in the cellular structure of plant cells [114].

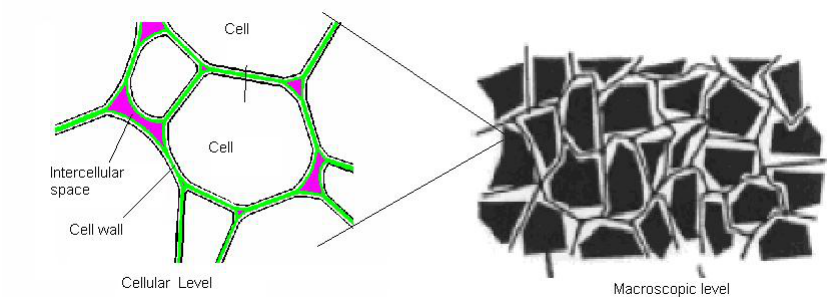

Figure 4.3: Drying process: from cellular level to macroscopic level [92].

shown in Figure 4.3, to illustrate how the macroscopic behavior of the drying process is related to cellular scale phenomena. During active drying processes, the principle transport of water in pores is through water vapour and this is taken to be the mechanism. Information on water transport within a detailed cellular structure description will ultimately be helpful in understanding the processes of drying at the macroscale level. We construct the theory of previous study of food structure, starting from a realistic picture of cellular tissue. A sketch of the macrostructure of an unconsolidated porous medium is shown in Figure 4.3 to distinguish the pores (intercellular space) and the cell. In this network, each pore is connected with its neighboring pores. The drying transport parameters can be identified and obtained as macroscopic properties by experiments. However, the physical effects of drying are on the microscopic level and modelling can be applied to help predict this physical effect, either directly or indirectly. Due to the difficulty of observing these phenomena by experiment at the pore scale, modelling of drying is also needed to provide the link to macroscopic drying behaviour, which is accessible experimentally.

Moisture in the drying of fruits is taken to exist in three categories: water vapour in the pores, free liquid water inside the individual cells and bound water held within the solid cell structures. The main assumptions for the model are based on the most physically significant aspects under drying conditions from experimental studies.

(a) Tropical fruits have an initially high moisture content which reduces significantly during the drying process.

(b) The drying process is maintained with moderate and sustained heating, typically for several hours.

(c) The internal structure of the food is cellular with its integrity maintained by internal cell walls/cell membranes and internal cell pressure(turgor). Turgor pressure is the main pressure on the cell contents determined by the water content in the vacuole and resulting from osmotic pressure(hydraulic pressure)

(d) Shrinkage can be considerable in some fruits as a result of drying that reduces the volume of water within the fruits. This is moderated by retention of water within some internal elements (bound water) and cell structure. Shrinkage is neglected in this model in the first instance.

(e) Bound water will be maintained by strong enzyme/chemical or biological bonds associated with internal structures within the cell. Water content, such as that contained within cell cytoplasm, that is relatively mobile is taken as 'free water'. Free water exists within the structures of the vacuole and is available for transport through the cell wall by the diffusion process or through cell pores. Bound water may diffuse into the structures holding free water at significantly low values of free water concentration.

(f) As a result of turgor pressure, a differential of pressure will exist between the cells with the intercellular space.

(g) Cell structure incorporates interconnected pathways of intercellular space containing water vapour.

(h) The local differential in temperature may exist between the intercellular water vapour and the cell during active drying from latent heat effects and from water evaporation.

(i) Intercellular water content during drying is dominated by water vapour; saturated water and associated capillary effects are negligible [37].

The macroscale representation of the physical structure associated with general foodstuffs and tissues for multicomponent systems have been addressed by numerous authors (e.g. Wood *et al.* [127], Whitaker [126], Datta [32]). In these papers, the processes of averaging or homogenisation from the cell or microscale processes to obtain macroscopic representations of processes are considered. Typically, microscale processes give rise to suitability modified diffusion, convective or sources or sink mechanisms on a macroscale, involving internal structurally related 'effective parameters'.

Following the basic concepts, we identify a representative macrostructure model for the multiphase transport of water relevant to tropical fruits in a typical drying phase. Key characteristics of the macroscopic models are noted.

(1) In the first instance the microstructure of the cellular and membranes are taken to provide sufficient support for shrinkage to the macrostructure to be negligible during drying.

(2) Intercellular space is sufficiently interconnected to provide a porous structure characterized by the porosity ϕ_i and an effective permeability k_i.

(3) Water transport in the intercellular spaces is as water vapour in a gas phase. Water in a saturated phase and associated capillary pressures are taken as negligible. The macroscopic representation of the internal cell structure is taken to comprise water, solid cell tissues and air. Compared with the water and solid phases, the air mass is taken as negligible ($\frac{\rho_a}{\rho_w} << 1$). The moisture levels within the cell are recognised as attributable to water content within the internal cell structure and the distinctions between free water and bound water are identified. Internal water mass transfer mechanisms (Kiranoudis *et al.* [71]) recognize that the availability of water within cell tissues on a macroscale can be associated with free and bound water phases. Within the initial phases of drying it is anticipated that transfer of moisture within the cell walls will be dominated by the diffusion of free water. At a lower moisture level, following significant drying, the more tightly bound water within the cell tissues must be converted to free water before further diffusion of water can occur. These processes would be important in the later, and much longer stages of drying to reduce residual levels of moisture.

(4) Transport of simultaneous heat and mass transfer in general food processes, where the food matrix is taken as a porous media, has been reviewed by Datta [32]. Models range in physical complexity from an elaborate multiphase porous medium that includes evaporation down to simple single phase isothermal models. Application of simple models to a range of experimental cases identifies the possibility of improving our fundamental understanding of food processes but depends on key effective parameters, optimised for the underlying process and which restricts their general applicability.

4.3.1 Three Compartments Representative of Macroscopic Volume

We identify a macroscopic model for the liquid content within the representative volume that falls into three categories shown schematically in Figure 4.4 as a three

compartment model. The component parts are identified as:

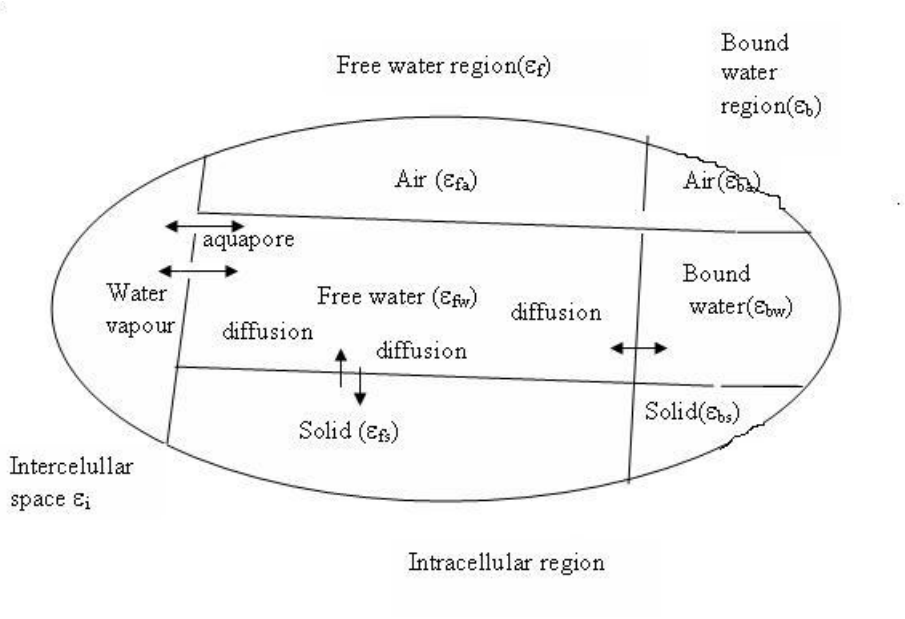

Figure 4.4: Macroscopic volume representation of three compartment model.

(a) Water vapour in the intercellular space that is transported by convective (pressure driven) and diffusive mechanisms.

(b) Bound water within the intracellular structure that is strongly linked to the internal cell structure but may be released by a local diffusion processes to the free water component.

(c) Free water retained within the intracellular structure that is readily available to be transported by cell to cell diffusion. In addition, water will be transferred to the intercellular space by diffusion through the wall of the space and membrane or from release by pore cells (plasmodesmata).

In a macroscopic representation, any typical volume is taken to comprise an intercellular space and an intracellular cell associated with free and bound water regions. Volume fractions for these three compartments are denoted by:

ε_i=Volume fraction of intercellular space;

ε_f=Volume fraction of the free water region within intracellular cell-comprising air, dry cell tissues and free water;

ε_b=Volume fraction of the bound water region within the intracellular cell-comprising bound water, dry cell tissue and air.

The total volume fractions provide a restriction

$$\varepsilon_i + \varepsilon_f + \varepsilon_b = 1.$$

In a non-shrinkage model, these are each taken as constant, although the individual composition of air and water within components will vary through the drying process. For a tropical fruit, typical values are ε_i=0.15-0.33, ε_f=0.6-0.9, and ε_b=0.1-0.2 (see [72]). These values are often characterized by the type of fruit and the ripeness stage of the fruit [72, 133]. Within the intracellular cell/tissue we separately identify components of dry solid, water and air but recognise the difference in internal structures where the availability of water for transport is given in terms of free water and bound water regions [44]. Hence we identify sub-regions as indicated in Figure 4.4, for model development.

Free water regions:

ε_{fw}=Volume fraction of water/unit volume within the free water region;

ε_{fs}=Volume fraction of solid/unit volume within the free water region;

ε_{fa}=Volume fraction of air/unit volume within the free water region.

A volume constraint is

$$\varepsilon_f = \varepsilon_{fa} + \varepsilon_{fw} + \varepsilon_{fs}.$$

Similarly within the bound water region:

ε_{bw}=Volume fraction of water/unit volume within the bound water region;

ε_{bs}=Volume fraction of solid/unit volume within the bound water region;

ε_{ba}=Volume fraction of air/unit volume within the bound water region.

A constraint is

$$\varepsilon_b = \varepsilon_{ba} + \varepsilon_{bw} + \varepsilon_{bs}.$$

We consider intercellular space as an interconnected porous media containing water vapour with density ρ_i varying within the foodstuff. Low velocity of air flow is anticipated and, correspondingly compressibility effects are negligible. For a non-shrinkage model, the porosity of the intercellular space is taken as constant $\varepsilon_i = \phi_i$.

Within the drying process, we anticipate $\rho_a << \rho_w$ and the air phase within the intracellular cell/tissue provide only minor dynamical or thermal impact and they are neglected where possible. The range of temperature will provide minor changes in density of liquid water and tissue but, compared with other changes, these are consistent with those of other authors [44, 111], taking ρ_w and ρ_s as constant.

Moisture content is defined as the quantity of water present in the moist sample. Two common ways are used to express the moisture content of a material in food science literature, dry-basis moisture content and wet-basis moisture content. The wet-basis moisture content expresses the ratio of water mass to the total mass of the food and the dry-basis moisture content expresses the ratio of the water mass present in the material to the mass of the dry matter. Useful related dependent variables enable comparison with previous one component models in food systems and introduce the non-dimensional moisture content (dry basis), gives

$$M_f = \frac{\varepsilon_{fw}\rho_w}{\varepsilon_{fs}\rho_s}, \tag{4.1}$$

$$M_b = \frac{\varepsilon_{bw}\rho_w}{\varepsilon_{bs}\rho_s}, \tag{4.2}$$

$$M_i = \rho_i\phi_i. \tag{4.3}$$

An overall average moisture content (dry basis) is given by a composite moisture value

$$M = \frac{\rho_i\phi_i + \rho_w(\varepsilon_{fw}\varepsilon_f + \varepsilon_{bw}\varepsilon_b)}{\rho_s(\varepsilon_{fs}\varepsilon_f + \varepsilon_{bs}\varepsilon_b)}.$$

This can be usually written as

$$M = \alpha_i\rho_i + \alpha_f M_f + \alpha_s M_b, \tag{4.4}$$

with

$\alpha_i = \dfrac{\phi_i}{\rho_s(\varepsilon_{bs}\varepsilon_b + \varepsilon_{fs}\varepsilon_f)}$, $\alpha_f = \dfrac{1}{1 + \dfrac{\varepsilon_{bs}\varepsilon_b}{\varepsilon_{fs}\varepsilon_f}}$, and $\alpha_s = \dfrac{\dfrac{\varepsilon_{bs}\varepsilon_b}{\varepsilon_{fs}\varepsilon_f}}{1 + \dfrac{\varepsilon_{bs}\varepsilon_b}{\varepsilon_{fs}\varepsilon_f}}$. Limiting cases, of the

above identified for later comparison with simpler models, will be discussed later in chapter 5.

(a) Taking the case of negligible intercellular space, $\phi_i \to 0$, gives $\alpha_i \to 0$ and gives two interacting diffusion processes within free and bound water. Thus, a global moisture content becomes

$$M = \alpha_f M_f + \alpha_s M_b.$$

(b) For a case of negligible bound water state, then $\varepsilon_b \to 0$ so $\alpha_s \to 0$. This gives $\alpha_f = 1$, and a global moisture content based on water vapour and cell water content by

$$M = \alpha_i \rho_i + M_f.$$

(c) For the limit of a single composite food comprising free water, solid and air only, such that no pore space is presented and only free water exists $\varepsilon_b \to 0$ so $\phi_i \to 0$, gives a global moisture variable

$$M = \frac{\rho_w}{\rho_s} \frac{\varepsilon_{fw}}{\varepsilon_{fs}} = M_f.$$

4.3.2 Mass transfer in drying fruit

We will consider modelling the individual transport mechanism within the food. During drying, water vapour is taken to collect within the intercellular network of spaces and to be convected to the food surface by a gradient of intercellular pressure P_i. Transfer of water between cells is ongoing but is anticipated to be less important during active drying processes as the flux of water vapour transport through the porous structure will be more significant.
Water vapour density ρ_i and pressure P_i are affected predominately by the following:

(a) Water is released from cells through membranes from intracellular cells to the intercellular phase regions. The release of water locally at cell level will depend on a local cell pressure difference $P_c - P_i$, where P_c is the cell turgor pressure.

(b) Water is released across the cell membranes bounding the intercellular space, arising from local diffusion processes through the membrane and dependent on the difference in local moisture levels.

Global models for transport of fluid (liquid and gas) through a porous food structure, for low Reynold number flow, have been well documented in terms of a Darcy Law [32]. For the structure of typical fruits, it will be assumed that the intercellular space comprises interconnected pores characterized by a porosity ϕ_i and permeability to gas flow k. Fluid flow within the intercellular space is assumed to be in a gas (water vapour form), with negligible unsaturated water; corresponding capillary forces and hydrostatic pressure are negligible.

Mass conservation for water vapour in the intercellular space is given by a general mass conservation equation [85] for a porous medium as

$$\frac{\partial(\phi_i \rho_i)}{\partial t} + \nabla . \boldsymbol{n}_i = j_{ip} + j_{ic}, \tag{4.5}$$

where $\phi_i \rho_i$ is local mass flux of water vapour in the intercellular space and $\boldsymbol{n}_i$ is a mass flux defined by

$$\boldsymbol{n}_i = \rho_i \boldsymbol{u}_i + \boldsymbol{J}_i, \tag{4.6}$$

where $\boldsymbol{u}_i$ is convective flow of water vapour and $\boldsymbol{J}_i$ is diffusive flow of water vapour. The source terms in equation (4.5) comprise:

> j_{ip}=mass flux of water vapour/unit volume, release into intercellular space due to release of water through cell membrane and cell wall pores, arising from internal cell pressure,
>
> j_{ic}=mass flux of water vapour/unit volume, released through the wall/membrane of intracellular space by diffusion.

According to Ho *et al.* [57], the intercellular space existing within a highly complicated network of pore channels can be considered as such porous media. The convective flow of water vapour $\boldsymbol{u}_i$ within the intercellular space is anticipated as driven by an internal pressure gradient and resisted by viscous resistance from local viscous shear forces arising from the internal connective geometry. With negligible shrinkage and negligible surface tension force, as supported by Datta [32] for the drying of wet food, capillary pressure is very small and consistent with the model developed. Appropriate transport of water vapour in porous material is due to pressure and provided by a Darcy Law relation

$$\boldsymbol{u}_i = -\frac{k_i}{\mu_i} \nabla P_i, \tag{4.7}$$

where k_i is the permeability of the food in the intercellular space and μ ia the viscosity of intercellular space.

A further mechanism of mass of flux of water vapour arises from any moisture gradient and will add to the convective flux. In this case, Bird *et al.* [11] modelled flux of water vapour that can be approximated by Fick's Law of diffusion as

$$\boldsymbol{J}_i = -D_i \nabla \rho_i, \tag{4.8}$$

where D_i is intercellular space diffusivity. Such an approach follows the approach of Crank [26] for a vapour diffusion equation through fabrics. A composite mass conservation equation for vapour becomes

$$\frac{\partial(\phi_i \rho_i)}{\partial t} = \nabla.(\frac{k_i \rho_i}{\mu_i} \nabla P_i) + \nabla.(D_i \nabla \rho_i) + j_{ip} + j_{ic}. \tag{4.9}$$

We note, according to Datta [33], if the pores are not large enough, the diffusion of water vapour in pores can be neglected. Curcio *et al.* [31] neglected diffusion of water vapour within dehydrated material where the void fraction value was less then 0.3.

a. Bound water

Within the cell structure, a small proportion of the water is identified as constrained by strong bonds to the cell structure and not freely available for transport by the more dominant diffusion mechanisms until water content is relatively low. Few studies have considered the migration of bound water, even though the transport characteristics are different from free water migration. Typically this bound water can be considered mobile only after conversion to the free water state and prior to removal processes that are active from that state (Kiranoudis *et al.* [71]). A common assumption is that the decrease in the drying rate at low moisture content is caused by the decreasing availability of free water molecules (Xiong *et al.* [129]; Kiranoudis *et al.*, [71]). Hence, the reduced drying rate results from a decreasing driving force, rather than from a decreasing diffusion coefficient is generally assumed. Many researchers have also tried to explain the reduced diffusion at low moisture content as due to the increase in energy requirement as drying progresses. As moisture content drops, such as through drying, the water molecules are more firmly bound to the material and more energy is required to remove the absorbed water molecules. This is illustrated, for example, by McMinn and Magee [77], Wang and Brennan [124], Xiong *et al.* [129]

where the effective diffusion coefficient remains constant with moisture until critical moisture content is reached. Below this critical moisture concentration, the diffusion coefficient shows a sharp decrease with decreasing water concentration. Following the model, the portion of free moisture content is initially very large. The free moisture molecules diffuse through the bulk and evaporate at the boundary of the material. The assumption is that only free water molecules are diffusing, see (Wang and Brennan [124], Xiong *et al.* [129]). As drying continues, the bound moisture molecules are in the majority. Then the conversion between bound and free water controls the overall mass transfer phenomenon, leading to the decreased drying rate.
The interaction of bound water within the macroscopic multiphase model is taken as

$$\frac{\partial M_b}{\partial t} = -r_b = -(n_1 M_b - n_2 M_f). \tag{4.10}$$

In (4.10), M_b is the moisture level in the bound state and r_b is a corresponding conversion rate. n_1 and n_2 are kinetic constant define by Kiranoudis *et al.* [71], a model that depends on local moisture levels for free and bound water content is given by a weighted balance between the local levels of bound and free water.

The difference between the two rates equals the decrease in bound water and the increase in free water inside the particle. This model recognizes that bound water within the cell structure will be controlled by biological (e.g. enzyme) systems. This binding of water to the cell structure is responsible for the high residual water content, even after significant drying and is responsible for maintaining much of the structural integrity of the food in the later stages of drying. Correspondingly the level of air/ shrinkage associated with the bound water region is anticipated to be negligible, other than in the final drying state. Therefore mass conservation of water in the bound phase is taken from equation (4.10). Equilibrium is given by relative moisture levels $M_b = (\frac{n_2}{n_1})M_f$. If the value of the kinetic constant of bound water n_1 is large, little bound water is present.

b. Free water

A relevant transfer of water within the intercellular cell structure is given by considering the more freely available water within the cell and the different transport mechanisms. It is assumed that only free water molecules are diffusing (Wang and

Brennan [122]). The driving force for diffusion thus is the gradient in free moisture content. In this setting, it is no longer necessary to assume that the diffusion coefficient itself depends upon the moisture content.

A cell level model for the localised transport of water within the free water region is characterized by the following internal mechanisms:
(a) Transport of water through the cell walls and membranes into the intercellular space. The two main mechanisms for free water transfer are:
i) diffusion across membranes of the intercellular space from relevant cells;
ii) local release of water across membranes because of pressure difference.
(b) Transport of free water from cell to cell through
i) diffusion within the cell matrix;
ii) release of water between cells from local pores within the cell structure.
(c) Interchange of water from the bound state to the free state within individual cells, which is anticipated to be of smaller magnitude during active drying periods.

The above mechanisms are operational at the microscale and, for the current modelling, must be represented by appropriate models within the macroscale equations. Formulation of such macroscopic equations for water transport in porous media has been conducted in detail by Whittaker [126], Slattery [109] and has been used in macroscopic model development for the water transport relevant to the free water region.
A mass conservation equation for free water is taken as

$$\rho_s \frac{\partial M_f}{\partial t} = -\nabla . \boldsymbol{J}_c - j_{ip} - j_{ic} + \rho_s r_b, \tag{4.11}$$

with

$$\boldsymbol{J}_c = \boldsymbol{J}_\alpha + \boldsymbol{J}_\beta$$

where $\boldsymbol{J}_\alpha$ is the flux of water due to the differential gradient of free moisture level in the cells, and $\boldsymbol{J}_\beta$ is the flux of water due to differential gradient pressure in cells. j_{ip} and j_{ip} are mass flux that release into intercellular space and r_b is a corresponding conversion rate.

In equation (4.11), a model for moisture transfer at the deeper cell to cell level has been formulated and represented by a macroscopic diffusion equation in terms of a suitable effective diffusivity. This transport is the transfer of water from one

cell to another, which requires molecules to cross both the cell membrane and the cell wall. This transport was included in the effective diffusion coefficient of water, characterizing the overall cell diffusion process. Correspondingly, the flux of free water forms a possible gradient of the free moisture level in the cells, and is given by

$$\boldsymbol{J}_{\alpha} = -\rho_s D_f \nabla M_f. \tag{4.12}$$

where D_f is effective diffusivity of free water.

A complementary flux of free water through cell wall pores (plasmodesmata) can be generated by the differential gradient of internal pressure. These give rise to a mass flux

$$\boldsymbol{J}_{\beta} = -D_p \rho_s M_f \nabla P_c, \tag{4.13}$$

which is dependent on the local level of free water(M_f) and the gradient of cell pressure P_c. D_p is effective diffusivity of plasmodesmata. Most of this transport is facilitated by small channels, known as the symplastic pathway [46]. The free water will be driven from the deeper cell through plasmodesmata (pores) by local pressure differences between the cells [86]. This assumption was used by Shi and Maguer [104] and Floury *et al.* [46] in the modelling of osmotic treatment of cellular porous material.

According to Nobel [86], the flux of water through the cell membrane under a chemical potential difference can be modelled using irreversible thermodynamics and this can be considered to depend on water activity and differences in pressure inside the cell and the intercellular space. Following this, we assumed that the release of free water from the cell into the intercellular space arises from differences between local pressure and moisture level and cumulatively occurs along the interconnected spaces. Thus, the mass flux of free water is associated with the differential pressure between the local cell and intercellular space and is taken as

$$j_{ip} = k_p(P_c - P_i). \tag{4.14}$$

In (4.14), k_p is a transfer coefficient and a measure of local cell pore permeability, number density and size.

The local transport of free water from cells across the cell membranes to the intercellular space will be dependent on the differential moisture levels across the

membrane. According to Toupin and Marcotte [114], transmembrane transport, defined as exchanges between the cell interior (cytoplasm and vacuole) and the cell exterior (cell wall and intercellular space) across the cell membrane, occurs in some instances. Correspondingly a macroscopic average of this cell transfer is taken to be in the form of a difference in volumetric densities, i.e.

$$j_{ic} = k_w(C_{fw} - C_i), \tag{4.15}$$

with C_{fw} as a concentration of water in cell (free water) and C_i as a concentration of water in intercellular space.

The concentration of water in the intercellular space is given by

$$C_i = \xi \rho_w,$$

where the density of intercellular space water vapour is given from the two-phase partition

$$\rho_i = \xi \rho_w + (1 - \xi)\rho_a.$$

where ξ is the level of liquid water within the intercellular space.
This gives

$$C_i = \left(\frac{\rho_i - \rho_a}{\rho_w - \rho_a}\right)\rho_w. \tag{4.16}$$

Concentration of water in the intracellular cell (free water region) is given by

$$C_{fw} = \frac{\varepsilon_{fw}\rho_w}{\varepsilon_{fs} + \varepsilon_{fw}}.$$

In terms of free water moisture, gives

$$C_{fw} = \frac{M_f}{\frac{\rho_w}{\rho_s} + M_f}\rho_w. \tag{4.17}$$

A corresponding macroscopic average of this cell transfer is taken

$$j_{ic} = k_w \rho_w(\eta - \xi), \tag{4.18}$$

where η is the level of free water within the cell, and ξ is the level of the water within intercellular space and given by $\eta = \dfrac{M_f}{\frac{\rho_w}{\rho_s} + M_f}$ and $\xi = \dfrac{\rho_i - \rho_a}{\rho_w - \rho_a}$.

A composite mass conservation equation for the free water from equations (4.12), (4.13), (4.14), (4.18) and (4.10) is taken as

$$\rho_s \frac{\partial M_f}{\partial t} = \nabla.(D_f \rho_s \nabla M_f) + \nabla.(D_p \rho_s M_f \nabla P_c) - k_p(P_c - P_i) - k_w \rho_w(\eta - \xi) + \rho_s r_b. \tag{4.19}$$

4.3.3 Heat transfer in drying fruit

On a microscopic scale, heat transfer within the drying of fruit is complex due to simultaneous transfer of mass and the multi-component nature of the cellular structure. Mechanisms that must be considered include:

(a) Convection of heat within water vapour present within the intercellular space,

(b) Conduction of heat within each phase, intercellular space and intracellular cell,

(c) Conversion to water vapour from water within the transfer to intercellular space through cell walls, cell membranes and cell pores,

(d) Heat transfer between intercellular space and intracellular cell.

Formal development processes for a microscopic model from local cell scale is given consideration by Whittaker [126] and Slattery [109]. These give relevant theoretical understanding to the governing balances of energy from a microscale to macroscale representation and form the basis of the energy equations. Most models of heat transfer on porous structures in food with interconnected pores assume the liquid and vapour phases remain in thermodynamic equilibrium at the local temperature [85, 35, 131, 44] but we note that Dincov [39] used two energy equations in the modelling of microwave heating: one for the liquid and solid phase and a second for the gas phase. Farkas *et al.* [43] also used two energy equations, core and crust and the findings showed that the temperature between these two regions was different. In this study, the formulation of an energy balance included the possibility that two representative temperatures are relevant: a representative temperature T_i of water vapour in the intercellular space may differ from a representative temperature T_c within the intracellular cell structure. This will utilize the principle of local non-equilibrium between the cell and the intercellular space at a given location.

a. Intercellular space energy equation

Within the intercellular space, heat is convected with the Darcy velocity within the intercellular space and also conducted within the vapour phase. Additional sources or sinks of heat are identified as

i) Heat transfer from the intracellular cell [32], and flux given by

$$q_c = h_i A_{spec}(T_c - T_i), \tag{4.20}$$

where h_i is an appropriate heat transfer coefficient, which will involve a measure of the interface area A_{spec} associated with the porous structure. Inflow of heat is due to the difference between the temperatures in the intercellular space and the intracellular tissue structure of the cell.

ii) Heat transfer from water released into the intercellular space from the cell is taken to be given by a flux

$$q_p = (j_{ic} + j_{ip})c_{pw}(T_c - T_i), \tag{4.21}$$

where c_{pw} is the heat capacity of water. Heat is transported from the intracellular cell into the intercellular space due to water release from the cell wall pores and cell membrane.

iii) Evaporation from water to water vapour requires an amount of heat for the phase transition with a flux

$$q_L = -\lambda(j_{ic} + j_{ip}), \tag{4.22}$$

where λ is the latent heat.

A composite energy equation for the intercellular space is given by a conservation balance, e.g. see [11], of the form

$$\phi_i \rho_i c_{pw}(\frac{\partial T_i}{\partial t} + \frac{\boldsymbol{n}_i}{\rho_i} \cdot \nabla T_i) = \nabla.(\phi_i \kappa_v \nabla T_i) + q_c + q_p + q_L. \tag{4.23}$$

Substituting for the source and sink terms gives an equation (4.20) to (4.22), which gives

$$\phi_i \rho_i c_i(\frac{\partial T_i}{\partial t} + \frac{\boldsymbol{n}_i}{\rho_i} \cdot \nabla T_i) = \nabla.(\phi_i \kappa_v \nabla T_i) + h_i A_{spec}(T_c - T_i) + (j_{ip} + j_{ic})c_i(T_c - T_i) - \lambda(j_{ip} + j_{ip}). \tag{4.24}$$

where c_i is the heat capacity of water vapour and will be taken to be the same as the effective heat capacity of the cell c_{pw} and $\boldsymbol{n}_i$ is a mass flux within intercellular space defined in equation (4.6).

b. Intracellular cell energy equation

Within the cellular tissues, the predominant heat transfer mechanism within the cells will arise from local conduction within the intracellular cell phase and heat

transfer within the intercellular space phase. A common temperature associated with the intracellular cell phase is taken as T_c, arising from the relatively high conductivity of water and solid tissues. The heat capacity of any air within the cell structure is taken as negligible.

A corresponding form for the energy equation for the intracellular cell phase, (see [11] [32] [69]), is given by

$$(1-\phi_i)\rho_c c_{pw}\frac{\partial T_c}{\partial t} = (1-\phi_i)\nabla.(\kappa_c \nabla T_c) - (q_c + q_p), \tag{4.25}$$

where c_{pw} is the effective heat capacity of the cell structure and κ_c is the effective conductivity. Substituting from (4.20) and (4.21) gives the energy balance equation

$$(1-\phi_i)\rho_c c_{pw}\frac{\partial T_c}{\partial t} = (1-\phi_i)\nabla.(\kappa_c \nabla T_c) - h_i A_{spec}(T_c - T_i) - (j_{ip}+j_{ic})c_{pw}(T_c - T_i). \tag{4.26}$$

4.3.4 Initial and boundary conditions

Five second order of differential equations have been derived to describe the heat and mass transfer in the intercellular space and the intracellular cell. Initially, the food material is at ambient pressure and temperature conditions, given by $P_i(t=0) = P_{atm}$, $T_i(t=0) = T_{i0}$ and $T_c(t=0) = T_{c0}$.

Depending on the composition of food material, the initial phase of the free water, bound water and water vapour is estimated. Initially, intercellular space contains air as given by $\rho_i(t=0) = \rho_a$. Free water and bound water initial conditions are given by, $M_f(t=0) = M_{f0}$ and $M_b(t=0) = M_{b0}$.

For each phase in the cellular system, equation (4.9), (4.10), (4.19), (4.24), (4.26) must be solved, along with the boundary conditions for the spatial distribution. In order to complete the set of equation listed above, the boundary conditions that connect the transport equations for three separated phases need to be specified. It is considered that between these two regions, the intercellular space and the intracellular cell, there is a transport of water with transmembrane flux transport, such as discussed in section §4.3. Boundary conditions on the closed boundary at x=0 for intercellular space and intracellular cell, assuming symmetry condition, the mass and heat flux are given below,

$\mathbf{n}.(\nabla T_i) = 0$, $\mathbf{n}.(\nabla T_c) = 0$, $\mathbf{n}.(\nabla M_f) = 0$, $\mathbf{n}.(\nabla M_b) = 0$, and $\mathbf{n}.(\nabla \rho_i) = 0$.

At the surface, there is an exchange of heat, liquid water, vapour and air. Moisture is transported to the air from the food surface in either liquid or vapour form, depending upon the intensity of drying. In the intercellular space, it is reasonable to assume that the moisture migrates to the interface in term of vapour form, and carried away by the hot air stream. Following Ousegui et al. [88], the boundary conditions for the intercellular space at the surface are obtained from flux balances and given by

$$-h_{m,v}(\rho_{i,sur} - C_{air}) = \frac{k_i \rho_i}{\mu_i} \nabla P_i + D_i \nabla \rho_i, \tag{4.27}$$

In the intracellular cell, the boundary conditions applied to the external surface of the food express the balance between the diffusive flux of liquid water coming from the core of the food and the flux of vapour leaving the food surface that is transferred to the drying air. The driving force for mass transfer at the interface of the food and the processing air is given by the difference in the moisture concentration at the surface and water concentration in the processing air. Assuming that processing air behaves like an ideal gas, this concentration difference can be expressed by vapour pressure difference. Correspondingly, the mass transfer boundary condition from intracellular cell tissues at the surface is given by

$$-h_{m,f}(C_{fw,sur} - C_{air}) = D_f \rho_s \nabla M_f + D_p M_f \rho_s \nabla P_c. \tag{4.28}$$

$C_{fw,sur}$ is the relationship between water vapour pressure and concentration of water vapour in the surface, such as C_{sur}, in chapter 2. The quantities $h_{m,v}$ and $h_{m,f}$ are associated with the mass transfer coefficient of vapour and the free water phase. The concentration of bound water only changes due to the conversion between free and bound water and, with this in mind, only the concentration of free water C_{fw} is considered at the surface of the intracellular cell.

An energy balance over the interface, the heat flux arriving at the surface from the interior of the materials equals the heat flux leaving the interface by convection. In the intercellular space, the boundary condition becomes

$$-\phi_i h_i (T_{isur} - T_{air}) = \phi_i \kappa_v \nabla T_i. \tag{4.29}$$

If mass is transferred from the food surface to the processing air, heat is needed to evaporate the moisture at the product surface. It is supplied by processing air so that

the intracellular cell boundary condition becomes

$$-(1-\phi_i)h_c(T_{csur}-T_{air}) = (1-\phi_i)\kappa_c\nabla T_c - \lambda\Big(D_f\rho_s\nabla M_f + D_p M_f\rho_s\nabla P_c\Big). \quad (4.30)$$

The quantities h_i and h_c are associated with the heat transfer coefficient of the intercellular space and the intracellular cell.

4.4 Non-dimensional formulation

The system of equations that governs the drying process is given in equations (4.9), (4.10), (4.19), (4.24) and equation (4.26). Free water M_f, bound water M_b, intercellular space density ρ_i, intracellular cell temperature T_c and intercellular space temperature T_i are dependent variables. To simplify the equations for numerical analysis, the following scaling groups are used, where the overbar corresponds to a non-dimensional variable,

$$\overline{x} = \frac{x}{L_0}, \quad \bar{\nabla} = L_0\nabla \quad \tau = \frac{D_0 t}{L_0^2},$$

$$\overline{\rho} = \frac{\rho_i}{\rho_a}, \quad \overline{P}_i = \frac{P_i}{P_{atm}}, \quad \overline{P}_c = \frac{P_c}{P_{atm}} \quad \overline{\rho}_c = \frac{\rho_c}{\rho_a}, \quad \overline{\rho}_s = \frac{\rho_s}{\rho_a}.$$

$$\overline{D}_i = \frac{D_i}{D_0}, \quad \overline{k} = \frac{k_i P_{atm}}{\mu D_0},$$

$$\overline{T}_i = \frac{T_i - T_0}{T_{air} - T_0}, \quad \overline{T}_c = \frac{T_c - T_0}{T_{air} - T_0}.$$

In the above L_0 is taken as characteristic dimension of the food and D_0 a suitable diffusion coefficient scaling. Other source or sink terms associated with the formulation are

$$\overline{j}_{ip} = \frac{L_0^2}{D_0\rho_a} j_{ip}, \quad \overline{j}_{ic} = \frac{L_0^2}{D_0\rho_a} j_{ic},$$
$$\overline{n}_1 = n_1\frac{L_0^2}{D_0}, \quad \overline{n}_2 = n_2\frac{L_0^2}{D_0}$$

(i) Intercellular space-water vapour mass conservation

Substituting these dimensional quantities into the equation (4.9), gives

$$\phi_i\frac{\partial\overline{\rho}}{\partial\tau} = \bar{\nabla}.(\overline{k}\overline{\rho}\bar{\nabla}\overline{P}_i) + \bar{\nabla}.(\overline{D}_i\bar{\nabla}\overline{\rho}) + \overline{j}_{ip} + \overline{j}_{ic}. \quad (4.31)$$

Choice of a scaling D_0 is informed by the drying process to be modelled. If the drying process is dominated by porous diffusivity(permeability) within the pore space, then a suitable value is $D_0 = \dfrac{k_i P_{atm}}{\mu}$, then $\overline{k} = 1$ and $\overline{D}_i = \dfrac{D_i}{D_0} = \dfrac{D_i \mu}{k_i P_{atm}} << 1$. If the drying process dominated by diffusion within pore space, then a suitable values is $D_0 = D_i$, so $\overline{D}_i = 1$ and $\overline{k} = \dfrac{k_i P_{atm}}{\mu D_0} << 1$. This latter equation is consistent with the case considered in chapter 2.

(ii) Bound water mass conservation

Substituting dimension quantities into equation (4.10) gives

$$\frac{\partial M_b}{\partial \tau} = -\overline{n}_1 M_b + \overline{n}_2 M_f. \tag{4.32}$$

(iii) Free water mass conservation

Substituting the dimension quantities into equation (4.13) gives

$$\overline{\rho}_s \frac{\partial M_f}{\partial \tau} = \bar{\nabla}.(\overline{\rho}_s \overline{D}_f \bar{\nabla} M_f) + \bar{\nabla}.(\overline{\rho}_s \overline{D}_p M_f \bar{\nabla} \overline{P}_c) - \overline{j}_{ip} - \overline{j}_{ic} + \overline{\rho}_s \overline{r}_b, \tag{4.33}$$

taking
$\overline{D}_f = \dfrac{D_f}{D_0}$, $\overline{D}_p = \dfrac{D_p P_a}{D_0}$, and $\overline{r}_b = \dfrac{r_b L_0^2}{D_0}$.

The expressions for the transfer fluxes (4.14) and (4.18) become

$$\overline{j}_{ip} = \overline{k}_p(\overline{P}_c - \overline{P}_i), \tag{4.34}$$

$$\overline{j}_{ic} = \overline{k}_w(\eta - \xi), \tag{4.35}$$

where
$\overline{k}_p = \dfrac{k_p P_a L_0^2}{D_0 \rho_a}$ and $\overline{k}_w = \dfrac{k_w L_0^2 \rho_w}{D_0 \rho_a}$, $\eta = \dfrac{M_f}{\dfrac{\rho_w}{\rho_s} + M_f}$ and $\xi = \dfrac{\overline{\rho} - 1}{\dfrac{\rho_w}{\rho_a} - 1}$.

(iv) Intercellular space energy equation

Substituting for the dimension quantities into the intercellular energy equation (4.24) gives the non-dimensional form

$$\phi_i \overline{\rho}\Big[\frac{\partial \overline{T}_i}{\partial \tau} + \frac{\overline{\boldsymbol{n}}_i}{\overline{\rho}} \bar{\nabla} \overline{T}_i\Big] = \bar{\nabla}.(\phi_i \overline{\kappa}_v \bar{\nabla} \overline{T}_i) + \overline{h}_i(\overline{T}_c - \overline{T}_i) + (\overline{j}_{ip} + \overline{j}_{ic})(\overline{T}_c - \overline{T}_i) - \overline{\lambda}(\overline{j}_{ip} + \overline{j}_{ic}), \tag{4.36}$$

where,
$\overline{\kappa}_v = \dfrac{\kappa_v}{D_0 c_{pw} \rho_a}$, $\overline{h}_i = \dfrac{h_i L_0^2 A_{spec}}{c_{pw} D_0 \rho_a}$, $\overline{\lambda} = \dfrac{\lambda}{c_{pw}(T_{air} - T_0)}$ and $\overline{\boldsymbol{n}}_i = \dfrac{\boldsymbol{n}_i L_0}{\rho_a D_0}$.

(v) Intracellular cell energy equation

Substituting the dimension quantities into an intracellular energy equation (4.26) gives the non-dimensional form

$$(1-\phi_i)\overline{\rho}_c \frac{\partial \overline{T_c}}{\partial \tau} = (1-\phi_i)\bar{\nabla}.(\overline{\kappa}_c \bar{\nabla}\overline{T}_c) - \overline{h}_i(\overline{T}_c - \overline{T}_i) - (\overline{j}_{ip} + \overline{j}_{ic})(\overline{T}_c - \overline{T}_i), \quad (4.37)$$

with $\overline{\kappa}_c = \dfrac{\kappa_c}{D_0 c_{pw} \rho_a}$.

(vi) Initial and boundary conditions

$\overline{P}_i = 1,\ \overline{\rho} = 1,\ \overline{T}_i = 0,\ \overline{T}_c = 0,\ M_f = M_{f0},\quad M_b = M_{b0}.$

Boundary conditions on the closed boundary at $\overline{x}$=0, assuming symmetry condition, the mass and heat flux are zero.

$\mathbf{n}.\bar{\nabla}\overline{T}_i = 0,\quad \mathbf{n}.\bar{\nabla}\overline{T}_c = 0,\quad \mathbf{n}.\bar{\nabla}M_f = 0,\quad \mathbf{n}.\bar{\nabla}M_b = 0,\quad \mathbf{n}.\bar{\nabla}\overline{\rho} = 0.$

Non-dimensional mass transfer boundary conditions at the surface for free water and intercellular space, at $\overline{x} = 1$, are given by

$$\overline{\rho}_s \overline{D}_f \bar{\nabla} M_f + \overline{\rho}_s \overline{D}_p M_f \bar{\nabla}\overline{P}_c = -Sh_f(\overline{C}_{fw,sur} - 1). \quad (4.38)$$

$$\text{and} \quad \overline{\rho}\overline{k}\bar{\nabla}\overline{P}_i + \overline{D_i}\bar{\nabla}\overline{\rho} = -Sh_i(\frac{\overline{\rho}}{\overline{C}_{air}} - 1), \quad (4.39)$$

with $\overline{C}_{fw,sur}$ as discussed in chapter 2 gives

$$\overline{C}_{fw,sur} = f(M_f)\overline{\beta}(\overline{T}_{sur}). \quad (4.40)$$

Non-dimensional surface convection mass transfer with respect to diffusivity in intercellular space and intracellular cell is estimated by the Sherwood number, given by

$$Sh_f = \frac{h_{m,f} L_0}{D_0}\frac{C_{air}}{\rho_a},\ Sh_i = \frac{h_{m,v} L_0}{D_0}\frac{C_{air}}{\rho_a}.$$

Non-dimensional energy balance at the surface for intercellular space and intercellular cell boundary, is given by

$$\phi_i \overline{\kappa}_v \bar{\nabla}\overline{T}_i = -\phi_i Nu_i \overline{\kappa}_v(\overline{T}_{isur} - 1). \quad (4.41)$$

$$\text{and} \quad (1-\phi_i)\overline{\kappa}_c\bar{\nabla}\overline{T}_c - \overline{\lambda}\,(\overline{D}_f\overline{\rho}_s\bar{\nabla}M_f + \overline{D}_p M_f\overline{\rho}_s\overline{\nabla P}_c) = -(1-\phi_i)\overline{\kappa}_c Nu_c(\overline{T}_{csur}-1). \tag{4.42}$$

Non-dimensional thermal diffusivity evolution with respect to water/vapour diffusivity evolution in the intercellular space and intracellular cell respectively is given by $\overline{\kappa}_c = \dfrac{\kappa_c}{\rho_a c_{pw} D_0}$, and $\overline{\kappa}_v = \dfrac{\kappa_v}{\rho_a c_{pw} D_0}$.

Convection at the surface with respect to conduction evolution for intercellular space and intracellular cell is given by the Nusset number as

$Nu_i = \dfrac{h_i L_0}{\kappa_v}$ and $Nu_c = \dfrac{h_c L_0}{\kappa_c}$.

Non dimensional latent heat given by $\overline{\lambda} = \dfrac{\lambda}{c_{pw}(T_{air}-T_0)}$.

The magnitude of each group was assessed by using literature values of physical, thermal and transport parameters in the capacity and kinetic coefficient. Information obtained from dimensionless equations is useful to predict the quantitative behaviour of temperature and moisture evaluation during food drying. From the dimensionless analysis some characteristic numbers were deduced. Using the magnitude of these numbers, it is possible predict the most significant transfer mechanisms that control food temperature and moisture evolution during drying.

4.5 Equation of state and phenomenological relations

To supplement the simultaneous heat and mass equations, closure of the system requires an equation of state and phenomenological physical relationships for the exchange processes between the intracellular cell and intercellular space.

(i) Equation of state of water vapour.

Water vapour released within the intercellular space phase is of sufficiency low density such that the water vapour is governed by the perfect gas law, hence

$$P_i = \rho_i R T_i. \tag{4.43}$$

Substituting a non-dimensional parameter in the perfect gas law gives

$$\overline{P}_i = \overline{\rho}\Big[1 + \frac{(T_{air} - T_0)}{T_0}\overline{T}_i\Big]. \tag{4.44}$$

(ii) Phase change.

Evaporation of water into water vapour during frying and drying processes has been implemented using an equilibrium formulation, whereby water in solid matrix is assumed to be in equilibrium with water vapour in the surrounding air at the surface. The relationship of vapour pressure and moisture content at equilibrium to temperature is given by a moisture isotherm and can be calculated using the water activity ratio such as discuss in chapter 2 and defined by

$$a_w = \frac{P_v}{P_{vs}}. \tag{4.45}$$

Many empirical equations have been developed (see for example [124, 8]) to express this relationship. Evaporation inside the food domain was ignored in that study ([124, 8]). However, in a recent work by Zhang and Datta [137], the actual vapour pressure in a fairly rapid process is seen to be lower than that given by equation (4.45). In most drying and frying processes, evaporation distributed inside the food domain exists, such as discussed by Zhang and Datta [137] and Halder *et al.* [53, 54, 51]. This suggests that the measure of vapour pressure and water activity may not be appropriate in modelling of fast transport processes of water vapour due to the time taken to reach equilibrium. Zhang and Datta [137], discuss the evaporation rate using a non-equilibrium approach that has been used in porous media models ([12]) to calculate the evaporation rate as given by

$$\dot{I} = K(P_{v,equi} - P_v), \tag{4.46}$$

where K is an empirical constant and $P_{v,equi}$ is the equilibrium vapour pressure. In a further investigation by Halder *et al.* ([52]), it was stated that the most appropriate value for K to best fit between experiment and simulation is $100s^{-1}(0.01)$ but Ousegi *et al.* suggest that this value is $1s^{-1}$. In our modelling, this formulation is appears in equations (4.14) and (4.18) and is related to the current formulation by

$$\dot{I} = j_{ic} + j_{ip}. \tag{4.47}$$

(iii) Internal pressure P_c

The mechanical and hydraulic properties of plant cells are critically important in determining both the physiological behaviour of plants and their behaviour in food processing [121]. The cell hydrostatic (turgor) pressure in intact plants cells was measured during experiments such as in work by [121, 112]. Most plant physiologists express hydrostatic pressure values (turgor) as above that of the atmosphere. Values of turgor in giant algal cells range from 0.1 to 0.6 MPa (100kPa-600kPa) [112]. Turgor pressure of 0.159 MPa (159 kPa) was measured for kiwi fruit tissue and 0.231 MPa (231kPa) for melon [100]. In this first instance the turgor pressure P_c remains constant and above the atmospheric pressure, that is $P_c > P_{atm}$ and given by,

$$P_c = B. \tag{4.48}$$

The value for the constant B=0.159 MPa and, in non-dimensional form $\overline{P}_c$ is taken as

$$\overline{P}_c = \frac{0.159}{P_{atm}} = 1.59. \tag{4.49}$$

On the other hand, in a simulation study by Ni *et al.* [84] for high-moisture material in microwave drying, the pressure increased rapidly during 3 minutes of drying at about 32kPa but the pressure eventually dropped as moisture was depleted by the end of drying. Following this, further models relevant to change of pressure related to the change of cellular volume, such as those discussed in Toupin *et al.* [114] and Zhiming and Le Maguer [140], were used. The difference in pressure is evaluated in relation to the change of cellular volume through a measure of the reversible elastic properties of the cell walls in the form of an empirical modulus ς ([86]) given by

$$dP_c = \varsigma \frac{dM_f}{M_f}, \tag{4.50}$$

where P_c is the osmotic pressure in the cellular cell above atmospheric pressure.

As discussed by Dianty [38], the empirical modulus, ς, is, in general, strongly affected by the internal pressure. Hence, integrating equation (4.50) yields

$$P_c = \varsigma \ln \frac{M_f}{M_{f0}} + P_{c0}. \tag{4.51}$$

Zhiming and Marc Le Maguer [140], stated at the incipient plasmolysis point where the turgor pressure is equal to the environment pressure, is given by non-dimensional

ς=3.5. The value of P_{c0}=159 kPa, as discussed in the case of constant internal pressure above. In non-dimensional form, equation (4.51) becomes

$$\overline{P}_c = 1.59 + 3.5 \ln \frac{M_f}{M_{f0}}. \tag{4.52}$$

An internal pressure P_c will correspond to the osmotic pressure and will reduce as the water content of cell is replaced by an air phase. On the other hand, the intercellular space pressure P_i will increase as evaporation takes place in this region.

4.6 Summary and conclusion

In this chapter, we have developed a multi-phase model for the movement of water and temperature by developing a representative model relevant to tropical fruits that is based on their cellular structure. We construct the theory of previous study of food structure, starting from a realistic picture of cellular tissue and the macrostructure of an unconsolidated porous medium to distinguish the pores (intercellular space) and the cell. Based on this cellular features, the model was derived using multiphase approach; each material constituent is taken as a distinct phase within the multiphase and with the constitutive law describing the material properties and its interaction with the neighbouring phase. To include interaction between neighbouring phases, we incorporate source terms $\overline{j}_{ip}$ and $\overline{j}_{ic}$ into the appropriate mass balance equations. Transfer fluxes $\overline{j}_{ip}$ and $\overline{j}_{ic}$ relates moisture transfer from intracellular cell into intercellular space lies at the heart of this new drying model. This is more relevant than the development of a formulation analogous to those equations well established for non-hydroscopic porous media such as discuss in section §1.3.3.

We identify the microscopic model for liquid content within the representative volume that falls into three categories: intercellular space, free water and bound water. We have considered the transport of water vapour in the intercellular space that is transported by convective (pressure driven) and diffusive mechanisms by considering the existence of intercellular space within a highly complicated network of pore channels, which can be considered as a porous medium. Free water, which is retained within the intracellular cell structure, is readily available to be transported by cell to cell diffusion. The model formulation was further extended to account for

bound water within the intracellular cell structure. This is strongly linked to the internal cell structure but may be released by local diffusion processes to the free water component.

In addition, the free water will also be transferred from cell to the intercellular space by diffusion through the wall of the space. In principle, this mechanism can be representation of the physical problem of phase changes between water and vapour inside the material during the drying process. The advantage of this multiphase model is that the movement of water can be modelled in greater detail than in single phase models, as we can track each phase. The ability to view each phase, we hope, will provide a more realistic interaction between phases as we can track each of them.

Furthermore, we have considered the formulation of an energy equation, with local moisture equilibrium on the cell scale, but within a macroscopic formulation that includes the representative temperature within the intercellular space T_i (water vapour) differing from a representative temperature T_c within the intracellular cell structure (free water). This will utilize the principle of local non-equilibrium between the cell and the intercellular space at a given location.

In the chapters that follow, we summarize the mathematical models we have developed and run a simulation for individual phase variables and consider the interaction between the intracellular cells with the intercellular space, as well as the effect of bound water within this cell.

Chapter 5

Multiphase one-dimensional isothermal conditions: case study of mango fruit

5.1 Introduction

The drying of foodstuffs is driven by moisture gradients within the cell matrix from drying conditions imposed at the surface. This is significantly enhanced by the addition of heat that also establishes thermal gradients and energy for conversion of water vapour to increase the drying rate. In this chapter, the multiphase model for drying under isothermal conditions is presented corresponding to the model developed in chapter 4. We analyse a mathematical model in order to identify the conditions under which the movement of water is not influenced by a thermal condition. Our model simulates the movement of water in terms of both a liquid phase and a vapour phase within a one-dimensional slab.

In this chapter, two sub-models are evaluated: firstly a simpler two-phase isothermal case, where bound water transfer is neglected. The modifying effect of including bound water transfer within the cellular structure is provided within a three-phase model. To enable closer identification of the transport mechanism, a one-dimensional geometry is taken, and this also provides an opportunity for comparison with previous simple models described in chapter 2.

5.2 Mathematical formulation

In this section, the formulation presented in chapter 4 is simplified by assuming that the sample undergoes one-dimensional movement parallel to the x-axis. A one-dimensional model is employed in the analysis since the sample approximates an infinite slab of thickness $2L$ with both ends insulated such as illustrated in Figure 5.1. The food is exposed to an air flow at the surface, for which the temperature is T_{air} with relevant relative humidity. Assuming symmetry at $x = 0$, only half of the domain requires computation i.e. $0 < x < L$ and symmetry conditions imposed at $x = 0$.

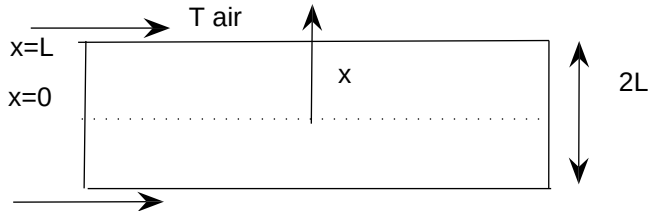

Figure 5.1: Schematic representation of food drying process

The corresponding set of governing equations for density of vapour $\overline{\rho}$ in the intercellular space, free water moisture M_f and bound water moisture M_b are given by equations (5.1)-(5.3) together with equations of transfer flux (equation (5.4) and (5.5)), in non-dimensional form. There are derived in chapter 4, given from (4.31), (4.32) and (4.33) together with the equations of transfer flux (4.34) and (4.35).
The mass conservation equation for a fixed intercellular space water vapour becomes

$$\phi_i \frac{\partial \overline{\rho}}{\partial \tau} = \frac{\partial}{\partial \overline{x}} \left[\overline{\rho}\, \overline{k} \frac{\partial \overline{P}_i}{\partial \overline{x}} + \overline{D}_i \frac{\partial \overline{\rho}}{\partial \overline{x}} \right] + \overline{j}_{ip} + \overline{j}_{ic}. \tag{5.1}$$

The conservation equation of bound water phase moisture is given by,

$$\frac{\partial M_b}{\partial \tau} = -\overline{n}_1 M_b + \overline{n}_2 M_f = -\overline{r}_b. \tag{5.2}$$

The conservation of free water moisture is given by

$$\overline{\rho}_s \frac{\partial M_f}{\partial \tau} = \frac{\partial}{\partial \overline{x}} \left[\overline{D}_f \overline{\rho}_s \frac{\partial M_f}{\partial \overline{x}} + \overline{D}_p\, M_f\, \overline{\rho}_s \frac{\partial \overline{P}_c}{\partial \overline{x}} \right] - \overline{j}_{ip} - \overline{j}_{ic} + \overline{r}_b\, \overline{\rho}_s. \tag{5.3}$$

The equation for mass flux of free water is associated with the differential pressure and concentration between the local cell and intercellular space, which is given by

$$\overline{j}_{ip} = \overline{k}_p(\overline{P}_c - \overline{P}_i), \tag{5.4}$$

$$\text{and} \quad \overline{j}_{ic} = \overline{k}_w(\eta - \xi). \tag{5.5}$$

In order to complete the set of equations listed above, the boundary conditions that connect the transport equations for two separated phases need to specified. The initial conditions are taken as uniform, i.e. $\overline{\rho} = 1, \;\; M_f = M_{f0}, \quad M_b = M_{b0}$.
Assuming the symmetry condition, boundary conditions at the centreline $x = 0$ become

$$\frac{\partial M_f}{\partial \overline{x}} = 0, \;\; \frac{\partial M_b}{\partial \overline{x}} = 0, \text{ and } \frac{\partial \overline{\rho}}{\partial \overline{x}} = 0. \tag{5.6}$$

The surface mass transfer intracellular cell/tissues boundary condition is given by

$$\overline{D}_f \overline{\rho}_s \frac{\partial M_f}{\partial \overline{x}} + \overline{D}_p M_f \overline{\rho}_s \frac{\partial \overline{P}_c}{\partial \overline{x}} = -Sh_f(\overline{C}_{fw,sur} - 1). \tag{5.7}$$

In equation (5.7), the term $\overline{C}_{fw,sur} = \beta(\overline{T}_{sur}) f(M_f)$ is the relationship between water vapour pressure and concentration of water vapour at the surface. $\beta(\overline{T}_{sur})$ is experimentally based relationship involving surface temperature as discussed in chapter 2, and given below,

$$\beta(\overline{T}_{sur}) = \frac{P_{\nu s}(\overline{T}_{sur})}{\overline{T}_{sur}} = A\,\overline{T}_{sur}^2 + B\,\overline{T}_{sur} + C, \tag{5.8}$$

The values of A, B and C will depend on air temperatures that are imposed during drying. Typical values for fruit are $A = 0.0364, B = 0.0108$ and $C = 0.0119$ for air temperature drying at 60^0C. Equation $f(M_f)$ using the relationship between water activity and moisture content M is given below,

$$\text{and } f(M_f) = \frac{\sigma\, M_f^{2.38}}{0.062^{2.38} + M_f^{2.38}}. \tag{5.9}$$

The value of $\sigma = \dfrac{84.55}{C_{air}}$, depends on the air temperature.
Corresponding mass transfer surface conditions for intercellular space at the surface are obtained from flux balances and given by

$$\overline{\rho}\overline{k}\frac{\partial \overline{P}_i}{\partial \overline{x}} + \overline{D}_i \frac{\partial \overline{\rho}}{\partial \overline{x}} = -Sh_i(\frac{\overline{\rho}}{\overline{C}_{air}} - 1). \tag{5.10}$$

In summary, our model comprises equations (5.1)-(5.3) with transfer fluxes, equations (5.4) and (5.5) together with boundary conditions given by equations (5.6) - (5.10). In the following sections, we present solutions to the model equations within various limits. In section §5.3 we consider the limit at which the intercellular space is large; in §5.3.1, analytical solutions are presented in the case for negligible diffusion and convection inside the intercellular space; in §5.3.2, numerical solutions are presented for the case with diffusion and convection inside intercellular space. In section §5.4 the corresponding two-phase model is presented, in which the drying processes are driven specifically by gradients in moisture content between intercellular space and the intracellular cell. The numerical solution results are presented in §5.4.2 and a parametric study is conducted in §5.5. The effect of pressure is considered in §5.6, which allows the effect of variable pressure to be included in the movement of free water. In §5.7, the model is further extended to include a third phase to incorporate the effect of bound water.

5.3 Drying through intercellular space dominance

From chapter 4, it will be assumed that the intercellular space comprises interconnected pores characterized by a porosity, ϕ_i. We consider the limit in which the intercellular space is large i.e ϕ_i=1 and derive appropriate equations and boundary conditions. Mass conservation for water vapour in the intercellular space is taken as

$$\frac{\partial(\phi_i \rho_i)}{\partial t} + \nabla . \boldsymbol{n}_i = j_{ip} + j_{ic}, \tag{5.11}$$

with

$$\boldsymbol{n}_i = \rho_i \boldsymbol{u}_i + \boldsymbol{J}_i, \tag{5.12}$$

Assuming constant temperature and using the perfect gas law of vapour, gives $\overline{P}_i = \gamma \overline{\rho}$. Using $\overline{\rho} = \dfrac{\rho_i}{\rho_a}$, in non-dimension form the mass conservation for water vapour is given by

$$\phi_i \frac{\partial \overline{\rho}}{\partial \tau} = \overline{k}\overline{\rho}\gamma[\frac{\partial^2 \overline{\rho}}{\partial x^2}] + \overline{D}_i \frac{\partial^2 \overline{\rho}}{\partial \overline{x}^2} + \overline{j}_{ip} + \overline{j}_{ic}, \tag{5.13}$$

The source of water into the intercellular space is provided by two mechanisms:

1. Transfer associated with the differential pressure between the local cell and inter-

cellular space and is taken as

$$\overline{j}_{ip} = \overline{k}_p(\overline{P}_c - \overline{P}_i). \tag{5.14}$$

Taking a constant pressure $\overline{P}_c = \overline{\rho}_c$, then

$$\overline{j}_{ip} = \overline{k}_p(\overline{\rho}_c - \gamma\overline{\rho}). \tag{5.15}$$

This value of $\overline{j}_{ip}$ will link water transfer between the intracellular cell with intercellular space.

2. Transfer dependent on the differential moisture levels across the membranes,

$$\overline{j}_{ic} = \overline{k}_w(C_{fw} - C_i). \tag{5.16}$$

Rewriting equation (5.16) gives $\overline{j}_{ic} = \overline{k}_w(\eta - \xi)$,
with $\eta = \dfrac{M_f}{\dfrac{\rho_w}{\rho_s} + M_f}$ and $\xi = \dfrac{\overline{\rho} - 1}{\dfrac{\rho_w}{\rho_a} - 1}$, and equation (5.16) will become

$$\overline{j}_{ic} = \overline{k}_w(\overline{\rho}_c - \overline{\rho}), \tag{5.17}$$

with $\overline{\rho}_c = \dfrac{M_f\rho_s + 1}{1 + \dfrac{\rho_s}{\rho_w}Mf}$. This value of $\overline{\rho}_c$ will link the intracellular cell water M_f with intercellular space $\overline{\rho}$.

In the case of intercellular space dominated drying, $\overline{j}_{ip}$ and $\overline{j}_{ic}$ are not strongly correlated with the free water M_f. We consider the dominant source of vapour release into intercellular space is given by

$$j = C(\overline{\rho}_c - \overline{\rho}).$$

with C is constant. These choices correspond with the assumption that the cell and intercellular space comprise of essentially the same matter i.e water vapour; the difference in vapour in the cell with intercellular space is therefore attributed to the flow of vapour. Model equation (5.13) is reduced to the form

$$\phi_i\frac{\partial\overline{\rho}}{\partial\tau} = \overline{k}\gamma\overline{\rho}[\frac{\partial^2\overline{\rho}}{\partial x^2}] + \overline{D}_i\frac{\partial^2\overline{\rho}}{\partial\overline{x^2}} + C(\overline{\rho}_c - \overline{\rho}). \tag{5.18}$$

5.3.1 Negligible diffusion and convective flow inside the intercellular space

In this case we consider the system with the limit in which the intercellular space is large i.e ϕ_i=1, where local values of vapour density $\overline{\rho}$ is determined from cells. The model equation will be in the form of

$$\frac{\partial \overline{\rho}}{\partial \tau} = C(\overline{\rho}_c - \overline{\rho}), \tag{5.19}$$

and the resulting equation becomes

$$\overline{\rho} = \overline{\rho}_c + A \exp^{-C\overline{\rho}\tau} \tag{5.20}$$

Using initial condition $\overline{\rho} = 1$, equation (5.20) becomes

$$\overline{\rho} = \overline{\rho}_c + (1 - \overline{\rho}_c) \exp^{-C\overline{\rho}\tau} . \tag{5.21}$$

Figure 5.2 shows the Figure of simplified case, τ=0 gives $\overline{\rho} = 1$ and if $\tau \to \infty$,

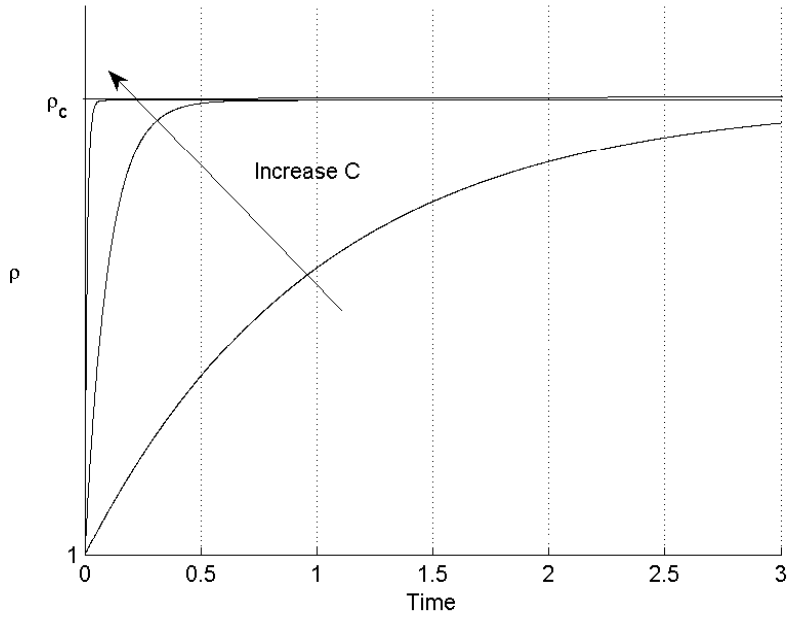

Figure 5.2: No diffusion and convection inside the intercellular space.

gives $\overline{\rho} = \overline{\rho}_c$. If C is bigger, the time taken to reach equilibrium of vapour is shorter,

given by Figure 5.2, where the bigger the value of C, the more quickly equilibrium is achieved. Value for parameter C, is not readily available in the literature since they will depend upon the characteristics of the cell membrane. We choose C=0.1 simply to illustrate the behaviour that can arise.

5.3.2 With diffusion and convective flow inside the intercellular space $\overline{D}_i$ and $\overline{k}$

In this simple case, we want to look at a system where the local value of vapour density is determined from the cell, is transferred into intercellular space and from intercellular space into the underlying air. Assuming uniform temperature and using non-dimension $\overline{\rho} = \dfrac{\rho_i}{\rho_c}$, in non-dimension form the mass conservation for water vapour is given by

$$\frac{\partial \overline{\rho}}{\partial \tau} = \frac{\partial}{\partial x}\left[(\overline{k}\gamma\overline{\rho} + \overline{D}_i)\right]\frac{\partial \overline{\rho}}{\partial \overline{x}} + j, \tag{5.22}$$

with $j = C(1 - \overline{\rho})$.

Initially, vapour density inside intercellular space is equal to the vapour density

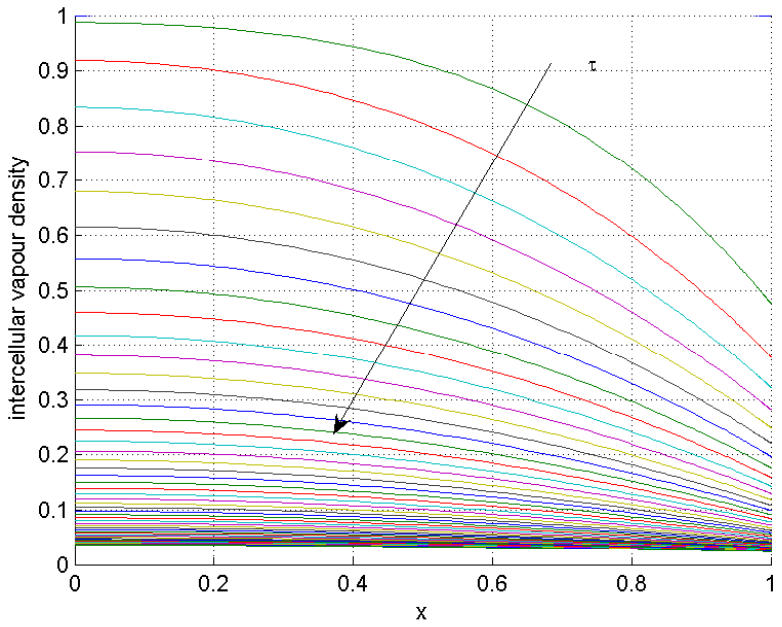

Figure 5.3: A plot of vapour density, $\overline{\rho}$ at τ=0-1, in steps of τ=0.01. Parameter values: $\overline{D}_i$=1, $\overline{k}$=1, Sh=5, C=0.01.

inside the cell, and is given by $\rho_i(t=0) = \rho_c$. In non-dimension form it gives $\overline{\rho} = 1$. The non-dimensional surface boundary at the intercellular space becomes

$$\left[(\overline{\rho}\,\overline{k}\gamma + \overline{D}_i)\right]\frac{\partial \overline{\rho}}{\partial \overline{x}} = -Sh_i(\frac{\overline{\rho}}{\overline{C}_{air}} - 1), \tag{5.23}$$

with $\overline{C}_{air} = \dfrac{C_{air}}{\rho_c}$

Equation (5.22) with initial and boundary conditions is solved numerically using initial value problem solver, pdepe in Matlab. The evolution of vapour density $\overline{\rho}$, is shown in Figure 5.3; arrows indicate the direction of increasing time. Figure 5.3 shows how the intercellular vapour density decreases because of diffusive and convective of vapour flow.

Case $\overline{k}$=0

In the case of $\overline{k}$=0, the resulting equation becomes

$$\frac{\partial \overline{\rho}}{\partial \tau} = \overline{D}_i \frac{\partial^2 \overline{\rho}}{\partial \overline{x}^2} + j, \tag{5.24}$$

with $j = C(1-\overline{\rho})$. In this case, the drying process dominated by diffusion within the pore space $\overline{k} << 1$.

Equation (5.24) with initial and boundary conditions was solved numerically and the effect of each varying parameter diffusivity $\overline{D}_i$ and transfer flux coefficient C was investigated. The evolution of vapour density $\overline{\rho}$, is shown in Figure 5.4: arrows indicate the direction of increasing time.

Figure 5.5(a), where fixed value of diffusivity $\overline{D}_i = 1$ and changes the value of transfer flux coefficient C from 0.001-1. From the graph, an increased value of the transfer flux coefficient C leads to a slow decrease in vapour density. Figure 5.5(b), where fixed value of transfer flux coefficient $C = 0.01$, changes the value of diffusivity $\overline{D}_i$ from 1-1000. From the graph, the increasing value of diffusion $\overline{D}_i$ leads to decreasing density of the intercellular space more quickly.

Case $\overline{D}_i = 0$

In the case of diffusivity $\overline{D}_i = 0$, the resulting equation becomes

$$\frac{\partial \overline{\rho}}{\partial \tau} = \overline{k}\gamma\overline{\rho}\frac{\partial^2 \overline{\rho}}{\partial \overline{x}^2} + j, \tag{5.25}$$

with $j = C(1-\overline{\rho})$. In this case, the drying process is dominated by porous diffusivity (permeability) within the pore space, $\overline{D}_i << 1$.

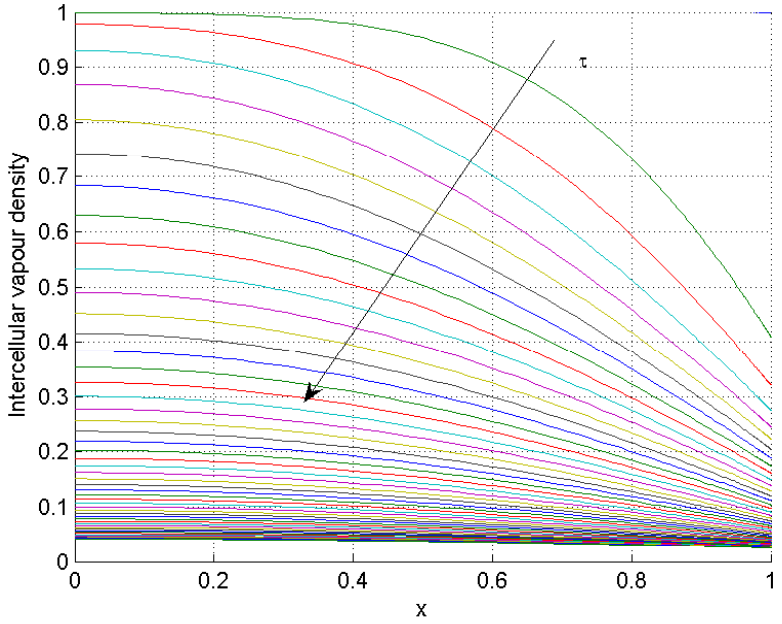

Figure 5.4: A plot of vapour density,$\overline{\rho}$ at τ=0-1, in steps of τ=0.01. Parameter values: $\overline{D}_i$=1, $\overline{k}$=0, Sh=5, C=0.01.

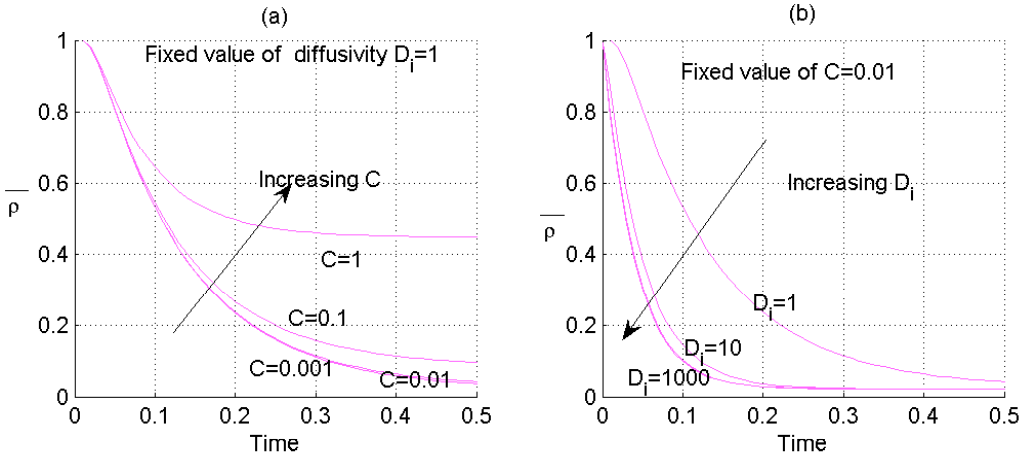

Figure 5.5: Centre profile plot of intercellular space density ($\overline{D}_i \neq 0$ and $\overline{k} = 0$) .

Simulations were conducted for equation (5.25) with initial and boundary conditions and the effect of varying parameter permeability $\overline{k}$ and transfer flux coefficient C were investigated. Figure 5.6 shows the evolution of vapour density decreasing with time. Vapour decreases much faster, especially at the surface and tends to become very slow at the end. Comparison of Figure 5.4 and 5.6 shows the different profiles of decreasing vapour density .

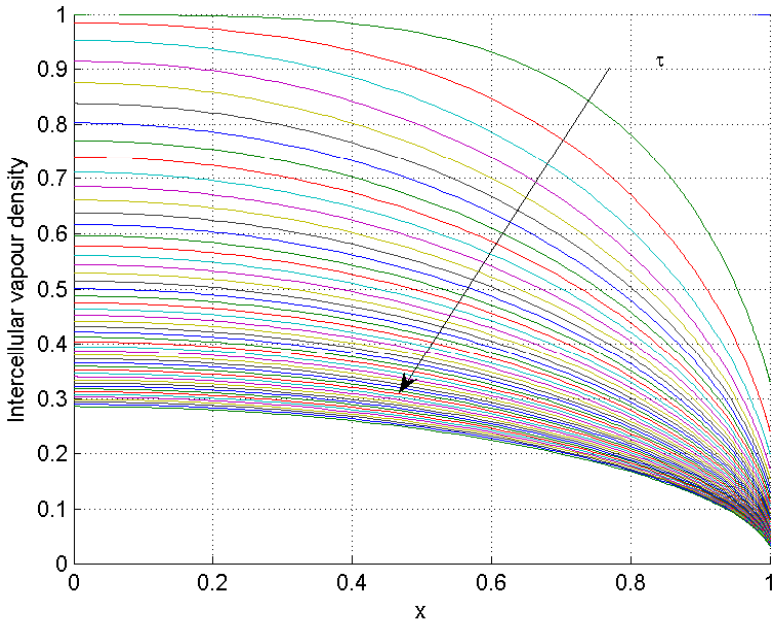

Figure 5.6: A plot of vapour density, $\overline{\rho}$ at τ=0-1, in steps of τ=0.01. Parameter values: $\overline{D}_i$=0, $\overline{k}$=1, Sh=5, C=0.01.

Figure 5.7(a) shows that, when we increase the value of C, there is more transfer of vapour into intercellular space, leading to a slow decrease of intercellular space vapour density. Figure 5.7(b) shows the increasing value of permeability $\overline{k}$ leading to decreasing density of vapour inside the intercellular space more qiuckly.

In this subsection, we have analysed the effect of vapour flow on a one-dimensional slab during drying, where the cell and intercellular space comprise of essentially the same matter i.e water vapour. A numerical solution was constructed at the limit of an asymptotically large intercellular space, for which diffusive and convective flow of vapour occurs. We have shown that diffusive flow of vapour has been captured,

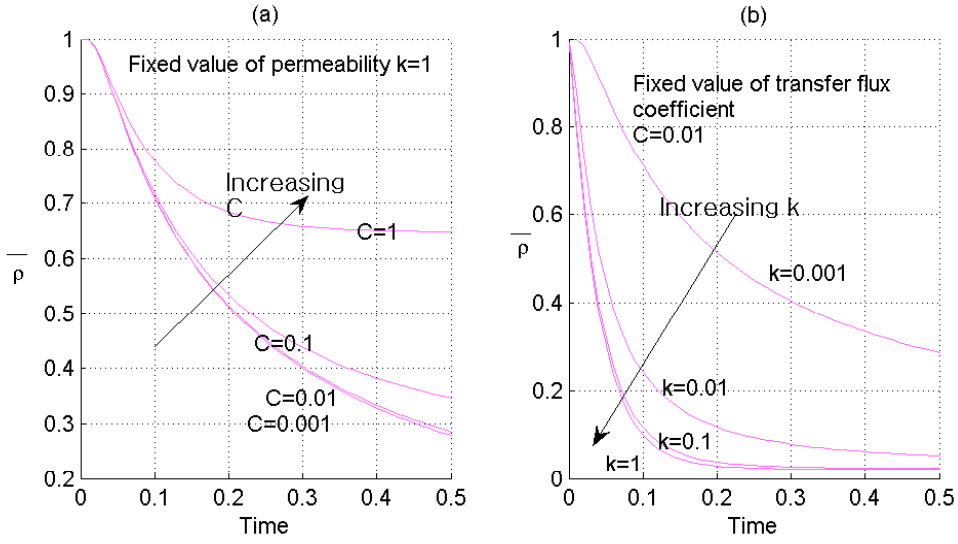

Figure 5.7: Centre profile plot of intercellular space density ($\overline{D}_i = 0$ and $\overline{k} \neq 0$).

showing the same behaviour as the flow of water in the cell as in chapter 2, but a different profile of the convective flow (permeability) of vapour has been detected. The result also tend to show the response of the intercellular water vapour is more sensitive to diffusive flow compared to permeability flow of water vapour.

5.4 Isothermal two-phase model

Solution for the isothermal model is given by solving the two coupled pdes (5.1) and (5.3). Analysis of this simplified case will enable insight into the drying processes, driven specifically by gradients in moisture content between intercellular space and intracellular cell components. Simplification is sought in the first instance by noting that the transfer of bound water is anticipated to be small i.e $\overline{n}_1, \overline{n}_2 << 1$ and its contribution to drying is negligible, other than in the final drying state; this gives the value $\overline{r}_b = 0$. A further simplification is taken that the value of internal turgor pressure $\overline{P}_c$ remains constant and above atmospheric pressure P_{atm} during the main drying stage. Initially, we take this value as $\overline{P}_c$=1.59, a value of turgor pressure for kiwi fruit tissue [100]; the effect of changing $\overline{P}_c$ will be analysed in later study.

For isothermal conditions, the drying is driven by moisture gradients with the temperature of the food remaining constant during drying and latent heat effects

taken as negligible. As discussed in chapter 2, the temperature increases rapidly to air temperature. Using the equation of state (4.44) gives $\overline{P}_i = \overline{\rho}\gamma$, where the value of γ corresponds to the value of T_{air}. For a special case of drying simulation, the air temperature is taken as 60^0C, and $\gamma = 1.09$. Simplification of equations (5.1)-(5.3) reduces to a system of two pdes,

$$\phi_i \frac{\partial \overline{\rho}}{\partial \tau} = \frac{\partial}{\partial x}\Big[(\overline{\rho}\,\overline{k}\,\gamma + \overline{D}_i)\frac{\partial \overline{\rho}}{\partial \overline{x}}\Big] + \overline{\dot{j}}_{ip} + \overline{\dot{j}}_{ic}, \tag{5.26}$$

$$\text{and} \quad \overline{\rho}_s \frac{\partial M_f}{\partial \tau} = \frac{\partial}{\partial \overline{x}}\Big[\overline{D}_f \overline{\rho}_s \frac{\partial M_f}{\partial \overline{x}}\Big] - \overline{\dot{j}}_{ip} - \overline{\dot{j}}_{ic}. \tag{5.27}$$

Transfer fluxes are given by

$$\overline{\dot{j}}_{ip} = \overline{k}_p(\overline{P}_c - \gamma\overline{\rho}), \tag{5.28}$$

$$\overline{\dot{j}}_{ic} = \overline{k}_w(\eta - \xi), \tag{5.29}$$

where η is the level of free moisture within the cell and ξ is the level of the water within the intercellular space, as discussed in chapter 4.

A set of initial conditions, typically prevailing in the drying process is necessary to perform the numerical simulations. In order to apply the model, a porous structure is supposed for a mango. A special case of drying simulation of a references food system based on mango with porosity ϕ_i=0.2 (see [72]). This will give the volume fraction of intracellular cell region as $\varepsilon_f = 0.8$. In the non-shrinkage model, these values are taken to be constant. It is also assumed that the volume fraction of free water in the intracellular cell region $\varepsilon_{fw} = 0.8$. The density of water and solid is fixed at 1000 kg/m^3 and 1080 kg/m^3 respectively. Using definitions of (4.1) and (4.3), gives associated initial conditions as M_f=3.70, and $\overline{\rho}$=1.

Boundary conditions on the symmetry boundary at $\overline{x} = 0$ are given by
$\dfrac{\partial M_f}{\partial \overline{x}} = 0, \quad \dfrac{\partial \overline{\rho}}{\partial \overline{x}} = 0.$
Boundary conditions on the surface, at $x = 1$, are given by

$$\overline{D}_f \overline{\rho}_s \frac{\partial M_f}{\partial \overline{x}} = -Sh_f(\overline{C}_{fw,sur} - 1). \tag{5.30}$$

$$\text{and} \quad \Big[(\overline{\rho}\,\overline{k}\gamma + \overline{D}_i)\Big]\frac{\partial \overline{\rho}}{\partial \overline{x}} = -Sh_i(\frac{\overline{\rho}}{\overline{C}_{air}} - 1). \tag{5.31}$$

with $\overline{C}_{fw,sur} = \beta(\overline{T}_{sur})f(M_f)$.
$\beta(\overline{T}_{sur}) = 0.0364\,\overline{T}^2_{sur} + 0.0108\,\overline{T}_{sur} + 0.0119$, β_1 for isothermal case and
$f(M_f) = \dfrac{84.55\,M_f^{\zeta}}{\varphi^{\zeta} + M_f^{\zeta}}$, with $\varphi = 0.062$ and $\zeta = 2.38$.

5.4.1 Numerical Solution

These equations were solved using COMSOL Multiphysics. COMSOL is a PDE-based multiphysics tool that makes use of finite element modeling (FEM). In FEM, a domain defining a continuum is discretized into simple geometric shapes called elements. Properties and the governing relationships are assumed over these elements and expressed mathematically in terms of unknown values at specific points (a odes) in the elements called nodes. The elements in the domain are linked by an assembly process. Solution of the governing equations of the phenomenon, initial conditions and boundary conditions in the domain give the approximate prediction of the results. A mesh consisting of 2400 quadrilateral elements was constructed and the equation for moisture was solved using UMFPACK solver. Equations (5.26) and (5.27) were input into COMSOL Multiphysics (PDE) solver with the general form for intercellular density of vapour and free water moisture. In the general equation system forms, the PDEs and boundary conditions are written in the following functional form (see [24]):

$$\begin{cases} e_a \dfrac{\partial^2 u}{\partial t^2} + d_a \dfrac{\partial u}{\partial t} + \nabla.\Gamma = F & \text{in } \Omega, \\ -\mathbf{n}.\Gamma = G - h^T \mu & \text{on } \partial\Omega, \\ 0 = R & \text{on } \partial\Omega. \end{cases}$$

Moreover, the transfer flux (5.28) and (5.29) gives the coupling effects for both the intercellular space and intercellular cell free water moisture.

In Comsol the isothermal two-phase, one-dimensional drying model, two dependent variables $\overline{\rho}$ and M_f are formulated

$$\phi_i \frac{\partial \overline{\rho}}{\partial \tau} + \frac{\partial}{\partial \overline{x}}\Big[- (\overline{\rho}\,\overline{k}\gamma + \overline{D}_i)\frac{\partial \overline{\rho}}{\partial \overline{x}}\Big] = \overline{j}_{ip} + \overline{j}_{ic}, \tag{5.32}$$

$$\text{and} \quad \overline{\rho}_s \frac{\partial M_f}{\partial \tau} + \frac{\partial}{\partial \overline{x}}\Big[- \overline{D}_f \overline{\rho}_s \frac{\partial M_f}{\partial \overline{x}}\Big] = -\overline{j}_{ip} - \overline{j}_{ic}. \tag{5.33}$$

Identifying the general form with equations (5.32) and (5.33), the following settings generate the equation (Table 5.1 and Table 5.2):

Two boundary conditions, boundary condition at the centreline $x = 0$ will give Neumann type boundary condition with $G = 0$ and influx boundary condition at the surface $x = 1$ will give Neumann type boundary condition with $G = -Sh_f(\overline{C}_{fw,sur} - 1)$ and $G = -Sh_i(\frac{\overline{\rho}}{\overline{C}_{air}} - 1)$ respectively.

Table 5.1: Equation generated for intercellular vapour density.

Coefficient	Value Expression
e_a	0
d_a	ϕ_i
Γ(flux vector)	$-(\overline{\rho}\,\overline{k}\gamma + \overline{D}_i)\frac{\partial \overline{\rho}}{\partial \overline{x}}$
F(source term)	$\overline{j}_{ip} + \overline{j}_{ic}$

Table 5.2: Equation generated for free water moisture.

Coefficient	Value Expression
e_a	0
d_a	$\overline{\rho}_s$
Γ(flux vector)	$-\overline{D}_f \overline{\rho}_s \frac{\partial M_f}{\partial \overline{x}}$
F(source term)	$-\overline{j}_{ip} - \overline{j}_{ic}$

The food domain was discretized into a total number of 320 elements. The time dependent problem was solved by an implicit time-stepping scheme, leading to non linear system of equations for each time step. Newton's method was used to solve each non-linear system of equations, whereas a direct linear system solver was adopted to solve the resulting systems of linear equations. The relative and absolute tolerance were set to 10^{-4} and 10^{-5}, respectively. The drying process is considered to be completed when the moisture content in the sample is asymptotic to a residual level.

We remark here that, due to the absence of experimental data on which to base our model parameter values and the fast timescale chosen, in all subsequent numerical simulations, the parameter values are selected from the literature data to illustrate the behaviour of the model under a particular movement regime. In the first instance, generic values of non-dimensional parameters are given as a constant value given from Table 5.3 and a range of non-dimension physically relevant values are shown in Table 5.4 below.

Non-dimensional parameters are
$Sh_f = \dfrac{h_{m,f} L_0}{D_0}\dfrac{C_{air}}{\rho_a}$, $Sh_i = \dfrac{h_{m,v} L_0}{D_0}\dfrac{C_{air}}{\rho_a}$, $\overline{D}_i = \dfrac{D_i}{D_0}$, $\overline{D}_f = \dfrac{D_f}{D_0}$,

Table 5.3: Input parameter values used in the simulation of mango drying.

Parameter	Value	Units and Source.
Gas and vapour intrinsic permeability (k_i)	10^{-14}	m^2 [85]
Viscosity of vapour in intercellular space (μ_i)	1.8×10^{-5}	Pa s[39]
Constant diffusivity (D_0)	$8.56 \times 10^{-10} - 8.121 \times 10^{-9}$	m^2 (refer chapter 2)
Vapour diffusivity in air (D_i)	2.6×10^{-5}	m^2 [131]
Effective diffusivity of cell (D_f)	$8.56 \times 10^{-10} - 8.121 \times 10^{-9}$	m^2 (refer chapter 2)
Ambient Pressure (P_{atm})	101325	Pa
Density of water (ρ_w)	1000	kg m^{-3}
Density of Vapour (ρ_v)	0.825	kg m^{-3}
Density of solid (ρ_s)	1080	kg m^{-3}
Density of air (ρ_i)	1.029	kg m^{-3}
Mass transfer coefficient of water vapour ($h_{m,v}$)	$8 \times 10^{-3} - 4 \times 10^{-4}$	m/s [131]
Mass transfer coefficient of water ($h_{m,f}$)	$0.0001 - 0.00031$	m/s (Refer chapter 2)
Gas Constant (R)	8.314	KJ $mol^{-1}K^{-1}$

Table 5.4: Non-dimensional parameter values.

Non-dimensional parameter	Value	Range of value.
Sh_i	5	1-20
Sh_f	20	0.1-20
$\overline{D}_f$	1	0-2
$\overline{D}_i$	1	1-10^4
$\overline{k}$	1	1-10^4
$\overline{k}_p$	10^{-3}	0-1
$\overline{k}_w$	10^{-3}	0-1

$\overline{k} = \dfrac{k_i P_{atm}}{\mu D_0}$, $\overline{k}_p = \dfrac{k_p P_a L_0^2}{D_0 \rho_a}$ and $\overline{k}_w = \dfrac{k_w L_0^2 \rho_w}{D_0 \rho_a}$.

The value for k_p is a measure of local cell pore permeability, number density and size but this value is not available in the case of drying. However, in an experimental study in the osmotic dehydration process, the permeability of the plasmodesmata, was taken as 1.14 x 10^{-10} kg mol $N^{-1}s^{-1}$ [113]. A similar analysis was reported Tyree [117], who showed that the permeability of the plasmodesmata to water was at least two orders of magnitude greater than that of the plasmalemma. Using this condition gives the non-dimension value of $\overline{k}_p$=10^{-3}.

Similarly, little is currently known about the value of k_w. As discussed by Halder *et al.* [50] in the case of flux of water inside the cell to the outside into intercellular space, the cell membrane exhibits three order of magnitude lower permeability. It is likely that this is the controlling limiting parameter of the transport of water. Based on their discussion, using potato membrane permeability, this value is computed to be order 10^{-11} m^2/s. This value gives the non-dimension value of $\overline{k}_w$=10^{-3}.

We pause to remark here that, in view of non-dimensionalisation $\tau = \dfrac{D_0 t}{L_0^2}$, the timescale of interest is the time taken for moisture to be diffused to the surface along the thickness of the fruits. The diffusion coefficient of free water $\overline{D}_f$ is given for the fruits around 10^{-9} m/s and the thickness of fruits of 5-10 mm (0.005-0.01 m). The time for drying to reach equilibrium was taken as 15000-36000 seconds [40] for drying of a mango slice, given a time scale of approximation 0.36-1.44. Using the same timescale for water vapour to transfer to the surface through the thickness, the diffusion coefficient of vapour D_i is 10^{-5}, which gives the time scale for vapour transfer approximately 10^3 faster than the timescale for water diffusion. We note that this is very short in comparison with the time for drying to reach equilibrium moisture. We therefore expect the ratio of the vapour timescale to flow of water timescale to be very large; however in this chapter (and the preceeding chapter of this thesis), we consider the ratio to be $\boldsymbol{O}(1)$, employing slow timescale rates for vapour to illustrate features of the system.

5.4.2 Analysis of isothermal two-phase model

In this section, the results of drying simulation with isothermal conditions for two-phase models are presented for the generic conditions given in section §5.4.1. The overbar notation in the graph is dropped as clarity. The time evolution of the free water moisture and intercellular vapour density is shown in Figure 5.8 and Figure 5.9. The arrows indicate the direction of increasing time. The corresponding free water moisture and intercellular vapour density at the surface and centreline are also shown in these figures. The effect of transfer fluxes to free water moisture and intercellular vapour density is shown in Figures 5.10, 5.11 and 5.12.

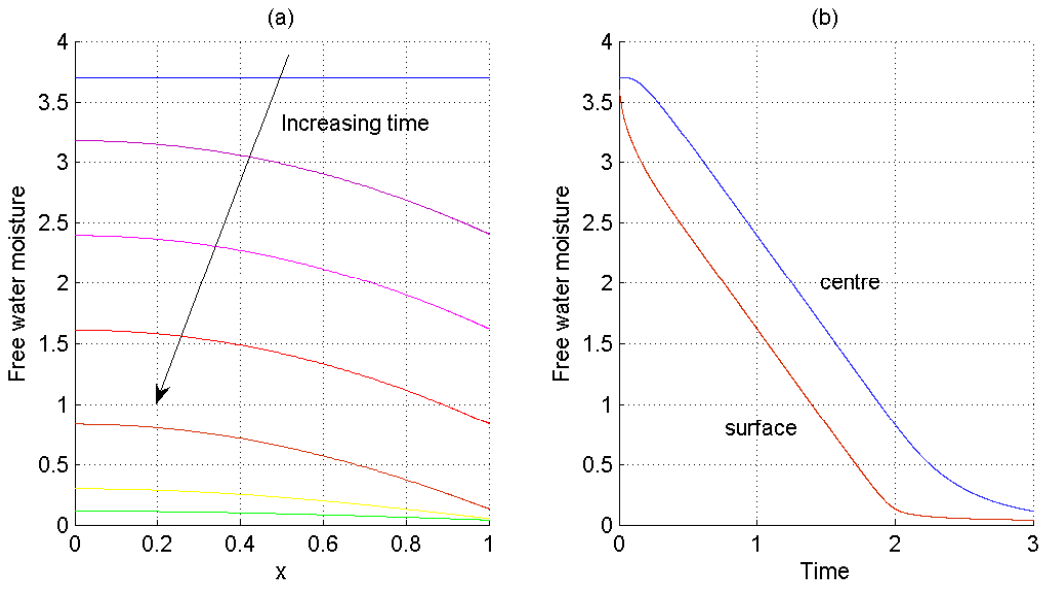

Figure 5.8: (a) Contour profile of free water moisture through the sample, with elapsed time τ=0-3 in step of 0.5 (b) Profile of free water moisture at the surface and centre. Dimensionless parameter values given by $Sh_f = 20$, Sh_i=5, $\overline{D}_f$=1, $\overline{D}_i$=1 $\overline{k}$=1, $\overline{k}_p$=0.01, and $\overline{k}_w$=0.01.

Figure 5.8(a) shows the contour profile of free water moisture(M_f) in the intracellular cell. The moisture profiles are plotted at points that correspond to the non-dimensional drying time of 0, 0.5, 1, 1.5, 2, 2.5 and 3. In the very initial stages of drying (time τ=0-1.5), there is a rapid decreased in moisture at the surface while the removal of moisture is slower at the centre of the product. The rapid surface

moisture removal, due to the large moisture gradient at the surface, prevents surface moisture from accumulating. After time τ=2, the removal of moisture becomes slower and relatively flat at the end of drying. In fact, at the beginning of the process, the profiles appear very well separated, while they tend to overlap as soon as drying rate decreases. This is similar to the results obtained in chapter 2, in which there was only a single phase of transfer of moisture.

Figure 5.8(b) shows the moisture profile of the free water moisture at the center and the surface of the product. It can be seen that the surface directly exposed to the drying air approaches the equilibrium moisture content faster (τ=2) and changes in the deeper layer are slow (τ=2.5). At the surface, moisture removal takes place straight after the start of drying but, in the centre, moisture is uniform at the beginning(τ=0-0.2) but as time increases, the moisture is no longer confined to the centre as water flows from the intracellular cell to the intercellular space and from the intracellular cell to the surface. As time increases, the rate of reduction of moisture becomes less, i.e., it reduces almost steadily with the progressing heating period. Starting from uniform initial moisture content, after a short warm up period, the free moisture content is reduced at a constant rate. At this stage, free water is bought to the surface by diffusion and by transfer fluxes to intercellular space. As the drying continues, the free water moisture is relatively flat and this will be investigated in the three-phase model where the bound water will take effect at this stage. It can be seen that moisture on the surface decreases rapidly compared to the centre of the fruit.

Figure 5.9 shows how the intercellular space is influenced by the present of source terms in the equations. The source of vapour from water inside intracellular cells is given by the transfer fluxes $\overline{j}_{ip}$ and $\overline{j}_{ic}$ in equations (5.28) and (5.29). The vapour density profile of intercellular space refers to water vapour flow through the intercellular air space of the tissues. The density of vapour profiles in the food during the period of drying decreases rapidly in the initial stage and becomes relatively flat at the end. Intercellular water vapour density profiles start decreasing due to the flow of water vapour from the fruit, is caused by convective flow and diffusive flow of water vapour. Vapour near the surface decreases rapidly compared to the centre of the fruit.

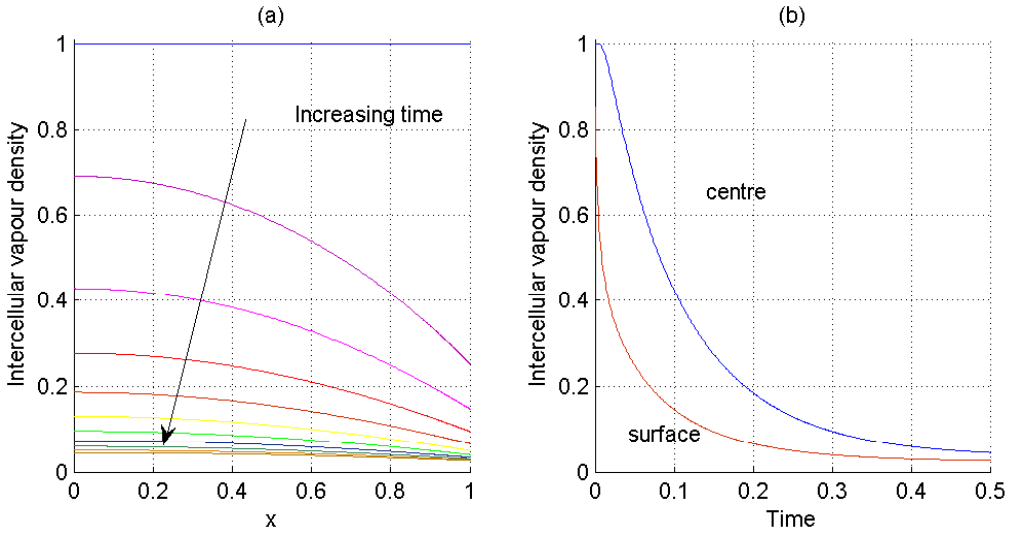

Figure 5.9: (a) Contour profile of intercellular vapour density, with elapsed time $\tau = 0 - 0.5$ in step of 0.05. (b) Profile of intercellular vapour density at the centre and surface. Parameter values as given in Figure 5.8.

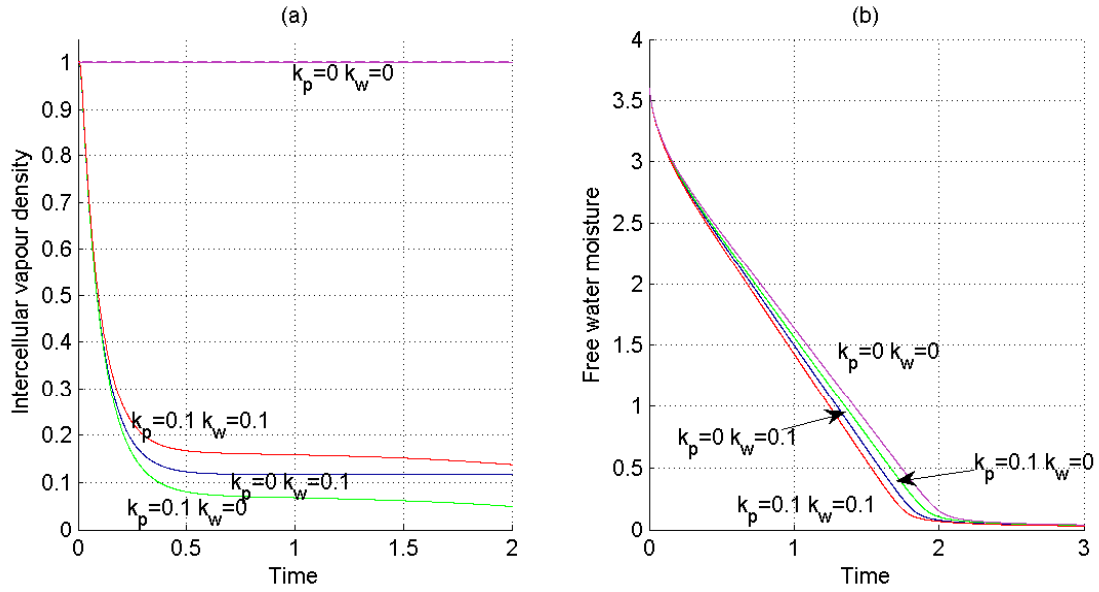

Figure 5.10: Profile at the surface of (a) intercellular vapour density (b) free water moisture with $\overline{k}_p$ and $\overline{k}_w$=0 compared with other values of $\overline{k}_p$ and $\overline{k}_w$.

The source and sink transfer fluxes will give a link between intracellular cell water and intercellular space. By putting this effect into drying, we have assumed that the water flux across the cell membrane and cell pores from cell to intercellular space can be expressed as $\overline{j}_{ip}$ and $\overline{j}_{ic}$. To see the effect of transfer flux, first we consider no transfer flux between intercellular space with intracellular cell ($\overline{j}_{ic}$=0 and $\overline{j}_{ip}$=0), in this case, for instance by putting the value of $\overline{k}_p$=0 and $\overline{k}_w$=0 and comparing it with the other values of $\overline{k}_p$ and $\overline{k}_w$. Figure 5.10(a) shows the intercellular vapour density and 5.10(b) shows the decrease in free water moisture in the cell with different values of $\overline{k}_p$ and $\overline{k}_w$. It was observed that, with no transfer flux $\overline{k}_p$=0 and $\overline{k}_w$=0, there is no water vapour in the intercellular space and the liquid water decreases more slowly. In this case, there is no exchange between liquid water to water vapour inside the fruit, evaporation occurs only at the external surface of cells leading to a slower decrease in free water moisture. The values of $\overline{k}_p$=0.1 and $\overline{k}_w$=0.1, show effects of transfer flux because of the pressure difference and concentration difference in which the intercellular vapour density increases but the convective and diffusive flow of vapour brings the vapour to the surface and leads to decrease vapour. Figure 5.10(b) shows that free water is transferred from the cell into vapour in the intercellular space that leads to a greater decrease in free water moisture in the cell. It was also observed that $\overline{k}_w$ term gives more effect compared to $\overline{k}_p$ term as the free water decreases rapidly when $\overline{k}_w$=0.1 compared to $\overline{k}_p$=0.1.

Specific values for the parameters, $\overline{k}_p$ and $\overline{k}_w$ are not readily available in the literature, since they will depend upon the characteristics of the selected fruits. Figure 5.11(a) shows the profile of the intercellular vapour density and of the free water moisture with the change in $\overline{k}_p$ from 0.001, 0.01, 0.1 and 0.5. As the value of $\overline{k}_p$, rises, the decrease in intercellular vapour density becomes slower. As shown by Figure 5.11, a slight increase in intercellular vapour density in the centreline was observed, due to the small values of $\overline{D}_i$ and $\overline{k}$ in the simulation. Figure 5.11(b) shows that, as the value of k_p increases, more vapour enters the intercellular space, leading to initial vapour build-up inside intercellular space. This also was observed by Halder and Datta [52] in their simulation based on a non equilibrium approach; more vapour rapidly accumulates during the first minute of frying and, with time, the vapour goes down steadily . We remark that the small value of diffusion $\overline{D}_i$ and permeability $\overline{k}$

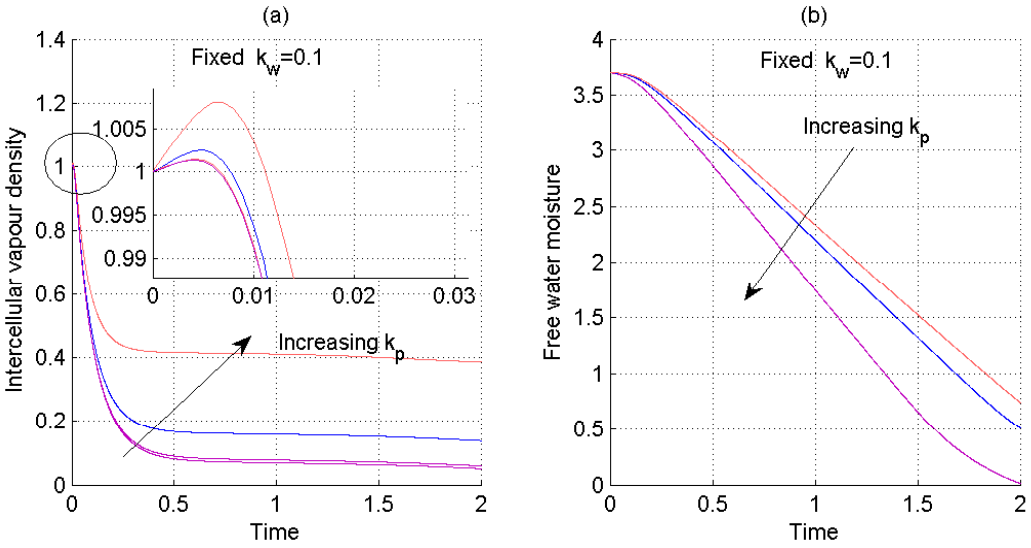

Figure 5.11: Effect of $\overline{k}_p$ into (a) intercellular vapour density (b) free water moisture at the centre. Parameter values as given in Figure 5.8.

has been chosen to be artificially small for illustrative purpose; the vapour build up, due to deviation of $\overline{k}_p$ and $\overline{k}_w$ represented by these solutions, would be small.

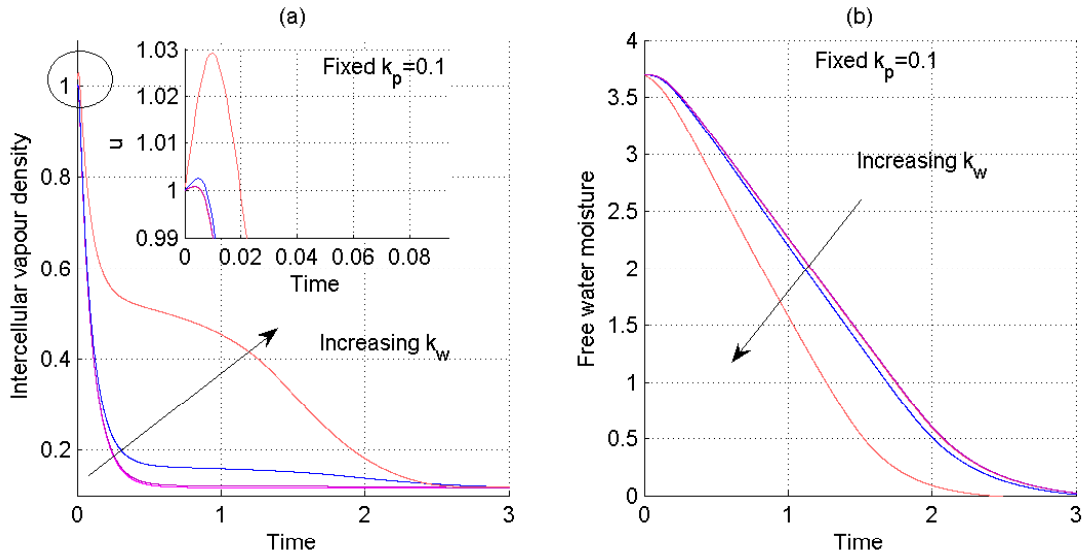

Figure 5.12: Effect of $\overline{k}_w$ (a) intercellular vapour density (b) free water moisture at the centre. Parameter values as given in Figure 5.8.

Figure 5.12 shows the effect of typical values of $\overline{k}_w$ as the value changes from 0.001,

0.01, 0.1, and 0.5. As we can see from Figure 5.12(a), we observe that a higher value of $\overline{k}_w$ leads to slow decrease in intercellular vapour density. The reason for the behaviour is explained as follows. The value of $\overline{k}_w$ is a measure of the membrane permeability of a cell, as discussed by Halder *et al.*[50], to provide controlling resistance of water to the intercellular space. As the value $\overline{k}_w$ increases, the resistance of the membrane becomes low, which will enable more water to push into intracellular space, resulting in pressure difference between these two regions. This leads to higher density of water vapour inside intercellular space. The transfer magnitude decreases with drying time, since the water vapour density decreases with the moisture content of free water. We also observed slightly increased vapour density at the beginning at the centreline arising from a small value of diffusion $\overline{D}_i$ and permeability $\overline{k}$ of vapour inside the intercellular space. Figure 5.12(b) shows the effect of $\overline{k}_w$ on the free water moisture. Higher values of $\overline{k}_w$, increase the transfer of free water into intercellular space, leading to a more rapid decrease in free water moisture.

5.5 Parametric study

For detailed modelling of tropical fruits, appropriate values remain uncertain. The aim of this section is to study the sensitivity of drying behaviour with respect to key model parameters, such as permeability and diffusivity of the intercellular space, diffusivity of free water moisture and parameters for convective mass transfer at the surface. The equations (5.26-5.31) for a two-phase model were solved and investigation carried out by varying this parameter numerically and comparing the numerical result with the reference case analysed in section §5.4.2 above.

5.5.1 Permeability and diffusivity of intercellular vapour density

By varying material properties, such as permeability and diffusivity, we investigate the transport of water influence of the drying process within the numerical solution developed in this section. The investigation is carried out by varying these parameters numerically. For the first instance, a fixed value of $\overline{D}_i = 1$ and varying values of

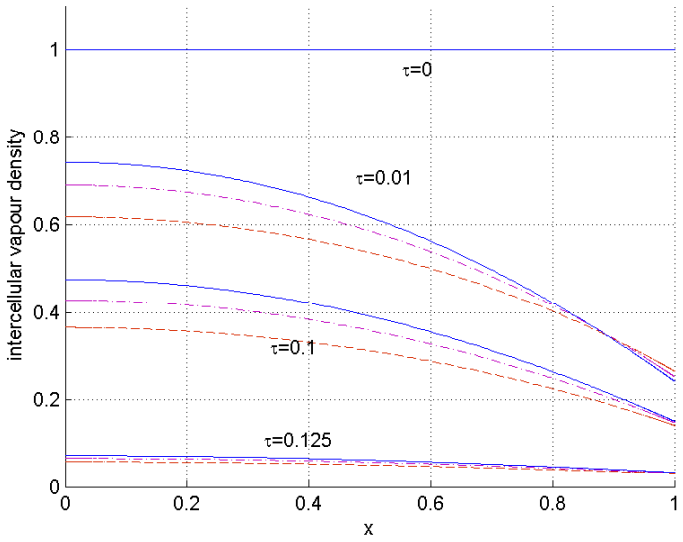

Figure 5.13: Profile of intercellular vapour density as permeability $\overline{k}$ changes. $\overline{k}$=0.5 (solid line), $\overline{k}$=1 (dotted dashed line), $\overline{k}$=2 (dashed line). Parameter values: Sh_f = 20, Sh_i=5, $\overline{D}_f$=1, $\overline{D}_i$=1, $\overline{k}_p$=0.01, and $\overline{k}_w$=0.01.

permeability $\overline{k}$ are used. As shown in Figure 5.13, the decrease in intercellular space density of water vapour becomes slower when smaller permeability was put into the model. The value of permeability depends on the pore structure of the material and the interaction within the solid.

Figure 5.14 shows simulations for a fixed value of permeability $\overline{k}$ and varying values of diffusivity in the intercellular space $\overline{D}_i$. When the value of diffusion of the vapour phase $\overline{D}_i$ is small ($\overline{D}_i = 0.5$), the vapour moves slowly towards the surface. Compared with the result in 5.13 with 5.14, this shows that the response of the intercellular space water vapour is more sensitive to change of diffusivity than the permeability.

5.5.2 Diffusivity of free water moisture

A profile of free water moisture within the cell can be seen in Figure 5.15. Varying the value of water diffusivity ($\overline{D}_f$) makes an impact on the transport of free water moisture. Increased diffusivity within the cell makes the diffusion of free water increase, leading to enhanced diffusion so that the total drying process is therefore shorter.

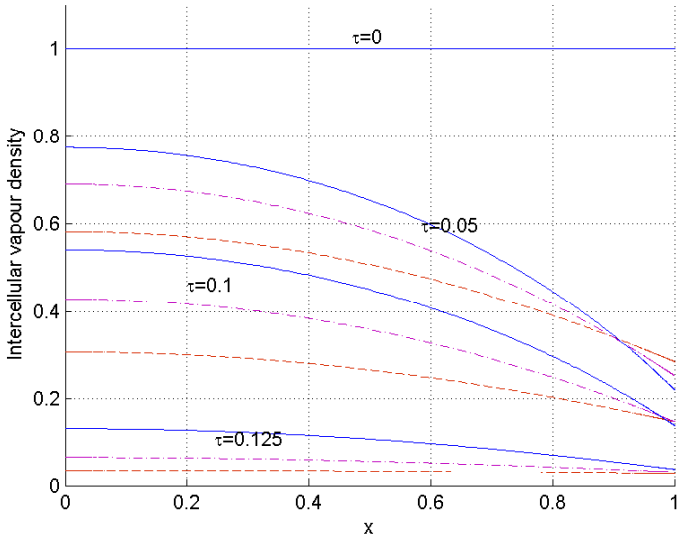

Figure 5.14: Profile of intercellular vapour density through food at τ=0.05, 0.1, 0.125 for values $\overline{D}_i$=0.5 (solid line), $\overline{D}_i$=1 (dotted dashed line), $\overline{D}_i$=2 (dashed line). Parameter values the same as Figure 5.13

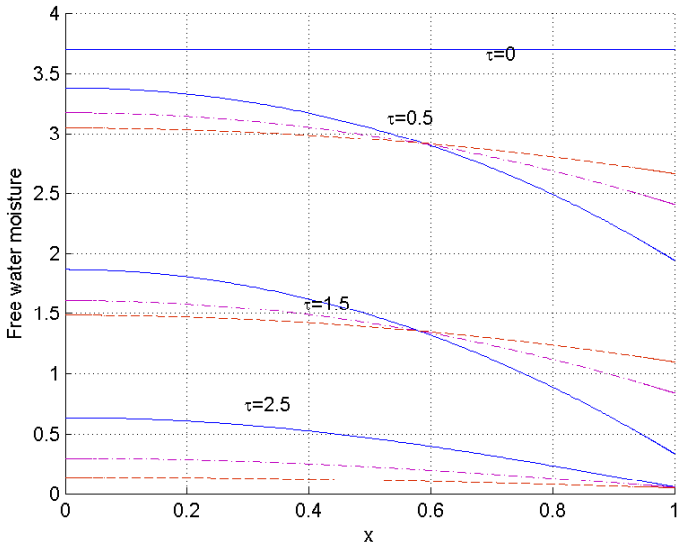

Figure 5.15: Profile of free water moisture at time τ=0.01, 1.5 and 2.5 with changes in diffusivity $\overline{D}_f$. Line plotted for $\overline{D}_i$=0.5 (solid line), $\overline{D}_i$=1 (dotted dashed line), $\overline{D}_i$=2 (dashed line). Parameter values the same as Figure 5.13

Figure 5.15 shows the contour profile of free water with different values of $\overline{D}_f$. It is apparent from the profile of free water that the diffusion coefficient is the guiding factor for diffusion of water during drying. If the value is higher, the water diffuses quickly to create the system equilibrium within the fruit earlier. When increasing the value of the diffusion coefficient $\overline{D}_f$, the flow of water will be moving faster toward the surface and the gradient between the surface and the centre of the fruit becomes small. As a result, more water will be removed from the surface in term of vapour.

5.5.3 Convective mass transfer

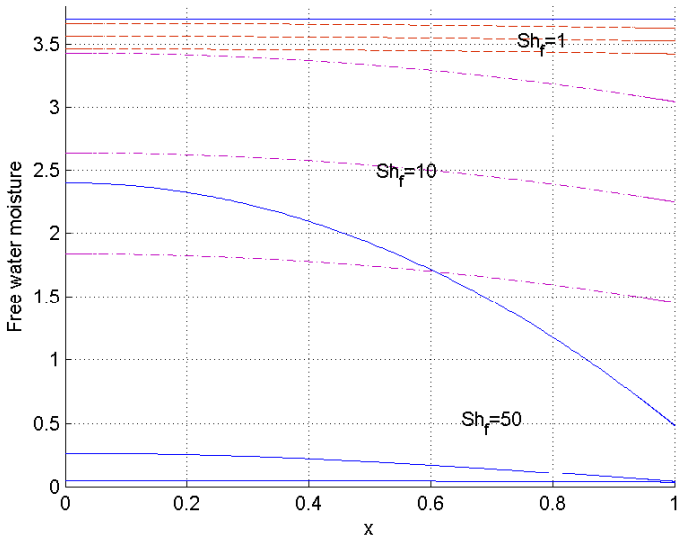

Figure 5.16: Plot showing free water moisture at time τ=0.5,1.5 and 2.5 with changes in Sh_f. Line plotted for Sh_f=50 (solid line), Sh_f=10 (dotted dashed line), Sh_f=1 (dashed line). Parameter values the same as Figure 5.13.

Figure 5.16 presents a decrease of free water moisture corresponding to the variation of Sh_f. Sh_f represents the surface convection mass transfer with respect to the diffusivity of water. Higher values of Sh_f correspond to more effective convective mass transfer at the surface relative to the diffusion of water inside the fruit. When Sh_f=1, there is a balance between convection mass transfer and diffusion leading to no gradient of free water moisture between the surface and centreline. Increasing Sh_f,

the gradient between the surface and the centreline becomes larger, which means that the convective mass transfer at the surface is more effective than diffusion of water from the inside to the surface. When this phenomenon happens, diffusion will be enhanced because the concentration gradient becomes large, having a significant effect on the movement of water and giving a shorter drying time.

5.6 Effect of cell pressure

As discussed in chapter 4, the cell pressure decreases due to loss of moisture; in this section we investigate the effect of changing cell pressure $\overline{P}_c$. The equation for cell pressure is given by,

$$\overline{P}_c = \delta + \varsigma \ln \frac{M_f}{M_{f0}}, \tag{5.34}$$

where δ is a turgor pressure of tissue at the beginning of drying, ς is an elastic modulus, which is given by incipient plasmolysis where the turgor pressure is equal to atmospheric pressure. Values of turgor pressure are typically in the range from 0.1 to 0.6 MPa (100kPa-600kPa) [112]. An experiment by Sajnin *et al.* [100] stated that turgor pressure of 0.159 MPa (159kPa) was measured for kiwi fruit tissue and 0.231 MPa(231kPa) for melon fruits. The elastic modulus ς value was given as 3.5 (non dimensional) by Zhiming and Le Maguer [140], 3.0 by Toupin *et al.* [113]. In this modelling, the value of δ=1.59 and ς=3.5.

When $\overline{P}_c$ is dependent on free water inside the intracellular cell, the equation (5.27) becomes

$$\overline{\rho}_s \frac{\partial M_f}{\partial \tau} = \frac{\partial}{\partial \overline{x}} \left[(\overline{D}_f \overline{\rho}_s + \overline{D}_p \, \overline{\rho}_s \, \varsigma \, M_{f0}) \frac{\partial M_f}{\partial \overline{x}} \right] - \overline{j}_{ip} - \overline{j}_{ic}. \tag{5.35}$$

In this section we investigated the effect of pressure on free water moisture and intercellular vapour density. We consider a constant pressure or pressure dependent on volume of water loss in cell. Figure 5.17 shows the free water moisture and intercellular vapour density, using different formulations of the cell pressure $\overline{P}_c$. In the case of constant pressure, only one method of transport of water is used i.e. release of water from the cell to the intercellular space by transfer fluxes $\overline{j}_{ip}$ and $\overline{j}_{ic}$. Using constant pressure in the transfer flux formulation, the free water moisture decreases more slowly compared with the use of variable pressure (Figure 5.17(a)). In the case of

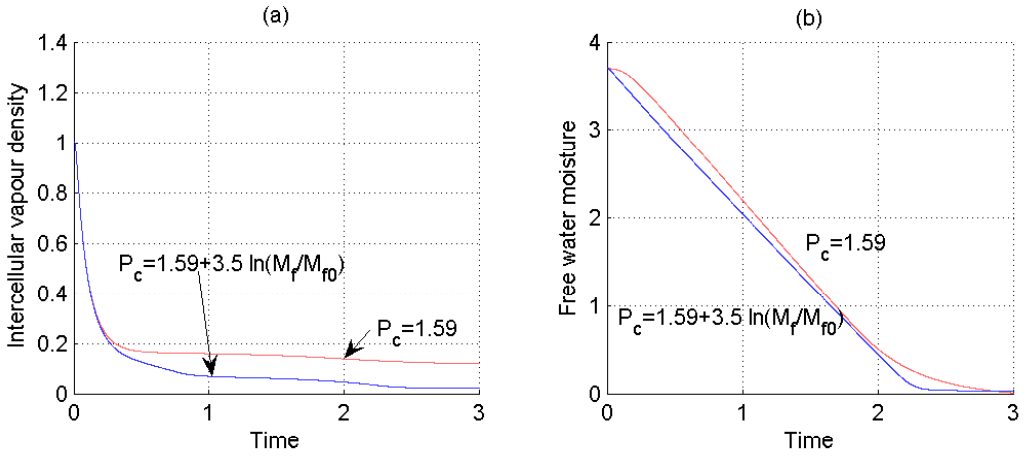

Figure 5.17: Comparison between constant with variable pressure formulation to intercellular vapour density and free water moisture at the centreline. Non-dimension parameter values given by $Sh_f = 20$, Sh_i=5, $\overline{D}_f$=1, $\overline{D}_i$=1 $\overline{k}$=1, $\overline{k}_p$=0.1, and $\overline{k}_w$=0.1.

variable pressure, there are two methods of transporting water: release of free water from the cell into intercellular space and the flux of free water through cell wall pores (plasmodesmata) generated by differential gradient of internal cell pressure. As a result of these two transport methods, free water moisture and intercellular vapour density will decrease more quickly compared to constant pressure.

In this section we also investigate the effect of values δ and ς by changing these parameters with time. Figure 5.18 shows the intercellular vapour density and free water moisture when we fix the value of initial pressure δ=1.59 and increase the value of the elastic modulus from ς=0.01 to ς=3.5. As we can see from Figure 5.18(a), increasing the value of ς gives a more rapid decrease in intercellular vapour density. This happens when bigger values of ς cause a faster drop of $\overline{P}_c$. This gives the transfer of water from intracellular cell to intercellular space from the pressure gradient, which becomes less and leads to free water decreasing more slowly (Figure 5.18(b)).

Figure 5.19 shows the intercellular vapour density and free water moisture when we fix the value of the elastic modulus ς=3.5 and change the value of the initial cell pressure δ from 1 (same as atmospheric pressure) to 5. From Figure 5.19(a), increasing values of δ causes more rapid decrease in intercellular vapour density. At atmospheric pressure δ=1 initially, no water will be transferred to the intercellular space because the pressure inside the intercellular space is much larger than from

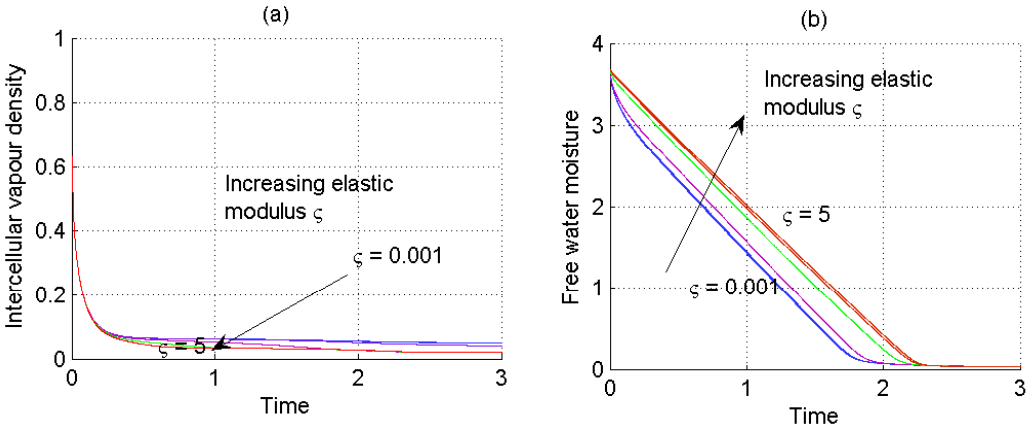

Figure 5.18: Effect of changing the value of elastic modulus ς to intercellular vapour density and free water moisture. Parameter values as given in Figure 5.17.

intracellular cell, so transfer flux is only from the concentration gradient. When the value of δ increases, the cell pressure $\overline{P}_c$ is more than intercellular space pressure $\overline{P}_i$, which leads to more vapour transfer from the cells to the intercellular space (Figure 5.19(a)) and a slow decrease in vapour. As the time increases, pressure inside cells will decrease and lead to a reduction of water vapour. Larger values of δ, lead to a faster decrease in free water moisture inside the cell (Figure 5.19(b)).

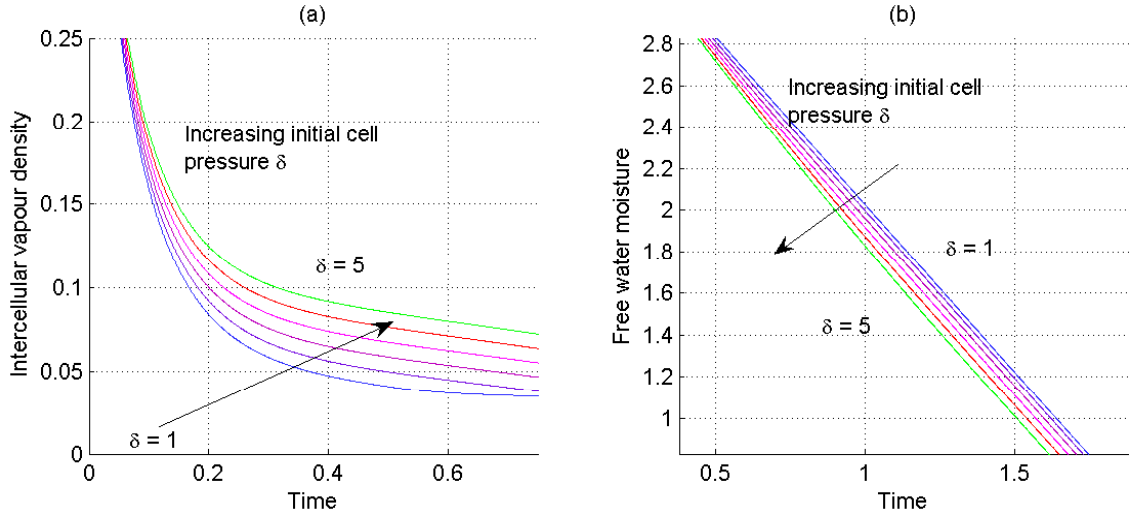

Figure 5.19: Effect of changing the value of initial pressure δ to intercellular space water vapour density and free water content. Parameter values as given in Figure 5.17.

5.7 Isothermal three-phase model

The model presented in section §5.4 is now extended to include a third phase to incorporate the effect of bound water. The modifying effect of including transfer inside the intracellular cells between the free water and bound water states is given from solving the three couple pdes (5.1)-(5.3). In this case, the intracellular cell comprises two-components i.e bound and free water, and the component exchanges from one phase to another. The previous simplification case is adapted so that the value of $\overline{P}_c$ remains constant and above atmospheric pressure during the main drying stage. For isothermal conditions, the temperature of the food remains constant during drying and $\overline{P}_i = \overline{\rho}\gamma$. Equations for intercellular space stay the same as equation (5.26) and the equations for free water and bound water are

$$\overline{\rho}_s \frac{\partial M_f}{\partial \tau} = \frac{\partial}{\partial \overline{x}}\left[\overline{D}_f \overline{\rho}_s \frac{\partial M_f}{\partial \overline{x}}\right] - \overline{j}_{ip} - \overline{j}_{ic} + \overline{r}_b\,\overline{\rho}_s. \tag{5.36}$$

$$\text{and} \quad \frac{\partial M_b}{\partial \tau} = -\overline{r}_b. \tag{5.37}$$

The constitutive equation for $\overline{r}_b$ is taken as

$$\overline{r}_b = \overline{n}_1 M_b - \overline{n}_2 M_f. \tag{5.38}$$

A set of initial conditions, typically prevailing in the drying process, are defined to perform the numerical simulations. In order to apply the model, a porous structure is supposed for mango. A special case of drying simulation of a reference food system, for example mango with porosity ϕ_i=0.2, is taken. With the assumption of the volume fraction of free water in the intracellular cell, $\varepsilon_f = 0.7$ and a small volume fraction of bound water in the intracellular cell, $\varepsilon_b = 0.1$ is considered. In the non shrinkage model, these values are taken as constant. It is also assumed that the volume fraction of free water in the free water region $\varepsilon_{fw} = 0.8$ and the volume fraction of bound water in the bound water region $\varepsilon_{bw} = 0.3$. The definitions of (4.1),(4.2) and (4.3) in chapter 4, give associated initial conditions as M_f=3.70,M_b=0.39 and $\overline{\rho}$=1.
Boundary conditions at the symmetry and surface are same as in two-phase models (section §5.4) together with flux conditions on the bound water as,

$$\frac{\partial M_b}{\partial \overline{x}} = 0, \quad \text{at} \quad \overline{x} = 0 \text{ and } \overline{x} = 1. \tag{5.39}$$

5.7.1 Analysis of the three-phase model

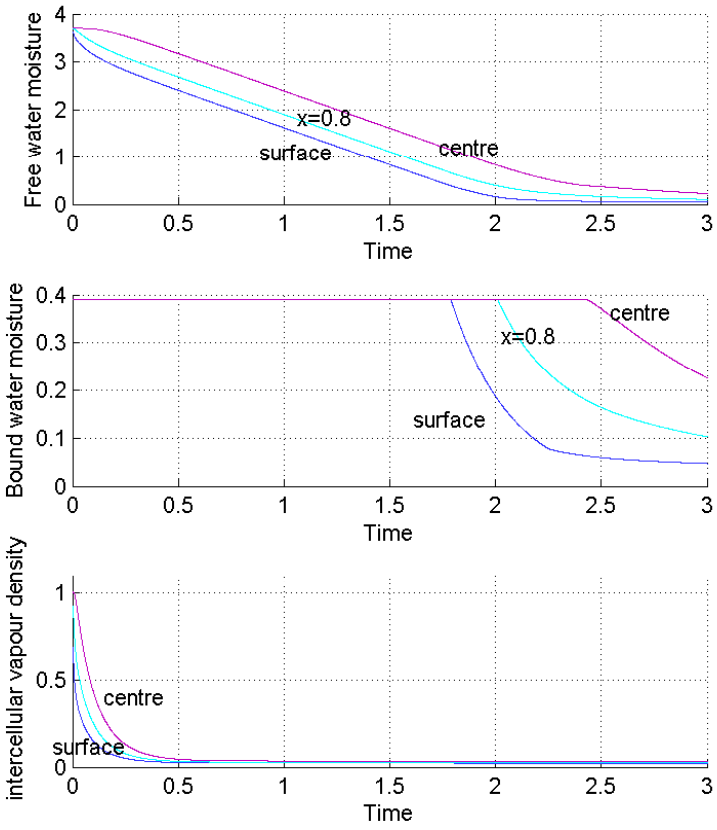

Figure 5.20: Moisture profile in free water moisture and bound water moisture at the centreline, x=0.8 and surface. The value of $\overline{n}_1 = 3.46$ and $\overline{n}_2 = 0.062$. Other parameter values $Sh_f = 20$, Sh_i=5, $\overline{D}_f$=1, $\overline{D}_i$=1 $\overline{k}$=1, $\overline{k}_p$=0.01, and $\overline{k}_w$=0.01.

Using the same parameter values as in section 5.4 for comparison, a simulation was run with the value of $\overline{n}_1 = 3.46$ and $\overline{n}_2 = 0.062$ (as discussed in [71]) to identify the effect of bound water. Figure 5.20 shows the profile of free water M_f and bound water M_b in the cell at selected points. This transfer corresponds to the transfer of bound water moisture to free water moisture, with movement to the intracellular cell component before it can transfer to the air. This profile shows that bound water decreases from the initial value of 0.39 to 0.01 at the later stage of drying, τ=1.8 at the

surface, τ=2 at $\overline{x}$=0.8 and τ=2.4 at the centreline. Within the initial phases of drying it is anticipated that the transfer of moisture within cell walls will be dominated by the diffusion of free water. At a lower moisture level, following significant drying, the more tightly bound water within the cell tissue must be converted to free water before further diffusion can occur. These processes would be important in the later stage when $M_f < M_b$ and the much longer stages of drying to reduce residual level of moisture.

To show the effect of free water moisture increase when $M_f < M_b$, the profile of free water in the three-phase model is compared with the profile of the two-phase model. This profile can be seen in Figure 5.21, where the profile of free water moisture is increasing at τ=1.8 when bound water is considered. This happens because of the change of bound water to free water at the later stage of drying. A similar profile was observed by Kiranoudis *et al.* [71] in a sensitivity test on the effect of bound water in their model.

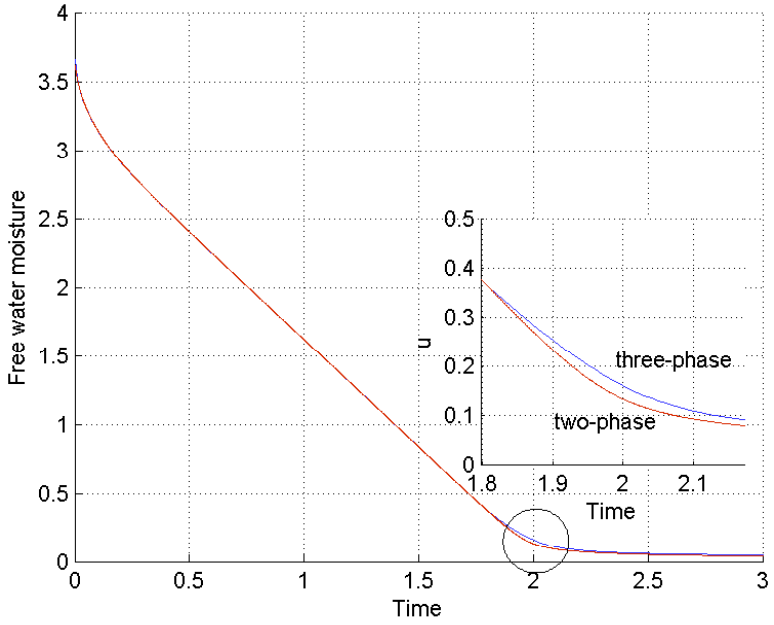

Figure 5.21: Moisture profile of the free water region in the three-phase and two-phase at the surface. The value of $\overline{n}_1 = 3.46$ and $\overline{n}_2 = 0.062$. Parameter values as given in Figure 5.20.

To help evaluate the kinetic constant $\overline{n}_1$ and $\overline{n}_2$, we investigate the situation with the values given in Table 5.5. For equilibrium then $\overline{n}_1 M_b = \overline{n}_2 M_f$, and for physically valid conditions $\dfrac{\overline{n}_1}{\overline{n}_2} > \dfrac{M_f}{M_b}$. Figure 5.22 shows the moisture content of bound water

Table 5.5: Different values of $\overline{n}_1$ and $\overline{n}_2$ and their ratios

$\overline{n}_1$	3.46	2.5	4.8
$\overline{n}_2$	0.062	0.062	0.1
Ratio	55.8	40.32	48

with drying time for three drying ratios. As we can see from the graph, profile shows that bound water start to decrease from the initial value of 0.39 at same time at τ=1.8 for each of the ratio. The larger the ratio of $\overline{n}_1$ with $\overline{n}_2$, the faster the decrease of bound water to free water moisture associated with the difference in level of bound water and free water in the intracellular cell.

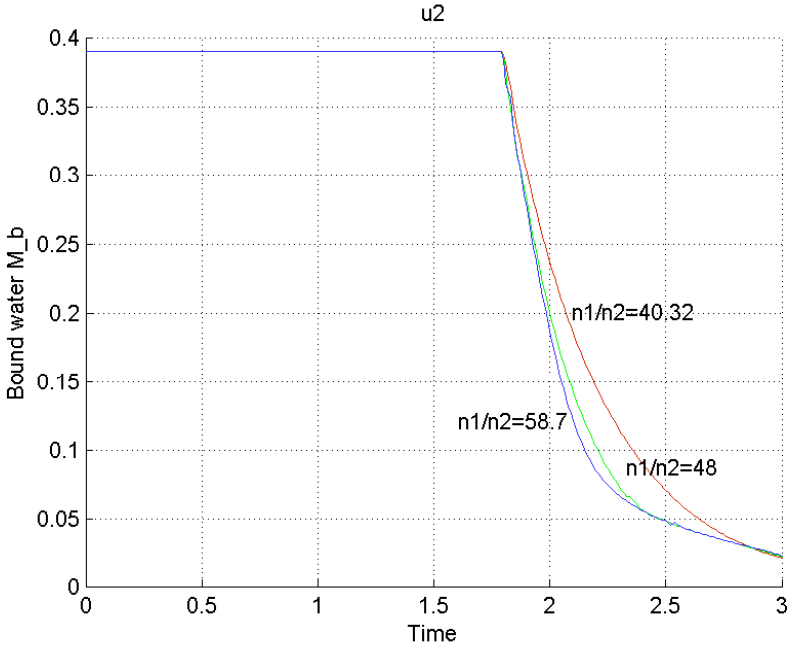

Figure 5.22: Bound water profile with different values of $\overline{n}_1$ and $\overline{n}_2$ at the surface. Parameter values the same as Figure 5.20

5.8 The special case of the one-phase model

As described earlier, much of the modelling for the drying of foodstuffs is restricted to a one-phase model. In this section we consider the approximation required to generate such a one-phase (composite) model from a multiphase model. Average moisture content (dry basis) is given by a composite moisture value (see section §4.3.1), given by

$$M = \alpha_i \rho_i + \alpha_f M_f + \alpha_s M_b. \tag{5.40}$$

The equation of this three-phase model and simulation is given and discussed in section §5.7 and the two-phase model is discussed in section §5.4.

We investigate the limits of a single composite food, comprising free water, solid and air only; i.e. the case with no intercellular space, $\phi_i \to 0$, and so $\alpha_i \to 0$. Correspondingly the water content is taken as

$$M = \alpha_f M_f + \alpha_s M_b, \tag{5.41}$$

With no intercellular space, there is no transfer flux $\overline{j}_{ip}$ and $\overline{j}_{ic}$ between these phases, the equation form reduces to

$$\frac{\partial M_f}{\partial \tau} = \frac{\partial}{\partial \overline{x}}\left(\overline{D}_f \frac{\partial M_f}{\partial \overline{x}}\right) + \overline{r}_b, \tag{5.42}$$

$$\text{and} \quad \frac{\partial M_b}{\partial \tau} = -\overline{n}_1 M_b + \overline{n}_2 M_f. \tag{5.43}$$

In the limit that only free water exists $\varepsilon_b \to 0$ so $\alpha_s = 0$ and $\alpha_f = 1$ and

$$M = \frac{\overline{\rho}_w}{\overline{\rho}_s}\frac{\varepsilon_{fw}}{\varepsilon_{fs}} = M_f.$$

The three-phase model reduces to the one-phase diffusion model

$$\frac{\partial M_f}{\partial \tau} = \frac{\partial}{\partial \overline{x}}\left(\overline{D}_f \frac{\partial M_f}{\partial \overline{x}}\right). \tag{5.44}$$

In this part, we made a comparison between the two-phase and three-phase models discussed in sections §5.4 and §5.7, with the case of no intercellular space. In the case of no intercellular space, the first case is with bound water and free water and a simplified case where only free water exists. A comparison is provided with a single phase result discussed in chapter 2. Figure 5.23 shows that the profile of free water

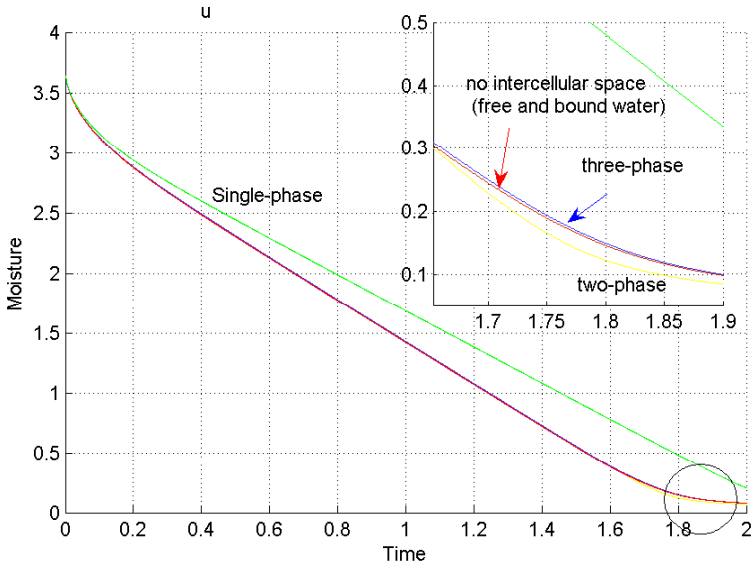

Figure 5.23: Moisture profile in the free water region in single-phase, two-phase and three-phase models at the centre. The value of $\overline{n}_1 = 3.46$ and $\overline{n}_2 = 0.062$. Dimensionless parameter values given by $Sh_f = 20$, Sh_i=5, $\overline{D}_f$=1, $\overline{D}_i$=1 $\overline{k}$=1, $\overline{k}_p$=0.1, and $\overline{k}_w$=0.1.

moisture in a three-phase and a two-phase model at the surface provides a similar trend but it is displaced from the one-phase model. From the graph, the profile of the single-phase shows the need for more drying time compared to the three-phase and two-phase models, as based on transfer of flux values k_p=0.1 and k_w=0.1. The small difference can be seen at the end of drying in the three-phase model, where the change from bound water to free water gives more free water at the end of drying.

5.9 Discussion

The general theory of mass transfer during the drying of cellular material, as developed in chapter four, has been applied to model the drying of mango tissue. In this chapter, we have presented a one-dimensional, time-dependent numerical solution of a two-phase and three-phase model with parameter values corresponding to the drying of fruit which shows the effect of a transfer flux between free water moisture with intercellular vapour density and the effect of bound water in the model. The

intercellular cell and intercellular space were modelled within a rigid slab.

An isothermal multiphase model was used to predict moisture in the food during drying. The model considers the transport of free water and water vapour separately. Water vapour, as a mixture of air and water, is considered as flow through a porous structure that interacts with the cell structure. The numerical solutions which solve the coupled mass equation for liquid water and water vapour movement through food material has been presented. The transfer fluxes $\overline{j}_{ip}$ and $\overline{j}_{ic}$, transfer quantities of moisture from the intracellular cell to intercellular space because of pressure difference and concentration gradient, which is an important consideration in this model. This transfer fluxes gives link between intracellular cell with intercellular space and the result shows that $\overline{j}_{ic}$ gives more effect compared to $\overline{j}_{ip}$. During active drying processes, transfer of free water moisture between cells is ongoing but the flux of water vapour transport through the porous structure will be more significant. Thus, higher values of transfer fluxes, the more faster the transfer of free water into intercellular space, the more significant of vapour transport through porous structure.

The effect of internal cell pressure was included in the model through constant pressure and pressure decreases due to lost of moisture. To include the transport of water from one cell to another cell through cell walls pores (plasmodesmata), variable pressure was put into the models. For this case, free water will be driven from deeper cells to the surface, by differential gradient of internal pressure. Simulations were presented showing that the flow of water in intracellular cell is faster for variable pressure compared to constant pressure.

Food material is typically hygroscopic, with some water tightly bound to the solid [131]. Within the initial phases of drying it is anticipated that transfer of moisture within cell will be dominated by the diffusion of free water. At lower moisture level, following significant drying the more tightly bound water within the cell tissues must be converted to free water before further diffusion of water can occur. To address this issue, consideration of bound water, particularly in the final drying state, is important. Thus, the modifying effect of including the transfer of intracellular cell compartments between the free and bound water are presented in the three-phase model. The inclusion of a third phase of bound water held within the cell structure allows consideration of the mechanism of a weighted balance between free and bound

water, associated with cell structure. This model addresses the existence of different classes of water in food products and the conversion between them. Simulations were presented, showing that the flow of moisture in the intracellular cell is profoundly altered by this effect, especially in the later stage of drying. This simulation demonstrates the importance of considering the effect of bound water within drying to low levels of moisture retention. We conclude that with the adding of bound water in the model gives influence in drying especially at the later stage of drying to reduce residual level of moisture.

In the system in which the intercellular space is large i.e. ϕ=1, numerical solutions were constructed whereby local values of vapour density were determined from cells transferred into intercellular space and from intercellular space into the underlying air. The result of vapour behaviour is similar to the results in the two-phase and three-phase models. This analysis indicated that we have confidence in the behaviour of vapour inside the intercellular space in the numerical simulation.

Comparison of a single phase model as a special case of the three-phase model identified the difference in the predictions in the profile of the moisture content; the single phase model under predicts the drying time during the main drying period, with inadequate details for long time taken to dry to low moisture concentrations. It was proved that the theory reduces to a simple case one equation diffusion model and that the model provides acceptable predictions. Previous efforts in developing a comprehensive governing equation for drying have often been hindered by lack of data for thermal and transport properties, such as relative permeability, effective moisture diffusivity and thermal conductivity. These parameters are essential to a realistic simulation of processes of practical problems. Unfortunately, for hygroscopic porous materials, data for these properties are often not available, especially for foods and agriculture. In order to overcome the difficulties, either constant values or a range of values were used in the drying simulation, thus weakening the reliability of the conclusions.

Chapter 6

Multiphase one-dimensional non-isothermal conditions: case study of mango fruit

6.1 Introduction

In chapter 5 we describe drying under isothermal conditions, where mass transfer within fruits is driven from prevailing concentration gradients of free water moisture and water vapour. Drying is typically a non-isothermal process and heat transfer can substantially affect drying behaviour through increasing concentration gradients and transfer of water between liquid and vapour phases. As drying is eminently a conjugate phenomenon. The transfer of mass and heat is solved simultaneously in both intercellular space and fluid phases, and strongly coupled through evaporation and variation of properties associated with moisture and temperature. In this chapter, the basic drying model has been extended to account for the availability of latent heat of evaporation. In the presence of thermal gradients, evaporation occurs in the partially saturated pore region and subsequent transfer of heat by vapor flow and conduction through the cells. Convection and moisture removal is evaluated within an extended model substrate, as reported in figure 5.1. During the drying process in fruit, heat is transferred mainly by convection from air to the product's exposed surface. Further, heat is transferred by conduction from the surface toward

the substrate interior. Meanwhile, moisture diffuses outwards to the surface, where it vaporizes. Liquid water inside food may also be converted into vapour, depending on the local thermal and liquid phase conditions.

In this chapter, a multiphase model for drying under thermal condition is presented corresponding to the model developed in chapter 4. Possible transfer of heat in a cell scale is put into the modelling, with the assumption that the representative temperature within the water vapour presented in the intercellular space $\overline{T}_i$ may differ from a representative temperature $\overline{T}_c$ within the intracellular cell structure. This will utilize the principle of local non-equilibrium between the cell and the intercellular space at any given location.

Two sub-models are evaluated, as identified in chapter 5: the two-phase and the three-phase model. We again distinguish between two types of mobility of water: free water is more readily available for transfer within cells and intercellular space and also introduces bound water into the cell region. Bound water can only be transferred if the free water concentration is low enough and is particularly relevant to final drying state.

6.2 Mathematical formulation for a non-isothermal one-dimensional drying model

The formulation presented in chapter 4 is simplified by assuming that the sample undergoes one-dimensional movement parallel to the x-axis, interacting with temperature between phases. As in chapter 5, there are two main phases: free water moisture and intercellular vapour density. The mechanism in the intercellular space is characterized by vapour through a porous food structure and inside the cell is based on diffusion and local pore (plasmodesmata) transport. In this study, we include the possibility of two representative temperatures, which are intercellular space temperature $\overline{T}_i$ and intracellular cell temperature $\overline{T}_c$. We now specify how our multiphase systems interact. The flow of water vapour from the fruit is caused by diffusive flow and permeability of gas flow. Thus, the mass conservation equation for vapour in the

intercellular space is given by

$$\phi_i \frac{\partial \overline{\rho}}{\partial \tau} = \frac{\partial}{\partial x}\left[(\overline{\rho}\overline{k}\gamma + \overline{D}_i)\frac{\partial \overline{\rho}}{\partial \overline{x}}\right] + \overline{j}_{ip} + \overline{j}_{ic}. \tag{6.1}$$

The chemical potential gradient of water in cell tissues can be considered to depend on water activity and pressure difference between the intercellular space and the intracellular cells (see Nobel [86], Shi and Le Maguer [104]). The key part of the formulation concerns transfer fluxes $\overline{j}_{ip}$ and $\overline{j}_{ic}$, where the intracellular cell moisture and energy equations interact with the intercellular space vapour and energy equations. To put this effect into the drying model, we assumed that the water flux across the cell membrane from cell to intracellular space can be expressed as $\overline{j}_{ic}$ and $\overline{j}_{ip}$. The formulation for water from intracellular cell across the cell membranes to the intercellular space will be dependent on the differential moisture levels across the membranes given by

$$\overline{j}_{ic} = \overline{k}_w(\eta - \xi), \tag{6.2}$$

where η and ξ are the measures of difference of level of water.

The release of free water from cells into the intercellular space arises from differences in local pressure that occurs along the interconnected spaces. According to Floury *et al.* [46], hydrostatic pressure is related to the unknown change of cellular volume difference between the two regions. Thus, the mass flux of free water is associated with the differential pressure between the local cell and intercellular space and is taken as

$$\overline{j}_{ip} = \overline{k}_p(\overline{P}_c - \overline{P}_i), \tag{6.3}$$

where $\overline{P}_c$ and $\overline{P}_i$ measure the difference in pressure between the cell with the intercellular space.

The sources of water in the intercellular space comes from the free water inside the intracellular cell. The interaction between the free water moisture inside the cell with the vapour density inside the intercellular space is given by transfer fluxes $\overline{j}_{ip}$ and $\overline{j}_{ic}$. Transfer of free water inside the cells to the intercellular space takes place and the conservation equation of free water moisture given by

$$\overline{\rho}_s \frac{\partial M_f}{\partial \tau} = \frac{\partial}{\partial \overline{x}}\left[\overline{D}_f \overline{\rho}_s \frac{\partial M_f}{\partial \overline{x}} + \overline{D}_p\, M_f\, \overline{\rho}_s \frac{\partial \overline{P}_c}{\partial \overline{x}}\right] - \overline{j}_{ip} - \overline{j}_{ic} + \overline{r}_b\, \overline{\rho}_s. \tag{6.4}$$

A further transfer mechanism comprises bound water transfer inside the cell. Where the bound water is not freely available for transport it can be converted to form free

water, when the availability of free water molecules becomes very low. The interaction of bound water to the free water state is given by,

$$\frac{\partial M_b}{\partial \tau} = -\overline{n}_1 M_b + \overline{n}_2 M_f. \tag{6.5}$$

The initial effect of temperature in drying comes in the governing equation of free water moisture through boundary conditions at the surface, $\overline{x} = 1$ and is given by

$$\left[\overline{D}_f \overline{\rho}_s \frac{\partial M_f}{\partial \overline{x}} + \overline{D}_p \, M_f \, \overline{\rho}_s \frac{\partial \overline{P}_c}{\partial \overline{x}}\right] = -Sh_f(\overline{C}_{fw,sur} - 1). \tag{6.6}$$

The term $\overline{C}_{fw,sur} = \beta(\overline{T}_{sur})f(M_f)$, defined at the surface, links surface conditions directly to surface temperature, as discussed in chapter 2 and is given by experiment correlation as,

$$\beta(\overline{T}_{sur}) = A\,\overline{T}^2_{sur} + B\,\overline{T}_{sur} + C,$$

Typical values for fruit are $A = 0.0364, B = 0.0108$ and $C = 0.0119$ for air temperature drying at 60^0C, in which the interaction of temperature comes to free water moisture. In isothermal case, when temperature is not considered, this is taken as β_1. A relationship between water activity and moisture content M is given by Wang and Brenann [123] as

$$f(M_f) = \frac{\sigma\, M_f^{2.38}}{0.062^{2.38} + M_f^{2.38}}.$$

The value of $\sigma = \dfrac{2.1667}{C_{air}}$, which depends on the air temperature.
The effect of temperature on intercellular vapour density also comes through boundary condition at the surface $\overline{x} = 1$ given by

$$\left[(\overline{\rho}\overline{k}\gamma + \overline{D}_i)\right]\frac{\partial \overline{\rho}}{\partial \overline{x}} = -Sh_i(\frac{\overline{\rho}}{\overline{C}_{air}} - 1). \tag{6.7}$$

Since non-thermal equilibrium is assumed to exist between the intercellular phase with the cell, the transfer fluxes $\overline{j}_{ip}$ and $\overline{j}_{ic}$ from intracellular cell structure to intercellular space, that occur by pressure difference and diffusion across cell membranes to give an interaction between cell temperature with intercellular space temperature. The first that is associated with transfer fluxes is flux of water release, which carries heat into intercellular space. This flux (in terms of water) also needs to turn to water vapour before it can flow to the external surface and is given by $\overline{\lambda}(\overline{j}_{ip} + \overline{j}_{ic})$. Furthermore, inflow of heat is also due to the difference between the temperatures at the intercellular

space and the intracellular cell structure. Thus, a representative intercellular space temperature equation is therefore given by,

$$\phi_i\overline{\rho}\Big[\frac{\partial\overline{T}_i}{\partial\tau}+\frac{\boldsymbol{n}_i}{\overline{\rho}}\cdot\frac{\partial\overline{T}_i}{\partial\overline{x}}\Big]=\frac{\partial}{\partial\overline{x}}\Big[\phi_i\overline{\kappa}_v\frac{\partial\overline{T}_i}{\partial\overline{x}}\Big]+\overline{h}_i(\overline{T}_c-\overline{T}_i)+(\overline{j}_{ip}+\overline{j}_{ic})(\overline{T}_c-\overline{T}_i)-\overline{\lambda}(\overline{j}_{ip}+\overline{j}_{ic}). \tag{6.8}$$

Furthermore, a representative intracellular cell structure temperature equation becomes

$$(1-\phi_i)\overline{\rho}_c\frac{\partial\overline{T}_c}{\partial\tau}=\frac{\partial}{\partial\overline{x}}\Big[(1-\phi_i)\overline{\kappa}_c\frac{\partial\overline{T}_c}{\partial\overline{x}}\Big]-\overline{h}_i(\overline{T}_c-\overline{T}_i)-(\overline{j}_{ip}+\overline{j}_{ic})(\overline{T}_c-\overline{T}_i). \tag{6.9}$$

At the surface $\overline{x}=1$ of intercellular space, heat flux arrives at the interface by convection balance with the conduction from surface to the interior of the fruit is given by

$$-\phi_i Nu_i\overline{\kappa}_v(T_{isur}-1)=\phi_i\overline{\kappa}_v\frac{\partial\overline{T}_i}{\partial\overline{x}}. \tag{6.10}$$

At local intracellular cell boundaries, free water moisture is transferred to the food surface and needs to convert to vapour before it can be released to the overlying air. Heat is supplied by the drying air and characterized by latent heat of evaporation of water $\overline{\lambda}$. The model boundary condition is given by

$$-(1-\phi_i)\overline{\kappa}_c Nu_c(T_{csur}-1)=(1-\phi_i)\overline{\kappa}_c\frac{\partial\overline{T}_c}{\partial\overline{x}}-\overline{\lambda}\left[\overline{D}_f\overline{\rho}_s\frac{\partial M_f}{\partial\overline{x}}+\overline{D}_p\,M_f\,\overline{\rho}_s\frac{\partial\overline{P}_c}{\partial\overline{x}}\right]. \tag{6.11}$$

Associated initial conditions (consistent with chapter 5) are taken as

M_f=3.7, M_b=0.39, $\overline{\rho}=1$, $\overline{T}_i$=0 and $\overline{T}_c$=0.

Symmetry boundary conditions at $\overline{x}=0$ are given by

$\dfrac{\partial M_f}{\partial\overline{x}}=0$, $\dfrac{\partial M_b}{\partial\overline{x}}=0$, $\dfrac{\partial\overline{\rho}}{\partial\overline{x}}=0$, $\dfrac{\partial\overline{T}_i}{\partial\overline{x}}=0$, and $\dfrac{\partial\overline{T}_c}{\partial\overline{x}}=0$.

6.3 Two-phase non-isothermal model

Solution to the two-phase non-isothermal model is obtained from solving four coupled pdes, corresponding to mass equations (6.1) and (6.4) and temperature equations (6.8) and (6.9), together with equation of transfer flux (6.2) and (6.3). As in chapter 5, the effect of pressure is assumed to take a constant value, $\overline{P}_c$=1.59. This will give the term $\overline{D}_p\,M_f\,\overline{\rho}_s\dfrac{\partial\overline{P}_c}{\partial\overline{x}}=0$ in equation (6.4), (6.6) and (6.11). In this non-isothermal model, the effect will be investigated later in section §6.4.

Numerical solutions were sought for the four dependent variables $\overline{\rho}$, M_f, $\overline{T}_i$ and $\overline{T}_c$. These equations are solved using COMSOL Multiphysics. Numerical formulation for $\overline{\rho}$ and M_f is explained in §5.4.1. Intercellular and cell temperature $\overline{T}_i$ and $\overline{T}_c$ are formulated as PDEs within the general format required for COMSOL.

Identifying the general form with equation (6.8) and equation (6.9), the following settings generate the equation (Table 6.1 and Table 6.2) :

Two boundary conditions, intracellular cell component and intercellular space are

Table 6.1: Equation generated for intercellular space temperature.

Coefficient	Value Expression
e_a	0
d_a	$\phi_i * \overline{\rho}$
Γ(flux vector)	$-\phi_i \overline{\kappa}_v \frac{\partial \overline{T}_i}{\partial \overline{x}}$
F(source term)	$(\overline{j}_{ip} + \overline{j}_{ic})(\overline{T}_c - \overline{T}_i) - \overline{\lambda}(\overline{j}_{ip} + \overline{j}_{ic}) + \overline{h}_i(\overline{T}_c - \overline{T}_i) - \phi_i \boldsymbol{n}_i \frac{\partial \overline{T}_i}{\partial \overline{x}}$

Table 6.2: Equation generated for intracellular cell temperature.

Coefficient	Value Expression
e_a	0
d_a	$(1-\phi_i) * \overline{\rho}_c$
Γ(flux vector)	$-(1-\phi_i)\overline{\kappa}_c \frac{\partial \overline{T}_c}{\partial \overline{x}}$
F(source term)	$-(\overline{j}_{ip} + \overline{j}_{ic}) * (\overline{T}_c - \overline{T}_i) - \overline{h}_i(\overline{T}_c - \overline{T}_i)$

given as in section §5.4.1. The temperature boundary condition at the centreline $\overline{x} = 0$ will give Neumann type boundary condition with $G = 0$ and influx boundary condition at the surface $\overline{x} = 1$ will give Neumann type boundary condition with

$$G = -\phi_i Nu_i \overline{\kappa}_v * (T_{isur} - 1),$$

$$\text{and} \quad G = -(1-\phi_i)\overline{\kappa}_c Nu_c (T_{csur} - 1) + \overline{\lambda D}_f \, \overline{\rho}_s \frac{\partial M_f}{\partial \overline{x}}.$$

The generic values of non-dimensional parameters for moisture are given as constant

values shown previously in Tables 5.3 and 5.4. Dimensional parameters associated with temperature formulations given as constant values are shown in Table 6.3 and a range of non-dimension physical relevant values are shown in Table 6.4 below. Initial conditions for a free water moisture and vapour density is given as in section §5.4.1. Initial condition for intercellular space temperature and intracellular cell temperature are given as $\overline{T}_i = 0$ and $\overline{T}_c = 0$.

Table 6.3: Input parameter values used in simulation of mango drying.

Parameter	Value	Unit and Source.
Heat transfer coefficient of cell water (h_c)	$20 - 250$	W/m^{2}K [85]
Heat transfer coefficient of intercellular space vapour (h_i)	$25 - 100$	W/m^{2}K [39]
Latent heat of evaporation (λ)	2.345×10^3	KJ/kg [84]
Specific heat capacity of water (c_{pw})	$1.9 - 3.683$	KJ/kg
Specific heat for vapour (c_{pv})	$1.84 - 1.9$	KJ/kg
Thermal conductivity of water (κ_c)	$0.475 - 0.567$	W/m K (refer chapter 2)
Thermal conductivity of intercellular space vapour (κ_v)	0.026	W/m K
Thermal diffusivity of water (α_w)	1.4×10^{-7}	m^2/s
Thermal diffusivity of vapour (α_v)	2.33×10^{-5}	m^2/s

Table 6.4: Non-dimensional parameter values.

Non-dimensional parameter	Value	Range of values
Nu_i	5	0-20
Nu_c	5	0-20
$\overline{\kappa}_v$	10	0.1-100
$\overline{\kappa}_c$	10	0.1-100
$\overline{\lambda}$	0.5	0-1

6.3.1 Analysis of two-phase non-isothermal model

In chapter 5, an isothermal model was evaluated with the assumption that the temperature of the food remains uniform during drying and latent heat is taken as negligible. In this section, the effect of temperature is included and compared with the numerical results given in chapter 5. We first focus on the effects of temperature during drying, which are characterized by the inclusion of a latent heat of evaporation ($\overline{\lambda}$). Evaporation is identified as transfer of liquid water to vapour within intercellular space and also from the external surface of the fruit. The intercellular space temperature equation (6.8) includes the evaporation of liquid water inside the intercellular space. The surface boundary condition for intracellular cell equation (6.11) includes evaporation of liquid water near the external surface.

In summary, the system comprises four equations (6.1), (6.4), (6.8) and (6.9) which are solved subject to (6.6), (6.7), (6.10), and (6.11) at the surface and symmetry boundary conditions at the centreline. The above systems were solved numerically using COMSOL. The time dependent problem was solved by an implicit time-stepping scheme, leading to a non-linear system of equations for each time step. Newton's method was used to solve each non-linear system of equations, whereas a direct linear system solver was adopted to solve the resulting systems of linear equations. The relative and absolute tolerance were set to 10^{-4} and 10^{-5}, respectively. The drying process is considered to be complete when the moisture content in the sample is asymptotic to a residual level.

In the following simulation, the dimensionless parameters for transfer flux are taken as $\overline{k}_p$=0.01 and $\overline{k}_w$=0.01. The parameters for conduction of heat $\overline{\kappa}_c$= 5, $\overline{\kappa}_v$= 5; this characterizes how quickly heat is conducted within the fruit. The convection heat transfer is given by Nu_i=5, Nu_c=5, which shows how convection takes place at the surface with respect to conduction evolution for both cell structure and the intercellular phase. Other parameter values for moisture transfer are the same as those defined in section §5.4. The overbar notation in the graph is dropped for clarity.

Profiles of local cell temperature, intercellular space temperature, free water moisture and intercellular density at the surface and centre are given by Figures 6.1 and 6.4. The time evolution of free water moisture, intercellular vapour density and temperature is shown in Figures 6.2 and 6.3; the arrows indicate the direction of increasing

time.

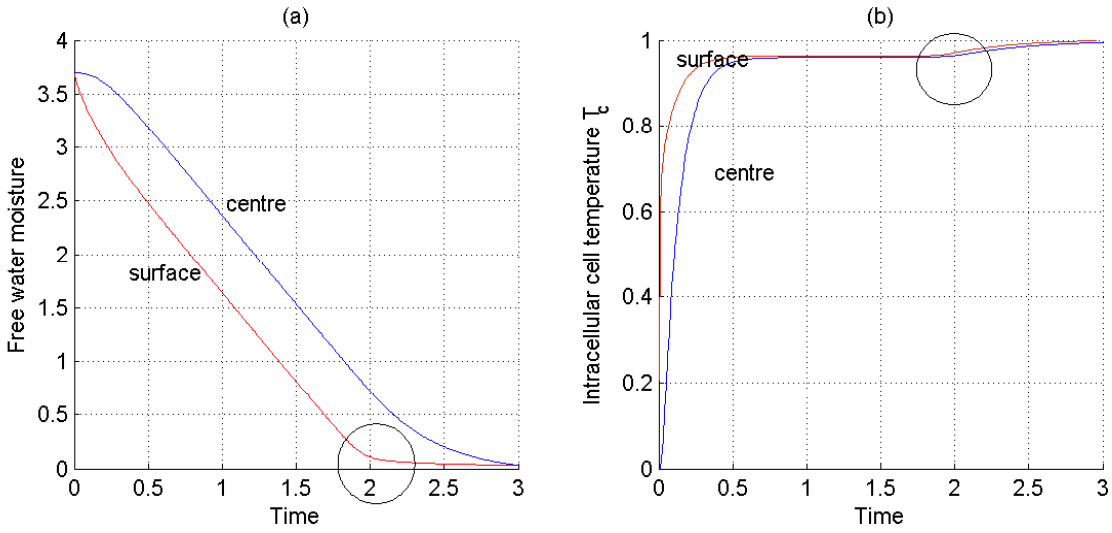

Figure 6.1: Profile of (a) free water moisture M_f (b) cell temperature $\overline{T}_c$ at the surface and the centre. Dimensionless parameter values given by Sh_f = 20, Sh_i=5, $\overline{D}_f$=1, $\overline{D}_i$=1 $\overline{k}$=1, $\overline{k}_p$=0.01, and $\overline{k}_w$=0.01, Nu_i=5, Nu_c=5, $\overline{\kappa}_c$= 5, $\overline{\kappa}_v$= 5 $\overline{\lambda}$ = 0.1.

Figure 6.1 shows the typical trends of the cell temperature and free water moisture at the surface and centre of the fruit during drying. From the cell temperature profile (figure 6.1(b)), three different stages can be defined: the initial steep temperature rise is the result of heat transfer, dependent on convection due to temperature difference between air and food; the temperature increases to a new constant and remains stationary while latent heat prevents a temperature rise and then there is a further rise to its maximum steady state temperature. A similar result for the drying of mango is reported by Tour and Kibangu-Nkembo [115], who studied the solar drying of mangos in a hurdle-dryer with a wire net bottom, observing that, during the constant rate period, the product temperature was lower than the ambient air temperature with an average difference of 2.3^{o}C and remaining at a constant temperature until a certain value of moisture. Figure 6.1(a) shows that, initially, when the process is controlled by external heat transfer and water leaving the surface was not bound to the food structure, the drying rate attained a maximum value (τ=0-0.3). Afterwards, when the process was controlled by mass transfer and the water leaving the surface was bound

to the food structure, a progressive decrease in the drying curve was observed (τ=0.3-1.8). As the free water moisture became very low at time $\tau = 2$, the latent heat $\overline{\lambda}$ at the boundary condition at the surface (equation (6.11)) was no longer effective and this led to a final decrease in moisture and a final increase in temperature at the end of drying. With respect to most work published in the literature, this typical trend of free water moisture shown in our simulations was observed in experimental drying, such as the drying of carrot [5], banana [67] and kiwi [107]. This will be investigated in more detail later in section §6.3.2.

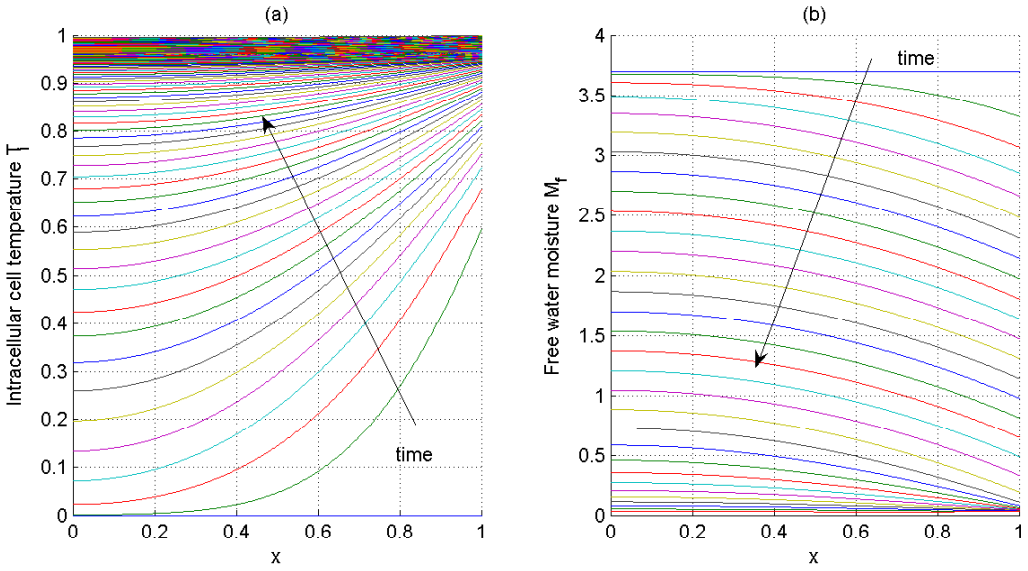

Figure 6.2: Evolution of (a) Cell temperature ($\overline{T}_c$) at time 0-3 (in step 0.01) (b) free water moisture (M_f) at time =0-3 (in step 0.1). Parameter values as Figure 6.1.

Figure 6.2 illustrates the time evolution of intracellular cell temperature $\overline{T}_c$ and free water moisture M_f, giving a detailed microscopic description of the process. Temperature in the fruit is initially constant, non-dimensionalised to zero, and reaches a final scaled steady value of $\overline{T}_c = 1$. As shown, cell temperature $\overline{T}_c$ rises sharply at the heating surface because of the large temperature difference between the surface and the drying air. At the beginning, the temperature difference between the surface and drying air is large; some heat is used for evaporation of water near the surface and some is conducted to the centre. At this time, the centre of the fruit is still

cooler than the outside. When time increases, the inside temperature starts to rise until equilibrium is attained between surface and centre. This is shown very clearly in the above mentioned variation of the drying rate; at the beginning of the process, the profile appears very well separated, whilst they tend to overlap as soon as the drying rate decreases. Figure 6.2(b) shows free water moisture decreasing as time initially increases; moisture reduces rapidly near the surface and establishes a gradient through-out the sample. The moisture gradient between the centre and the surface decreases as time increases.

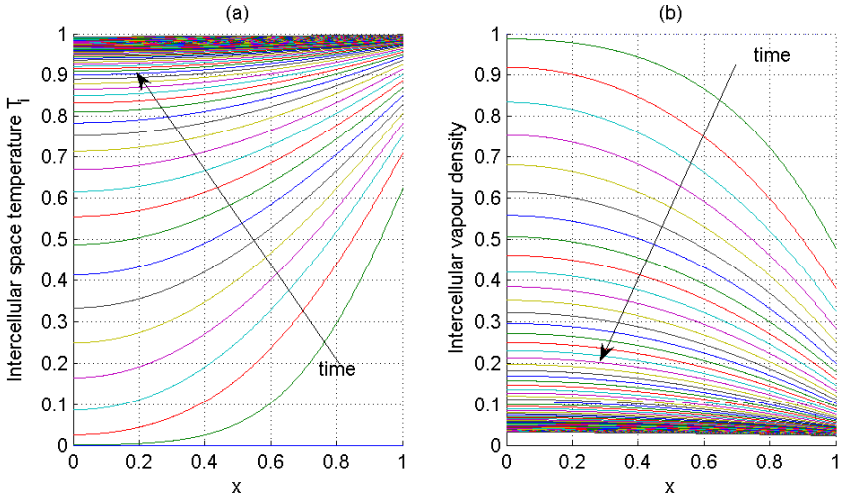

Figure 6.3: Evolution of (a) intracellular space temperature $\overline{T}_i$ at time 0-3 (in step 0.01) (b)intercellular vapour density ($\overline{\rho}$) at time =0-3 (in step 0.01). Parameter values as Figure 6.1.

Figure 6.3 illustrates time evolution of representative intercellular temperature $\overline{T}_i$ and intercellular vapour density during drying. The increase in intercellular space temperature $\overline{T}_i$ (Figure 6.3(a)) is faster at the surface due to the heat transferred, mainly by convection, from air to the exposed surface, indicating that the process is controlled by external heat transfer. As time increases, the gradient along the moist regions is negligible and the temperature increases uniformly with time. It was also observed that the temperature profile increases rapidly during early heating; the source of heat from air drying is very effective at the beginning. As heating progresses, the rise in temperature attains an almost uniform profile indicating that the process

has basically approached a steady state. Figure 6.3(b) shows intercellular vapour density decreasing with time. The sources of vapour inside the intercellular space are from the transfer fluxes. As a result of water advected to the pores (intercellular space), the water inside the intercellular space increases. Then the thermal process occurs, which induces strong water evaporation in this area. As a result, more vapour is produced inside the pores. Intercellular vapour density decreases due to the flow of vapour from the surface due to permeability and diffusive flow. Some studies (for example see [37]) have stated that a decrease in the local density of vapour causes the water to evaporate at a lower temperature, depend on permeability to gas flow and water vapour diffusion.

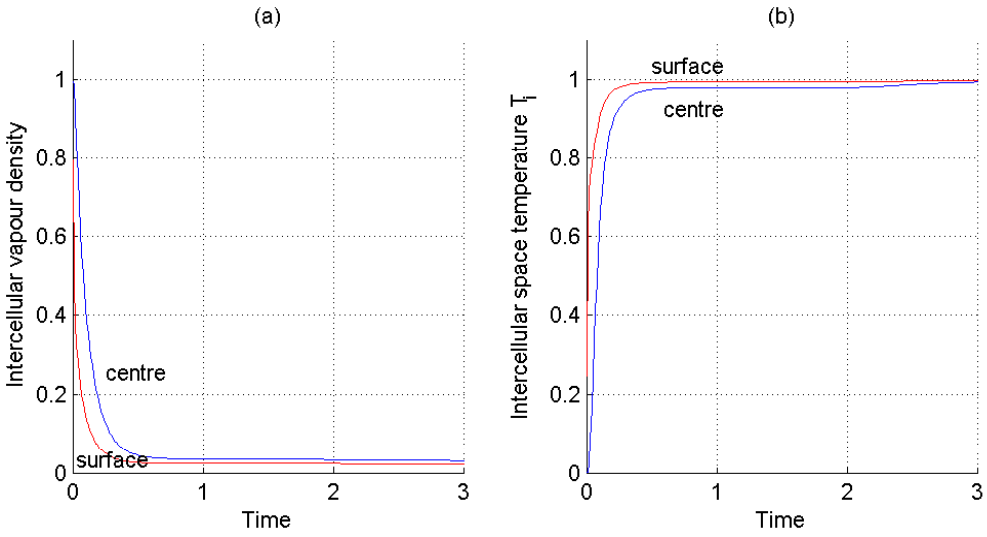

Figure 6.4: Profile of (a) intercellular vapour density $\overline{\rho}$ (b) intercellular temperature $\overline{T}_i$ at the surface and the centreline. Parameter values as in Figure 6.1.

Figure 6.4 represents the intercellular temperature and intercellular vapour density at the centre and surface of the fruit. The temperature is higher at the surface and intercellular vapour density decreases much faster at the surface. Comparing 6.1 with 6.4, the time taken for free water to reach equilibrium at the surface is $\tau = 2$ but, for vapour, the time taken is $\tau = 0.4$, and consistent with other study [37] that shows the rate of water vapour transfer to the sample surface to be much faster than the free water transport to the drying front by several orders of magnitude. We observed

that the intercellular space temperature $\overline{T}_i$ is not in equilibrium to 1 compared to the intercellular cell. This will be investigated later in section §6.5.

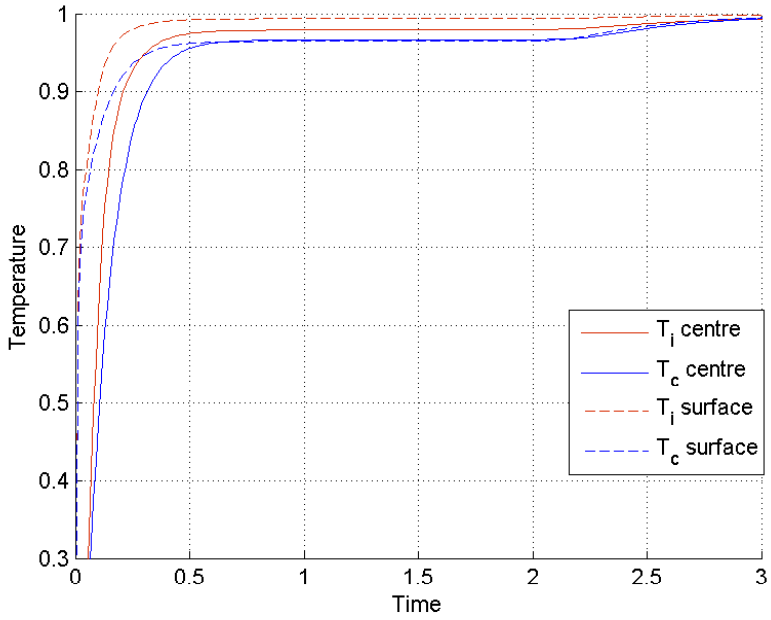

Figure 6.5: The profile of intracellular cell temperature and intercellular space temperature at the surface and the centre. Parameter values as Figure 6.1.

Figure 6.5 shows a comparison between the intercellular space temperature$\overline{T}_i$ with intracellular cell temperature $\overline{T}_c$. Intercellular space temperature $\overline{T}_i$ rises more rapidly compared to intercellular cell temperature $\overline{T}_c$. By inspection equation (6.8), heat was used for internal evaporation inside the intercellular space for water evaporation but the source of heat for the intercellular space comes from convection from overlying air and transfer fluxes from the cell. This leads to a higher increase in temperature inside intercellular space. Similar conclusions have been drawn by other study: for instance, Farkas *et al.* [43] have shown temperature is higher inside the crust region, which is characterized by vapour flow, compared to the core region, which is dominated by the liquid phase. Different increasing profiles of cell temperature $\overline{T}_c$ compared to intercellular space temperature $\overline{T}_i$ were observed. At the beginning, intercellular cell temperature ($\overline{T}_c$) surface and centre temperature increase. The difference between the surface and centre is large, but after $\tau = 0.6$, the same

temperature was observed between the surface and the centre. Representative intercellular space temperature, $\overline{T}_i$, also shows rise in temperature at the beginning before a uniform profile was observed, but the same temperature is not observed at the centre and the surface.

6.3.2 Study of movement of water and vapour

We now present at a detailed study of the behaviour of the solution of the two-phase non-isothermal model. Using numerical simulation, we illustrate the effect of varying the parameters that are associated with transfer flux and evaporation. In order to provide insight into the factors that affect the behaviour of the intracellular cell and intercellular space moisture and temperature, solutions are presented for a variety of parameter values that highlight how the interaction influences behaviour during drying.

Transfer flux

The model parameters pertinent to the study of movement of water from cell structure into intercellular space at cell scale are $\overline{k}_p$ and $\overline{k}_w$. The effect of varying each parameter is investigated below, exploiting the numerical scheme developed in this section. Figure 6.6 shows how the movement of water from intracellular cell into intercellular space is affected by increasing the value of the transfer flux coefficient rate $\overline{k}_p$. We observed that increasing $\overline{k}_p$, increases the rate of transfer of liquid water when liquid free water is advected into the intercellular space, leading to the formation of more water inside the intercellular space. Increasing $\overline{k}_p$, gives decreased values of free water M_f (figure a) and also affects the intracellular cell temperature $\overline{T}_c$. The intracellular cell temperature $\overline{T}_c$ decreases as $\overline{k}_p$ is increased (figure c): when the liquid water is advected into intercellular space, it brings associated heat with it. This gives a lower cell temperature $\overline{T}_c$ when larger values of $\overline{k}_p$ are used in the model. Increasing $\overline{k}_p$ gives more liquid water inside the intercellular space so that more heat is required to evaporate liquid water into water vapour. Intercellular space temperature $\overline{T}_i$ decreases when $\overline{k}_p$ is increased (figure d).

Figure 6.7 shows how the movement of water from cell into intercellular space is affected by increasing the value of transfer flux coefficient $\overline{k}_w$. Similar behaviour is observed, such as $\overline{k}_p$, and this transfer is more important than $\overline{k}_p$. The parameter

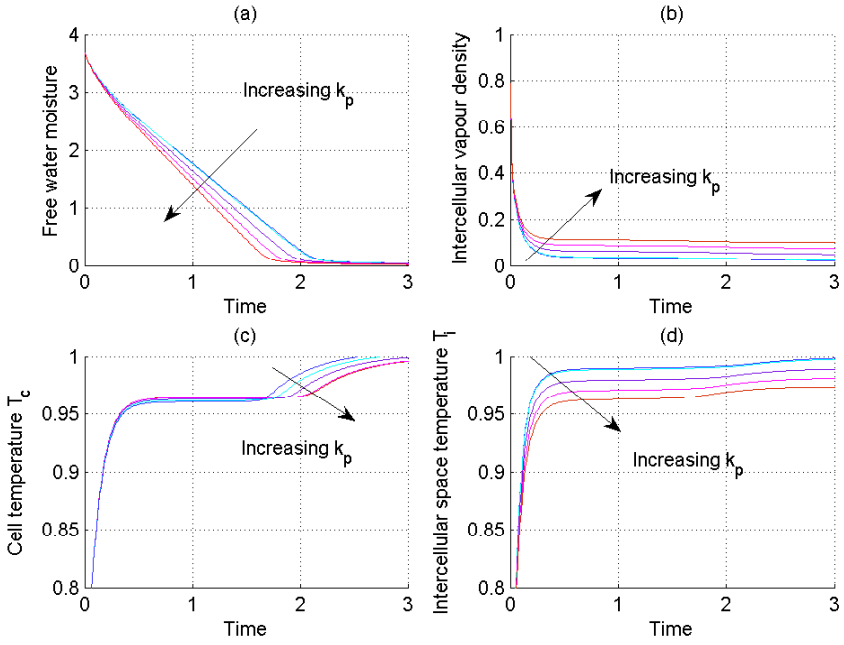

Figure 6.6: Profile of (a) free water moisture (b) intercellular vapour density (c) cell temperature (d) intercellular space temperature at the surface. Parameter values given by $Sh_f = 20$, Sh_i=5, $\overline{D}_f$=1, $\overline{D}_i$=1 $\overline{k}$=1, $\overline{k}_w$=0.1, Nu_i=5, Nu_c=5, $\overline{\kappa}_c$= 5, $\overline{\kappa}_v$= 5, $\overline{\lambda} = 0.1$ and $\overline{k}_p$=0.001, 0.01, 0.1, 0.2, 0.3, 0.5

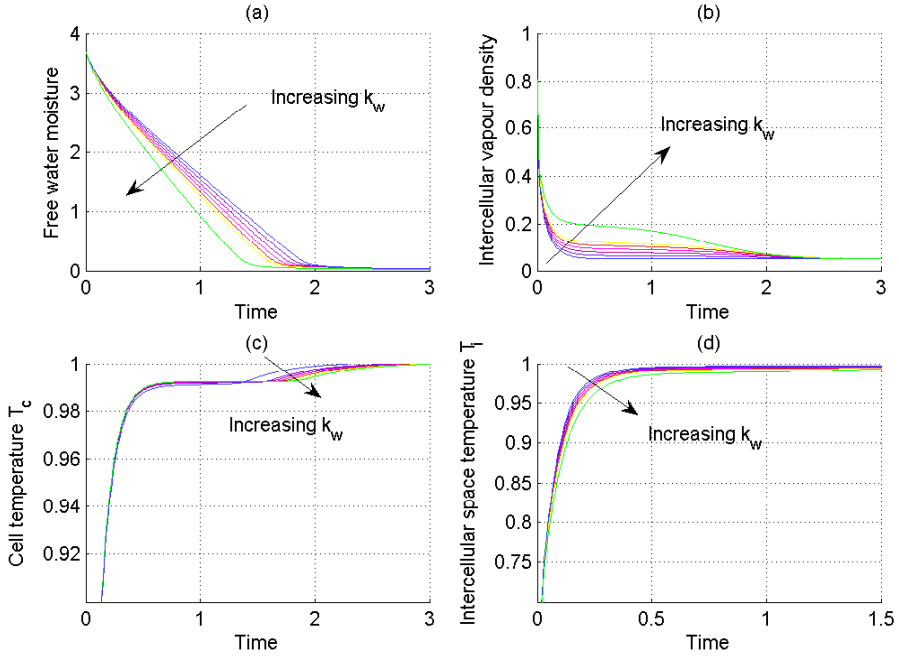

Figure 6.7: Profile of (a) free water moisture (b) intercellular vapour density (c) cell temperature (d) intercellular space temperature at the surface. Parameter values the same as Figure 6.6. $\overline{k}_w$=0.001, 0.01, 0.1, 0.2, 0.3, 0.5 and 1

$\overline{k}_w$ quantifies the resistance of cell membranes to the flow of water from cell to pores because of concentration difference. The cell membrane is considered to be 'semi-permeable' and allows water to pass through. This behaviour has been reported by, for instance, Zhiming and Maguer [139], Toupin and Marcotte [114] in osmosis dehydration. An increase in $\overline{k}_w$ therefore represents the increased rate of water to be pumped through cell membranes. As the rate increases, resulting in increasing advection, equations (6.8) and (6.9), show that temperature is also affected by this advection.

For a lower value of $\overline{k}_p$ and $\overline{k}_w$, the representative cell temperature $\overline{T}_c$ increases more quickly, due particularly to the low value of $(j_{ip} + j_{ic})(T_c - T_i)$ in the intracellular cell temperature equation (6.9). Representative intercellular space temperature $\overline{T}_i$ also increases more quickly for a lower value of $\overline{k}_p$ and $\overline{k}_w$, due particularly to the low value of $\overline{\lambda}(\overline{j}_{ip} + \overline{j}_{ic})$ in the intercellular space temperature equation (6.8). For higher values of $\overline{k}_p$ and $\overline{k}_w$, this term is more important and therefore more energy is devoted to evaporation.

Latent Heat

We now consider the effect of varying the latent heat $\overline{\lambda}$ to the temperature of intracellular cell structure and intercellular space. Figure 6.8(c) shows the effect of increasing the latent heat $\overline{\lambda}$ at the intracellular cell surface ($\overline{x}$=1). With negligible latent heat ($\overline{\lambda}$=0), at the surface, temperature $\overline{T}_c$ (figure (c)) increases rapidly, as most heat conducted to the fruit (the time scale for temperature changes rapidly compared to the change in moisture discussed in chapter 5 for isothermal case). In this case, it was found that the temperature profile rises rapidly in the early period of heating ($0 < \tau < 0.3$) and, as the heating period progresses, the rise in temperature is almost uniform. Thus, after the initial transient period, which is relatively short compared to the total drying time, the food remains nearly uniform during the entire drying period. The numerical solution shows that increasing values of $\overline{\lambda}$ cause a slower rise in surface temperature $\overline{T}_c$ (figure (c)). This effect is due to the heat required to evaporate water near the surface. For high values of $\overline{\lambda}$, the temperature rise at the surface is slower because most energy is used up as latent heat of evaporation. Comparing figure 6.8(a) with 6.8(c), the behaviour of cell temperature $\overline{T}_c$ shows the increasing profile at the end of drying due to low level of free water, giving the term $\overline{\lambda}\overline{\rho}_s\overline{D}_f\dfrac{\partial M_f}{\partial \overline{x}}$

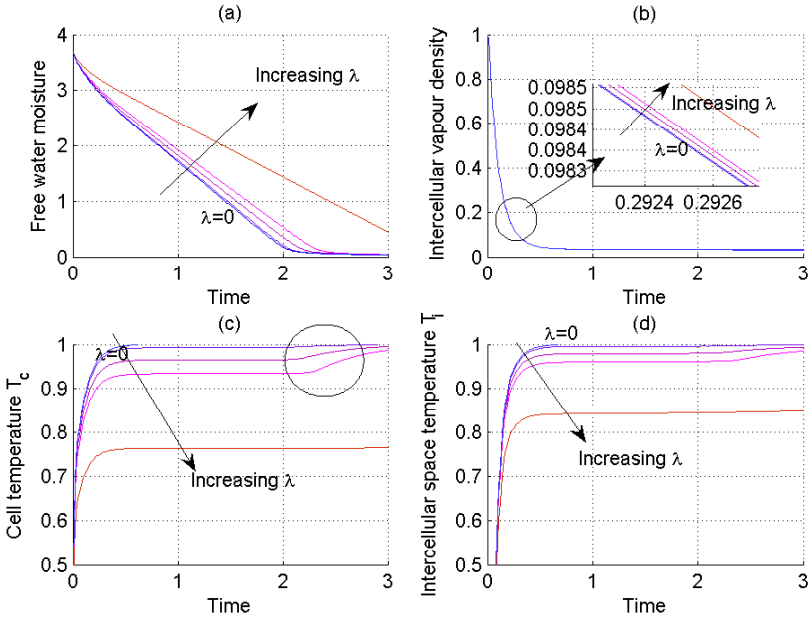

Figure 6.8: Profile of (a) free water moisture (b) intercellular vapour density (c) intracellular cell temperature at the surface (d) intercellular space temperature the centreline. Parameter values given by $Sh_f = 20$, Sh_i=5, $\overline{D}_f$=1, $\overline{D}_i$=1 $\overline{k}$=1, $\overline{k}_w$=0.01,$\overline{k}_p$=0.01 Nu_i=5, Nu_c=5, $\overline{\kappa}_c$= 5, $\overline{\kappa}_v$= 5 and $\overline{\lambda} = 0 - 5$

in equation (6.11) is smaller. This leads to faster increased of cell temperature $\overline{T}_c$.

Figure 6.8(d) shows the effect of increasing the latent heat $\overline{\lambda}$ at the intercellular space centreline ($\overline{x} = 0$). With negligible latent heat ($\overline{\lambda}$=0), at the centre, intercellular space temperature $\overline{T}_i$ (figure (d)) increases rapidly. Similar in behavior to cell temperature, the temperature profile rises rapidly in the early period of heating ($0 < \tau < 0.3$) and as the heating period progresses, the rise in temperature attains an almost uniform level. Increasing values of $\overline{\lambda}$ cause a slower increase of intercellular space temperature $\overline{T}_i$ at the centreline (figure (d)). Inspection of equation (6.8) indicates that $\overline{\lambda}$, enters the model in the combination of transfer flux $\overline{\lambda}(\overline{j}_{ip} + \overline{j}_{ic})$ inside the intercellular space. Increasing this value gives a slower increase in temperature inside the intercellular space.

Our simulations clearly demonstrate the importance of putting the evaporation term ($\overline{\lambda}$) into the model at the surface of the intercellular cell energy equation and inside the intercellular space energy equation. By doing this, evaporation can take place at the external surface and can also be distributed inside the intercellular space. A more realistic model can be drawn, which is of crucial importance especially in the drying of fruits that have high moisture content. Similar trends have been drawn by other studies; for instance, Ni and Datta [84], Yamsaengsung and Moreira [130] have shown evaporation to be distributed over the zone of the model.

6.4 Effect of pressure

In section §5.6, the modifying effect of pressure due to the loss of water was put into the model equation (6.4) and through the boundary condition, such as equation (6.6). In this section we investigate the effect of pressure inside the cell through pressure dependent on the volume of water loss. Figure 6.9 shows how the centreline free water moisture and intercellular vapour density, representative cell temperature and intercellular space temperature profile are created by the modifying effect of pressure. As in the two-fluid model, under constant pressure, free water flow will be driven by pressure to the intercellular phase, but there is no pressure driven from the deeper cell through plasmodesmata and so $\overline{D}_p\, M_f\, \overline{\rho}_s \dfrac{\partial \overline{P}_c}{\partial \overline{x}} = 0$. This leads to a slower decrease of free water M_f (figure (a)). High pressure water driven into the intercellular space,

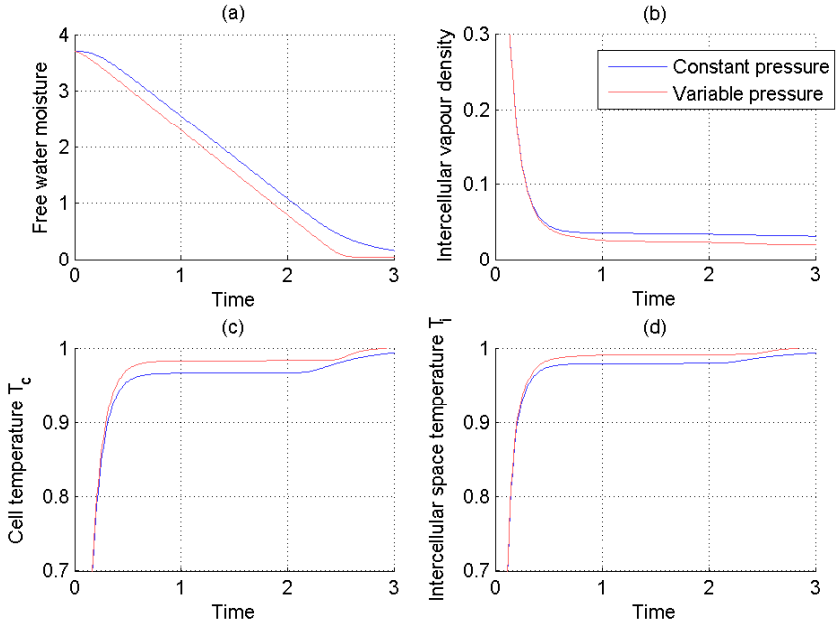

Figure 6.9: Profile of intercellular space temperature, vapour density, intracellular cell temperature and free water moisture at the centreline. Dimensionless parameter values given by $Sh_f = 20$, Sh_i=5, $\overline{D}_f$=1, $\overline{D}_i$=1 $\overline{k}$=1, $\overline{k}_w$=0.01, $\overline{k}_p$=0.01, Nu_i=5, Nu_c=5, $\overline{\kappa}_c$= 5, $\overline{\kappa}_v$= 5 and $\overline{\lambda} = 0.5$

brings heat with it, leading to a slow increase in cell temperature $\overline{T}_c$ (figure (c)). The intercellular vapour density will decrease more slowly due to higher pressure driven water to flow from the cell structure (figure (b)). With increased water in the intercellular space, more heat is needed for water evaporation, leading to a lower intercellular space temperature (figure (d)).

For variable pressure, there is a convective flow because pressure is driven from deeper cells to the surface, in addition to transfer flux because of pressure driven flow into intercellular space. These two flows will give faster transfer of free water compared to constant pressure (figure (a)). Due to the balance between pressure mechanisms, the flow will be distributed within transfer flux to the intercellular space and convective driven flow to the external surface, so that the intercellular vapour density produced will be lower (figure (b)). This leads to a higher intercellular space temperature $\overline{T}_i$ because less heat is needed for evaporation (figure (d)). At the same time, because of the balance between pressure mechanisms, cell temperature $\overline{T}_c$ will also be higher in the case of variable pressure.

6.5 Drying through intercellular space dominant fruit

To validate the numerical solution for the non-isothermal model, we consider the limit in which the intercellular space is asymptotically large, as discussed in section §5.3. In this case, water is transferred from the cell into the intercellular space and from the intercellular space into the drying air. At the same time, heat is also transferred from the cell to the intercellular space. The source of heat from the cell into the intercellular space as discussed in chapter 4 i.e. water is released into the intercellular space from the cell and inflow of heat due to the difference in temperatures between intercellular space and intracellular cell. The sink of heat will be from latent heat to evaporate water to water vapour. The non-dimensional model equation becomes

$$\overline{\rho}\Big[\frac{\partial \overline{T}_i}{\partial \tau}+\frac{\boldsymbol{n}_i}{\overline{\rho}}\cdot\frac{\partial \overline{T}_i}{\partial \overline{x}}\Big]=\frac{\partial}{\partial \overline{x}}\Big[\phi_i\overline{\kappa}_v\frac{\partial \overline{T}_i}{\partial \overline{x}}\Big]+\overline{h}_i(1-\overline{T}_i)+C(1-\overline{\rho})(1-\overline{T}_i)-\overline{\lambda}(C(1-\overline{\rho})). \quad (6.12)$$

Initially, temperature of the intercellular space is $\overline{T}_i$=0. To simplify the model for temperature, we consider the limit in which the interface between the intercellular

space with drying air is insulated and we impose a no-flux boundary condition on both boundaries given by

$$\frac{\partial \overline{T}_i}{\partial \overline{x}} = 0. \tag{6.13}$$

Simulation was conducted for equations (5.22) and (6.12) with boundary condi-

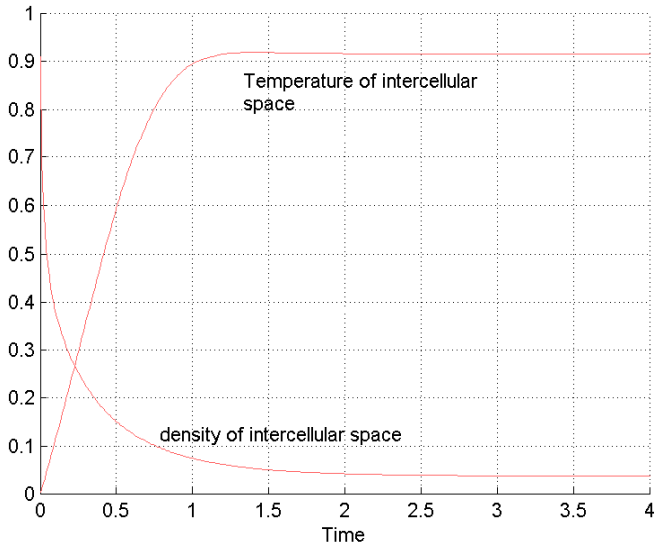

Figure 6.10: Density/temperature of water vapour in intercellular space at the surface. Parameter values $\overline{h}_i$=1 C=0.1 λ=1.

tions, equations (5.23) and (6.13). Figure 6.10 shows the profile of intercellular space density and temperature at the surface of the intercellular space. The equilibrium temperature will be attained with the limit that the flow of heat from the cell will be larger from the heat required for evaporation, given by

$$\overline{h}_i(1-\overline{T}_i) + C(1-\overline{\rho})(1-\overline{T}_i) > \overline{\lambda}(C(1-\overline{\rho})).$$

Rearranging

$$\overline{T}_i < 1 - \frac{\overline{\lambda}[C(1-\overline{\rho})]}{\overline{h}_i + C(1-\overline{\rho})}.$$

The behaviour of intercellular temperature for changing parameter values is shown in Figures 6.11 and 6.12. Figure 6.11 shows how the increasing the evaporation term, $\overline{\lambda}$ results in temperature decrease. The same behaviour has been seen in Figure 6.8(d) in section §6.3.2

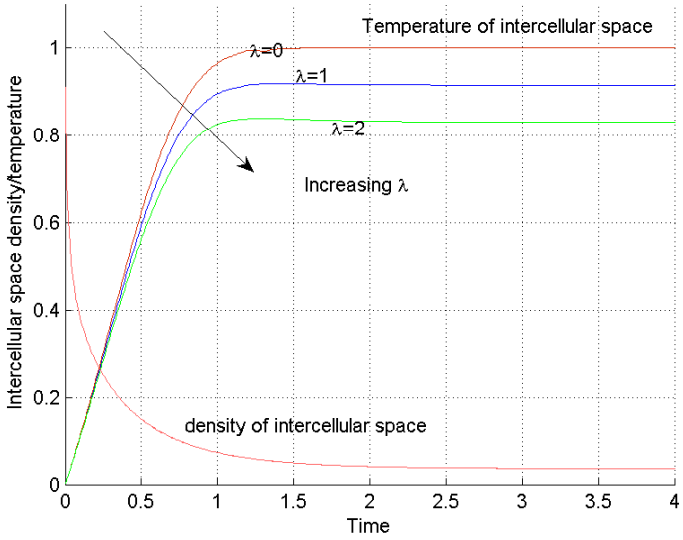

Figure 6.11: Density/temperature of water vapour in intercellular space at the surface with different values of $\overline{\lambda}$. Parameter values $\overline{h}_i$=1 C=0.1.

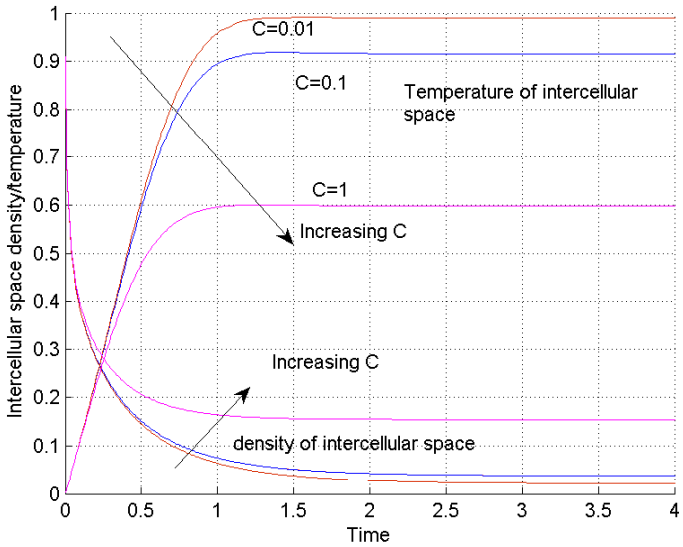

Figure 6.12: Density/temperature of water vapour in intercellular space at the surface with different values of C. Parameter values $\overline{h}_i$=1 $\overline{\lambda}$=1.

The effect of increasing the flux parameter C is shown in Figure 6.12. As this parameter is increased, the long time residual temperature decreases. The same behaviour has been seen in Figure 6.6(d) in section §6.3.2.

Values for parameter $\overline{\lambda}$, $\overline{h}_i$ are associated with fruits are not readily available in the literature, since they will depend upon the characteristics of the intercellular space. In the following, we take representative values $\overline{\lambda}$=0.5, $\overline{h}_i$=1, these parameter values being chosen to illustrate the type of behaviour that can arise.

6.6 Three-phase non-isothermal model

The modifying effect of transfer inside the intracellular cell structure between free water and bound water is included in this three-phase model for the five dependent variables $\overline{\rho}$, M_f, M_b, $\overline{T}_i$ and $\overline{T}_c$. A solution for the three-phase non-isothermal model is given by solving five coupled pde, three for mass equations (6.1), (6.4) and (6.5), two for energy equations (6.8) and (6.9), together with equations of transfer flux (6.3) and (6.2). These equations were solved using COMSOL Multiphysics as discussed in chapter 5. $\overline{\rho}$ and M_f are formulated as in section §5.4.1. $\overline{T}_i$ and $\overline{T}_c$ are formulated as in section §6.3. Generic values of non-dimensional parameters are given as constant, as discussed in section §5.4.1 and §6.3

6.6.1 Analysis of non-isothermal three-phase model

Figure 6.13 shows comparison profiles of free water moisture, bound water moisture, intercellular vapour density at the surface for the three-phase isothermal (Chapter 5) and three-phase non-isothermal model. Variable cell pressure was put into the modelling for each case. Results shown in Figure 6.13 show that free water moisture for the isothermal case decreases more quickly than the non-isothermal case. In the case of isothermal, we assume that the temperature increases rapidly and gives the value of $T_{sur} = 1$ and the solution is based on uncoupled behaviour between moisture and temperature. When the free water moisture is in a relatively small quantity, change of the bound water moisture to the free water moisture happens especially at later stages of drying. The transfer between the bound water moisture to the free water moisture increases the level of free water, which happens at time τ=2.2 for

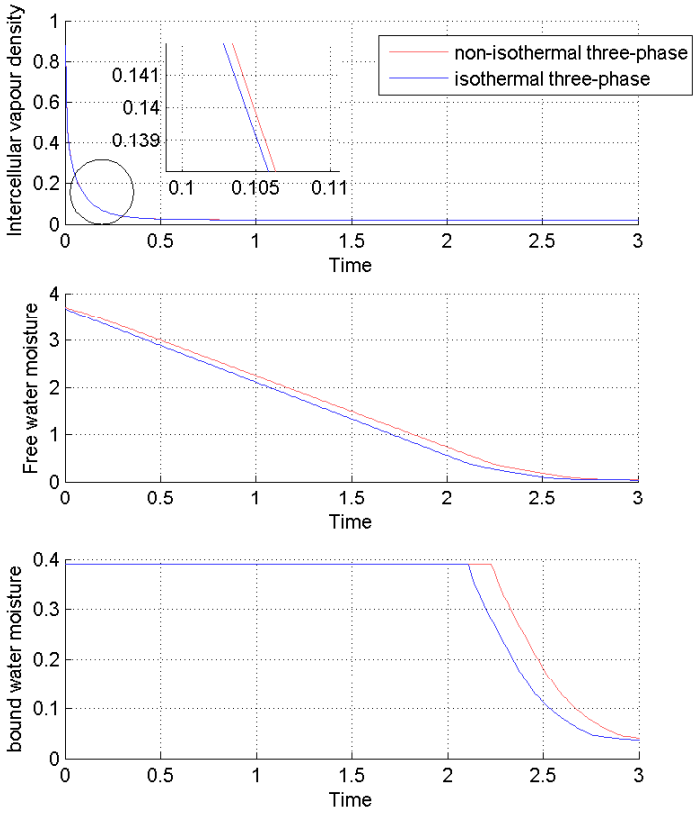

Figure 6.13: Profile of intercellular vapour density, free water moisture and bound water moisture for isothermal and non-isothermal three-phase at the surface. Dimensionless parameter values given by $Sh_f = 20$, $\overline{Sh}_i$=5, $\overline{D}_f$=1, $\overline{D}_i$=1 $\overline{k}$=1, $\overline{k}_p$=0.01, $\overline{k}_w$=0.01, Nu_i=5, Nu_c=5, $\overline{\kappa}_c$= 5, $\overline{\kappa}_v$= 5 and $\overline{\lambda}$=0.5

isothermal condition and time τ=2.3 for non-isothermal condition.

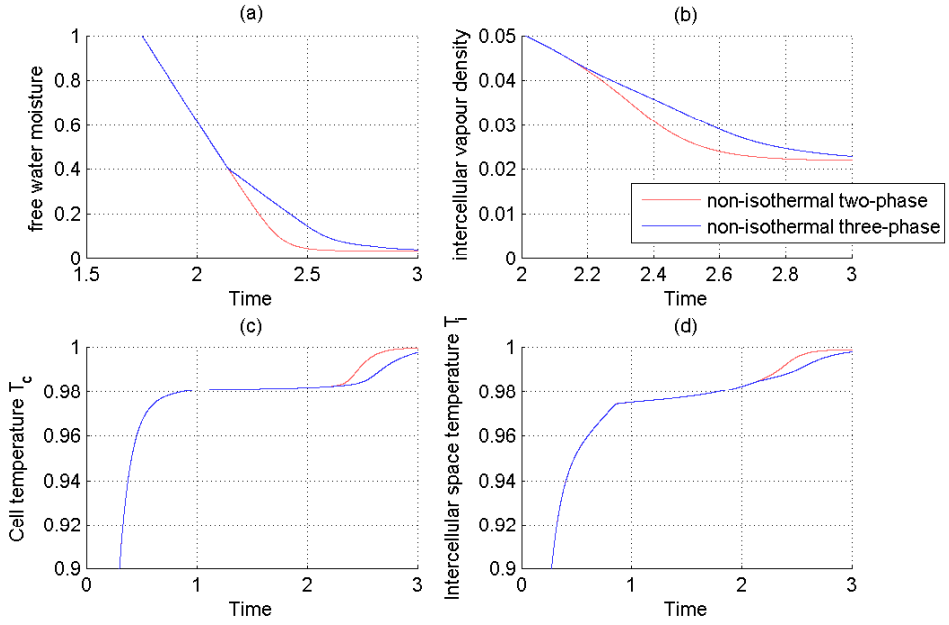

Figure 6.14: Profile of free water moisture, intercellular vapour density, cell temperature and intercellular temperature for two-phase and three-phase non-isothermal case at the surface. Parameter values the same as Figure 6.13.

Figure 6.14 shows a profile of free water moisture, intercellular vapour density, cell temperature and intercellular space temperature for two-phase and three-phase non isothermal cases at the centre. Comparison of the two-phase and the three-phase models shows the decrease in free water as nearly the same, but at a later stage in the three-phase model, the transfer of bound water to free water increases the level of free water moisture in cell (refer Figure 6.13) leads to increasing transfer flux into intercellular space. This happens in the later stage (τ = 2.3) when $M_f < M_b$. This gives the intercellular vapour density to be higher at the end of drying. A similar profile was also found in the isothermal case (Chapter 5). Figures 6.14(c) and 6.14(d) show a profile of temperature at the surface of the intercellular space and the intracellular cell. The temperature of three-phase model is little bit lower at τ=2.3, which happens as the transfer of bound water to free water leads to increased of free water moisture levels. This water is advected to the intercellular space, particularly

increasing the intercellular vapour density. This gives the increase in cell temperature $\overline{T}_c$ and intercellular space temperature $\overline{T}_i$ at a later stage in the three-phase model, which is slower than the two-phase model.

6.7 Model validation

Closely coupled with an accurate formulation of the problem is validation of the model and accuracy of the computations.

6.7.1 Time step and convergence

In simulations, convergence of the numerical results was verified through mesh convergence, going up to 800 nodes in the 1 non-dimensionless thickness to achieve a numerically accurate and converged solution. The time step used in the simulation is 0.01 in terms of non-dimensionless time steps. The effects of changing the number of nodes on moisture and temperature distribution gives an absolute error of 10^{-5} . Tests with finer meshes were made but no influence on the results was observed. The input parameters used in this study are shown in Table 5.4.

The numerical test was also conducted using different time steps. The mesh value was fixed at 800 , with time steps of change from 300 to 3000. The effect of changing the number of time steps on moisture and temperature gives absolute error of 10^{-6}. From Figure 6.15, the results from different numbers of time step agree well.

6.7.2 Comparison with the literature data

A direct comparison of predicted values with the experiments is not possible at this time due to limitations of the parameter estimations. There is only limited experimental transport data for cellular tissues available in the literature. Most data are expressed as diffusion coefficients and are obtained from solution of the diffusion coefficient along with the experiment drying curve on the basis of physical models unlike those presented in this work. Alternatively, prediction used in the theoretical model result can be compared on the basis of some assumptions in the literature data. Comparison was made with the work of Dissa *et al.* [40], who investigated

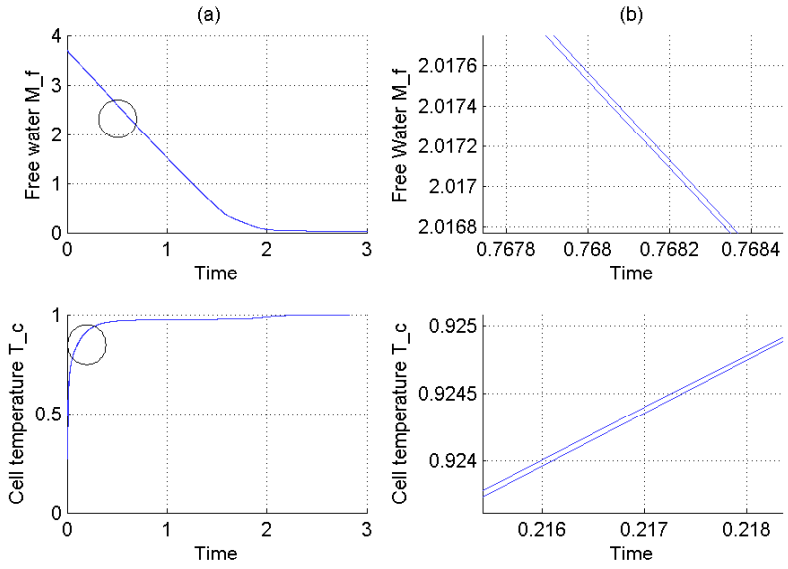

Figure 6.15: Convergence checks for different numbers of time steps. (a) Evolution of free water and cell temperature at the surface position.(b) a magnified region to show the detail more clearly. Parameter values the same as section §6.6.

the convective drying of mango with the effects of shrinkage and that of Velic *et al.* [118] for apple drying. Figure 6.16 shows the variation in average moisture content by drying time for air velocity=0.8 m/s, RH=15%, temperature=70^{o}C and length=5mm for mango drying and velocity=1 m/s, temperature=60^{o}C, RH=9%, length=5mm for apple drying. As seen, the comparison between experiment results of average moisture and model prediction matches closely with the results of Dissa *et al.* [40] and Velic *et al.* [118]. At the beginning, there is close agreement between experiment data simulation at high moisture content; at low moisture contents, the predicted value begins to separate from experiment data. This departure is to be expected because the model is built on the assumption that cellular structure remains functional. This is less and less realistic as moisture content decreases, because of an increasing portion of tissue becoming non functional. This similar behaviour was also observed by Crapiste *et al.*[28] when they compared experiment data with their simulation. As our model considers vapour transport to be distributed across the cell structure at the later stage of drying; this transport leads to a faster decrease at the end of drying compared to their model. Such close agreement between experiment measurements

and model prediction confirms the effectiveness of the model and serves to validate it.

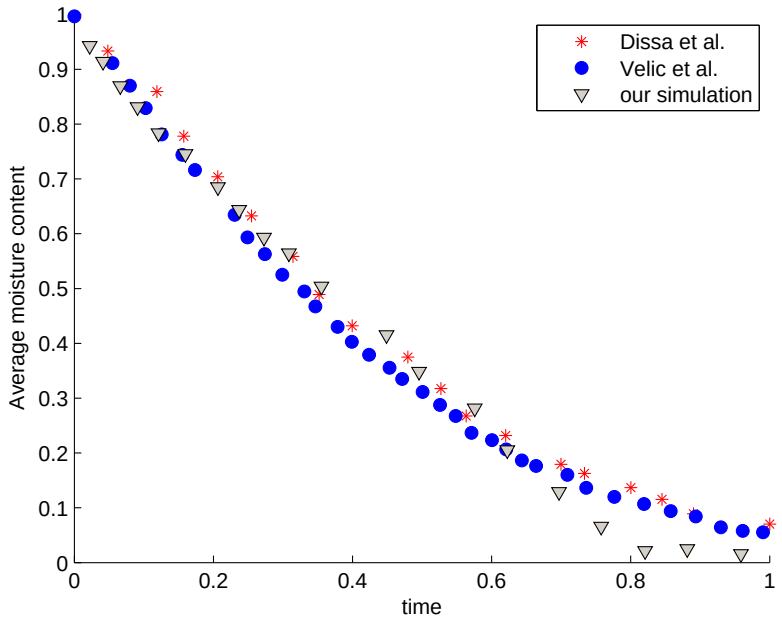

Figure 6.16: Comparison between numerical solutions for average moisture with experiment data from the literature by Dissa *et al.* [40] and Velic *et al.* [118]. Dimensionless parameter values the same as §6.6

6.8 Conclusion

In this chapter we have presented a one-dimensional two-phase model and a three-phase model in which the effect of heat was put into the more relevant the model. Numerical solutions of the model equations are presented using constant value of parameters.

In chapter 5, only mass transfer has been assumed in the model. However, drying is a non-isothermal process and heat transfer can substantially affect drying behavior. Therefore, drying model has been extended to account for the latent heat of evaporation and the temperature dependencies of saturation vapor pressure $\beta(T_{sur})$. In the presence of thermal gradients, evaporation occur in the partially saturated pore

region. Most studies in the literature include only surface evaporation as a boundary condition for the energy equation, and equate the rate of surface evaporation to the rate of diffusive moisture loss at the surface. Thus, evaporation has been excluded inside the food even though temperatures inside reached higher than 100^oC. Recent studies ([42] and [135]) have shown that evaporation is not instantaneous and non-equilibrium exists during rapid evaporation between water and vapour in the gas phase. As evaporation takes place, the vapour produced expels the air and occupies its space, resulting in increased of vapour. Furthermore, if evaporation occurs, pressure will produce a significant convective flow (Darcy) in the intercellular space, leading to decrease in vapour, which leaves the surface. We remark that, as we have modelled this phase as a rigid porous material and have divided our system into two different phases, water phase in the intracellular cell and vapour phase in the intercellular space and different temperatures are observed between this regions. Moisture in the water vapour phase inside intercellular space is at a higher temperature than the moisture in the liquid phase inside intracellular cell.

Our model reveals that temperature gives significant effects in both intercellular space and intracellular cells. This prediction has important implications for food engineering applications, suggesting that a uniform temperature is crucial, as temperature is the main source of drying. This is characterized by Nu_i and Nu_c, the bigger these values, the more non-uniform the temperature inside the fruit.

The separated modelling of the intercellular space and intracellular cell has revealed an important facet of the system. Furthermore, such a model provides a means to investigate the interplay between the liquid phase and the water vapour phase on the movement of water during drying. It has been shown that water transport during drying occurs by the contribution of two mains fluxes: cell to cell and through intercellular spaces.

Chapter 7

Two-dimensional Multiphase drying model

7.1 Introduction

In chapters 5 and 6, numerical solution for the one-dimension multiphase model was performed using the COMSOL solver. In this chapter, we want to extend the model developed in chapter 4 to a two-dimensional multiphase model. Modelling of overall food behaviour is important and local and transient features can help to establish firmer knowledge for modelling applications. Modelling can provide insight into fundamental and critical processing variables to improve product quality and safety. In this respect, the simple model discussed in chapter 4 for drying of food using cellular features will be further analysed for two-dimensional drying, integrated with evaporation and transfer flux.

A two-dimensional model for drying under thermal conditions is evaluated using COMSOL and the results will be presented and compared with the results found in earlier chapters for one-dimensional model.

7.2 Mathematical formulation

In this chapter, the two-dimensional multiphase model for drying under non-isothermal conditions is presented, corresponding to the model developed in chapter 4. To rep-

resent the moisture/temperature distribution system, we choose a (dimensionless) Cartesian coordinate system $\mathbf{u}=(x, y)$. A two-dimensional model is employed in the analysis using slab of thickness a and length b, as shown in Figure 7.1. The food is exposed to an air flow at the surface ($d\Omega_3$ and $d\Omega_4$) for which the temperature $T_{air} = 60^oC$, the relative humidity(RH)=20%; this will give the concentration of air as constant C_{air}=0.025. Due to the geometric symmetry and suitable initial and boundary condition ($d\Omega_1$ and $d\Omega_2$), only a quarter of the product requires computation ($0 < x < a$ and $0 < y < b$). On the same figure, three characteristic points inside the fruit were selected: point A-located at the top surface; Point B-located in the middle of the fruit; point C- is located in the symmetry point of the fruit. One line across the thickness was also selected (line D).

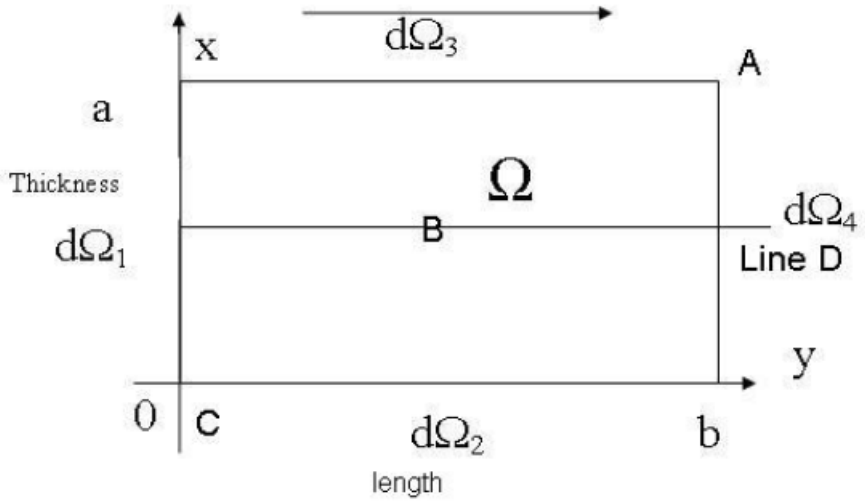

Figure 7.1: Schematic of two-dimension slab.

The corresponding set of governing equations in non-dimensional form as derived in chapter 4, is given from (4.31), (4.32), (4.33), (4.36) and (4.37), together with the equation of transfer flux (4.34) and (4.35). The overbar notation is dropped for clarity. The conservation equations for intercellular vapour density for a fixed intercellular

space become

$$\phi_i \frac{\partial \rho}{\partial \tau} + \frac{\partial}{\partial x}\Big[- (\rho k \gamma + D_i)\frac{\partial \rho}{\partial x}\Big] + \frac{\partial}{\partial y}\Big[- (\rho k \gamma + D_i)\frac{\partial \rho}{\partial y}\Big] = j_{ip} + j_{ic}. \tag{7.1}$$

The conservation of free water moisture is given by,

$$\rho_s \frac{\partial M_f}{\partial \tau} + \frac{\partial}{\partial x}\Big[- (D_f \rho_s + D_p\, M_{f0}\, \rho_s\, \varsigma)\frac{\partial M_f}{\partial x}\Big] \;+\; \frac{\partial}{\partial y}\Big[- (D_f \rho_s + D_p\, M_{f0}\, \rho_s\, \varsigma)\frac{\partial M_f}{\partial y}\Big] = -j_{ip} - j_{ic} + \rho_s r_b. \tag{7.2}$$

The conservation equation of bound water moisture is given by,

$$\frac{\partial M_b}{\partial \tau} = -n_1 M_b + n_2 M_f = -r_b. \tag{7.3}$$

The equation for mass flux of free water is associated with differential pressure between the local cell and the intercellular space given by

$$j_{ip} = k_p(P_c - P_i), \quad \text{and} \quad j_{ic} = k_w(\eta - \xi). \tag{7.4}$$

Intercellular space temperature equation becomes

$$\phi_i\Big[\rho \frac{\partial T_i}{\partial \tau} - \frac{\partial}{\partial x}\Big(\kappa_v \frac{\partial T_i}{\partial x}\Big) - \frac{\partial}{\partial y}\Big(\kappa_v \frac{\partial T_i}{\partial y}\Big)\Big] = h_i(T_c - T_i) + (j_{ip} + j_{ic})(T_c - T_i - \lambda) - \phi_i \boldsymbol{n}_i \cdot \frac{\partial T_i}{\partial x} - \phi_i \boldsymbol{n}_i \cdot \frac{\partial T_i}{\partial y}. \tag{7.5}$$

Intracellular cell temperature equation becomes

$$(1 - \phi_i)\Big[\rho_c \frac{\partial T_c}{\partial \tau} - \frac{\partial}{\partial x}\Big(\kappa_c \frac{\partial T_c}{\partial x}\Big) - \frac{\partial}{\partial y}\Big(\kappa_c \frac{\partial T_c}{\partial y}\Big)\Big] = -h_i(T_c - T_i) - (j_{ip} + j_{ic})(T_c - T_i). \tag{7.6}$$

Associated initial conditions are taken as

M_f=3.7, M_b=0.39, $\rho = 1$, T_i=0 and T_c=0.

Boundary condition on the symmetry boundary (boundary $\mathrm{d}\Omega_1$) at $y = 0$ and $0 < x < b$ is given by

$$\frac{\partial M_b}{\partial y} = 0, \quad \frac{\partial \rho}{\partial y} = 0 \quad \frac{\partial T_i}{\partial y} = 0 \quad \text{and} \quad \frac{\partial T_c}{\partial y} = 0.$$

Boundary condition on the axi symmetry boundary (boundary $\mathrm{d}\Omega_2$) at $x = 0$ and $0 < y < a$ is given by

$$\frac{\partial M_f}{\partial x} = 0, \quad \frac{\partial M_b}{\partial x} = 0, \quad \frac{\partial \rho}{\partial x} = 0 \quad \frac{\partial T_i}{\partial x} = 0 \quad \text{and} \quad \frac{\partial T_c}{\partial x} = 0$$

Boundary condition at the surface (boundary $d\Omega_3$), at $x = a$ and $0 < y < b$ is given by

$$\Big[(D_f\rho_s + D_pM_{f0}\rho_s\varsigma)\Big]\frac{\partial M_f}{\partial x} = -Sh_f(\overline{C}_{fw,sur} - 1), \tag{7.7}$$

$$\Big[(\rho k\gamma + D_i)\Big]\frac{\partial \rho}{\partial x} = -Sh_i(\frac{\rho}{C_{air}} - 1), \tag{7.8}$$

$$\phi_i\kappa_v\frac{\partial T_i}{\partial x} = -\phi_i Nu_i\kappa_v(T_{isur} - 1), \tag{7.9}$$

$$\text{and} \quad (1-\phi_i)\kappa_c\frac{\partial T_c}{\partial x} = -(1-\phi_i)\kappa_c Nu_c(\overline{T}_{csur} - 1) + \lambda D_f\frac{\partial M_f}{\partial x}. \tag{7.10}$$

Boundary condition at the surface (boundary $d\Omega_4$), at $y = b$ and $0 < x < a$ is given by

$$\Big[(D_f\rho_s + D_pM_{f0}\rho_s\varsigma)\Big]\frac{\partial M_f}{\partial y} = -Sh_f(\overline{C}_{fw,sur} - 1), \tag{7.11}$$

$$\Big[(\rho k\gamma + D_i)\Big]\frac{\partial \rho}{\partial y} = -Sh_i(\frac{\rho}{C_{air}} - 1), \tag{7.12}$$

$$\phi_i\kappa_v\frac{\partial T_i}{\partial y} = -\phi_i Nu_i\kappa_v(T_{isur} - 1), \tag{7.13}$$

$$\text{and} \quad = (1-\phi_i)\kappa_c\frac{\partial T_c}{\partial y} = -(1-\phi_i)\kappa_c Nu_c(T_{csur} - 1) + \lambda D_f\frac{\partial M_f}{\partial y}. \tag{7.14}$$

7.3 Numerical solution

The COMSOL Multiphysics program is used to simulate the dehydration process in a drying system that corresponds to the numerical solution of these model equations as seen in the one-dimensional problem in section §2.3.1 . The above system of non linear partial differential equations, together with the described set of initial and boundary conditions, has been solved by Finite Element Method implementation by COMSOL Multiphysics 3.4.

The coefficients of the equations were formulated such that the equations led to constitutive equations for intercellular vapour density and free water moisture and bound water moisture, intercellular space temperature and intracellular cell temperature i.e., equations (7.1), (7.2), (7.3), (7.5) and (7.6). Moreover, the transfer fluxes (7.4) were included in the equations to give the coupling effects for both the intercellular vapour density and free water moisture. All the equations were input into COMSOL Multiphysics using a partial differential equation (PDE) solver with the

general form for moisture content and temperature. Details of the numerical procedure can be found in Appendix C.

7.3.1 Results and analysis

In this section, the results of drying simulation with two-dimensional non-isothermal conditions for the three-phase model are presented for generic conditions given in section §5.4.1 and §6.3. For the non-isothermal three-phase two-dimensional drying model, five dependent variables ρ, M_f, M_b, T_i and T_c were used to describe the characteristics of drying models. For the first simulation, the thickness and length is taken as aspect ratio (AR) $b/a = 1$. The simulation is then repeated with aspect ratios, $b/a = 2$ and $b/a = 0.5$ and compared with $b/a = 1$. The thickness of the food is maintained at constant value $a = 1$ and the length of the food is changed according to the corresponding aspect ratio (AR). Simulation result are presented in the form of free water moisture, intercellular vapour density, cell temperature T_c and intercellular space temperature T_i.

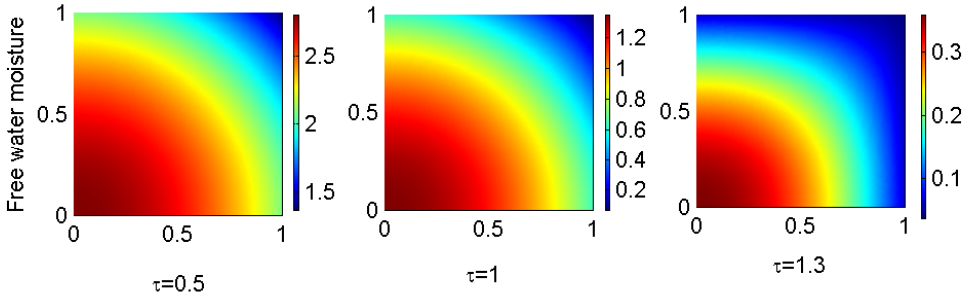

Figure 7.2: Surface plot of residual free water moisture field at different time $\tau = 0.5$, $\tau = 1$ and $\tau = 1.3$. Parameter values given by $Sh_f = 20$, Sh_i=5, D_f=1, D_i=1 k=1, k_p=0.01, and k_w=0.01, Nu_i=5, Nu_c=5, κ_c= 5, κ_v= 5 and $\lambda = 0.1$.

A surface plot of residual free water moisture is given in Figure 7.2, which shows the free water moisture residual inside the fruit as the time period increases as a result of drying. Fruit loses a significant amount of water during the initial phase of drying, free water moisture decreases from its initial value of 3.7 kg/kg to 1.4 kg/kg after τ=0.5 at the surface. A different region of moisture forms almost immediately after

just τ=0.5 of drying, while the central portion retains a high moisture content. After τ=1, a distinct layer has been formed, with a considerable amount of water within the centre of the fruit. After τ=1.3, most of the free water moisture is eliminated from the fruit and a small amount of residual moisture is still left. Thus, the moisture loss is highest at the top edge, lowest in the centre. After heating of about τ=1, almost 92% of the moisture is lost near the top edge. Hence, the 2-D model is able to present the transient change of moisture and its steady movement towards the centre of the fruit.

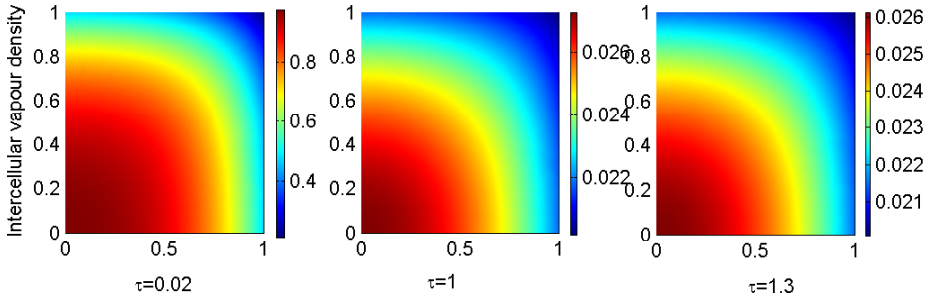

Figure 7.3: Surface plot of intercellular vapour density field at different time $\tau = 0.02$, $\tau = 1$ and $\tau = 1.3$. Parameter values the same as Figure 7.2.

Figure 7.3 shows a surface plot of residual intercellular vapour density at different times. From the figure, the intercellular vapour density reduces as the time increases. As drying proceeds, when nearly all free water moisture is eliminated, the intercellular vapour density decreases.

Figure 7.4 shows the profile of free water moisture, cell temperature, intercellular vapour density and intercellular space temperature drawn across the section line passing through the centre of thickness (line D). The figure shows that the free water moisture and intercellular vapour density continues to decrease with time and cell temperature and intercellular space temperature increase with time. A similar profile is also seen in one-dimensional drying. The temperature at all points across the thickness approaches a level close to the temperature of the air; however, the temperature in the middle increases more slowly than at other points. The moisture gradient in the fruit drives the flow of free water moisture upstream through the sur-

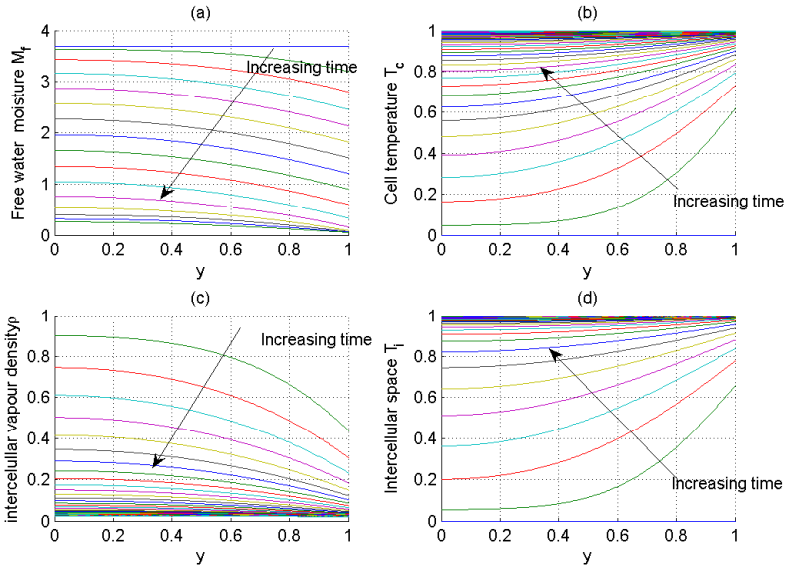

Figure 7.4: Profile of (a) M_f (in step of 0.1) (b) T_c, (c) ρ and (d) T_i cross the section line through the centre of thickness x (Line D) with increasing time τ=0-1.5 (in step of 0.01). Parameter values the same as Figure 7.2.

face, which gradually decreases as the moisture equalizes with the exterior moisture (air moisture).

Changes in local values of free water moisture, intercellular vapour density, intercellular temperature and cell temperature inside the fruit at several points and also compared with moisture and temperature profiles of a one-dimension model are shown in Figure 7.5. It can be seen that the free water moisture at the surface of the slab (point A) achieves its equilibrium faster (Figure 7.5(b)). On the same figure we can observe that the higher the distance of the point analysed from the centre, the lower the free water moisture at that point. This also happens in a one-dimensional model but it takes longer than in the two-phase model because of the smaller surface area in the one-dimension model. This same behaviour is also observed from intercellular vapour density (Figure 7.5(d)). Changes in cell temperature at selected points are also shown in Figure 7.5. Cell temperatures at all points were raised to a level close to temperature of air (Figure 7.5(a)). It can be observed that cell temperature at the middle point (C and B) is lower that the temperature of surface point (A). The increase in cell temperature at the surface occurs rapidly at the beginning

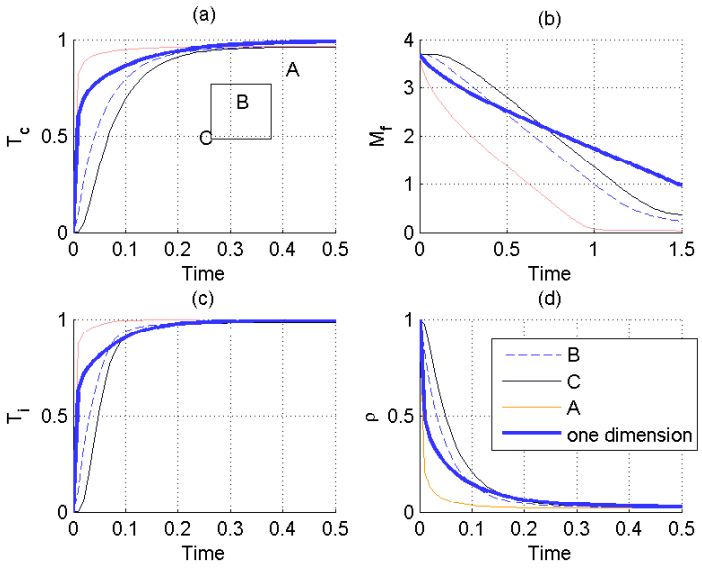

Figure 7.5: Change in (a) T_c (b) M_f, (c) T_i and (d) ρ at selected point and compared with one-dimension model at the surface. Parameter values the same as Figure 7.2.

until there is no significant change in temperature, suggesting that the system has reached very close to equilibrium with drying air. Cell temperature at the surface of the one-dimension model increases more slowly compared to the two-dimension model. As expected, the cell temperature increases faster at the surface because the air temperature starts at the surface, especially in the two-phase model, where the surface area is larger. The same behaviour is also observed for intercellular space temperature (Figure 7.5(c)).

A surface plot of residual bound water moisture at different times is given by Figure 7.6. Initially, when $M_f > M_b$, at any location inside the fruit, there will be no change of bound water to free water. At τ=0.5, bound water moisture still contains 0.39 kg/kg, there is no change of bound water to free water at this stage as $M_f > M_b$. At τ=1, there are some areas near the surface corner (point A), where the transfer of bound water to free water leads to decreased bound water moisture.

Figure 7.7 shows profile of free water, bound water and intercellular vapour density at selected points. This profile shows that bound water decreases from the initial value of 0.39 to 0.01 at the later stage of drying, started at time τ=0.8 at A, τ=1 at B and τ=1.1 at C and τ=2.6 for one-dimensional model. Change of bound water to

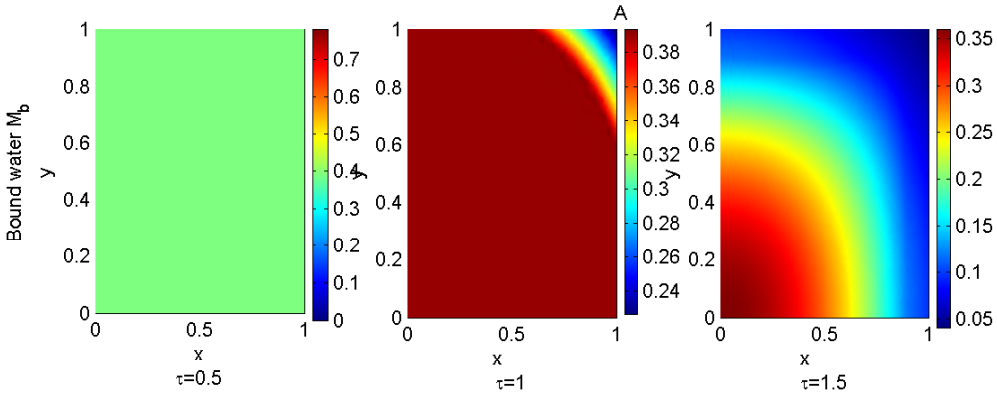

Figure 7.6: Surface plot of residual bound water moisture at different time $\tau = 0.5$, $\tau = 1$ and $\tau = 1.5$. Parameter values the same as Figure 7.2.

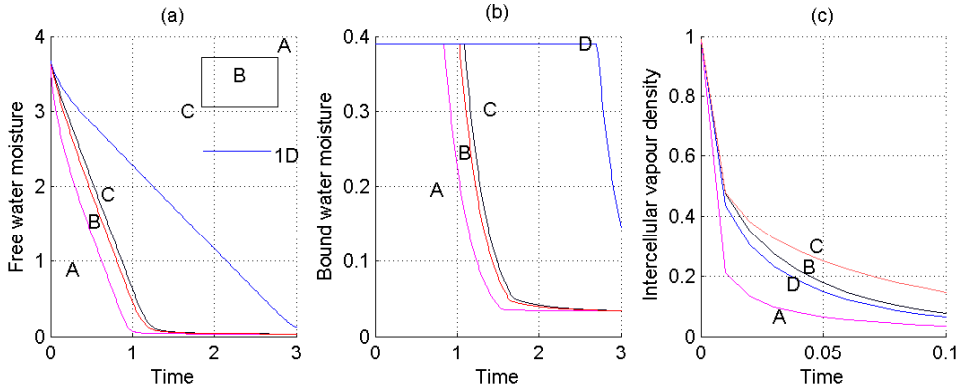

Figure 7.7: Moisture profile (a) free water moisture (b) bound water moisture (c) intercellular density at selected points A , B and C compared with one dimensional model at surface. Parameter values the same as Figure 7.2.

free water is faster at the surface and slower at the centre. As discussed in chapter 5, when the free water moisture is in a relatively small quantity, change of bound water to free water happens. These processes would be important in the later stage when $M_f < M_b$ and much longer stages of drying to reduce residual levels of moisture. For a one-dimensional model, free water decreases more slowly than in the two-dimensional model. The slower decrease of free water in the one-dimensional model leads to time taken for bound water to start decreasing at the surface at time τ=2.6.

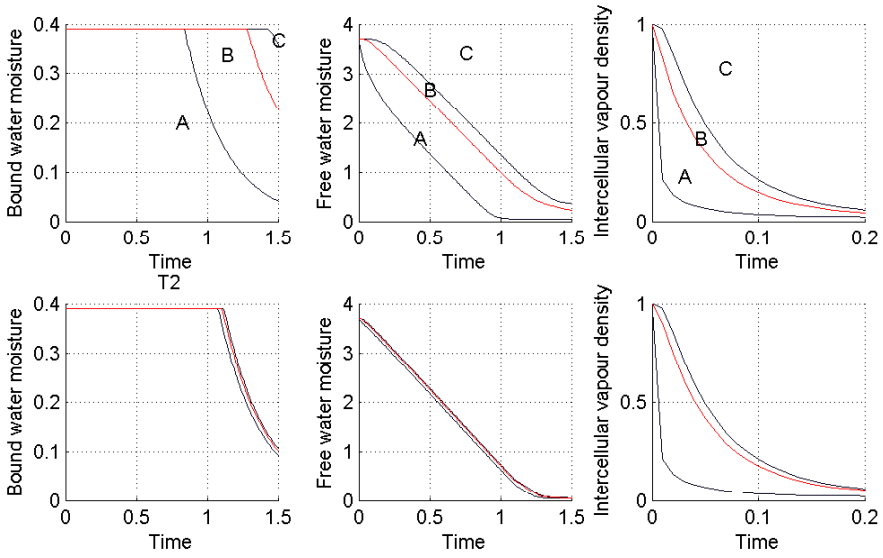

Figure 7.8: Comparison between moisture profiles of bound water moisture, free water moisture and intercellular vapour density at selected points A , B and C for constant pressure (above) and variable pressure (below) inside cell structure. Parameter values the same as Figure 7.2.

Figure 7.8 shows a comparison of bound water moisture, free water moisture and intercellular vapour density between the models using constant pressure and variable pressure inside the cell structure. When using constant pressure, the gradient between the surface and centreline of free water moisture and bound water moisture is much bigger. The drying curves of free water moisture and bound water moisture at selected points practically overlap when using variable pressure in the model. This happens because the constant rate of water is advected to intercellular space for constant

pressure but this rate increases with variable pressure.

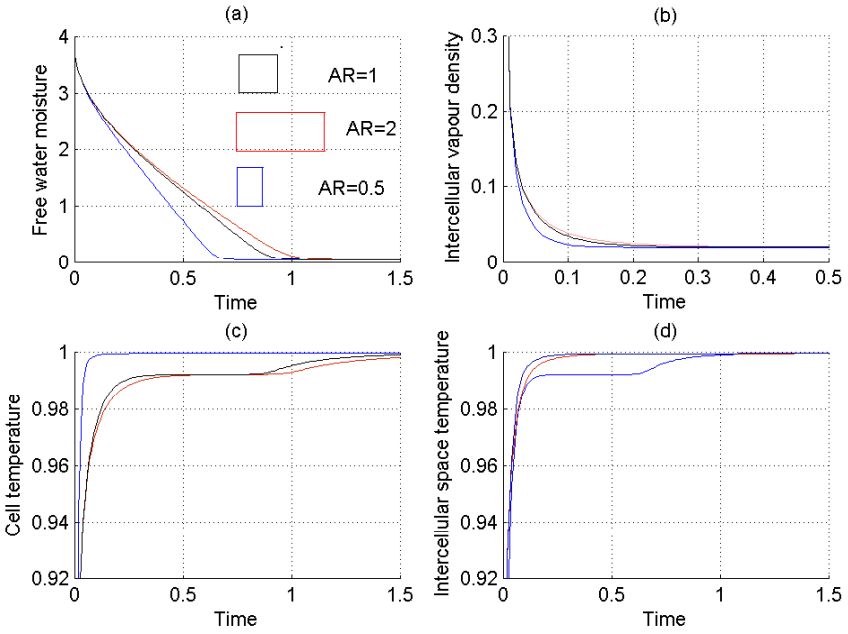

Figure 7.9: Effect of aspect ratio on (a) M_f (b) ρ (c) T_c and (d) T_i at the surface top edge corner. Parameter values the same as Figure 7.2.

Variation of moisture and temperature inside the fruit with different aspect ratio (AR) products is shown in Figure 7.9. Results for free water moisture, intercellular vapour density, cell temperature and intercellular space temperature at the top edge point (A) are shown. Free water moisture reduces more quickly for smaller aspect ratio (Figure 7.9(a)) and cell temperature increase more quickly for smaller aspect ratio (Figure 7.9(c)). Intercellular vapour density decreases more quickly for smaller aspect ratio but intercellular temperature increases slowly for smaller aspect ratio. When drying is accompanied with evaporation inside the fruit, the energy consumption necessary for intensive vaporization of moisture inside the fruit. This gives the intercellular temperature a slower for smaller aspect ratio. It was observed that smaller aspect ratios provide shorter drying times than higher aspect ratios, which is consistent with findings by Kaya *et al.* [68]. Dissa et al. [40] and Villa *et al.* [119] found that the drying rate decreases 4.5% with 1mm increase in mango thickness because the diffusion path of moisture to reach the drying surface increases.

7.4 Conclusion

The full two-dimensional system was investigated in this chapter allowing the effect of geometry to be included. Numerical simulations were used to show that the effect of temperature on the movement of water during drying. It was again found that the moisture maximum is near the centre and the minimum at the surface. The temperature is higher at the surface but lower at the centre, similar to the behaviour observed in a one-dimension model. We remark that the movement of temperature is faster than the movement of moisture. The proposed model was able to provide information about water and temperature profiles at all times, thus allowing detection of the regions within the fruit, where high moisture content promote microbial growth. Hence the 2-D model is able to present a transient change in the temperature and moisture of the fruit and its steady movement toward the centre of the product.

The aspect ratio of a slab directly influences the drying process, and this is directly related to the area/volume ratio, i.e., the lower the area/volume ratio, the faster the drying. During the drying process the smallest moisture gradients are found close to the center and the highest are found close to the surface. The moisture content depends on thickness and length coordinates. The closer to the surface of the slab, the lower the moisture content will be.

As covered in chapter 2, it has been postulated that temperature is higher at the surface corner of leading edge and lower at the symmetry leading edge. The results in this chapter suggest that variable pressure inside the cell is likely to lead to uniform temperature and moisture and, hence, may allow for the formation of isothermal processes during drying.

Chapter 8

Future work and Recommendation

In this thesis we have used two different approaches to model the drying process in foods: a continuum single phase homogenous model (chapter 2), and a continuum multiphase model based on a cellular feature framework (chapter 4), suitable for a macroscale modelling of drying. The significant achievements that can be observed in this thesis are the successful development of the continuum model with embedded of shrinkage and multiphase model based on cellular features. In this chapter we assess the relative merits of each modelling framework and discuss their suitability for use in the drying of fruits. We consider a tropical fruit of fixed size (mango) and run a test problem using each approach. We also discuss insights gained from each model and consider how well they agree with experimental findings.

Following many studies of drying models which exploit single phase continuum formulation, discussed in chapter 2, we initially restricted attention to the flow of water due to the concentration gradient based on diffusion theory and flow of heat, which enhances the diffusion process by, heat conduction transfer. Motivated by the range of experimental studies, we isolated two crucial factors of key importance in the drying of tropical fruits and arising from cellular structure: (i) the interaction between adjacent cells and between cell-airspace, and (ii) the impact of mechanisms (that is, the process by which water is converted to water vapour inside the pores influencing, for example, temperature, moisture and pressure) on drying. The emphasis of this thesis was on these factors. The formulation employed was necessarily simple, but the relevance of the model, by including more detailed physics, provides insight into

the physical processes in a more precise and reliable manner.

This chapter is structured in the following way: summaries of each model is presented in §8.1 before further work and conclusions are discussed in §8.2.

8.1 Summary of the models

A simulation model of heat and mass transfer during drying of tropical fruits was developed. Each model exhibits features of temperature and moisture that are observed experimentally in the drying model. Experimental results by Wang and Brenann [122] suggest that, during drying, there exist temperature differences in the vertical direction (thickness), i.e. from the surface to the bottom of the sample but there are no significant differences between temperatures in the horizontal direction (length). This suggests that a one dimensional model can be used in the modelling of food drying. Further experimental [136] evidence has shown that evaporation occurs inside the food. Non-equilibrium conditions may exist during rapid evaporation between water-vapour in gas phase but consideration of water in pores [50] is justified and our modelling incorporates this in terms of suitable transfer fluxes.

8.1.1 Continuum model

In chapter 2, we developed a continuum model to describe the movement of water inside a fruit. Following Wang and Brenann [123], Balaban and Pigoet [8], water movement was modelled using Fick's Law of diffusion which is characterized by a diffusion coefficient. Two distinct forms of diffusion coefficients were considered: constant and dependent on temperature and moisture. The transfer of water through food is a slow process characterized by the diffusion coefficient; the movement of heat was modelled by the Fourier equation of heat conduction. In drying, two linked processes are considered: the evaporation of water at the solid surface and the internal diffusion of water to the surface. The internal diffusion of water to the surface is given by a diffusion equation and the evaporation of water at the solid surface is given by convective boundary condition. At the surface, overlying hot air was assumed to evaporate water and gives a latent heat effect at the surface. Internally, heat was used to evaporate water near the surface and some of the heat was conducted to

the inside, characterized by Fourier's law of heat conduction. These processes occur simultaneously.

In general two stages can be identified during the drying process. Initially the drying is determined by the external conditions, i.e., the moisture transport in the material is faster than the mass transfer out of the material by the underlying air flow. As a result, the moisture profiles in the material will be rather flat and uniform. However, as soon as the surface becomes dry a drying front will enter the material. Now it is the internal moisture transport that limits the drying rate of the material. During this stage, the moisture profiles, which exhibit a moving drying front, are determined by the material properties such as moisture diffusivity. In general from drying experiment, this can be considered as isothermal. However, for typical drying process, it was found that temperature is an important aspect, this gives a coupled heat and mass transfer have to be taken into account in the simulation. This situation is given in case of non-isothermal model.

The main finding of the model was the ability of the equations to represent the movement of moisture and temperature inside the fruit with high moisture content and, consistent with experiment findings, results providing physical contents were assigned appropriate numerical values. In both mass and heat transfer, two resistances towards transfer play a role. The two relevant mass transfer phenomena are diffusion and convection. Diffusion controls the transfer of moisture inside the material. Convection controls the transfer of moisture from the surface of the material to the air. For heat transfer, conduction controls the heat transfer within the material and convection control the transfer from the air to the foods surface. The ratio between the intensities to internal and external transfer determines whether distributions of either mass or energy arise in the food. For example: when the controlling resistance for drying is the internal mass transfer resistance, the transfer of water from the inside of the food to the surface is much slower than the transport from the surface to the air. Therefore, the moisture content at the surface will be much lower than its concentration in the centre. Clearly, a distribution of water arises inside the food. The ratio between the internal and external resistances is evaluated with the corresponding Sherwood (Sh) numbers. They depend on drying parameters as well as material properties. The controlling of heat transfer is deduced by Nu and $\overline{\lambda}$. If this number

is similar and of the same order of magnitude, the fruit temperatures increase slowly while the process develops. In general, all these numbers depend upon the type of fruit under study and such consideration remains valid with validation of experiment results.

8.1.2 Continuum model with shrinkage effect

Chapter 3, developed a model that extended the heat and mass transfer model to include shrinkage. In previous models, shrinkage effects are very dependent on data from experiment, where the adjustment of shrinkage is done at each time step, using equations derived from experimental measurement. Chapter 3 focussed on the continuum model that based the effect of shrinkage on changes of volume rate from the volumetric reduction of water during drying. The equation for the shrinkage was derived from overall mass conservation balance of liquid water in the fruits in the absence of any void creation.

Model simulation yielded behaviour similar to the non-shrinkage heat and mass transfer model. The comparison between this shrinkage model and the non shrinkage model shows that with shrinkage, the time for drying is much shorter. Physically, the thickness of the sample decreases due to the shrinkage, the moisture has less distance to cover and hence reaches the surface faster, before it can diffuse to the air. This is consistent with experimental findings reported in [122, 107, 40].

A detailed investigated into the effect of diffusivity on drying behaviour is provided by consideration of temperature and moisture dependency; simulation revealed that the temperature has more effect than moisture on the diffusion coefficient. Physically, a combination of these two effects makes changes to fruit, known as glass transition.

8.1.3 Multiphase model

A homogeneous model does not allow us to incorporate more detailed ongoing processes inside the cell/tissues within the single cell as a continuum. Chapter 4 focussed on the heterogenous properties of tissue and detailed cellular structures that can better represent the physical model. An aim is to include subcellular models to develop an enhanced macrostructure model for the multiphase transport of water.

In most multiphase models in the literature, food is considered as a porous medium. The mass transfer equations are solved for the components inside the food whose mass is changing significantly. These components are identified as phases and all the balance equations (mass, momentum and energy) for each of the phases are solved. Phases identified are solid, liquid water, and gas (mixture of vapour and air). The solid phase plays an important role in energy conservation. For fluid phases, all three balance equations are solved within a porous structure. Darcy's law is assumed to be valid. The basic physics of heat and mass transfer remains but is adapted to simulate different processes in this category with appropriate changes in boundary conditions or with the addition/removal of a phase.

In our model, the cells are treated as cellulose capsules filled with liquid. Surrounding the cell are intercellular spaces (pores) that are separated by cell membranes and cell walls. Plasmodesmata connect a cell to the neighbouring cell. Based on these features at cell level, we consider two different regions: an intracellular cell and intercellular spaces (pores). Basic transport of moisture during drying is taken to exist in three categories: water vapour transport in the pores (intercellular spaces), transport of liquid free water inside the individual cell and transport of bound water that is held within the solid cell structure. The model was derived using a multiphase approach; each material constituent is taken as a distinct phase within the multiphase and with the constitutive law describing the material properties and its interaction with the neighbouring phase. To include interaction between neighbouring phases, we incorporate source terms $\overline{j}_{ip}$ and $\overline{j}_{ic}$ into the appropriate mass balance equations. Formal averaging techniques were not used as we describe the process in macroscopic property but the precise details at the microscopic level.

Simulations of the model were based on isothermal and non-isothermal conditions for a two-phase model. The modifying effect of including bound water within the cellular structure is provided within a three-phase model. Model simulation results show the behaviour changes in liquid water and water vapour during drying. Model simulations yielded behaviour of liquid water transport similar to that seen in the single phase model. The multi-phase model also generates results not evident in the homogenous model, such as the bahaviour of water vapour inside the intercellular space. The additional effect of heat considers the principal of local non-equilibrium

between the cell and intercellular space at given locations. This given by representative temperature in the intercellular space $\overline{T}_i$ which is different from representative temperature within the intracellular cell $\overline{T}_c$. This could not be seen in the single phase model, which assumed heat transfer remains in equilibrium at the local temperature.

In further chapters we investigated the key parameters in the multiphase model. In chapter 5, an isothermal model evaluates the effect of transfer fluxes. Simulations reveal that, the transfer fluxes $\overline{j}_{ip}$ and $\overline{j}_{ic}$ relates moisture transfer from intracellular cell into intercellular space is important. In Zhang and Datta [134], the use of non-equilibrium approach was discussed along with a more realistic representation of the physical problem. Discussion in Halder *et al.* [52], the use of non-equilibrium formulation in frying, stated that the assumption of equilibrium between liquid water and water vapour might not always be true and, based on this, the evaporation rate is estimated using the Hertz-Knudsen Law. From our simulation, it is realistically possible to include interaction between water and water vapour inside the material by using the transfer flux equations. Transfer fluxes $\overline{j}_{ip}$ and $\overline{j}_{ic}$ relates moisture transfer from intracellular cell into intercellular space lies at the heart of this new drying model. Currently, modelling studies are limited by the knowledge of phase changes between water and vapour inside the material during the drying process.

A multi-phase model allowed us to incorporate the movement of vapour inside the intercellular space. This enabled evaluation that cell-pores have an effect on drying behaviour. The effect of changes in permeability influence behaviour inside the intercellular space more than diffusivity. Convective transport near the surface also influences drying less than diffusion inside the intracellular cell.

In this thesis, we have laid the foundations for mathematical investigation into the mechanisms by which movement of water and movement of heat occur simultaneously. This work has yielded a number of interesting results, many of which merit further investigation. We have shown how homogenous models and multiphase models can replicate experimental findings and give new insight into the study of drying methods. We hope this body of work will prove useful to mathematics in industry and experimental industries with an interest in the development of new drying methods

8.2 Further work and conclusion

Although we have been able to show the main physical features in the models, further work is needed to gain a comprehensive understanding. The models analysed within this thesis were necessarily complex since they attempted to capture the complex interplay between a number of phases within a biologically relevant framework. We have therefore employed reasonable simplifying limits such as internal turgor pressure P_c, which remains constant during the main drying stage, but may need modifying in later studies. Furthermore, due to lack of experimental data in term of dimensionless parameters, we have made a number of biologically-motivated constitutive and modelling choices and estimated many of the parameter values. These approximations point the way to a myriad of interesting and challenging extensions. Starting with the available data, we have obtained the desired output for a range of data. The enhanced models provided in this study will show important trends and promote understanding of food drying systems, even when precise data are not available. A simple way to increase the realism of the models developed in this thesis would be to work more closely with industries and biologists to obtain better estimates of the parameters for specific food applications. Furthermore, such collaboration would allow the estimation of more accurate functional forms for our constitutive modelling choices, such as consideration of the effect of internal turgor pressure P_c.

In developing the three-phase model that included the effect of bound water, we have exploited the model by Kiranoudis *et al.* [71] which details the conversion between two forms of water molecules as a reversible reaction, relevant to the later stage of drying. The interaction between water and solid is modelled through the adsorption of free water to become bound water and the desorption of bound water to become free water. This needs further investigation. Mayor and Sereno [76] have stated that loss of water and heating cause stresses in the cellular structure of the food, leading to change in shape and reduction in size. This suggests that cellular structure collapse during drying is associated with the removal of bound water at a later stage of drying, due to microstructure stresses. This thesis provides a first opportunity to thoroughly investigate the effect of bound water and to include the shrinkage effect in the model.

An important advantage of the fully predictive theory, suggested here, is to provide considerable insight into the mechanisms that influence water transport. Care should be taken in the estimation of transport parameters and cell properties and additional work is recommended in this area. It has been shown that water transport during drying occurs by the contribution of two main fluxes: cell to cell and cell to intercellular space. All these mechanisms are relevant and their contribution to the total moisture transport, changes significantly as drying proceeds. Even though the study was restricted to a particular case of mass transport during drying, the theoretical approach presented in this work should have wide application in the analysis of a variety of transport problems involving cellular materials.

Within this thesis, we have demonstrated the benefits of different theoretical frameworks for studying the movement of moisture and temperature within a fruit slab. We have shown how a multiphase model and a singlephase model can replicate experiment findings and give insight into moisture and temperature movement during drying. Although we have generated some interesting results, there are many model extensions we could consider. These include simulating the models in a more realistic geometry or applying the model to include more subcellular effects. It would also be interesting to create a fully three-dimensional model for drying, modelled as three-dimensional shapes. With a three-dimensional model, we would be able to model the movement of water more accurately as we could calculate the contact area between cells, rather than assuming that all the cells are of the same size. The results could be compared with those from a homogenous model.

Our models incorporated moisture isotherm using Wang and Brenann's [122] model of potato. As mentioned in chapter 1, several other isotherm models could be considered, using the numerous relationships outlined by Mujumdar [79]. It would be interesting to study the effect on our system if other moisture isotherm model were used.

The most detailed of the physically based models have been solved by specialist codes. These codes are often unavailable to the public or difficult to use by anyone other than author. As a result, the food industry and academia are unable to use such simulations for the design of products [52]. To overcome this problem, implementing in commercial software, is a good option and work is needed to organize the

information and integrate it into a user friendly package known as Graphical User Interface.

Towards the end of our project, Halder *et al.* [50], in their experiment, identified how cellular structure influences the transport of water during the drying of porous media. They found that the transport of water depends on its pathways, either intercellular pathways (from cell to cell) or extracellular (from cell to pores) pathways depending on temperature. They also found that $\approx 95\%$ of water is in the intracellular cell at lower temperature and this water becomes intercellular space water at temperatures above 52^{o}C. Consequently, cell membranes are not damaged when drying at low temperature and cell membranes rupture at higher temperature. Taking this effect into our transfer fluxes and incorporating it into our model would certainly result in a more detailed model.

To be able to model the drying behaviour of living plant foods, such as fruit and vegetables, in detail we suggest that not only physical and chemical mechanisms but also biological mechanisms such as pore size distribution and capillary pressure (intercellular space) should be included. The example of biological mechanism experiments, such as classical pressure plate experiments and liquid extrusion porosimetry to measure the flow of water at an applied pressure, and bioelectrical impedance analysis (BIA) could be performed to determine the fraction of water in a tissue/cell. Biological mechanisms could be important for water release during a significant part of the drying time during convective drying. A direct investigation of the ultrastructural changes could be used to better describe biological mechanisms such as experimental study by Halder *et al.* [50].

Bibliography

[1] S. Achanta, M. R. Okos, J. H. Cushman, and D. P. Kessler. Moisture transport in shrinking gels during saturated drying. *AIChE Journal*, 43:2112–2122, 1997.

[2] E. Akpinar, A. Midilli, and Y. Bicer. Single layer drying behaviour of potato slices in a convective cyclone dryer and mathematical modelling. *Energy Conversion and Management*, 44:1689–1705, 2003.

[3] B. J. Aldous, F. Franks, and A. L. Greer. Diffusion of water within an amorphous carbohydrate. *Journal of Materials Science*, 32:301–308, 1997.

[4] W. F. Ames. *Numerical Method for Partial Differential Equations*. Academic Press, Boston, 3th edition, 1992.

[5] M. Aversa, S. Curcio, V. Calabro, and G. Iorio. An analysis of the transport phenomena occuring during food drying process. *Journal of Food Engineering*, 78:922–932, 2007.

[6] P. Baggio, C. Bonacina, and B. A. Schrefler. Some considerations on modelling heat and mass transfer in porous media. *Transport in Porous media Chemical Engineering Science*, 28:233–251, 1997.

[7] R. Baini and T. A. G. Langrish. Choosing an approriate drying model for intermittent and continuous drying of banana. *Journal of Food Engineering*, 79:330–343, 2007.

[8] M. Balaban and G. M. Pigott. Mathematical model of simulteous heat and mass transfer in food with dimensional changes and variable transport parameters. *Journal of Food Science*, 53:935–939, 1988.

[9] B. R. Bhandari and T. Howes. Implication of glass transition for the drying and stability of dried foods. *Journal of Food Engineering*, 40:71–79, 1999.

[10] I. Bialobrzewski. Determination of the mass transfer coefficient during hot-air-drying of celery root. *Journal of Food Engineering*, 78:1388–1396, 2007.

[11] R. Bird, W. Stewart, and E. Lightfoot. *Transport phenomena*. John Wiley and son, 2002.

[12] N. E. Bixler. Noria a finite element computer program for. analyzing water, vapor, air, and energy transport in porous media. Technical report, Report No. SAND842057, UC-70; Sandia National. Laboratories: Albuquerque, New Mexico 87185, 2006.

[13] J. Bon, H. Vaquiro, J. Benedito, and J. Telis-Romero. Thermophysical properties of mango pulp (mangifera indica l. cv. tommy atkins). *Journal of Food Engineering*, 97:563–568, 2010.

[14] N. Boudhrioua, C. Michon, G. Cuvelier, and C. Bonazzi. Influence of ripeness and air temperature in banana texture during drying cavendish and gros michel banana slices. *Journal of Food Engineering*, 55:115–120, 2002.

[15] M. Bouraoui, P. Richard, and T. Durance. Microwave and convective drying of potato slices. *Journal of Food Process Engineering*, 17:353–363, 1994.

[16] D. B. Brooker. Mathematical model of the psychrometric chart. *Transactions of ASAE*, 10(4):558–560, 1967.

[17] H. S. Carslaw and J. C. Jaeger. *Conduction of Heat in Solids*. Clarendon Oxford - Sciences Publication, 2th edition, 1959.

[18] I. Ceylan. Energy analysis of pid controlled heat pump dryer. *Engineering*, 1:188–195, 2009.

[19] I. Ceylan, M. Aktas, and A. Dogan. Mathematical modelling of drying characteristics of tropical fruits. *Applied Thermal Engineering*, 27:1931–1936, 2007.

[20] S. Chemkhi, F. Zagrouba, and A. Bellagi. Modelling and simulation of drying phenomena with rheological behavior. *Brazilian Journal of Chemical Engineering*, 22(2):153–163, 2005.

[21] P. Chen and D. C. T. Pei. A mathematical model of drying processes. *International Journal of Heat and Mass Transfer*, 32:297–310, 1989.

[22] K. J. Chou, S. K.and Chua. New hybrid drying technologies for heat sensitive foodstuffs. *Trends in Food Science and Technology*, 12:359–369, 2001.

[23] K. J. Chua, S. K. Chou, M. N. A. Hawlader, A. S. Mujumdar, and J. C. Ho. Modelling the moisture and temperature distribution within the agricultural product undergoing time-varying drying schemes. *Biosystem Engineering*, 81:99–111, 2002.

[24] COMSOL. Comsol multiphysic: Modelling guide. COMSOL Multiphysics Modeling Guide COPYRIGHT 19982008 by COMSOL AB., Nov. 2008.

[25] T. Constant, C. Moyne, and P. Perré. Drying with internal heat generation: Theoretical aspect and application to microwave heating. *AIChE Journal*, 42:359–368, 1996.

[26] J. Crank. *The Mathematics of Diffusion*. Oxford Sciences Publication, 1975.

[27] J. Crank. *Free and moving boundary problems*. Clarendon Press - Oxford Sciences Publication, 1984.

[28] G. H. Crapiste, S. Whitaker, and E. Rotstein. Drying of cellular structure-i. a mass transfer theory. *Chemical Engineering Science*, 43:2919–2928, 1988.

[29] G. H. Crapiste, S. Whitaker, and E. Rotstein. Drying of cellular structure-ii. experiment and numerical results. *Chemical Engineering Science*, 43:2929–2936, 1988.

[30] S. Curcio and M. Aversa. Transport phenomena and shrinkage modelling during convective drying of vegetable. In *Proceedings of COMSOL Conferences 2009 Milan*, 2009.

[31] S. Curcio, M. Aversa, V. Calabro, and G. Iorio. Simulation of food drying: Fem analysis and experimental validation. *Journal of Food Engineering*, 87:541553, 2008.

[32] A. Datta. Porous media approaches to studying simultaneous heat and mass transfer in food processes i:problem formulation. *Journal of Food Engineering*, 80:80–95, 2007.

[33] A. K. Datta. Porous media approaches to studying simultaneous heat and mass transfer in food processes ii:property data and representative results. *Journal of Food Engineering*, 80:96–110, 2007.

[34] A. K. Datta. Status of physics-based models in the design of food products, processes, and equiptment. *Comprehensive Review In Food Science and Food Safety*, 7:121–129, 2008.

[35] A. K. Datta and H. Ni. Infrared and hot-air-assisted microwave heating of foods for control of surface moisture. *Journal of Food Engineering*, 51:355–364, 2002.

[36] H. Desmorieux, C. Diallo, and Y. Coulibaly. Operation simulation of a convective and semiindustrial mango dryer. *Journal of Food Engineering.*, 89:119–127, 2008.

[37] C. Di Blasi. Multi-phase moisture transfer in high-temperature drying of wood particles. *Chemical Engineering Sciences*, 53:353–366, 1997.

[38] J. Dianty. Water relations of plant cells. In U. Luttge and M. G. Pitman, editors, *Transport in plants II. Part A.*, pages 279–326. New York, USA: Academic Press, Springer-Verlag., 1976.

[39] D. D. Dincov, K. A. Parrott, and K. A. Pericleous. Heat and mass transfer in in two phase porous materials under intensive microwave heating. *Journal of Food Engineering*, 65:403–412, 2004.

[40] A. O. Dissa, H. Desmorieux, J. Bathiebo, and J. Koulidiati. Convective drying characteristics of amelie mango(mangifera indica l. cv. amelie) with correction for shrinkage. *Journal of Food Engineering*, 88:429–437, 2008.

[41] G. J. Dunn, S. K. Wilson, B. R. Duffy, S. David, and K. Sefiane. A mathematical model of the evaporation of a thin sessile liquid droplet: Comparison between experiment and theory. *Colloids and Surface A: Physicochemical and Engineering Aspects*, 323:50–55, 2008.

[42] G. Fang, , and C. Ward. Examination of the statistical rate theory expression for liquid evaporation rates: statistical physics, plasma fluids and related interdisciplinary topics. *Physics Review*, 59:441–453, 1999.

[43] B. Farkas, R. Singh, and T. Rumsey. Modeling heat and mass transfer in immersion frying. i, model development. *Journal of Food Engineering*, 29:211–226, 1996.

[44] H. Feng, J. Tang, R. P. Cavalieri, and O. A. Plumb. Heat and mass transport in microwave drying of porous materials in a spouted bed. *AIChE Journal*, 47:1499–1512, 2001.

[45] F. A. N. Fernandes, S. Rodrigues, C. L. Law, and A. S. Mujumdar. Drying of exotic tropical fruits: A comprehensive review. *Food Bioprocess Technology*, 4:163–185, 2009.

[46] A. L. Floury, J.and Bail and Q. Pham. A three-dimensional numerical simulation of the osmotic dehydration of mango and effect of freezing on the mass transfer rates. *Journal of Food Engineering*, 85:1–11, 2008.

[47] J. Frauhammer, H. Klein, G. Eigenberger, and U. Nowak. Solving moving boundary problems with an adaptive moving grid method: Rotary heat exchangers with condensation and evaporation. *Chemical Engineering Science*, 53(19):3393–3411, 1998.

[48] R. P. F. Guiné, A. E. Rodrigued, and M. M. Figueiredo. Modelling and simulation of pear drying. *Applied Mathematics and Computation*, 192:69–77, 2007.

[49] B. Hadrich and N. Kechaou. Mathematical modelling and simulation of heat and mass transfer in a shrinking cylinder during drying. *Proceedings of the 14th International Drying Simposium (IDS)(Sao Paulo,Brazil, August 22-25, 2004)*, A:533–541, 2004.

[50] A. Halder, A. Datta, and M. Spanswick. Water transport in cellular tissues during thermal processing. *Trans IChemE, Food and Bioproducts Processing*, 00:1–15, 2010.

[51] A. Halder, A. Dhall, and A. Datta. Modeling transport in porous media with phase change: Application to food processing. *Journal of Heat Transfer*, 133:1–13, 2011.

[52] A. Halder, A. Dhall, and A. K. Datta. Modeling of frying and related processes involving strong evaporation:a porous media approach. In *Proceedings of the COMSOL user conferences, Boston*, pages 28–30, 2006.

[53] A. Halder, A. Dhall, and A. K. Datta. An improved, easily implementable, porous media based model for deep fat frying part i: Model development and input parameter. *Trans IChemE, Food and Bioproducts Processing*, 85:209–219, 2007.

[54] A. Halder, A. Dhall, and A. K. Datta. An improved, easily implementable, porous media based model for deep fat frying part ii: Result, validation and sensitivity analysis. *Trans IChemE, Food and Bioproducts Processing*, 85:220–230, 2007.

[55] L. Hassini, S. Azzouz, R. Peczalski, and A. Belghith. Estimation of potato diffusivity from convective drying kinetics with correction for shrinkage. *Journal of Food Engineering*, 79:47–56, 2007.

[56] J. A. Hernandez, G. Pavon, and M. Garcia. Analytical solution of mass transfer equation considering shrinkage for modelling food-drying kinetics. *Journal of Food Engineering*, 45:1–10, 2000.

[57] Q. Ho, B. Verlinden, P. Verboven, S. Vandewalle, and M. Nicolai. A permeation-diffusion-reaction model of gas transport in cellular tissues of plant material. *Journal of Experiment Botany*, 57:4215–4224, 2006.

[58] A. Husain, C. S. Chen, J. T. Clayton, and L. F. Whitney. Mathematical simulation of mass and heat transfer in high moisture food. *Transactions of the ASAE*, 15:732–736, 1972.

[59] M. M. Hussain and I. Dincer. Two-dimensional heat and moisture transfer analysis of a cylindrical moist object subjected to drying: A finite-difference approach. *Journal of Heat and Mass Transfer*, 46:4033–4039, 2003a.

[60] M. M. Hussain and I. Dincer. Analysis of two-dimensional heat and moisture transfer during drying of spherical objects. *International Journal of Energy Research*, 27:703–713, 2003b.

[61] S. Janjai, N. Lamlert, P. Intawee, B. Mahayothee, M. Haewsungcharern, B. Bala, and J. Muller. Finite element simulation of drying of mango. *Biosystem Engineering*, 99:523–531, 2008.

[62] K. Javaherdeh, H. Deylemi, M. Hanifi, and M. Naghashdegan. Drying characteristics of banana: Theoretical modelling and experimental verification. *Proceding of 2nd International Congress on Computational Mechanics and Simulation Dec 8-10, 2006*, A, 2005.

[63] V. Karathanos, S. Angela, and M. Karel. Collapse of structure during drying of celery. *Drying Technology*, 5:1005–1024, 1993.

[64] M. A. Karim and M. N. A. Hawladar. Drying characteristic of banana: Theoritical modelling and experiment validation. *Journal of Food Engineering*, 70:4914–4925, 2005.

[65] M. A. Karim and M. N. A. Hawladar. Mathematical modelling and experimental investigation of tropical fruits drying. *Journal of Heat and Mass Transfer*, 48:4914–4925, 2005.

[66] M. E. Katekawa and M. A. Silva. A review of drying models including shrinkage effects. *Drying Technology*, 24:5–20, 2006.

[67] M. E. Katekawa and M. A. Silva. On the influence of glass transition on shrinkage in convective drying of fruits: a case study of banana drying. *Drying Technology*, 25:1659–1666, 2007.

[68] A. Kaya, O. Aydin, and I. Dincer. Numerical modelling of heat and mass transfer during force convection drying of rectangular moist objects. *Journal of Food Engineering*, 49:3094–3103, 2006.

[69] A. Khaled and K. Vafai. The role of porous media in modeling flow and heat transfer in biological tissues. *International Journal of Heat and Mass Transfer.*, 46:4989–5003, 2003.

[70] M. M. Khraisheh, T. J. R. Cooper, and T. R. A. Magee. Transport mechnanism of moisture during drying process. *Trans IChemE*, 75:34–40, 2000.

[71] C. T. Kiranoudis, Z. B. Maroulis, and D. Marinos-Kouris. Heat and mass transfer model building in drying with multiresponse data. *International Journal of Heat and Mass Transfer*, 38(3):463–480, 1995.

[72] W. Kyamuhangire, T. Krekling, E. Reed, and R. Pehrson. The microstructure and tannin content of banana fruit and their likely influence of juice extraction. *Journal of the Sciences of Food and Agriculture*, 86:1908–1915, 2006.

[73] F. T. Lewis. The geometry of growth and cell division in epithelial mosaics. *American Journal of Botany*, 30:766–776, 1943.

[74] A. G. B. Lima, M. R. Quiroz, and S. A. Nebra. Simulteneous moisture transport and shrinkage during drying of solids with ellipsoidal configuration. *Chemical Engineering Journal*, 86:85–93, 2002.

[75] A. V. Luikov. System of differential equations of heat and mass transfer in capillary-porous bodies (review). *International Journal of Heat and Mass Transfer*, 18:1–14, 1975.

[76] L. Mayor and A. M. Sereno. Modelling shrinkage during convective drying of food materials: a review. *Journal of Food Engineering*, 61:373–386, 2004.

[77] W. A. M. McMinn and T. R. A. Magee. Studies on the effect of temperature on the moisture sorption characteristics of potato. *Journal of Food Process Engineering*, 22:113–128, 1999.

[78] H. K. Mebatsiona, P. Verbovena, A. Melese Endalewa, J. Billenb, Q. T. Ho, and B. M. Nicolaa. Modelling fruit (micro) structures, why and how? *Trends in Food Science and Technology*, 19:59–66, 2008.

[79] A. S. Mujumdar. *Handbook of industrial drying*. Marcel Dekker, Inc, New York, Basel (1995), 2nd. edition, 1995.

[80] A. Mulet. Drying modeling and water diffusivity in carrots and potatoes. *Journal of Food Engineering*, 22:329–348, 1994.

[81] S. B. Nasrallah and P. Perre. Detailed study of a model of heat and mass transfer during convective drying of porous media. *International Journal of Heat Mass Transfer*, 31:975–967, 1988.

[82] M. N. Nguyen and W. E. Price. Air drying of banana: Influence of experimental parameter slab thickness, banana maturity and harvesting season. *Journal of Food Engineering*, 79:200–206, 2007.

[83] P. T. Nhan. *Understanding Viscoelasticity: Basics of Rheology*. Springer, 2002.

[84] H. Ni and A. K. Datta. Moisture, oil and energy transport during deep fat frying of food materials. *Trans IChem*, 77:194–204, 1999.

[85] H. Ni, A. K. Datta, and K. E. Torrance. Moisture transport in intensive microwave heating of biometerial: a multiphase porous media approach. *Internationl Journal of Heat and Mass Transfer*, 42:1501–1512, 1999.

[86] P. S. Nobel. *Biophysical Plant Physiology and Ecology*. W.H. Freeman and Co., 1983.

[87] P. S. Nobel. *Physichemical and enviromental Plant Physiology*. Elsevier Academic Press, 3th edition, 2004.

[88] A. Ousegui, C. Moresoli, M. Dostie, and B. Marcos. Porous multiphase approach for baking process-explicit formulation of evaporation rate. *Journal of Food Engineering*, 100:535–554, 2010.

[89] T. Padfield. The role of absorbent building materials in moderating changes of relative humidity. *Published as a report from the Department of Structural Engineering and Materials, The Technical University of Denmark. Series R no. 54, 1999*, 11(1):2–57, 1999.

[90] G. Pavón-Melendez, J. A. Hernández, M. A. Salgado, and M. A. García. Dimensionless analysis of the simultaneous heat and mass transfer in food drying. *Journal of Food Engineering*, 51:347–353, 2002.

[91] Q. A. Plumb. Transport phenomena in porous media: Modelling the drying process. In K. Vafai, editor, *Handbook of Porous Media*, pages 755–786. Taylor and Francis, 2000.

[92] M. Prat. Recent advances in pore-scale for drying of porous media. *Journal of Food Engineering*, 86:153–164, 2002.

[93] M. Quintard and S. Whitaker. Theoretical analysis of transport in porous media. In K. Vafai, editor, *Handbook of Porous Media*, pages 1–52. Taylor and Francis, 2000.

[94] M. R. Quiroz and S. A. Nebra. Theoretical and experimental analysis of the drying kinetics of banana. *Journal of Food Engineering*, 47:127–132, 2001.

[95] S. Radomkit, E. Kaewmaneechai, P. Kuwichitjaru, B. Mahayothee, and S. Samuhasaneetoo. Physicochemical changes during hot air drying of banana. In *The 9th Agro-Industrial Conference: Food Innovation Asia 2007: Q Food for Good Life, 14-15 June 2007. BITEC, Bangkok, Thailand*, pages 1–6, 2007.

[96] M. S. Rahman. Glass transition and other structure changes in foods. In M. S. Rahman, editor, *Handbook of Food Preservation*, pages 75–94. Marcel Dekker New York, 1999.

[97] M. S. Rahman, I. M. Al-Marhubi, and A. Al-Mahrouqi. Measurement of glass transition temperature by mechanical(DTMA), thermal (DSC and MDSC), water diffusion and density method: a comparison study. *Chemical Physics Letters*, 440:372–377, 2007.

[98] R. M. Reeve. Histological survey of condition influencecing texture in potato. i. effect of heat treatment on structure. *Journal of Food Science*, 19:323–332, 1954.

[99] I. Ruiz-Lopez, A. Cordova, G. Rodriguez-Jimenes, and Garcia-AlvaradoM.A. Moisture and temperature evolution during drying: effect of variable properties. *Journal of Food Engineering*, 63:117–124, 2004.

[100] C. Sajnin, L. N. Gerschenson, and A. Rojas. Turgor pressure in vegetable tissues: Comparison of the performance of incipient plasmolysis technique using mannitol and polyethylenglycol. *Food Research International*, 32:531–537, 1999.

[101] D. Salvatori, A. Andres, A. Chiralt, and P. Fito. Osmotic dehydration progression in apple tissue i: Spatial distribution of solutes and moisture content. *Journal of Food Engineering*, 42:125–132, 2008.

[102] W. E. Schiesser. *The Numerical Method of Lines*. Academic Press, San Diego, 1991.

[103] W. Senadeera, B. Bhandari, G. Young, and B. Wijesinghe. Physical property changes of fruits and vegetables during hot air drying. In A. S. Mujumdar, editor, *Drying Technology in Agriculture and Food Sciences*, pages 149–190. Science Publishers, Inc., 2000.

[104] J. Shi and M. Le Maguer. Mass transfer flux at solid-liquid contacting interface. *Food Science and Technologies*, 9:193–199, 2003.

[105] A. Simal, A. Femenia, J. A. Carcel, and C. Rossello. Mathematical modelling of the drying curves of kiwi fruits: Influances of ripening stage. *Journal of Science of Food and Agriculture*, 85:425–432, 2005b.

[106] A. Simal, A. Femenia, M. C. Garau, and C. Rossello. Use of exponential, page's and diffusional models to simulate the drying kinetics of kiwi fruit. *Journal of Food Engineering*, 66:323–328, 2005a.

[107] A. Simal, C. Rosselló, A. Berna, and A. Mulet. Drying of shrinking cylinder-shaped bodies. *Journal of Food Engineering*, 37:423–435, 1998.

[108] R. Singh. Heating and cooling process for foods. In D. R. Heldman and D. B. Lund, editors, *Handbook of Food Engineering*, pages 247–276. Marcel Dekker Inc., 1992.

[109] J. C. Slattery. *Momentum, Energy and Mass Transfer in Continua*. Robert E. Krieger, 1978.

[110] M. A. Stanish, G. S. Schajer, and F. Kayihan. A mathematical model of drying for hygroscopic porous media. *AIChE Journal*, 32:1301–1311, 1986.

[111] K. Thorvaldsson and H. Janestad. A model for simulteneous heat, water and vapour diffusion. *Journal of Food Engineering*, 40:167–172, 1999.

[112] A. D. Tomos and R. A. Leigh. The pressure probe: A versatile tool in plant cell physiology. *Annu. Rev. Plant Physiol. Plant Mol. Biol.*, 50:447–472, 1999.

[113] C. Toupin and M. Marcotte. Osmotically-induced mass transfer in plant storage tissues: A mathematical model. part ii. *Journal of Food Engineering*, 10:97–121, 1989.

[114] C. J. Toupin, M. Marcotte, M. L. Maguer, and C. J. Michkle. Osmotically-induced mass transfer in plant storage tissues: A mathematical model. part i. *Journal of Food Engineering*, 10:13–38, 1989.

[115] S. Touré and S. Kibangu-Nkembo. Comparative study of natural solar drying of cassava, banana and mango. *Renewable Energy*, 29:975–990, 2004.

[116] I. W. Turner and W. J. Ferguson. An unstructured mesh cell-centered control volume method for simulating heat and mass transfer in porous media: application to softwood drying, part i: the isotropic model. *Applied Mathematics Modelling*, 19:654–666, 1995.

[117] M. T. Tyree. The symplast concept. a general theory of symplastic transport according to the thermodynamics of irreversible processes. *J. Theor. Biol.*, 26:181–214, 1970.

[118] D. Velič, M. Planinič, S. Tomas, and S. Bilič. Influance of air velocity on kinetics of convection of apple drying. *Journal of Food Engineering*, 64:97–102, 2004.

[119] L. Villa-Corrales, J. Flores-Prieto, J. Xaman-Villasenor, and E. Garcia-Hernandez. Numerical and experimental analysis of heat and moisture transfer during drying of ataufo mango. *Journal of Food Engineering*, 98:198–206, 2010.

[120] J. Waewsak, S. Chindaruksa, and C. Punlek. A mathematical modelling study of hot air drying for some agriculture products. *Thammast Int. J. Sc. Tech.*, 11:14–20, 2006.

[121] L. Wang, D. Hukin, J. Pritchard, and C. Thomas. Comparison of plant cell turgor pressure measurement by pressure probe and micromanipulation. *Biotechnology Letters*, 28:11471150, 2006.

[122] N. Wang and J. Brennan. Effect of water binding on the drying behaviour of potato. In A. S. Mujumdar, editor, *Drying*, pages 1350–1359. Elsevier Amsterdem, 1992.

[123] N. Wang and J. Brennan. Changes in structure, density and porosity of potato during dehydration. *Journal of Food Engineering*, 24:61–76, 1995.

[124] N. Wang and J. Brennan. A mathematical model of simultenuous heat and moisture transfer during drying of potato. *Journal of Food Engineering*, 24:47–60, 1995.

[125] Z. Wang and G. H. Chen. Heat and mass transfer during intensity convection drying. *Chemical Engineering Science*, 54:3899–3908, 1999.

[126] S. Whitaker. Simultaneous heat, mass, and momentum transfer in porous media: a theory of drying. *Advances in Heat Transfer*, 13:119–203, 1977.

[127] B. D. Wood, M. Quintard, and S. Whitaker. Calculation of effective diffusivities for biofilms and tissues. *Biotechnology and Bioengineering*, 77:495–516, 2002.

[128] B. D. Wood and S. Whitaker. Diffusion and reaction in biofilms. *Chemical Engineering Sciences*, 53:397–425, 1998.

[129] X. Xiong, G. Narsimhan, and M. R. Okos. Effect of composition and pore structure on binding energy and effective diffusivity of moisture on porous food. *Journal of Food Engineering*, 15:187–208, 1991.

[130] R. Yamsaengsung and R. Moreira. Modeling the transport phenomena and structural changes during deep fat frying part ii: Model solution and validation. *Journal of Food Engineering*, 53:11–25, 2002.

[131] R. Yamsaengsung and R. G. Moreira. Modeling the transport phenomena and structural changes during deep fat frying part i: Model developement. *Journal of Food Engineering*, 53:1–10, 2002.

[132] Z. Yan, M. J. Sousa-Gallagher, and F. A. R. Oliveira. Shrinkage and porosity of banana, pineapple and mango slice during air-drying. *Journal of Food Engineering*, 84:430–440, 2008.

[133] H. M. Yashoda, T. N. Prabha, and R. N. Tharanathan. Mango ripening:changes in cell wall constitution in relation to textural softening. *Journal of the Sciences of Food and Agriculture*, 86:713–721, 2006.

[134] A. Zhang and A. K. Datta. Mathematical modeling of bread baking process. *Journal of Food Engineering*, 75:78–89, 2006.

[135] A. Zhang, A. K. Datta, and S. Mukherjee. Transport processes and large deformation during baking of bread. *AIChE Journal*, 51 no 9:2569–2580, 2005.

[136] A. Zhang, A. K. Datta, and V. Rakesh. Investigation of non-equilibrium in water evaporation. In *3rd Inter-American Drying conference, Montreal Canada*, 2005.

[137] J. Zhang and A. K. Datta. Some consideration in modelling of moisture transport in heating of hygroscopic materials. *Drying Technology*, 22:1983–2008, 2004.

[138] Z. Zhang, S. Yang, and D. Liu. Mechanism and mathematical model of heat and mass trensfer during convective drying of porous materials. *Heat Transfer-Asian research*, 28:337–351, 1999.

[139] Y. Zhiming and M. Le Maguer. Mathematical modelling and simulation of mass tansfer in osmotic dehydration processes. part i:conceptual and mathematical model . *Journal of Food Engineering*, 29:349–360, 1997.

[140] Y. Zhiming and M. Le Maguer. Mathematical modelling and simulation of mass tansfer in osmotic dehydration processes. part ii: Simulation and verification. *Journal of Food Engineering*, 32:21–32, 1997.

[141] L. Zhou, V. M. Puri, R. Anantheswaran, and G. Yeh. Finite element modeling of heat and mass transfer in food materials during microwave heating- model development and validation. *Journal of Food Engineering*, 25:509–529, 1995.

[142] N. P. Zogzas and Z. B. Maroulis. Effective moisture diffusivity estimation from drying data. a comparison between various methods of analysis. *Drying Technology*, 14:1542–1573, 1996.

Appendix A

Numerical solution using Comsol - one-dimension

In the general equation system forms, the PDEs and boundary conditions are written in the following form:

$$\begin{cases} e_a \dfrac{\partial^2 u}{\partial t^2} + d_a \dfrac{\partial u}{\partial t} + \nabla.\Gamma = F & \text{in } \Omega, \\ -\mathbf{n}.\Gamma = G - h^T \mu & \text{on } \partial\Omega, \\ 0 = R & \text{on } \partial\Omega. \end{cases}$$

For non-isothermal one-dimensional drying model, two dependent variable $\overline{M}$ and $\overline{T}$ is formulated such as a PDEs general form below

$$\frac{\partial \overline{M}}{\partial \tau} - \frac{\partial}{\partial \xi}(\frac{\partial \overline{M}}{\partial \xi}) = 0. \tag{A.1}$$

$$\frac{\partial \overline{T}}{\partial \tau} - \frac{\partial}{\partial \xi}(Le\frac{\partial \overline{T}}{\partial \xi}) = 0. \tag{A.2}$$

The space coordinate in the model is ξ. Identifying the general form with equations A.1 and A.2, the following settings generate the equation (Table A.1, Table A.2) :

Two boundary conditions, boundary condition at the centreline $\xi = 0$ will give Neumann type boundary condition with $G = 0$ and influx boundary condition at the surface ξ will give Neumann type boundary condition with $G = -\overline{Sh}(\overline{C}_{f,sur} - 1)$ and $G = LeNu_c(\overline{T}_{csur} - 1) + \overline{\lambda}\frac{\partial \overline{M}}{\partial \overline{x}}$ respectively.

The food domain was discretized into a total number of 320 elements. The time dependent problem was solved by an implicit time-stepping scheme, leading to non

Table A.1: Equation generated for moisture.

Coefficient	Value Expression
e_a	0
d_a	1
Γ(flux vector)	$-\frac{\partial \overline{M}}{\partial \xi}$
F(source term)	0

Table A.2: Equation generated for temperature.

Coefficient	Value Expression
e_a	0
d_a	1
Γ(flux vector)	$-Le\,\frac{\partial \overline{T}}{\partial \xi}$
F(source term)	0

linear system of equations for each time step. Newton's method was used to solve each non-linear system of equations, whereas a direct linear system solver was adopted to solve the resulting systems of linear equations. The relative and absolute tolerance were set to 10^{-4} and 10^{-5}, respectively. The drying process is considered to be completed when the moisture content in the sample is asymptotic to a residual level.

Appendix B

Numerical solution using Comsol - two-dimension

In the general equation system forms, the PDEs and boundary conditions are written in the following form:

$$\begin{cases} e_a \dfrac{\partial^2 u}{\partial t^2} + d_a \dfrac{\partial u}{\partial t} + \nabla.\Gamma = F & \text{in } \Omega, \\ -\mathbf{n}.\Gamma = G - h^T \mu & \text{on } \partial\Omega, \\ 0 = R & \text{on } \partial\Omega. \end{cases}$$

For non-isothermal two-dimensional drying model, two dependent variable $\overline{M}$ and $\overline{T}$ is formulated such as a PDEs general form below

$$\frac{\partial \overline{M}}{\partial \tau} = \frac{\partial^2 \overline{M}}{\partial \xi_1^2} + \frac{\partial^2 \overline{M}}{\partial \xi_2^2}, \tag{B.1}$$

$$\frac{\partial \overline{T}}{\partial \tau} = Le\Big[\frac{\partial^2 \overline{T}}{\partial \xi_1^2} + \frac{\partial^2 \overline{T}}{\partial \xi_2^2}\Big]. \tag{B.2}$$

The space coordinate in the model is ξ_1 and ξ_2. Identifying the general form with equation B.1 and B.2, the following settings generate the equation (Table B.1, Table B.2):

Four boundary conditions, boundary conditions at the centreline ξ_1=0 and ξ_2=0 will give Neumann type boundary condition with $G = 0$ and influx boundary conditions at the surface $\xi_1 = 1$ will give Neumann type boundary conditions with $G = -\overline{Sh}(\overline{C}_{f,sur} - 1)$ and $G = LeNu_c(\overline{T}_{csur} - 1) + \overline{\lambda}\frac{\partial \overline{M}}{\partial \xi_1}$ respectively. For ξ_2=1 will give Neumann type boundary condition $G = -\overline{Sh}(\overline{C}_{f,sur} - 1)$ and $G = LeNu_c(\overline{T}_{csur} - 1) + \overline{\lambda}\frac{\partial \overline{M}}{\partial \xi_2}$ respectively.

Table B.1: Equation generated for moisture.

e_a	0	
d_a	1	
Γ(flux vector)	$-\frac{\partial \overline{M}}{\partial \xi_1}$	$-\frac{\partial \overline{M}}{\partial \xi_2}$
F(source term)	0	

Table B.2: Equation generated for temperature.

e_a	0	
d_a	1	
Γ(flux vector)	$-Le\,\frac{\partial \overline{T}}{\partial \xi_1}$	$-Le\,\frac{\partial \overline{T}}{\partial \xi_2}$
F(source term)	0	

The food domain was discretized into a total number of 320 elements. The time dependent problem was solved by an implicit time-stepping scheme, leading to non linear system of equations for each time step. Newton's method was used to solve each non-linear system of equations, whereas a direct linear system solver was adopted to solve the resulting systems of linear equations. The relative and absolute tolerance were set to 10^{-4} and 10^{-5}, respectively. The drying process is considered to be completed when the moisture content in the sample is asymptotic to a residual level.

Appendix C

Numerical solution using Comsol for multiphase model - Two dimension

In the general equation system forms, the PDEs and boundary conditions are written in the following form:

$$\begin{cases} e_a \dfrac{\partial^2 u}{\partial t^2} + d_a \dfrac{\partial u}{\partial t} + \nabla.\Gamma = F & \text{in } \Omega, \\ -\mathbf{n}.\Gamma = G - h^T \mu & \text{on } \partial\Omega, \\ 0 = R & \text{on } \partial\Omega. \end{cases}$$

Identifying the general form with equations (7.1), (7.2), (7.3), (7.5) and (7.6) in a framework to use COMSOL solver, the following settings generate the equations (Table C.1, Table C.2, Table C.3, Table C.4, Table C.5) :

Table C.1: Equation generated for intercellular vapour density.

Coefficient	Value Expression	
e_a	0	
d_a	ϕ_i	
Γ(flux vector)	$-(\rho k\gamma + D_i)\frac{\partial \rho}{\partial x}$	$-(\rho k\gamma + D_i)\frac{\partial \rho}{\partial y}$
F(source term)	$j_{ip} + j_{ic}$	

Table C.2: Equation generated for free water moisture.

Coefficient	Value Expression	
e_a	0	
d_a	ρ_s	
Γ(flux vector)	$-(D_f\rho_s + D_p\, M_{f0}\, \rho_s\, \varsigma)\frac{\partial M_f}{\partial x}$	$-(D_f\rho_s + D_p\, M_{f0}\, \rho_s\, \varsigma)\frac{\partial M_f}{\partial y}$
F(source term)	$-(j_{ip} + j_{ic}) + \rho_s r_b$	

Table C.3: Equation generated for bound water moisture.

Coefficient	Value Expression	
e_a	0	
d_a	1	
Γ(flux vector)	0	0
F(source term)	$-r_b$	

Table C.4: Equation generated for intercellular space temperature .

Coefficient	Value Expression	
e_a	0	
d_a	$\phi_i * \rho$	
Γ(flux vector)	$-\phi_i\kappa_v\frac{\partial T_i}{\partial x}$	$-\phi_i\kappa_v\frac{\partial T_i}{\partial y}$
F(source term)	$(j_{ip} + j_{ic})(T_c - T_i - \lambda) + h_i(T_c - T_i) - \phi_i\boldsymbol{n}_i \cdot \frac{\partial T_i}{\partial x}$-$\phi_i\boldsymbol{n}_i \cdot \frac{\partial T_i}{\partial y}$	

Table C.5: Equation generated for intracellular cell temperature.

Coefficient	Value Expression	
e_a	0	
d_a	$(1-\phi_i) * \rho_c$	
Γ(flux vector)	$-(1-\phi_i)\kappa_c\frac{\partial T_c}{\partial x}$	$-(1-\phi_i)\kappa_c\frac{\partial T_c}{\partial y}$
F(source term)	$-(j_{ip} + j_{ic})(T_c - T_i) - h_i(T_c - T_i)$	

Boundary condition at the centreline $y = 0$ and $0 < x < b$, $x = 0$ and $0 < y < a$ will give Neumann type boundary condition with $G = 0$ and influx boundary condition at the surface $x = 1$ and $y = 1$ will give Neumann type boundary condition with $G = -Sh_f(\overline{C}_{fw,sur} - 1)$, $G = -Sh_i(\frac{\rho}{C_{air}} - 1)$, $G = -\phi_i Nu_i \kappa_v (T_{isur} - 1)$ and $G = -(1 - \phi_i)\kappa_c Nu_c(T_{csur} - 1) + \lambda D_f \frac{\partial M_f}{\partial x}$ respectively.